Université de Provence

Habilitation à Diriger les Recherches

Interaction de la lumière avec les milieux hétérogènes tridimensionnels

Présentée par

Brian STOUT

Institut Fresnel : Equipe **C.L.A.R.T.E.**

29 septembre 2006

Composition du jury :

Jean-Jacques GREFFET (Président)
Jacques LAFAIT (Rapporteur)
Gérard GRANET (Rapporteur)
Evgeny POPOV   (Rapporteur)
Jean-Marc LAYET
Gérard TAYEB

Habilitation à diriger des recherches

Interaction de la lumière avec les milieux hétérogènes tridimensionnelles

Brian Stout

29 septembre 2006

Table des matières

1 Remerciements

Ce mémoire a été l'occasion de me pencher sur mon parcours passé et de réaliser que j'ai beaucoup de personnes à remercier :

– Aux U.S.A. à l'Université de Stony Brook (State University of New York) où j'ai préparé mon doctorat dans l'équipe de physique nucléaire de P^r Gerry Brown que je remercie tout particulièrement ainsi que mon directeur de thèse, le P^r T.T.S. Kuo qui m'a appris à bien comprendre «les petites bêtes» dans un programme de recherche.
– En France je remercie beaucoup les chercheurs
   – Yves-Patrick Pellegrini et Jean-Jacques Niez au C.E.A.
   – Jacques Lafait (Université de Paris VI - CNRS)
   – Michel Nevière, Evgeny Popov, Gerard Tayeb - Professeurs à l'Université d'Aix-Marseille (I / III)
   ainsi que :
   – Sophie Stout (mon épouse)
   et les anciens étudiants de thèse
   – Jean-Claude Auger et Olivier Moine

Pour leur soutient constant je remercie mes parents Don et Beverly Stout et mon frère Tim et sa famille.

Un autre grand merci ma belle-famille Michel et You Fournier ainsi que Jean et les siens.

Pour notre fils Jacques et à la mémoire de Sophie

2   Curriculum vitae

D. Brian Stout   Nationalité française
Résidence Les Prairies ; Bâtiment C20   Date de naissance 01/09/1962
153 Chemin de Château Gombert
13013 Marseille

E-mail : brian.stout@fresnel.fr   Page web : http ://www.fresnel.fr/perso/stout/index.htm

Expérience Professionnelle

Nov. 2000 – présent Maître de conférences, Université de Provence, Equipe CLARTE, Institut Fresnel, UMR CNRS 6133, Case 161, Faculté des Sciences et Techniques de St. Jérôme, Marseille

Oct.99 – sept.00 A.T.E.R. Université de Provence, Laboratoire d'Optique électromagnétique, Marseille

Juin 98 – sept. 99 Stage post-doctoral au Laboratoire d'Optique des Solides, Université Paris VI, UMR CNRS 7601

Janv. 97 – juin 98 Visiteur au C.E.N.B.G. de l'Université de Bordeaux Gradignan

Mai 94 – jan. 97 Stage post doctoral dans l'équipe de Jean-Jacques Niez : Etudes des Propriétés Electromagnétique des Matériaux (Furtivité) Centre d'Etudes Scientifiques et Techniques d'Aquitaine, C.E.A./C.E.S.T.A, Le Barp, Gironde

Janv. 92 - dec. 93 Stage post doctoral à l'Institut de Physique Nucléaire, Université de Paris Sud, ORSAY

Dec. 1991 «Ph.D.» (thèse de doctorat) en physique théorique, «State University of New York at Stony Brook» , U.S.A. Titre de la thèse : **Neutrino Mass and Nuclear Double Beta Decay**

Sept. 86 - Dec. 91 Assistant, Groupe de physique nucléaire théorique, State University of New York at Stony Brook, Stony Brook, New York, U.S.A.

Eté 88-90 Assistant en physique théorique, Laboratoire National de Los Alamos, Nouveau Mexique, U.S.A.

3   Introduction

Je décrirai dans ce mémoire une sélection des activités d'encadrement et de recherche que j'ai menées au sein du groupe C.L.A.R.T.E. de l'Institut Fresnel depuis octobre 1999 et au sein du groupe Optique des Solides (de l'Institut de nano-science à Paris) de 1998-1999. J'espère qu'il va servir de base pour de nouveaux travaux dans les prochaines années. Mes articles publiés ou acceptés en 2005-2006 (Références [1]-[8]) sont joints à la fin de ce document. Mes articles antérieurs sont disponibles sur le site :
http ://www.fresnel.fr/perso/stout/index.htm

Je passerai essentiellement sous silence mes travaux antérieurs en milieux effectifs effectués pour la plupart au CEA/CESTA. Je passerai aussi sous silence mes travaux liés au problème à N-Corps et la physique des neutrinos. Bien que ces études antérieures aient eu une influence et continuent d'en avoir une sur mes travaux actuels, les inclure dans ce mémoire mènerait à un document trop hétéroclite. Je me suis donc concentré sur mes travaux les plus récents qui permettent de comprendre les travaux que je compte mener et diriger dans les prochaines années. On trouve néanmoins dans la section 11 de courts résumés de tous mes travaux, où j'essaie d'étayer les grandes lignes des objectifs et les résultats obtenus.

Le fil conducteur de mes recherches récentes est l'interaction de la lumière avec des systèmes méso-scopiques complexes ou composites en trois dimensions. Par «mésoscopiques», on veut dire que le système comporte des objets de taille comparable aux phénomènes ou ondes concernées mais suffisamment grandes afin qu'on puisse discuter leur comportement sans être obligé de considérer les atomes individuels.

De tels milieux suivent deux classifications principales : les systèmes ordonnés et les systèmes dés-ordonnés. Les deux classifications se trouvent naturellement dans la nature et ont des applications tech-nologiques.

Les structures ordonnées permettent une manipulation de la lumière pour la technologie. L'importance des applications des réseaux à la spectroscopie et ailleurs ne nécessite plus de rappel. Les structures du type cristaux photoniques offrent de nouvelles possibilités pour le contrôle et le guidage de la lumière.

En ce qui concerne les milieux désordonnés, une des applications de telles études est l'optimisation des propriétés volontairement diffusantes et/ou absorbantes comme les peintures ou les revêtements furtifs. Une autre application en est les études de télédétection et le problème inverse où la diffusion peut nous renseigner sur les caractéristiques d'un milieu étudié ou empêcher la détection d'un objet enfoui.

La grande majorité de mes travaux scientifiques a utilisé des techniques analytiques afin d'améliorer les performances de la modélisation par ordinateur de phénomènes complexes. Ce manuscrit va refléter ce thème en expliquant les grandes lignes des certains calculs que j'ai effectués ces dernières années. Les diverses applications seront traitées de façon relativement succincte, mais on peut trouver des discussions d'applications dans certains de mes articles ci-joints.

4   Bref résumé de carrière

J'ai commencé ma carrière en tant que physicien nucléaire. Je me suis tout d'abord intéressé au calcul des états d'excitation des noyaux[27, 31] et des amplitudes de transition[29] dans les noyaux atomiques, en utilisant la méthodologie du problème à N-corps. J'ai ensuite appliqué les méthodes de calcul que j'ai développées à plusieurs types de problèmes différents. Notamment, j'ai étudié dans ma thèse certaines transitions «exotiques» des noyaux afin d'explorer les propriétés des neutrinos.[26] En dehors de ma thèse, j'ai étudié le comportement de noyaux chauffés lors des collisions dans les accélérateurs[28], et les interactions nucléaires dans les étoiles en fin de vie avant le stade de supernovae.[30] J'ai également étudié l'utilité du développement en $1/N$ pour le calcul de potentiels effectifs des noyaux.[25]

J'ai commencé mes travaux en électromagnétisme lors d'un emploi doctoral au CEA/CESTA, en appli-quant les méthodes du problème à N-corps à la propagation d'ondes en milieux micro-hétérogènes.[23, 24] Nous avons étudié la détermination du milieu effectif et le transport radioactif dans de tels milieux. Nous avons souligné le besoin dans une théorie de milieu aléatoire d'une matrice-T du type «hors couche de masse». Vu la complexité d'une telle matrice-T exacte, nous avons proposé un modèle de matrice-T plus simple qui nous a permis d'étendre les calculs de milieux effectifs au-delà du domaine quasi-statique. En dehors de nos publications, nos résultats principaux ont été exposés dans une thèse.[a)] (liste d'encadre-ments : page 6)

Mes travaux au CEA/CESTA m'ont incité à diversifier mes intérêts dans différents problèmes de diffusion et d'absorption au sein du Laboratoire d'Optique des Solides de Paris VI. Lors de l'encadrement

d'un étudiant en thèse, [b) page 6)] j'ai développé de nouvelles méthodes pour une résolution quasi-analytique et récursive du problème de diffusion multiple d'un nombre fini de diffuseurs.[13, 14, 15, 16, 17, 18, 21, 22] Ces études ont permis l'étude de la diffusion dépendante qui a tendance à diminuer l'efficacité de systèmes volontairement diffusants comme les peintures, les cosmétiques, le papier et les revêtements pour la furtivité. Cette technique de calcul fut utilisée dans plusieurs contrats et collaborations industrielles menées sur la diffusion, l'absorption et la non-linéarité induite dans des systèmes diffusants divers.

Je suis arrivé à l'Université de Provence en tant qu'ATER en novembre 1999, et j'ai poursuivi mes recherches au sein du groupe C.L.A.R.T.E. de l'Institut Fresnel, UMR CNRS 6133. J'ai été ensuite nommé Maître de Conférence à l'Université de Provence en novembre 2000.

Une de mes premières activités a été une collaboration avec le Pr. Nevière avec qui nous avons développé un modèle unidimensionnel de cristaux photoniques.[20] Nous avons appliqué cette méthode au problème de fibres optiques structurées avec guidage dans un cœur d'air enrobé d'un cristal photonique. Le but était de mettre en évidence la possibilité de guidage de faisceaux laser haute puissance. Notre méthode numérique rapide et stable nous a permis de calculer les caractéristiques des modes de propagation dans de telles fibres. Nous avons mis en évidence le comportement «mono-mode» de ces fibres et l'importance du choix des propriétés du cœur afin d'éviter les «fuites» de lumière induites par diffraction. Actuellement, je m'intéresse à nouveau aux cristaux photoniques mais cette fois à des modèles tridimensionnels.

Par la suite, j'ai dirigé une thèse et un DEA sur le calcul quasi-analytique des forces optiques sur des objets micrométriques en faisant appel à la matrice T des objets.[5, 8] [c), d) page 6)] L'utilisation des forces optiques sur de petits objets trouve actuellement des applications dans la manipulation de petits objets en biologie et chimie, et dans une variété de techniques de mesure. Parmi les nombreuses applications en perspective, on trouve les lasers à micro-cavité et les cristaux photoniques.

J'ai continué les études sur la diffusion multiple.[2, 6, 9, 10, 11, 12, 13, 14, 15, 16, 17, 18] au sein de l'Institut Fresnel en travaillant à une meilleure compréhension du transport radiatif[10, 11, 12, 14] et à la modélisation d'agrégats aléatoires de plus en plus grands.[2, 6] Concernant la diffusion par des agrégats de grande taille, avec Pierre Sabouroux et Jean-Michel Geffrin de L'Institut Fresnel nous avons entamé une étude en collaboration avec le CETHIL (Centre d'Etudes Thermiques de Lyon). Nous avons commencé à comparer les résultats de notre modélisation avec des mesures, en amplitude et en phase dans le domaine des micro-ondes. L'accord observé entre théorie et expérience a été jusqu'ici d'une grande qualité.[2] Cette étude concerne des agrégats du type suie qui actuellement posent des problèmes dans les environs des aérogares. Nos études trouvent également une utilité dans la modélisation des poussières interstellaires.[2]

Dans la plupart des études sur les agrégats de diffuseurs, que j'ai menées d'abord à l'Université de Paris VI et ensuite à l'Institut Fresnel, nous prenions pour diffuseurs individuels des sphères homogènes et isotropes. Cette idéalisation nous a permis de traiter rapidement les propriétés des diffuseurs individuels en utilisant la théorie de Mie et de nous concentrer sur le problème de diffusion multiple. Compte tenu des progrès réalisés dans le domaine de la diffusion multiple, nous avons récemment commencé à étudier des hétérogénéités ayant une forme et/ou une structure plus complexe.

Une première étude concernait des diffuseurs volontairement plus complexes comme les sphères enrobées du type de celles actuellement fabriquées à l'Institut Fresnel.[10, 11] Dans le cadre d'un contrat industriel, nous avons étudié les moyens d'augmenter l'absorption dans des matériaux composites composés de sphères enrobées. Cette étude nous a permis d'avancer sur l'utilisation de la diffusion afin d'augmenter l'absorption dans les matériaux. Elle a également permis le développement de nouvelles techniques dans le calcul des effets de diffusion dépendante.

Afin d'élargir encore le type de diffuseurs individuels, j'ai développé une théorie différentielle de la diffraction par des objets tridimensionnels décrits en coordonnées sphériques.[7] Elle fournit la matrice-T d'un objet de forme quelconque. Cette méthode a intégré et généralisé les progrès récents réalisés par les Pr. Nevière et Popov dans la théorie différentielle de réseaux de diffraction. Dernièrement, nous avons étendu cette théorie à des sphères composées de matériaux anisotropes,[5] et ensuite à des objets anisotropes de forme quelconque.[4] Les applications de ces théories sont en cours.[1]

La théorie que nous avons développée pour traiter la sphère anisotrope fournit une solution quasi-analytique. Il est à remarquer qu'alors que la théorie de Mie fournissant la solution du problème de la diffraction par une sphère isotrope date de 1908, aucune solution n'avait depuis été élaborée pour une sphère anisotrope arbitraire. Bien que certains travaux résolvaient quelques cas particuliers d'anisotropie, un article publié en 2004 signalait encore que le cas d'anisotropie générale échapperait à toute résolution analytique, pour la raison qu'une anisotropie générale brise la symétrie sphérique. Nos travaux ont infirmé cette prédiction. Ils trouvent des applications immédiates dans le domaine de l'astrophysique, la diffusion

par les poussières interstellaires anisotropes conditionnant l'évolution des étoiles.

5   Contrats et collaborations

06- Collaboration ANR avec le CETHIL (Centre Thermique de Lyon), Pierre Sabouroux, et Jean-Michel Geffrin sur la diffusion par des agrégats du type suie.

05-06 Collaboration avec un projet NASA visant la réalisation de futurs télescopes spatiaux de grandes dimensions.

02-03 Contrat industriel avec le «Centro d'Investigacion en Polïmeros» COMEX, Mexique. visant l'amélioration de peintures.

01-02 Contrat industriel visant l'amélioration des panneaux solaires, IMRA-Europe.

98-99 Contrat industriel (Rhodia-Rhône-Poulenc) visant l'amélioration de peintures.

98-99 Etude en micro-ondes pour un consultant sur des particules sphériques ayant des couches sphériques (Université de Paris VI).

94-97 Etude de furtivité radar pour le C.E.A.

6   Encadrement de jeunes chercheurs

Responsable principal d'une thèse et d'un stage de D.E.A

d) 2002-2005 Modélisation de forces optiques : Thèse, Olivier Moine, Aix-Marseille (Soutenance : Novembre 2005)

c) 2001-2002 Modélisation de Pincettes Optiques pour la nanotechnologie : stage de DEA, Olivier Moine , Aix-Marseille

Participation à l'encadrement de 2 thèses

b) 98-99 Etude expérimentale et modélisation optique des milieux hétérogènes diffusants : Thèse de Jean-Claude Auger ; Université de Paris VI (Soutenance : Décembre 1999)

a) 94-97 Propriétés électromagnétiques dynamiques effectives des milieux aléatoires : Thèse de P. Thibaudeau ; C.E.A., Université de Bordeaux (Soutenance : Juin 1997)

7   Communications à des congrès et séminaires

Mars 2006 Communication PIERS Cambridge, USA

Mars 2006 Communication : GDR Couleurs : Paris France

Mai 2005 Communication : Elect. Light Scat. Non-Sph. Part. Grenada Espagne

Mars 2004 Communication : PIERS Pise Italie

Déc. 2003 Communication : GDR Ondes : ORSAY France

Sept. 2003 Communication : Horizons d'Optique : Toulouse France

Avril 2003 Séminaire invité : Centro d'Investigacion en Polímeros COMEX, México

Nov. 2002 Communication : GDR Ondes : ORSAY France

Juillet 2002 2 communications : Congrès ETOPIM Salt Lake City, Utah

March 2002 Communication : Elect. Light Scat. Non-Sph. Part. Gainseville Floride

Août 2001 3 communications : Electromagnetic Optics 2, Paris, France

Août 2001 Communication : Int. Mat. Research Congress , Cancun, Mexique

Août 2000 2 communications : Elect. Light Scat. Non-Sph. Part. Halifax Canada

Août 1999 Communication, Ecole d'été, Cargèse, Corse, France

Juillet 1999 Présentation invité ETOPIM 99, Hong-Kong

Juin 1996 Séminaire invité C.E.A./Bruyères le Chatel, Paris, France

Juin 1995 Séminaire invité CENBG, Bordeaux, France

Juin 1995 Communication, Journées Maxwell 95, June 6-9, Bordeaux-Lac, France

Mars 1995 Séminaire invité CENBG, Bordeaux, France

Avril 1993 Séminaire invité GANIL Caen, France

Mai 1992 Séminaire invité ORSAY, France

Avril 1991 Communication donnée à la Conférence Nuclear Physics in the 90's, Santa Fe, Nouveau Mexique, Etats-Unis

1989 Communication donnée à la réunion de l'«American Physical Society», Baltimore Maryland, Etats-Unis

1988 Communication donnée à la réunion de l' l'«American Physical Society», Washington D.C., Etats-Unis.

8   Techniques de base et notation

Ce chapitre, donne une introduction / rappel des techniques, concepts et notations utilisés afin de comprendre les diverses applications de la technique «matrice-T» pour la diffusion par des systèmes tridimensionnels.

8.1   Le problème

On commence en écrivant les équations de Maxwell pour un milieu homogène.

8.1.1   Rappel sur les champs «microscopiques» et «macroscopiques»

Les équations de Maxwell dans le vide sont :

$$\nabla \times \mathbf{E}\left(\mathbf{r},t\right) = -\frac{\partial \mathbf{B}\left(\mathbf{r},t\right)}{\partial t} \tag{1a}$$

$$\nabla \cdot \mathbf{E}\left(\mathbf{r},t\right) = \frac{\rho\left(\mathbf{r},t\right)}{\epsilon_0} \tag{1b}$$

$$\nabla \times \mathbf{B}\left(\mathbf{r},t\right) = \frac{1}{c^2}\frac{\partial \mathbf{E}\left(\mathbf{r},t\right)}{\partial t} + \mu_0 \mathbf{J}\left(\mathbf{r},t\right) \tag{1c}$$

$$\nabla \cdot \mathbf{B}\left(\mathbf{r},t\right) = 0 \tag{1d}$$

où $c \equiv 299\,792\,458$ m/s est la célérité de la lumière, et la perméabilité du vide, μ_0, est définie par :

$$\mu_0 \equiv 4\pi\,10^{-7}\text{henry/m} \tag{2}$$

La permittivité du vide, ϵ_0, est donné par :

$$\epsilon_0 \equiv \frac{1}{c^2\mu_0} = \frac{10^7}{4\pi c^2} \tag{3}$$

Les équations de Maxwell décrivent l'évolution des champs, mais seraient stériles sans l'équation de la force de Lorentz qui décrit l'interaction du champ électromagnétique avec la matière. L'équation dit que la force sur une charge q qui se déplace avec la vitesse $\mathbf{v}$ est :

$$\mathbf{F} = q\left(\mathbf{E} + \mathbf{v} \wedge \mathbf{B}\right) \tag{4}$$

Dans l'ensemble de nos modélisations, nous considérons que la matière est entièrement décrite par une densité de polarisation dipolaire électrique, $\mathbf{P}\left(\mathbf{r},t\right)$, et une densité de polarisation magnétique, $\mathbf{M}\left(\mathbf{r},t\right)$. Des considérations microscopiques habituelles nous amènent à définir des charges de polarisation, ρ_{pol} :

$$\rho_{\text{pol}}\left(\mathbf{r},t\right) \equiv -\nabla \cdot \mathbf{P}\left(\mathbf{r},t\right) \tag{5}$$

ainsi que des courants de polarisation :

$$\mathbf{J}_{\text{pol}}\left(\mathbf{r},t\right) \equiv \frac{\partial}{\partial t}\mathbf{P}\left(\mathbf{r},t\right) \tag{6}$$

et des courants de magnétisation :

$$\mathbf{J}_{\text{mag}}\left(\mathbf{r},t\right) = \nabla \times \mathbf{M}\left(\mathbf{r},t\right) \tag{7}$$

En insérant explicitement ces définitions de charge et courant matériel dans les équations (1b) et (1c) on obtient :

$$\nabla \cdot \mathbf{E}\left(\mathbf{r},t\right) = \frac{\rho_{\text{src}}\left(\mathbf{r},t\right) + \rho_{\text{pol}}\left(\mathbf{r},t\right)}{\epsilon_0}$$

$$\frac{1}{\mu_0}\nabla \times \mathbf{B}\left(\mathbf{r},t\right) = \epsilon_0\frac{\partial \mathbf{E}\left(\mathbf{r},t\right)}{\partial t} + \mathbf{J}_{\text{src}}\left(\mathbf{r},t\right) + \mathbf{J}_{\text{mag}}\left(\mathbf{r},t\right) + \mathbf{J}_{\text{pol}}\left(\mathbf{r},t\right) \tag{8}$$

où ρ_{src} et $\mathbf{J}_{\text{src}}$ sont les courants sources en dehors du système matériel étudié. Insérant les équations (5) (6) (7) dans cette équation on obtient :

$$\nabla \cdot (\epsilon_0 \mathbf{E}(\mathbf{r}, t) + \mathbf{P}(\mathbf{r}, t)) = \rho_{\text{src}}(\mathbf{r}, t) \tag{9}$$

$$\nabla \times \left(\frac{\mathbf{B}(\mathbf{r}, t)}{\mu_0} - \mathbf{M}(\mathbf{r}, t) \right) = \frac{\partial}{\partial t} (\epsilon_0 \mathbf{E}(\mathbf{r}, t) + \mathbf{P}(\mathbf{r}, t)) + \mathbf{J}_{\text{src}}(\mathbf{r}, t) \tag{10}$$

On définit ensuite les champs «macroscopiques», $\mathbf{D}$ et $\mathbf{H}$:

$$\mathbf{D}(\mathbf{r}, t) \equiv \epsilon_0 \mathbf{E}(\mathbf{r}, t) + \mathbf{P}(\mathbf{r}, t)$$

$$\mathbf{H}(\mathbf{r}, t) \equiv \left(\frac{\mathbf{B}(\mathbf{r}, t)}{\mu_0} - \mathbf{M}(\mathbf{r}, t) \right) \tag{11}$$

En termes du champs $\mathbf{D}$ l'équation (9) s'écrit :

$$\nabla \cdot \mathbf{D}(\mathbf{r}, t) = \rho_{\text{src}}(\mathbf{r}, t) \tag{12}$$

qui peut remplacer l'équation (1b) quand un milieu matériel est présent. L'équation (10) s'écrit également en termes des champs $\mathbf{D}$ et $\mathbf{H}$. Si on prend la conservation de charge comme principe de base, l'équation (10) et l'équation (1a) forment les deux équations «macroscopiques» de l'électromagnétisme :

$$\nabla \times \mathbf{E}(\mathbf{r}, t) = -\frac{\partial \mathbf{B}(\mathbf{r}, t)}{\partial t} \tag{13a}$$

$$\nabla \times \mathbf{H}(\mathbf{r}, t) = \frac{\partial \mathbf{D}(\mathbf{r}, t)}{\partial t} + \mathbf{J}_{\text{src}}(\mathbf{r}, t) \tag{13b}$$

Les équations «macroscopiques» (13) ne sont utiles que si l'on connaît les relations entre $\mathbf{D}$ et $\mathbf{H}$ et les champs $\mathbf{E}$ et $\mathbf{B}$. Pour la plupart des matériaux, $\mathbf{D}$ ne dépend que de $\mathbf{E}$ et $\mathbf{H}$ ne dépend que de $\mathbf{B}$. Dans ce mémoire, on va considérer que le milieu *externe* au système est linéaire, homogène, isotrope, et spatialement local. Dans un tel milieu, on peut relier les champs $\mathbf{D}$ et $\mathbf{H}$ aux champs $\mathbf{E}$ et $\mathbf{B}$ via les «relations» constitutives temporellement non-locales $R_\varepsilon(t - t')$ et $R_\mu(t - t')$:

$$\mathbf{D}(\mathbf{r}, t) = \epsilon_0 \int_{-\infty}^{t} dt' \, R_\varepsilon(t - t') \, \mathbf{E}(\mathbf{r}, t')$$

$$\mathbf{B}(\mathbf{r}, t) = \mu_0 \int_{-\infty}^{t} dt' \, R_\mu(t - t') \, \mathbf{H}(\mathbf{r}, t') \tag{14}$$

Typiquement, on adresse le problème de non-localité temporelle en travaillant dans le domaine harmonique avec une dépendance en $\exp(-i\omega t)$ des champs, afin que les relations entre $\mathbf{D}$ et $\mathbf{E}$ ainsi que celles entre $\mathbf{B}$ et $\mathbf{H}$ puissent être écrites de manières «locales» dans le domaine harmonique :

$$\mathbf{D}(\omega) = \epsilon_0 \varepsilon_r(\omega) \mathbf{E}(\omega) \quad \text{et} \quad \mathbf{B}(\omega) = \mu_0 \mu_r(\omega) \mathbf{H}(\omega) \tag{15}$$

où la permittivité électrique relative $\varepsilon_r(\omega)$ est la transformée de Fourier de $R_\varepsilon(t - t')$ et la perméabilité magnétique relative $\mu_r(\omega)$ est la transformée de Fourier de $R_\mu(t - t')$.

On remarque que la présence de l'absorption dans le milieu impose que $\varepsilon_r(\omega)$ et/ou $\mu_r(\omega)$ soient des nombres complexes avec des parties imaginaires positives. Néanmoins, dans certaines situations, le milieu sera presque transparent et on préféra faire l'approximation de ε_r et μ_r réels et indépendants de la fréquence.

Dans un milieu homogène, il est souvent pratique de combiner les équations (13a) et (13b) dans le domaine harmonique afin d'obtenir une seule équation de deuxième ordre entièrement en termes du champ électrique :

$$\nabla \times (\nabla \times \mathbf{E}) - \left(\frac{\omega}{c} \right)^2 \varepsilon_r \mu_r \mathbf{E} = i\omega \mu_r \mu_0 \mathbf{J}_{\text{src}} \tag{16}$$

8.1.2   Milieux hétérogènes

On considère maintenant une structure inhomogène immergée dans le milieu homogène. Donc ε_r (et potentiellement μ_r) sont des fonctions de coordonnées spatiales. Dans ce mémoire, on va considérer

seulement des matériaux ayant des propriétés constitutives constantes par morceau, même s'il est possible de généraliser ces techniques aux matériaux ayant des dépendances spatiales plus complexes. Par contre, suite à mes travaux récents, on peut maintenant aborder des situations où le matériau composant l'objet n'est plus décrit par une constante diélectrique isotrope, mais est un matériau intrinsèquement anisotrope, comme c'est le cas pour de nombreux cristaux dans la nature.

Le problème qu'on veut traiter est de prédire la distribution du champ électromagnétique en présence d'un courant source ou d'un champ incident quelconque. On peut être amené à interroger le champ électromagnétique soit loin du système, soit près du système, voir même à l'intérieur du système étudié. Le fait qu'on étudie des systèmes tri-dimensionnels et que le champ électromagnétique soit de nature vectorielle a tendance à rendre ce problème assez difficile à traiter et à visualiser. Notre solution à cette difficulté consiste à décrire le champ à travers sa projection sur une base d'ondes «multipolaires» (décrite en section 8.2). De cette manière, les descriptions du champ électromagnétique reviennent à spécifier les coefficients de sa projection sur cette base.

On remarque qu'on veut surtout étudier les systèmes où les composants sont comparables en taille à la longueur d'onde caractéristique du rayonnement incident sur le système. Nous appelons de tels systèmes des systèmes résonants parce qu'il est courant dans de tels systèmes d'exciter des résonances électromagnétique liées aux formes géométriques des inhomogénéités. Si les composants sont très grands devant la longueur d'onde, on considère qu'on peut utiliser l'optique géométrique. Si les composants sont petits par rapport à la longueur d'onde, on invoque des approximations du style quasi-électrostatique ou dipolaire. Ces deux limites sont moins définies que l'on pourrait croire mais nous considérons pour la plupart qu'elles sont relativement bien maîtrisées et nous n'allons pas en parler souvent dans ce mémoire.

Les types de système que nous avons regardés le plus souvent sont des systèmes comme ceux de la figure 1 où les inhomogénéités ordonnées ou désordonnées sont immergées directement dans le milieu extérieur homogène. Un deuxième type de système plus réaliste qu'on peut traiter actuellement est celui des systèmes inhomogènes immergés dans une région homogène sphérique comme celle sur la figure 2.
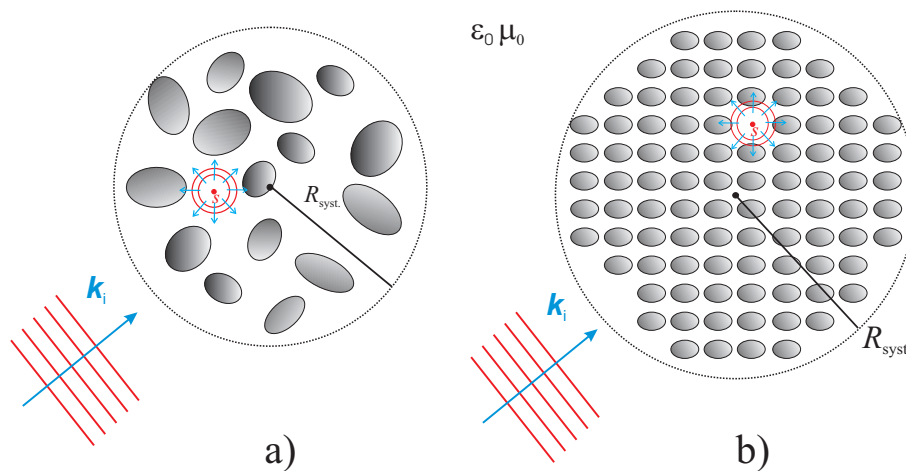
FIG. 1 – Système inhomogène immergé directement dans le milieu externe. Les inhomogénéités sont contenues dans une sphère de rayon R_{syst} et le champ incident vient soit de sources à l'extérieur du système, soit à l'intérieur du système.

Parfois, on est amené à étudier des modes ou des quasi modes de propagation dans des systèmes hétérogènes, surtout quand la structure est étendue et/ou périodique. Nous avons parfois adapté les techniques de diffusion discutées dans ce mémoire au problème de propagation des modes en cherchant des solutions en l'absence d'onde incidente.

Bien que les géométries des figures 1 et 2 aient des applications intéressantes, la géométrie d'une couche inhomogène qui s'étale à l'infini comme celle des figures 3a) et 3b) nous intéresse plus particulièrement. A l'heure actuelle, on ne peut traiter de tels systèmes qu'en faisant des approximations, comme la théorie de transfert radiatif. Un des intérêts majeurs des géométries des régions sphériques est que les solutions semi-analytiques obtenues pour les géométries sphériques peuvent nous permettre d'améliorer les traitements des systèmes de géométrie en couches.
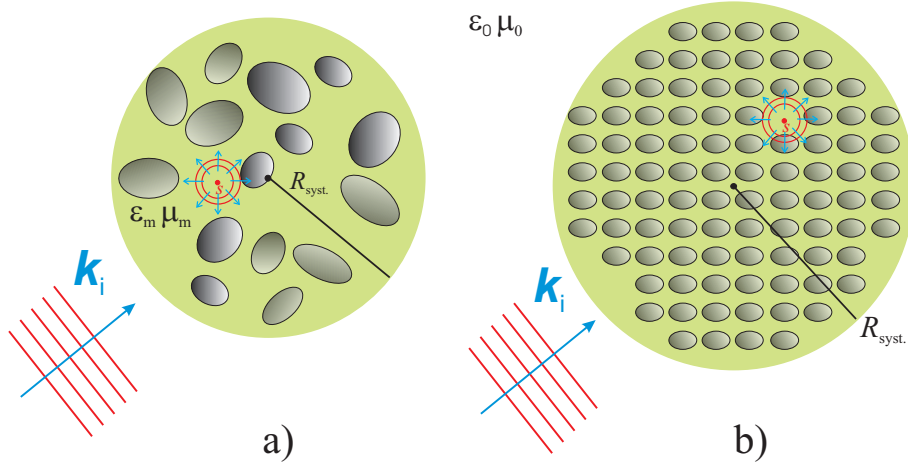
FIG. 2 – Système inhomogène immergé dans un milieu sphérique de géométrie sphérique de rayon R_{syst} et ayant des paramètres constitutifs $\varepsilon_m \neq \varepsilon_0$ et $\mu_m \neq \mu_0$.

Dans tous ces types de systèmes, l'équation de base qui gouverne le champ électrique est :

$$\nabla \times \frac{1}{\mu_r(\mathbf{r})}(\nabla \times \mathbf{E}) - \left(\frac{\omega}{c}\right)^2 \varepsilon_r(\mathbf{r})\,\mathbf{E} = i\omega\mu_0\mathbf{J}_{\text{src}} \tag{17}$$

où $\varepsilon_r(\mathbf{r})$ et $\mu_r(\mathbf{r})$ peuvent être des fonctions de position.

8.2 Ondes multipolaires

Quand le milieu extérieur est isotrope et homogène, l'invariance par rotation dans ce milieu permet de définir une base des solutions aux équations de Maxwell dans ce milieu ayant des propriétés sous rotation particulièrement intéressantes. On appelle les fonctions de cette base les «ondes multipolaires» ou les «ondes partielles» («partial waves»). L'étude des propriétés des ces ondes multipolaires est très riche et fait intervenir la théorie spectrale, la théorie des groupes et pourrait facilement être le sujet d'un livre à elle seule. Dans cette section, on se contentera d'introduire les ondes multipolaires.

Puisque le milieu extérieur est homogène, isotrope et local en régime harmonique, les paramètres constitutifs relatifs du milieu «partial waves», ε_{e} et μ_{e} ne sont pas des tenseurs et on peut les décrire en domaine harmonique par des constantes complexes. L'indice «e» signifie désormais le milieu *externe*. Les équations de Maxwell harmoniques sans sources donnent dans ce cas que le champ électrique satisfait l'équation :

$$\nabla \times (\nabla \times \mathbf{E}) - k_0^2 \varepsilon_{\text{e}}\mu_{\text{e}}\,\mathbf{E} = \mathbf{0} \tag{18}$$

où nous avons défini $k_0 \equiv \omega/c$.

Il est habituel de construire les solutions de l'équation (18) à partir d'ondes multipolaires scalaires. Désignons par φ une solution de l'équation de Helmholtz scalaire :

$$\Delta\varphi + k_{\text{e}}^2\varphi = 0 \tag{19}$$

où $k_{\text{e}}^2 \equiv k_0^2\varepsilon_{\text{e}}\mu_{\text{e}}$. On peut écrire les solutions ondes sortantes de cette équation, $\varphi_{nm}(k_{\text{e}}\mathbf{r})$ par :

$$\varphi_{nm}(k\mathbf{r}) \equiv h_n^+(kr)Y_{nm}(\theta,\phi) \tag{20}$$

où $h_n^+(\rho)$ sont les fonctions de Bessel sphériques sortantes définies par $h_n^+(\rho) \equiv j_n(\rho) + iy_n(\rho)$, et $Y_{nm}(\theta,\phi)$ sont les harmoniques sphériques scalaires normalisés (on donne leurs définitions en 8.3 ci-dessous). Les $\varphi_{nm}(k\mathbf{r})$ ont la particularité qu'elles divergent à l'origine. Elles sont caractérisées par leurs indices n et m qui sont des nombres entiers tel que :

$$n = 0, 1, \ldots, \infty \quad \text{et} \quad m = -n, \ldots, n \tag{21}$$
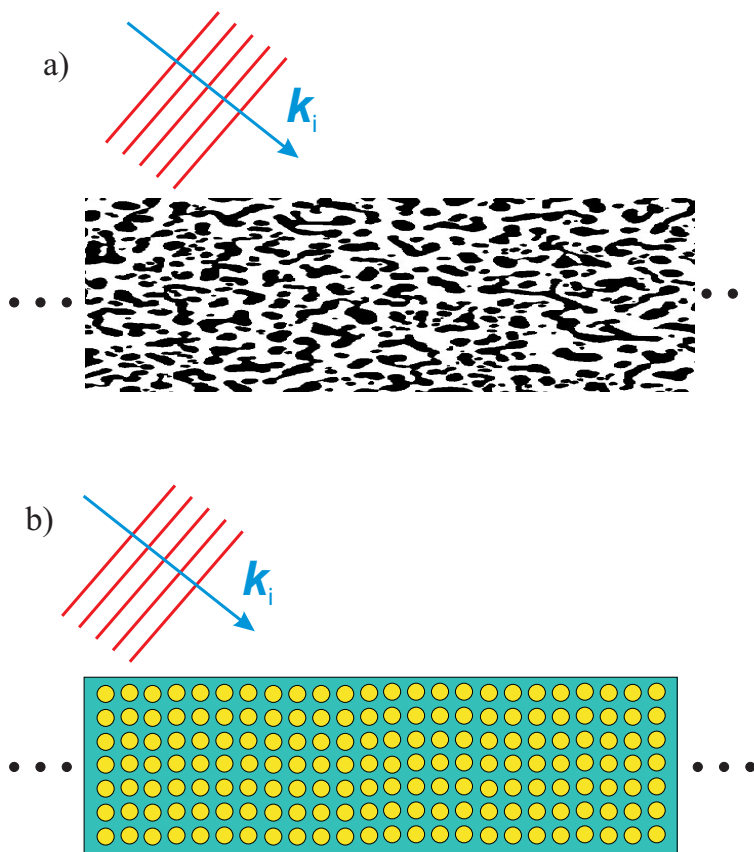
Fig. 3 – a) Système inhomogène dans une couche avec une géométrie aléatoire. b) Système inhomogène dans une couche avec une géométrie ordonnée.

L'indice n correspond au nombre quantique azimutal (habituellement dénoté l en mécanique quantique) et m à la projection du moment cinétique.

On peut également définir des solutions «régulières» de l'équation (18), dénoté $Rg\{\varphi_{nm}(k\mathbf{r})\}$, qui ne divergent pour aucune valeur de $|\mathbf{r}|$ fini :

$$Rg\{\varphi_{nm}(k\mathbf{r})\} = j_n(kr)Y_{nm}(\theta, \phi) \tag{22}$$

où les $j_n(x)$ sont les fonction de Bessel sphériques. Les fonctions d'ondes régulières, $Rg\{\varphi_{nm}(k\mathbf{r})\}$, sont orthogonales dans le sens que :

$$\int d\mathbf{r}\, Rg\{\varphi_{n,m}(k\mathbf{r})\}\, Rg\{\varphi_{\nu\mu}(k'\mathbf{r})\} = \frac{\pi}{2k^2}\delta(k-k')\,\delta_{n,\nu}\delta_{m,\mu} \tag{23}$$

Revenons maintenant à l'équation vectorielle des ondes électromagnétiques de l'équation(18), On peut maintenant construire une solution en coordonnés sphériques de l'équation (18) et qui satisfait la condition d'onde sortante[7]. Elles s'écrivent $\mathbf{M}_{nm}(k_e\mathbf{r})$ où :

$$\mathbf{M}_{nm}(k\mathbf{r}) \equiv \frac{\nabla \times [\mathbf{r}\varphi_{nm}(k\mathbf{r})]}{\sqrt{n(n+1)}} \tag{24}$$

Un deuxième type de solution de l'équation (18) satisfaisant la condition d'onde sortante $\mathbf{N}_{nm}(k_e\mathbf{r})$ est obtenu à partir de l'équation :

$$\mathbf{N}_{nm}(k\mathbf{r}) \equiv \frac{\nabla \times [\mathbf{M}_{nm}(k\mathbf{r})]}{k} \tag{25}$$

Ces deux types d'ondes ont des singularités essentielles à l'origine. On remarque que la notation $\mathbf{M}$ et $\mathbf{N}$ est conventionnelle dans la littérature.

On peut également définir des ondes vectorielles régulières qui n'ont pas de singularités pour $|\mathbf{r}|$ fini.

$$Rg\left\{\mathbf{M}_{nm}\left(k\mathbf{r}\right)\right\} = \frac{\nabla \times \left[\mathbf{r}Rg\left\{\varphi_{nm}\left(k\mathbf{r}\right)\right\}\right]}{\sqrt{n\left(n+1\right)}}$$

$$Rg\left\{\mathbf{N}_{nm}\left(k\mathbf{r}\right)\right\} \equiv \frac{\nabla \times \left[Rg\left\{\mathbf{M}_{nm}\left(k\mathbf{r}\right)\right\}\right]}{k} \tag{26}$$

Le facteur $1/\sqrt{n\left(n+1\right)}$ dans les définitions de $\mathbf{M}_{nm}\left(k\mathbf{r}\right)$ et $\mathbf{N}_{nm}\left(k\mathbf{r}\right)$ est choisi afin que $Rg\left\{\mathbf{M}_{nm}\left(k\mathbf{r}\right)\right\}$ et $Rg\left\{\mathbf{N}_{nm}\left(k\mathbf{r}\right)\right\}$ aient des relations d'orthogonalité analogues à celles des ondes scalaires :

$$\int d\mathbf{r}\, Rg\left\{\mathbf{M}_{nm}^{*}(k\mathbf{r})\right\} \cdot Rg\left\{\mathbf{M}_{\nu\mu}(k'\mathbf{r})\right\} = \frac{\pi}{2k^2}\delta\left(k-k'\right)\delta_{n,\nu}\delta_{m,\mu}$$

$$\int d\mathbf{r}\, Rg\left\{\mathbf{N}_{nm}^{*}(k\mathbf{r})\right\} \cdot Rg\left\{\mathbf{N}_{\nu\mu}(k'\mathbf{r})\right\} = \frac{\pi}{2k^2}\delta\left(k-k'\right)\delta_{n,\nu}\delta_{m,\mu}$$

$$\int d\mathbf{r}\, Rg\left\{\mathbf{M}_{nm}^{*}(k\mathbf{r})\right\} \cdot Rg\left\{\mathbf{N}_{\nu\mu}(k'\mathbf{r})\right\} = 0 \tag{27}$$

où δ_{ij} est le symbole delta de Kronecker, et $\delta\left(k-k'\right)$ la fonction δ de Dirac.

Il est à remarquer que les fonctions ψ, $Rg\left\{\psi_{nm}\right\}$, $\mathbf{M}_{\nu\mu}$, $\mathbf{N}_{\nu\mu}$ $Rg\left\{\mathbf{M}_{nm}\right\}$, et $Rg\left\{\mathbf{N}_{nm}\right\}$ sont ici toutes définies en coordonnées sphériques. Donc, elles dépendent du choix de l'origine du système. Ce point est important dans le développement des théories de diffraction utilisant ces fonctions.

8.3   Harmoniques sphériques vectorielles

Les fonctions harmoniques sphériques scalaires, $Y_{nm}(\theta,\phi)$, sont exprimées en termes de fonctions de Legendre associées $P_n^m(\cos\theta)$ définies par [32] :

$$Y_{nm}(\theta,\phi) = \left[\frac{2n+1}{4\pi}\frac{(n-m)!}{(n+m)!}\right]^{\frac{1}{2}} P_n^m(\cos\theta)\exp(im\phi)$$

$$\equiv \overline{P}_n^m\left(\cos\theta\right)\exp(im\phi) \tag{28}$$

où dans la deuxième ligne nous avons introduit les fonctions de Legendre normalisées, $\overline{P}_n^m$:

$$Y_{nm}(\theta,\phi) = \overline{P}_n^m\left(\cos\theta\right)\exp(im\phi) \tag{29}$$

Ces fonctions harmoniques sphériques sont normalisées par rapport à une intégration sur l'angle solide :

$$\int_0^{4\pi} d\Omega\, Y_{\nu\mu}^{*}(\theta,\phi) \cdot Y_{nm}(\theta,\phi) \equiv \int_0^{\pi} \sin\theta d\theta \int_0^{2\pi} d\phi\, Y_{\nu\mu}^{*}(\theta,\phi) \cdot Y_{nm}(\theta,\phi) = \delta_{n,\nu}\delta_{m,\mu} \tag{30}$$

Les fonctions harmoniques sphériques vectorielles sont décrites dans plusieurs livres de référence [33, 34, 32, 35], mais leurs définitions et notations varient avec les auteurs. Elles forment une base complète et orthogonale pour décrire les variations angulaires de n'importe quel champ vectoriel. Nous les définissons par les équations suivante :

$$\mathbf{Y}_{nm}(\theta,\phi) \equiv \widehat{\mathbf{r}}\, Y_{nm}(\theta,\phi) \tag{31}$$

$$\mathbf{X}_{nm}(\theta,\phi) \equiv \mathbf{Z}_{nm}(\theta,\phi) \wedge \widehat{\mathbf{r}} \tag{32}$$

où

$$\mathbf{Z}_{nm}(\theta,\phi) \equiv \frac{r\boldsymbol{\nabla}Y_{nm}(\theta,\phi)}{\sqrt{n(n+1)}} \tag{33}$$

L'éq.(32) implique que :

$$\mathbf{Z}_{nm}(\theta,\phi) = \widehat{\mathbf{r}} \wedge \mathbf{X}_{nm}(\theta,\phi) \tag{34}$$

Toutes les harmoniques sphériques vectorielles sont mutuellement orthogonales dans le sens où si $\mathbf{W}_{nm}^{(i)}$ $(i=1,2,3)$ dénotent respectivement les harmoniques vectorielles $\mathbf{Y}_{nm}$, $\mathbf{X}_{nm}$, or $\mathbf{Z}_{nm}$, on a :

$$\left\langle \mathbf{W}_{nm}^{(i)} \mid \mathbf{W}_{\nu\mu}^{(j)} \right\rangle \equiv \int_0^{4\pi} \mathbf{W}_{nm}^{(i)*} \cdot \mathbf{W}_{\nu\mu}^{(j)}\, d\Omega = \delta_{ij}\delta_{n\nu}\delta_{m\mu} \tag{35}$$

où la définition du produit Hermitien a été étendue aux champs vectoriels.

On introduit maintenant les fonctions $\overline{u}_n^m$ et $\overline{s}_n^m$ définies par :

$$\overline{u}_n^m(\cos\theta) = \frac{1}{\sqrt{n(n+1)}} \frac{m}{\sin\theta} \overline{P}_n^m(\cos\theta) \tag{36}$$

$$\overline{s}_n^m(\cos\theta) = \frac{1}{\sqrt{n(n+1)}} \frac{d}{d\theta} \overline{P}_n^m(\cos\theta) \tag{37}$$

On peut facilement calculer ces fonctions par des relations de récurrence. Les harmoniques vectorielles $\mathbf{X}_{nm}$ et $\mathbf{Z}_{nm}$ ont des expressions simples en fonction de $\overline{u}_n^m$ et de $\overline{s}_n^m$:

$$\mathbf{X}_{nm}(\theta,\phi) = i\overline{u}_n^m(\cos\theta)\exp(im\phi)\widehat{\boldsymbol{\theta}} - \overline{s}_n^m(\cos\theta)\exp(im\phi)\widehat{\boldsymbol{\phi}} \tag{38}$$

$$\mathbf{Z}_{nm}(\theta,\phi) = \overline{s}_n^m(\cos\theta)\exp(im\phi)\widehat{\boldsymbol{\theta}} + i\overline{u}_n^m(\cos\theta)\exp(im\phi)\widehat{\boldsymbol{\phi}} \tag{39}$$

Les équations (38-39), prises ensemble avec l'éq.(31), montrent que pour des indices n, m donnés que les $(\mathbf{Y}_{nm}, \mathbf{X}_{nm}, \mathbf{Z}_{nm})$ sont mutuellement «*perpendiculaires*» dans le sens que $\mathbf{W}_{nm}^{(i)} \cdot \mathbf{W}_{nm}^{(j)} = 0$ pour $i \neq j$.

Il est très pratique dans la suite de ce mémoire d'écrire les ondes multipolaires en fonction des harmoniques sphériques vectorielles et des fonctions de *Hankel* sphériques :

$$\mathbf{M}_{nm}(k\mathbf{r}) \equiv h_n^+(kr)\,\mathbf{X}_{nm}(\theta,\phi)$$
$$\mathbf{N}_{nm}(k\mathbf{r}) \equiv \frac{1}{kr}\left[\sqrt{n(n+1)}h_n^+(kr)\,\mathbf{Y}_{nm}(\theta,\phi) + \xi_n'(kr)\,\mathbf{Z}_{nm}(\theta,\phi)\right] \tag{40}$$

De même, les ondes multipolaires *régulières* sont exprimées en fonction des harmoniques sphériques vectorielles et des fonctions de *Bessel* sphériques :

$$Rg\{\mathbf{M}_{nm}(k\mathbf{r})\} \equiv j_n(kr)\,\mathbf{X}_{nm}(\theta,\phi)$$
$$Rg\{\mathbf{N}_{nm}(k\mathbf{r})\} \equiv \frac{1}{kr}\left[\sqrt{n(n+1)}j_n(kr)\,\mathbf{Y}_{nm}(\theta,\phi) + \psi_n'(kr)\,\mathbf{Z}_{nm}(\theta,\phi)\right] \tag{41}$$

Dans les équations (40) et (41) nous avons introduit les fonctions de Ricatti-Bessel ψ_n et ξ_n définies par :

$$\psi_n(x) \equiv xj_n(x) \quad \text{et} \quad \xi_n(x) \equiv xh_n^+(x) \tag{42}$$

et le prime exprime la dérivée par rapport à l'argument, c'est-à-dire :

$$\psi_n'(x) = j_n(x) + xj_n'(x)$$
$$\xi_n'(x) = h_n^+(x) + x\left[h_n^+(x)\right]'. \tag{43}$$

8.4   Développements du champ dans des milieux homogènes

N'importe quel champ satisfaisant l'équation (18) et incident sur un système de diffuseurs peut être développé sur la base des ondes multipolaires régulières :

$$\mathbf{E}_{\text{inc}}(\mathbf{r}) = E \sum_{n=1}^{n_{\max}} \sum_{m=-n}^{m=n} \left[Rg\{\mathbf{M}_{nm}(k_{\text{e}}\mathbf{r})\}\,a_{nm}^{(h)} + Rg\{\mathbf{N}_{nm}(k_{\text{e}}\mathbf{r})\}\,a_{nm}^{(e)}\right]$$
$$= E \sum_{p=1}^{\infty} \left[Rg\{\mathbf{M}_p(k_{\text{e}}\mathbf{r})\}\,a_p^{(h)} + Rg\{\mathbf{N}_p(k_{\text{e}}\mathbf{r})\}\,a_p^{(e)}\right] \tag{44}$$

où $a_p^{(h)}$ et $a_p^{(e)}$ sont les coefficients respectifs des ondes sphériques $\mathbf{M}_p$ et $\mathbf{N}_p$. La constante E a la dimension d'un champ électrique. Si le champ incident est une onde plane, on la choisit telle que $\|\mathbf{E}_{\text{inc}}\|^2 = E^2$ (pour un champ incident plus général voir la réf.[8]).

La dernière ligne de l'éq.(44) introduit le procédé communément admis de remplacer les double indices n, et m, par un unique indice généralisé p où l'indice p correspond à une unique paire n, m pair par la relation :[35]

$$p = n(n+1) + m \tag{45}$$

Les relations inverses entre une valeur de p et le couple n, m correspondant sont données par :

$$n\left(p\right) = \mathrm{Int}\sqrt{p}$$
$$m\left(p\right) = p - n\left(p\right)\left[n\left(p\right) + 1\right] \tag{46}$$

Il faut se rappeler que les $\mathbf{M}$ et $\mathbf{N}$ s'expriment ici en coordonnées sphériques. L'origine du système est typiquement choisie à un endroit pratique, soit vis-à-vis du système, soit vis-à-vis du faisceau incident.

On définit une matrice en ligne :

$$Rg\left\{\boldsymbol{\Psi}^{t}\left(k\mathbf{r}\right)\right\} \equiv \left\{Rg\left\{\mathbf{M}_{1}\right\}, \ldots, Rg\left\{\mathbf{M}_{\infty}\right\}, Rg\left\{\mathbf{N}_{1}\right\}, \ldots, Rg\left\{\mathbf{N}_{\infty}\right\}\right\} \tag{47}$$

et a une matrice colonne :

$$a \equiv \begin{bmatrix} \vdots \\ a_{p}^{(h)} \\ \vdots \\ \hline \vdots \\ a_{p}^{(e)} \\ \vdots \end{bmatrix} \tag{48}$$

Cette notation nous permet d'écrire le champ incident sous la forme compacte et transparente :

$$\mathbf{E}_{\mathrm{inc}}\left(\mathbf{r}\right) = E Rg\left\{\boldsymbol{\Psi}^{t}\left(k\mathbf{r}\right)\right\} a \tag{49}$$

Puisqu'on va étudier des systèmes ayant plusieurs «composants» par une méthode de diffusion multiple, il est pratique de distinguer le champ *incident* envoyé sur tout le système et le champ d'*excitation* sur une particule du système (parfois appelé, champ «local»). Le champ d'excitation sur une particule est le champ qui serait présent si la particule n'était pas présente. N'importe quelle onde d'*excitation* sur une particule peut être développée sur la base des ondes multipolaires régulières :

$$\mathbf{E}_{\mathrm{exc}}^{(j)}\left(\mathbf{r}\right) = E \sum_{p=1}^{\infty}\left[Rg\left\{\mathbf{M}_{p}(k_{\mathrm{e}}\mathbf{r}_{j})\right\}\left[e^{(j)}\right]_{p}^{(h)} + Rg\left\{\mathbf{N}_{p}(k_{\mathrm{e}}\mathbf{r}_{j})\right\}\left[e^{(j)}\right]_{p}^{(e)}\right]$$
$$= E Rg\left\{\boldsymbol{\Psi}^{t}\left(k_{\mathrm{e}}\mathbf{r}_{j}\right)\right\} e^{(j)} \tag{50}$$

où $\mathbf{r}_{j} \equiv \mathbf{r} - \mathbf{x}_{j}$ est la position du point champ par rapport au «centre» de l'objet j. Ce centre est arbitraire dans une certaine mesure, mais on peut le prendre d'une façon générale comme le centre de la sphère circonscrite entourant l'objet. On doit remarquer pourtant que le développement du champ d'excitation n'est parfaitement fiable qu'à l'extérieur de la sphère circonscrite autour de l'objet, c'est-à-dire à des rayons où l'on est partout dans le milieu homogène à l'extérieur de la particule.

Le champ à l'intérieur d'une sphère inscrite à l'intérieur du diffuseur peut s'écrire :

$$\mathbf{E}_{\mathrm{int}}^{(j)}\left(\mathbf{r}\right) = E \sum_{p=1}^{\infty}\left[Rg\left\{\mathbf{M}_{p}(k_{\mathrm{s}}\mathbf{r})\right\}\left[s^{(j)}\right]_{p}^{(h)} + Rg\left\{\mathbf{N}_{p}(k_{\mathrm{s}}\mathbf{r})\right\}\left[s^{(j)}\right]_{p}^{(e)}\right]$$
$$= E Rg\left\{\boldsymbol{\Psi}^{t}\left(k_{\mathrm{s}}\mathbf{r}\right)\right\} s^{(j)} \tag{51}$$

où k_{s} est le nombre d'onde du milieu homogène à l'intérieur de la sphère inscrite.

8.5   Matrice-T

On prend un système de plusieurs objets qu'on va dénombrer par $j = 1, \ldots, N$. Le champ diffusé par le j^{e} objet du système, $\mathbf{E}_{\mathrm{s}}^{(j)}$, peut être développé en termes des fonctions d'ondes partielles $\mathbf{M}$ et $\mathbf{N}$ qui satisfont la condition d'onde sortante :

$$\mathbf{E}_{\mathrm{diff}}^{(j)}\left(\mathbf{r}_{j}\right) = E \sum_{p=1}^{\infty}\left[\mathbf{M}_{p}(k_{\mathrm{e}}\mathbf{r}_{j})\left[f^{(j)}\right]_{p}^{(h)} + \mathbf{N}_{p}(k_{\mathrm{e}}\mathbf{r}_{r})\left[f^{(j)}\right]_{p}^{(e)}\right]$$
$$= E \boldsymbol{\Psi}^{t}\left(k_{\mathrm{e}}\left(\mathbf{r} - \mathbf{x}_{j}\right)\right) f^{(j)} \tag{52}$$

où la matrice colonne $f^{(j)}$ contient les coefficients du champ diffusé.

Une solution pour un système composé d'un seul diffuseur est «simplement» de déterminer les coefficients du champ diffusé, $f^{(j)}$, à partir des coefficients du champ incident a en assurant que les équations de Maxwell sont satisfaites à l'intérieur du diffuseur et que les conditions aux limites sur les champs sont satisfaites aux interfaces entre le diffuseur et le milieu extérieur.

Si par contre, l'objet fait simplement partie d'un système contenant d'autres objets, et que l'on veuille traiter le système complet par la technique de diffusion multiple, on ne connaît pas à l'avance l'onde d'excitation sur la particule, puisque l'onde d'excitation sur l'objet est composée de l'onde incidente, et des champs diffusés par les autres objets du système. Pour de tels systèmes de diffusion multiple, on a besoin d'une solution complète de l'objet qu'on représente le plus souvent par la *matrice-T* .

Par définition, la matrice-T d'une particule j exprimée sur la base des ondes partielles s'exprime par :

$$f^{(j)} \equiv t^{(j)} e^{(j)} \tag{53}$$

où $e^{(j)}$ et $f^{(j)}$ dénotent respectivement les coefficients du champ d'excitation et de diffusion de la particule j. On choisit d'utiliser le symbole «t » plutôt que «T» pour la matrice-T d'un objet seul afin de réserver le symbole «T » pour des matrices-T décrivant la diffusion multiple (voir section 8.8).

8.6   Développements du champ dans des milieux hétérogènes

Si le milieu n'est pas homogène, le champ électrique n'est pas une solution de l'équation (18), et l'on ne peut pas généralement développer le champ en fonction des ondes multipolaires. Les harmoniques sphériques vectorielles restent néanmoins un bon moyen d'écrire le champ. Notamment, n'importe quel champ vectoriel peut être décrit comme des fonctions de la distance radiale r qui multiplient des harmoniques sphériques vectorielles.

Prenons un objet non-sphérique composé d'un milieu isotrope et homogène comme illustré sur la figure 4. N'importe quel champ vectoriel peut être décrit comme des fonctions radiales qui multiplient des harmoniques sphériques vectorielles :

$$\begin{aligned}
\mathbf{E}(\mathbf{r}) &= \sum_{n=0}^{\infty} \sum_{m=-n}^{m=n} \left[E_{nm}^{(Y)}(r) \mathbf{Y}_{nm}(\theta, \phi) + E_{nm}^{(X)}(r) \mathbf{X}_{nm}(\theta, \phi) + E_{nm}^{(Z)}(r) \mathbf{Z}_{nm}(\theta, \phi) \right] \\
&= \sum_{p=0}^{\infty} \left[E_p^{(Y)}(r) \mathbf{Y}_p(\theta, \phi) + E_p^{(X)}(r) \mathbf{X}_p(\theta, \phi) + E_p^{(Z)}(r) \mathbf{Z}_p(\theta, \phi) \right]
\end{aligned} \tag{54}$$

Un avantage de cette représentation des champs $\mathbf{E}$, $\mathbf{D}$ et $\mathbf{H}$ est la simplicité de l'action du rotationnel sur cette base. L'équation $\nabla \times \mathbf{E} = i\omega \mu_e \mu_0 \mathbf{H}$ devient dans la représentation de l'équation (54) :

$$a_p \frac{E_{Xp}}{r} = i\omega \mu_e \mu_0 H_{Yp} \tag{55a}$$

$$a_p \frac{E_{Yp}}{r} - \frac{E_{Zp}}{r} - \frac{dE_{Zp}}{dr} = i\omega \mu_e \mu_0 H_{Xp} \tag{55b}$$

$$\frac{E_{Xp}}{r} + \frac{dE_{Xp}}{dr} = i\omega \mu_e \mu_0 H_{Zp} \tag{55c}$$

De façon similaire, l'équation $\nabla \times \mathbf{H} = -i\omega \mathbf{D}$ s'écrit :

$$a_p \frac{H_{Xp}}{r} = -i\omega D_{Yp} \tag{56a}$$

$$a_p \frac{H_{Yp}}{r} - \frac{H_{Zp}}{r} - \frac{dH_{Zp}}{dr} = -i\omega D_{Xp} \tag{56b}$$

$$\frac{H_{Xp}}{r} + \frac{dH_{Xp}}{dr} = -i\omega D_{Zp} \tag{56c}$$

Pour un milieu homogène, on peut résoudre ces équations et l'on retombe sur les ondes partielles de la section 8.4. On verra dans section 9.5 comment on a pu exploiter ces équations ainsi que les récents progrès dans la théorie différentielle des réseaux afin de construire une nouvelle théorie différentielle pour des objets tridimensionnels.
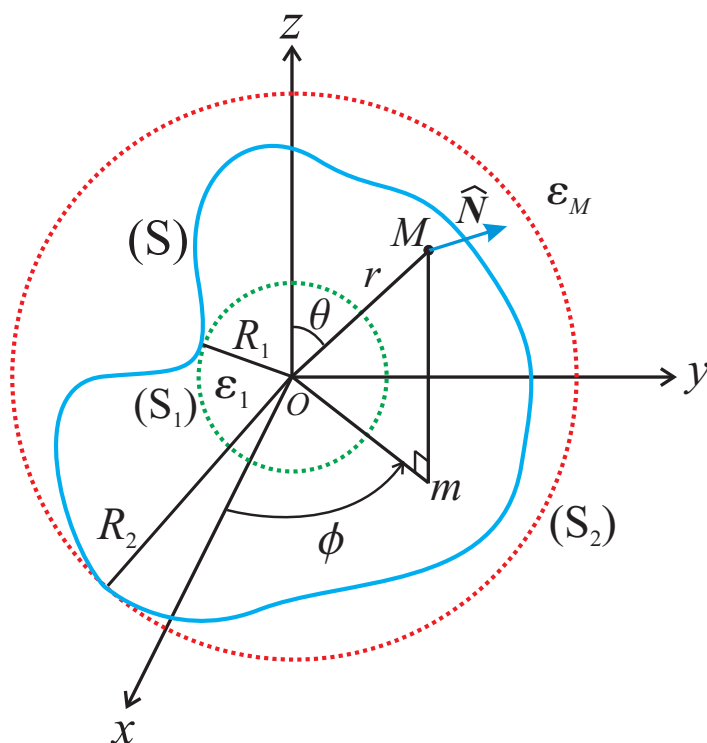
Fig. 4 – Objet de forme arbitraire. La sphère inscrite (verte) et la sphère circonscrite (rouge) sont en pointillées. La surface de l'objet est en trait plein (bleu).

8.7 Matrice-T d'une sphère isotrope (Théorie de Mie)

Comme exemple de l'utilité des harmoniques sphériques vectorielles, on montre dans cette section qu'elles facilitent l'obtention de la matrice-T d'une sphère isotrope. On tombe sur les résultats donnés par la célèbre théorie de Mie (1908). Toutefois la théorie de Mie était formulée directement en réponse à une onde plane incidente, alors que la matrice-T s'applique à n'importe quelle onde incidente. Cette section sert également à préparer le terrain pour notre théorie récente de la matrice-T d'une sphère anisotrope.[1, 3]

Le champ à l'extérieur d'une sphère se décompose en champ d'excitation, $\mathbf{E}_{\text{exc}}$, et en champ diffusé, $\mathbf{E}_{\text{diff}}$. Les champ $\mathbf{E}_{\text{exc}}$ et $\mathbf{E}_{\text{diff}}$ sont respectivement développés sur les ondes partielles selon les équations (50) et (52).

Une comparaison entre ces développements en ondes multipolaires et les développement généraux d'un champ en termes des harmoniques sphériques vectorielles de l'équation (54) (voir aussi les éqs.(40) et (41)), montre que les fonctions $E_{\text{e},p}^{(Y)}$, $E_{\text{e},p}^{(X)}$, et $E_{\text{e},p}^{(Z)}$ du champ à l'extérieur de la sphère sont :

$$E_{\text{e},p}^{(Y)}\left(r\right) = E\sqrt{n\left(n+1\right)}\left[\frac{j_n\left(k_{\text{e}}r\right)}{k_{\text{e}}r}e_p^{(e)} + \frac{h_n^+\left(k_{\text{e}}r\right)}{k_{\text{e}}r}f_p^{(e)}\right]$$

$$E_{\text{e},p}^{(X)}\left(r\right) = \frac{E}{k_{\text{e}}r}\left[\psi_n\left(k_{\text{e}}r\right)e_p^{(h)} + \xi_n\left(k_{\text{e}}r\right)f_p^{(h)}\right]$$

$$E_{\text{e},p}^{(Z)}\left(r\right) = \frac{E}{k_{\text{e}}r}\left[\psi_n'\left(k_{\text{e}}r\right)e_p^{(e)} + \xi_n'\left(k_{\text{e}}r\right)f_p^{(e)}\right] \tag{57}$$

De même, un regard sur le développement du champ à l'intérieur donne :

$$E_{s,p}^{(Y)}(r) = E\sqrt{n(n+1)}\frac{j_n(k_s r)}{k_s r}s_p^{(e)}$$

$$E_{s,p}^{(X)}(r) = \frac{E}{k_s r}\psi_n(k_s r)s_p^{(h)}$$

$$E_{s,p}^{(Z)}(r) = \frac{E}{k_s r}\psi_n'(k_s r)s_p^{(e)} \tag{58}$$

où $k_s^2 \equiv \varepsilon_s\mu_s k_0^2$ et ε_s et μ_s sont respectivement la permittivité relative et la perméabilité relative du diffuseur. Les champs $\mathbf{H}$ correspondants peuvent être déduits de l'équation Maxwell-Faraday :

$$\mathbf{H} = \frac{1}{i\omega\mu_r\mu_0}(\nabla \times \mathbf{E}) \tag{59}$$

où μ_r est la perméabilité magnétique relative du matériau (soit μ_e à l'extérieur de la sphère soit μ_s à l'intérieur). Insérant les développements en ondes partielles des équations (52)-(50) et utilisant les relations :

$$\nabla \times \mathbf{M}_p(k\mathbf{r}) = k\mathbf{N}_p(k\mathbf{r}) \qquad\qquad \nabla \times \mathbf{N}_p(k\mathbf{r}) = k\mathbf{M}_p(k\mathbf{r}) \tag{60}$$

on obtient pour le champ $\mathbf{H}$ diffusé, $\mathbf{H}_{\text{diff}}$, et le champ $\mathbf{H}$ d'excitation, $\mathbf{H}_{\text{exc}}$, les développements :

$$\mathbf{H}_{\text{diff}}(\mathbf{r}) = \frac{k_e}{i\omega\mu_e\mu_0}E\sum_{p=1}^{\infty}\left[\mathbf{N}_p(k_e\mathbf{r})f_p^{(h)} + \mathbf{M}_{nm}(k_e\mathbf{r})f_p^{(e)}\right]$$

$$\mathbf{H}_{\text{exc}}(\mathbf{r}) = \frac{k_e}{i\omega\mu_e\mu_0}E\sum_{p=1}^{\infty}\left[Rg\{\mathbf{N}_p(k_e\mathbf{r})\}e_p^{(h)} + Rg\{\mathbf{M}_{nm}(k_e\mathbf{r})\}e_p^{(e)}\right] \tag{61}$$

d'ou l'on peut écrire par analogie avec l'éq.(57) :

$$H_{e,p}^{(Y)}(r) = \frac{a_p}{i\omega\mu_e\mu_0}\frac{E}{r}\left[j_n(k_e r)e_p^{(h)} + h_n(k_e r)f_p^{(h)}\right]$$

$$H_{e,p}^{(X)}(r) = \frac{1}{i\omega\mu_e\mu_0}\frac{E}{r}\left[\psi_n(k_e r)e_p^{(e)} + \xi_n(k_e r)f_p^{(e)}\right]$$

$$H_{e,p}^{(Z)}(r) = \frac{1}{i\omega\mu_e\mu_0}\frac{E}{r}\left[\psi_n'(k_e r)e_p^{(h)} + \xi_n'(k_e r)f_p^{(h)}\right] \tag{62}$$

De la même manière, le champ $\mathbf{H}$ à l'intérieur du diffuseur s'écrit :

$$H_{s,p}^{(Y)}(r) = \frac{\sqrt{n(n+1)}}{i\omega\mu_s\mu_0}\frac{E}{r}j_n(k_s r)s_p^{(h)}$$

$$H_{s,p}^{(X)}(r) = \frac{1}{i\omega\mu_s\mu_0}\frac{E}{r}\psi_n(k_s r)s_p^{(e)}$$

$$H_{s,p}^{(Z)}(r) = \frac{1}{i\omega\mu_s\mu_0}\frac{E}{r}\psi_n'(k_s r)s_p^{(h)} \tag{63}$$

On remarque qu'à la surface d'une sphère que les composantes $H_p^{(Y)}(r)\mathbf{Y}_p$ et $E_p^{(Y)}(r)\mathbf{Y}_p$ des champs sont normales à la surface, alors que les composantes $E_p^{(X)}(r)\mathbf{X}_p$, $H_p^{(X)}(r)\mathbf{X}_p$, $E_p^{(Z)}(r)\mathbf{Z}_p$, $H_p^{(Z)}(r)\mathbf{Z}_p$, sont tangentielles à la surface. Combinant la continuité des composantes tangentielles des champs $\mathbf{E}$ et $\mathbf{H}$ et l'orthogonalité des harmoniques sphériques vectorielles, nous obtenons les quatre équations :

$$\frac{E}{k_e R}\left[\psi_n(k_e R)e_p^{(h)} + \xi_n(k_e R)f_p^{(h)}\right] = \frac{E}{k_s R}\psi_n(k_s R)i_p^{(h)}$$

$$\frac{E}{k_e R}\left[\psi_n'(k_e R)e_p^{(e)} + \xi_n'(k_e R)f_p^{(e)}\right] = \frac{E}{k_s R}\psi_n'(k_s R)i_p^{(e)}$$

$$\frac{1}{i\omega\mu_e\mu_0}\frac{E}{R}\left[\psi_n(k_e R)e_p^{(e)} + \xi_n(k_e R)f_p^{(e)}\right] = \frac{1}{i\omega\mu_s\mu_0}\frac{E}{R}\psi_n(k_s R)i_p^{(e)}$$

$$\frac{1}{i\omega\mu_e\mu_0}\frac{E}{R}\left[\psi_n'(k_e R)e_p^{(h)} + \xi_n'(k_e R)f_p^{(h)}\right] = \frac{1}{i\omega\mu_s\mu_0}\frac{E}{R}\psi_n'(k_s R)i_p^{(h)} \tag{64}$$

ce qu'on peut récrire comme :

$$\frac{k_{\mathrm{s}}}{k_{\mathrm{e}}}\left[\psi_n\left(k_{\mathrm{e}}R\right)e_p^{(h)}+\xi_n\left(k_{\mathrm{e}}R\right)f_p^{(h)}\right]=\psi_n\left(k_{\mathrm{s}}R\right)i_p^{(h)}$$

$$\frac{k_{\mathrm{s}}}{k_{\mathrm{e}}}\left[\psi_n'\left(k_{\mathrm{e}}R\right)e_p^{(e)}+\xi_n'\left(k_{\mathrm{e}}R\right)f_p^{(e)}\right]=\psi_n'\left(k_{\mathrm{s}}R\right)i_p^{(e)}$$

$$\frac{1}{\mu_{\mathrm{e}}}\left[\psi_n\left(k_{\mathrm{e}}R\right)e_p^{(e)}+\xi_n\left(k_{\mathrm{e}}R\right)f_p^{(e)}\right]=\frac{1}{\mu_{\mathrm{s}}}\psi_n\left(k_{\mathrm{s}}R\right)i_p^{(e)}$$

$$\frac{1}{\mu_{\mathrm{e}}}\left[\psi_n'\left(k_{\mathrm{e}}R\right)e_p^{(h)}+\xi_n'\left(k_{\mathrm{e}}R\right)f_p^{(h)}\right]=\frac{1}{\mu_{\mathrm{s}}}\psi_n'\left(k_{\mathrm{s}}R\right)i_p^{(h)} \tag{65}$$

Changeant l'ordre des équations et en arrangeant les expressions, on obtient :

$$\psi_n\left(k_{\mathrm{s}}R\right)s_p^{(h)}=\rho_{\mathrm{s}}\psi_n\left(k_{\mathrm{e}}R\right)e_p^{(h)}+\rho_{\mathrm{s}}\xi_n\left(k_{\mathrm{e}}R\right)f_p^{(h)} \tag{66a}$$

$$\mu_{\mathrm{e}}\psi_n'\left(k_{\mathrm{s}}R\right)s_p^{(h)}=\mu_{\mathrm{s}}\psi_n'\left(k_{\mathrm{e}}R\right)e_p^{(h)}+\mu_{\mathrm{s}}\xi_n'\left(k_{\mathrm{e}}R\right)f_p^{(h)} \tag{66b}$$

$$\psi_n'\left(k_{\mathrm{s}}R\right)s_p^{(e)}=\rho_{\mathrm{s}}\psi_n'\left(k_{\mathrm{e}}R\right)e_p^{(e)}+\rho_{\mathrm{s}}\xi_n'\left(k_{\mathrm{e}}R\right)f_p^{(e)} \tag{66c}$$

$$\mu_{\mathrm{e}}\psi_n\left(k_{\mathrm{s}}R\right)s_p^{(e)}=\mu_{\mathrm{s}}\psi_n\left(k_{\mathrm{e}}R\right)e_p^{(e)}+\mu_{\mathrm{s}}\xi_n\left(k_{\mathrm{e}}R\right)f_p^{(e)} \tag{66d}$$

où $\rho_{\mathrm{s}}\equiv\frac{k_{\mathrm{s}}}{k_{\mathrm{e}}}=\frac{n_{\mathrm{s}}}{n_{\mathrm{e}}}=\sqrt{\frac{\varepsilon_{\mathrm{s}}\mu_{\mathrm{s}}}{\varepsilon_{\mathrm{e}}\mu_{\mathrm{e}}}}$. On obtient la matrice en éliminant les coefficients $s_p^{(h)}$ et $s_p^{(e)}$ de ces équations. En éliminant $s_p^{(h)}$ des équations (66a) et (66b), on obtient :

$$f_p^{(h)}=\frac{\mu_{\mathrm{s}}\psi_n'\left(k_{\mathrm{e}}R\right)\psi_n\left(k_{\mathrm{s}}R\right)-\rho_{\mathrm{s}}\mu_{\mathrm{e}}\psi_n'\left(k_{\mathrm{s}}R\right)\psi_n\left(k_{\mathrm{e}}R\right)}{\rho_{\mathrm{s}}\mu_{\mathrm{e}}\psi_n'\left(k_{\mathrm{s}}R\right)\xi_n\left(k_{\mathrm{e}}R\right)-\mu_{\mathrm{s}}\xi_n'\left(k_{\mathrm{e}}R\right)\psi_n\left(k_{\mathrm{s}}R\right)}e_p^{(h)} \tag{67}$$

De même, en éliminant $s_p^{(e)}$ des équations (66c) et (66d) on obtient :

$$f_p^{(e)}=\frac{\mu_{\mathrm{s}}\psi_n'\left(k_{\mathrm{s}}R\right)\psi_n\left(k_{\mathrm{e}}R\right)-\rho_{\mathrm{s}}\mu_{\mathrm{e}}\psi_n\left(k_{\mathrm{s}}R\right)\psi_n'\left(k_{\mathrm{e}}R\right)}{\rho_{\mathrm{s}}\mu_{\mathrm{e}}\psi_n\left(k_{\mathrm{s}}R\right)\xi_n'\left(k_{\mathrm{e}}R\right)-\mu_{\mathrm{s}}\xi_n\left(k_{\mathrm{e}}R\right)\psi_n'\left(k_{\mathrm{s}}R\right)}e_p^{(e)} \tag{68}$$

Donc, on voit qu'on peut écrire la solution sous la forme :

$$\left[\begin{array}{c}f_p^{(h)}\\f_p^{(e)}\end{array}\right]=t\left[\begin{array}{c}e_p^{(h)}\\e_p^{(e)}\end{array}\right] \tag{69}$$

où la matrice t est de la forme

$$[t]=\left[\begin{array}{cc}\left[t^{(h,h)}\right]&\left[t^{(e,h)}\right]\\\left[t^{(h,e)}\right]&\left[t^{(e,e)}\right]\end{array}\right] \tag{70}$$

avec

$$\left[t^{(h,h)}\right]_{pp'}=\delta_{pp'}t_n^{(h)}\qquad\left[t^{(e,e)}\right]_{pp'}=\delta_{pp'}t_n^{(e)}\qquad\left[t_n^{(h,e)}\right]_{pp'}=\left[t_n^{(e,h)}\right]_{pp'}=0 \tag{71}$$

et les éléments diagonaux s'écrivent :

$$t_n^{(h)}=\frac{\frac{\mu_{\mathrm{s}}}{\mu_{\mathrm{e}}}\psi_n'\left(k_{\mathrm{e}}R\right)\psi_n\left(k_{\mathrm{s}}R\right)-\rho_{\mathrm{s}}\psi_n'\left(k_{\mathrm{s}}R\right)\psi_n\left(k_{\mathrm{e}}R\right)}{\rho_{\mathrm{s}}\psi_n'\left(k_{\mathrm{s}}R\right)\xi_n\left(k_{\mathrm{e}}R\right)-\frac{\mu_{\mathrm{s}}}{\mu_{\mathrm{e}}}\xi_n'\left(k_{\mathrm{e}}R\right)\psi_n\left(k_{\mathrm{s}}R\right)}$$

$$t_n^{(e)}=\frac{\frac{\mu_{\mathrm{s}}}{\mu_{\mathrm{e}}}\psi_n'\left(k_{\mathrm{s}}R\right)\psi_n\left(k_{\mathrm{e}}R\right)-\rho_{\mathrm{s}}\psi_n\left(k_{\mathrm{s}}R\right)\psi_n'\left(k_{\mathrm{e}}R\right)}{\rho_{\mathrm{s}}\psi_n\left(k_{\mathrm{s}}R\right)\xi_n'\left(k_{\mathrm{e}}R\right)-\frac{\mu_{\mathrm{s}}}{\mu_{\mathrm{e}}}\xi_n\left(k_{\mathrm{e}}R\right)\psi_n'\left(k_{\mathrm{s}}R\right)} \tag{72}$$

On peut également vouloir connaître les coefficients du champ à l'intérieur de la sphère. En éliminant $e_p^{(h)}$ des équations (66a) et (66b), on obtient :

$$\left[\mu_{\mathrm{s}}\psi_n'\left(k_{\mathrm{e}}R\right)\psi_n\left(k_{\mathrm{s}}R\right)-\rho_{\mathrm{s}}\psi_n\left(k_{\mathrm{e}}R\right)\mu_{\mathrm{e}}\psi_n'\left(k_{\mathrm{s}}R\right)\right]s_p^{(h)}=\rho_{\mathrm{s}}\mu_{\mathrm{s}}\left[\psi_n'\left(k_{\mathrm{e}}R\right)\xi_n\left(k_{\mathrm{e}}R\right)-\psi_n\left(k_{\mathrm{e}}R\right)\xi_n'\left(k_{\mathrm{e}}R\right)\right]f_p^{(h)}$$

Utilisant la relation du Wronskien :

$$\psi_n\left(x\right)\xi_n'\left(x\right)-\psi_n'\left(x\right)\xi_n\left(x\right)=i \tag{73}$$

on obtient :

$$s_p^{(h)} = \frac{i\mu_s\rho_s}{\mu_e\rho_s\psi_n'\left(k_sR\right)\psi_n\left(k_eR\right) - \mu_s\psi_n\left(k_sR\right)\psi_n'\left(k_eR\right)} f_p^{(h)} \tag{74}$$

De même, en éliminant $e_p^{(e)}$ des équations (66c) et (66d) et utilisant la relation du Wronskien, on obtient :

$$s_p^{(e)} = \frac{i\mu_s\rho_s}{\mu_s\psi_n\left(k_eR\right)\psi_n'\left(k_sR\right) - \mu_e\rho_s\psi_n\left(k_sR\right)\psi_n'\left(k_eR\right)} f_p^{(e)} \tag{75}$$

Les relations entre les coefficients du champ à l'intérieur et ceux du champ diffusé peuvent être écrites sous une forme matricielle :

$$\begin{bmatrix} s_p^{(h)} \\ s_p^{(e)} \end{bmatrix} = \Lambda \begin{bmatrix} f_p^{(h)} \\ f_p^{(e)} \end{bmatrix} \tag{76}$$

où la matrice Λ a la forme :

$$\Lambda = \begin{bmatrix} \left[\Lambda^{(h,h)}\right] & \left[\Lambda^{(e,h)}\right] \\ \left[\Lambda^{(h,e)}\right] & \left[\Lambda^{(e,e)}\right] \end{bmatrix} \tag{77}$$

avec

$$\left[\Lambda^{(h,h)}\right]_{pp'} = \delta_{pp'}^{(h)}\Lambda_n^{(h)} \qquad \left[\Lambda_n^{(e,e)}\right]_{pp'} = \delta_{pp'}\Lambda_n^{(e)} \qquad \left[\Lambda_n^{(h,e)}\right]_{pp'} = \left[\Lambda_n^{(e,h)}\right]_{pp'} = 0 \tag{78}$$

et où les $\Lambda_n^{(h)}$, $\Lambda_n^{(e)}$ sont exprimés par :

$$\Lambda_n^{(h)} = \frac{i\frac{\mu_s}{\mu_e}\rho_s}{\rho_s\psi_n'\left(k_sR\right)\psi_n\left(k_eR\right) - \frac{\mu_s}{\mu_e}\psi_n\left(k_sR\right)\psi_n'\left(k_eR\right)}$$

$$\Lambda_n^{(e)} = \frac{i\frac{\mu_s}{\mu_e}\rho_s}{\frac{\mu_s}{\mu_e}\psi_n\left(k_eR\right)\psi_n'\left(k_sR\right) - \rho_s\psi_n\left(k_sR\right)\psi_n'\left(k_eR\right)} \tag{79}$$

Nous avons donc constaté que la matrice-T d'une sphère isotrope s'obtient directement grâce à l'emploi des ondes multipolaires et leurs propriétés. Nous continuerons à constater que l'emploi des ondes multipolaires et des harmoniques sphériques va simplifier les dérivations de formules susceptibles d'avoir des applications numériques intéressantes.

8.8   Diffusion multiple par la technique de la fonction de Green

Il est possible d'aborder le problème de la diffusion multiple avec la technique de la fonction de Green, $\mathbf{G}$, du système. Pour cette construction, il nous faut la fonction de Green d'un milieu homogène, $\mathbf{G}_0$, les matrices-T individuelles, $\mathbf{t}^{(j)}$, et le concept de champ d'excitation. Nous verrons que toute cette discussion sera facilitée en adoptant un formalisme opérateur.

8.8.1   La forme opérateur de la fonction de Green

En l'absence d'un contraste de perméabilité magnétique (c'est à dire $\mu_r\left(\mathbf{r}\right) = 1$ partout), la fonction de Green correspondant à l'équation (17) est :

$$\nabla \times \left[\nabla \times \mathbf{G}\left(\mathbf{r}, \mathbf{r}'\right)\right] - \left(\frac{\omega}{c}\right)^2 \varepsilon_r\left(\mathbf{r}\right)\mathbf{G}\left(\mathbf{r}, \mathbf{r}'\right) = \mathbb{I}\delta\left(\mathbf{r} - \mathbf{r}'\right) \tag{80}$$

où $\mathbb{I}$ est l'identité dans un espace vectoriel et $\mathbf{G}\left(\mathbf{r}, \mathbf{r}'\right)$ est la projection d'un opérateur $\mathbf{G}$ dans l'espace direct.

Explicitement, l'opérateur $\mathbf{G}$ peut s'écrire :

$$\mathbf{G} = \iint d\mathbf{r}\, d\mathbf{r}' \left|\mathbf{r}\right\rangle \left\langle\mathbf{r}\right| \mathbf{G} \left|\mathbf{r}'\right\rangle \left\langle\mathbf{r}'\right| \tag{81}$$

où

$$\left\langle\mathbf{r}\right| \mathbf{G}_0 \left|\mathbf{r}'\right\rangle \equiv \mathbf{G}_0\left(\mathbf{r}, \mathbf{r}'\right) \tag{82}$$

Les états de position $\left|\mathbf{r}\right\rangle$ ont une normalisation en fonction delta tridimensionnel :

$$\left\langle\mathbf{r}'|\mathbf{r}\right\rangle = \delta\left(\mathbf{r} - \mathbf{r}'\right) \tag{83}$$

et forment une base complète :

$$\int d\mathbf{r} \, |\mathbf{r}\rangle \langle\mathbf{r}| = 1 \tag{84}$$

La fonction de Green, $\mathbf{G}$, d'un système quelconque constitue une solution complète du problème électromagnétique puisque n'importe quel champ électrique, $\mathbf{E}(\mathbf{r})$, produit par un courant source $\mathbf{J}_{\mathrm{src}}$ est obtenu grâce à une intégrale de convolution ; c'est-à-dire que le champ $\mathbf{E}(\mathbf{r})$ s'écrit :

$$\mathbf{E}(\mathbf{r}) = \langle\mathbf{r}|\mathbf{E}\rangle = \langle\mathbf{r}|\, \mathbf{G} \,|\mathbf{J}_{\mathrm{src}}\rangle = \int d\mathbf{r}' \, \langle\mathbf{r}|\, \mathbf{G} \,|\mathbf{r}'\rangle \langle\mathbf{r}'|\mathbf{J}_{\mathrm{src}}\rangle \tag{85}$$

où $\langle\mathbf{r}'|\mathbf{J}_{\mathrm{src}}\rangle \equiv i\omega\mu_{\mathrm{e}}\mu_0\mathbf{J}_{\mathrm{src}}(\mathbf{r}')$ est proportionnel à la distribution de courants sources du problème. Utilisant la définition donnée par l'équation (80), on peut vérifier que $\mathbf{E}$ est une solution de l'équation (17) avec $\mu_r(\mathbf{r}) = 1$.

Une *fonction* de Green n'existe pas à proprement parler, mais on peut la définir comme une distribution. La définition de la «fonction de Green» comme une distribution convient puisque notre but est de l'utiliser dans les intégrales telles que celle de l'équation (85). L'évaluation des distributions est souvent facilitée en travaillant dans l'espace réciproque. Le passage à l'espace réciproque dans le formalisme opérateur est obtenu en définissant des états $|\mathbf{k}\rangle$ tels que :

$$\langle\mathbf{r}|\mathbf{k}\rangle \equiv \frac{e^{i\mathbf{k}\cdot\mathbf{r}}}{(2\pi)^{3/2}} \qquad\qquad \langle\mathbf{k}|\mathbf{r}\rangle \equiv \frac{e^{-i\mathbf{k}\cdot\mathbf{r}}}{(2\pi)^{3/2}} \tag{86}$$

Les états $|\mathbf{k}\rangle$, comme les états de position $|\mathbf{r}\rangle$, ont une normalisation en fonction delta :

$$\langle\mathbf{k}'|\mathbf{k}\rangle = \int d\mathbf{r} \, \langle\mathbf{k}'|\mathbf{r}\rangle \langle\mathbf{r}|\mathbf{k}\rangle = \int d\mathbf{r} \, \frac{e^{i(\mathbf{k}-\mathbf{k}')\cdot\mathbf{r}}}{(2\pi)^3} = \delta(\mathbf{k}-\mathbf{k}') \tag{87}$$

et forment une base complète :

$$\int d\mathbf{k} \, |\mathbf{k}\rangle \langle\mathbf{k}| = 1 \tag{88}$$

Une représentation alternative de l'opérateur $\mathbf{G}$ est donc :

$$\mathbf{G} = \iint d\mathbf{k}\, d\mathbf{k}' \, |\mathbf{k}\rangle \langle\mathbf{k}|\, \mathbf{G} \,|\mathbf{k}'\rangle \langle\mathbf{k}'| \tag{89}$$

où

$$\begin{aligned}
\langle\mathbf{k}|\, \mathbf{G} \,|\mathbf{k}'\rangle &= \iint d\mathbf{r}\, d\mathbf{r}' \, \langle\mathbf{k}|\mathbf{r}\rangle \langle\mathbf{r}|\, \mathbf{G} \,|\mathbf{r}'\rangle \langle\mathbf{r}'|\mathbf{k}'\rangle \\
&= \frac{1}{(2\pi)^3} \iint d\mathbf{r}\, d\mathbf{r}' e^{-i\mathbf{k}\cdot\mathbf{r}} \mathbf{G}(\mathbf{r},\mathbf{r}') \, e^{i\mathbf{k}'\cdot\mathbf{r}'}
\end{aligned} \tag{90}$$

Nous constaterons que le formalisme opérateur nous apportera de la flexibilité dans les manipulations qui mènent à des solutions des fonctions de Green.

8.8.2   Fonction de Green dans un milieu homogène

L'équation de Green pour un milieu homogène s'écrit dans l'espace direct :

$$\nabla\times [\nabla\times \mathbf{G}_0(\mathbf{r},\mathbf{r}')] - k_{\mathrm{e}}^2 \, \mathbf{G}_0(\mathbf{r},\mathbf{r}') = \mathbb{I}\delta(\mathbf{r}-\mathbf{r}') \tag{91}$$

où $k_{\mathrm{e}}^2 = \varepsilon_{\mathrm{e}}\mu_{\mathrm{e}}k_0^2$ ne dépend pas de la position. Il n'est pas pratique de résoudre cette équation directement dans l'espace direct. On choisit donc de passer à l'espace réciproque où l'équation de Green s'écrit :

$$-\mathbf{k}\wedge \mathbf{k}\wedge \mathbf{G}_0(\mathbf{k},\mathbf{k}') - k_{\mathrm{e}}^2 \, \mathbf{G}_0(\mathbf{k},\mathbf{k}') = \delta(\mathbf{k}-\mathbf{k}') \tag{92}$$

En utilisant l'identité :

$$\mathbf{k}\wedge \mathbf{k}\wedge \mathbf{A} = -k^2 \left(\mathbb{I} - \widehat{\mathbf{k}}\widehat{\mathbf{k}}\right) \mathbf{A} \tag{93}$$

on obtient :

$$k^2 \left(\mathbb{I} - \widehat{\mathbf{k}}\widehat{\mathbf{k}} \right) \mathbf{G}_0 \left(\mathbf{k}, \mathbf{k}' \right) - k_{\mathrm{e}}^2 \, \mathbf{G}_0 \left(\mathbf{k}, \mathbf{k}' \right) = \delta \left(\mathbf{k} - \mathbf{k}' \right) \tag{94}$$

qui a pour solution :

$$\mathbf{G}_0 \left(\mathbf{k}, \mathbf{k}' \right) = \langle \mathbf{k} | \, \mathbf{G}_0 \, | \mathbf{k}' \rangle = \delta \left(\mathbf{k} - \mathbf{k}' \right) \left[\frac{\mathbb{I} - \widehat{\mathbf{k}}\widehat{\mathbf{k}}}{k^2 - k_{\mathrm{e}}^2} - \frac{\widehat{\mathbf{k}}\widehat{\mathbf{k}}}{k_{\mathrm{e}}^2} \right] \tag{95}$$

On peut maintenant obtenir la fonction de Green dans l'espace direct en faisant une transformée de Fourier inverse :

$$\langle \mathbf{r}_1 | \, \mathbf{G}_0 \, | \mathbf{r}_2 \rangle = \mathbf{G}_0 \left(\mathbf{r}_1, \mathbf{r}_2 \right) = \mathbf{G}_0 \left(\mathbf{r} \right)$$

$$= \frac{e^{ik_{\mathrm{e}}r}}{4\pi k_{\mathrm{e}}^2 r^3} \mathrm{V.P.} \left\{ \left(1 - ik_{\mathrm{e}}r - k_{\mathrm{e}}^2 r^2 \right) \left(\mathbb{I} - \widehat{\mathbf{r}}\widehat{\mathbf{r}} \right) - 2 \left(1 - ik_{\mathrm{e}}R \right) \widehat{\mathbf{r}}\widehat{\mathbf{r}} \right\} + \frac{1}{3k_{\mathrm{e}}^2} \delta \left(\mathbf{r} \right) \tag{96}$$

où $\mathbf{r} \equiv \mathbf{r}_1 - \mathbf{r}_2$. La valeur principale indique qu'il faut exclure un volume infinitésimal sphérique ou cubique autour du point $\mathbf{r} = \mathbf{0}$. On peut utiliser d'autres formes pour le volume d'exclusion, mais il faut modifier le terme en fonction delta afin que son application dans les équations intégrales telles que l'équation (85) reste invariante. (voir Ref.[36] chap. 8)

On appelle désormais *champ incident*, le champ électrique $\mathbf{E}_{\mathrm{inc}} \left(\mathbf{r} \right)$ produit par un courant source $\mathbf{J}_{\mathrm{src}}$ dans ce milieu. On peut l'obtenir par la formule :

$$\mathbf{E}_{\mathrm{inc}} \left(\mathbf{r} \right) = \langle \mathbf{r} | \mathbf{E}_{\mathrm{inc}} \rangle = \langle \mathbf{r} | \, \mathbf{G}_0 \, | \mathbf{J}_{\mathrm{src}} \rangle = \int d\mathbf{r}' \, \langle \mathbf{r} | \, \mathbf{G}_0 \, | \mathbf{r}' \rangle \, \langle \mathbf{r}' | \mathbf{J}_{\mathrm{src}} \rangle \tag{97}$$

où $\langle \mathbf{r}' | \mathbf{J}_{\mathrm{src}} \rangle \equiv i\omega \mu_{\mathrm{e}} \mu_0 \mathbf{J}_{\mathrm{src}} \left(\mathbf{r}' \right)$.

8.8.3 Le potentiel d'un diffuseur discret

On introduit des inhomogénéités dans le système en appelant un «diffuseur», chaque région ayant des permittivités et perméabilités constantes et différentes de celles du milieu externe. Chaque diffuseur j est caractérisé par ses paramètres constitutifs relatifs ε_j et μ_j et par une fonction de Heaviside, $\varkappa$:

$$\varkappa^{(j)}(\mathbf{r}) = 1 \qquad \text{si } \mathbf{r} \text{ est à l'intérieur du diffuseur } j$$
$$\varkappa^{(j)}(\mathbf{r}) = 0 \qquad \text{si } \mathbf{r} \text{ est à l'extérieur du diffuseur } j \tag{98}$$

La position de chaque diffuseur est dénotée par $\mathbf{x}_j$ qui est le centre de la sphère circonscrite au diffuseur (voir la figure 5).

Si il n'y a pas de contraste de la perméabilité magnétique (c'est-à-dire on prend la perméabilité relative $\mu\left(\mathbf{r}\right) = 1$ partout), on peut écrire l'équation (17) gouvernant l'évolution du champ $\mathbf{E}$ dans un milieu inhomogène en termes des potentiels, $\mathbf{u}^{(j)}$:

$$\nabla \times \left(\nabla \times \mathbf{E} \right) - \left(\frac{\omega}{c} \right)^2 \varepsilon_{\mathrm{e}} \mathbf{E} - \sum_{j=1}^{N} \mathbf{u}^{(j)} \mathbf{E} = i\omega \mu_0 \mathbf{J}_{\mathrm{src}} \tag{99}$$

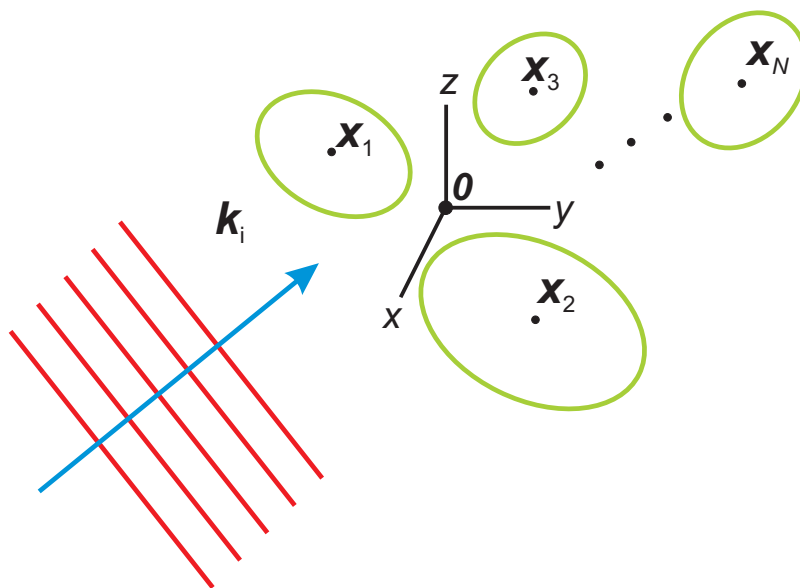où *l'opérateur* $\mathbf{u}^{(j)}$ dans la représentation des coordonnées s'écrit :

$$\langle \mathbf{r} | \, \mathbf{u}^{(j)} \, | \mathbf{r}' \rangle = \left(\frac{\omega}{c} \right)^2 \left(\varepsilon_j - \varepsilon_{\mathrm{e}} \right) \varkappa^{(j)}(\mathbf{r}) \delta \left(\mathbf{r} - \mathbf{r}' \right) \mathbb{I} \tag{100}$$

La fonction de Green associée à l'équation (99) est donc définie par :

$$\nabla \times \left(\nabla \times \mathbf{G} \right) - \left(\frac{\omega}{c} \right)^2 \varepsilon_{\mathrm{e}} \mathbf{G} - \sum_{j=1}^{N} \mathbf{u}^{(j)} \mathbf{G} = \mathbb{I} \tag{101}$$

Finalement, il est pratique pour la suite de reformuler l'équation (101) en termes de la fonction de Green «non-perturbée», $\mathbf{G}_0$, du milieu homogène externe :

$$\mathbf{G} = \mathbf{G}_0 + \mathbf{G}_0 \sum_{j=1}^{N} \mathbf{u}^{(j)} \mathbf{G} \tag{102}$$

Fig. 5 – Système de N objets soumis à un champ incident.

L'équation (102) n'est pas encore sous une forme très pratique à résoudre. Bien que le potentiel soit de forme assez pratique dans l'espace direct (voir l'éq.(100)), $\mathbf{G}_0$ est assez compliqué dans l'espace direct (voir l'éq.(96)). On pourrait être tenté de résoudre (102) dans l'espace de Fourier puisque $\mathbf{G}_0$ y est relativement simple (voir l'éq.(95)). Il est par contre difficile de calculer la transformée de Fourier de $\mathbf{u}^{(j)}$ pour un objet de forme arbitraire. Pour une sphère isotrope, on peut effectuer la transformée de Fourier et l'on obtient :

$$\mathbf{u}^{(j)}(\mathbf{k}|\mathbf{k}') = \langle \mathbf{k} | \, \mathbf{u}^{(j)} \, | \mathbf{k}' \rangle = \frac{R_j^2}{2\pi^2} \left(\frac{\omega}{c} \right)^2 (\varepsilon_\mathrm{s} - \varepsilon_\mathrm{e}) \frac{j_1(R_j \, |\mathbf{k}' - \mathbf{k}|)}{|\mathbf{k}' - \mathbf{k}|} \mathbb{I} \tag{103}$$

où R_j est le rayon de la j^e sphère. Même dans ce cas simple, la valeur absolue dans le potentiel rendrait la résolution de l'éq.(102) assez difficile.

8.8.4 La forme opérateur de la matrice-T

L'équation (102) n'est un bon départ pour résoudre les équations de diffusion multiple que dans le cas où le contraste d'indice serait suffisamment petit. Dès que le contraste d'indice devient notable, il est avantageux de reformuler les équations de diffusion multiple en terme de matrices T.

On définit la matrice T d'un diffuseur isolé j, dénotée $\mathbf{t}^{(j)}$, comme la solution d'une équation du type Lippmann-Schwinger :

$$\mathbf{t}^{(j)} = \mathbf{u}^{(j)} + \mathbf{u}^{(j)} \mathbf{G}_0 \mathbf{t}^{(j)} \tag{104}$$

Cette équation a l'air simple, mais il faut se rappeler qu'elle représente une équation intégrale. Dans l'espace de Fourier par exemple, l'équation (104) s'écrit :

$$\mathbf{t}^{(j)}(\mathbf{k}|\mathbf{k}') = \mathbf{u}^{(j)}(\mathbf{k}|\mathbf{k}') + \int d^3\mathbf{k}_1 \, \mathbf{u}^{(j)}(\mathbf{k}|\mathbf{k}_1) \mathbf{G}_0 \left(\mathbf{k}_1 | \mathbf{k}_2 \right) \mathbf{t}^{(j)}(\mathbf{k}_2|\mathbf{k}') \tag{105}$$

Si l'on insère les résultats des équations (95) et (103) pour $\mathbf{G}_0 \left(\mathbf{k}_1 | \mathbf{k}_2 \right)$ et $\mathbf{u}^{(j)}(\mathbf{k}|\mathbf{k}')$ dans l'équation (105), on s'aperçoit immédiatement de la difficulté à résoudre une telle équation, même pour une sphère isotrope (l'essentiel de la difficulté venant des facteurs $|\mathbf{k}' - \mathbf{k}|$ dans le potentiel). Dans le langage de la théorie quantique des champs ou dans celui du problème à N-corps, on appellera cette matrice-T opérateur une

matrice-T *hors couche de masse* en empruntant une expression de la physique des particules, «off mass shell». Grâce à l'utilisation des ondes partielles introduites en section 8.2, on va pouvoir éviter de résoudre l'équation (105) dans beaucoup de circonstances, notamment quand il y a un nombre fini de diffuseurs par exemple.

Pour l'instant, il nous suffit de remarquer qu'une solution formelle de l'équation (104) s'écrit :

$$\mathbf{t}^{(j)} = \left(\mathbb{I} - \mathbf{u}^{(j)} \mathbf{G}_0\right)^{-1} \mathbf{u}^{(j)}$$
$$= \mathbf{u}^{(j)} \left(\mathbb{I} - \mathbf{G}_0 \mathbf{u}^{(j)}\right)^{-1} \tag{106}$$

S'il n'y a qu'un seul objet j dans le système, la matrice $\mathbf{t}^{(j)}$ constitue une solution complète de la fonction de Green. Explicitement, s'il n'y a qu'un seul objet la fonction de Green s'écrit :

$$\mathbf{G} = \mathbf{G}_0 + \mathbf{G}_0 \mathbf{u}^{(j)} \mathbf{G} \tag{107}$$

On peut réécrire cette relation comme :

$$\mathbf{u}^{(j)} \mathbf{G} = \mathbf{u}^{(j)} \left(\mathbb{I} - \mathbf{G}_0 \mathbf{u}^{(j)}\right)^{-1} \mathbf{G}_0 \tag{108}$$

Une comparaison avec les éqs.(106) et (107) montre alors que la fonction de Green pour un objet isolé s'écrit :

$$\mathbf{G} = \mathbf{G}_0 + \mathbf{G}_0 \, \mathbf{t}^{(j)} \, \mathbf{G}_0 \tag{109}$$

En présence d'un courant source $\mathbf{J}_\mathrm{s}$, le champ incident s'écrit $\mathbf{E}_\mathrm{i} = \mathbf{G}_0 \left| \mathbf{J}_\mathrm{s} \right\rangle$ et le champ total s'écrit $\mathbf{E}_\mathrm{t} = \mathbf{G} \left| \mathbf{J}_\mathrm{s} \right\rangle$. On peut en déduire que le champ diffusé par la particule j est donné par :

$$\mathbf{E}_\mathrm{s} = \mathbf{G}_0 \mathbf{t}^{(j)} \mathbf{G}_0 \left| \mathbf{J} \right\rangle \tag{110}$$

On peut évaluer les opérateurs $\mathbf{G}_0$ et $\mathbf{t}^{(j)}$ sur la base des ondes multipolaires, et après un certain nombre de manipulations, on trouve qu'aux positions $\mathbf{r}$ à l'extérieur d'une sphère circonscrite autour de l'objet, le champ électrique diffusé s'exprime par :

$$\mathbf{E}_\mathrm{s}\left(\mathbf{r}\right) = \boldsymbol{\Psi}^t \left(k_\mathrm{e}\mathbf{r}_j\right) \, t^{(j)} J^{(j,0)} a \tag{111}$$

où $t^{(j)}$ est la matrice t de l'objet j, «sur couche de masse» dans la représentation des ondes multipolaires (voir l'équation (53)). Ici nous avons utilisé la notation condensée de la section 8.4 afin d'exprimer les développements en ondes multipolaires. La matrice $J^{(j,0)} \equiv J(k_\mathrm{e}\mathbf{x}_j)$ est une matrice de translation régulière dont les éléments ont des expressions analytiques (voir l'appendice A). L'utilisation du symbole J dans la matrice de translation sert à rappeler que $J^{(j,0)}$ s'écrit en termes de fonctions de Bessel sphériques, $j_n\left(k_\mathrm{e}x_j\right)$.[37] La matrice colonne «a» est composée des coefficients de l'onde incidente et ces coefficients peuvent en principe être calculés directement à partir des courants sources par les intégrales :

$$[a]_{nm}^{(e)} = -k_\mathrm{e}\omega\mu_0\mu_\mathrm{e} \int d\mathbf{x}' h_n^+\left(k_\mathrm{e}x'\right) \mathbf{X}_{nm}^*\left(\theta', \phi'\right) \cdot \mathbf{J}_\mathrm{s}\left(\mathbf{x}'\right)$$
$$[a]_{nm}^{(h)} = -k_\mathrm{e}\omega\mu_0\mu_\mathrm{e} \int d\mathbf{x}' h_n^+\left(k_\mathrm{e}x'\right) \mathbf{Z}_{nm}^*\left(\theta', \phi'\right) \cdot \mathbf{J}_\mathrm{s}\left(\mathbf{x}'\right) \tag{112}$$

où $\mathbf{J}_\mathrm{s}\left(\mathbf{x}\right)$ est la densité des courants sources.

On souligne que l'expression multipolaire du champ diffusé de l'éq.(111) constitue un énorme progrès pratique puisqu'un grand nombre de techniques numériques peuvent générer la matrice $t^{(j)}$ d'un objet isolé.

8.8.5   La matrice-T à diffusion multiple

On peut récrire l'équation de diffusion multiple de l'équation (102) en définissant des matrices-T à diffusion multiple, dénotées $\mathbf{T}^{(j)}$. Les matrices $\mathbf{T}^{(j)}$ sont définies par N équations couplées :

$$\mathbf{T}^{(j)} = \mathbf{t}^{(j)} + \mathbf{t}^{(j)} \mathbf{G}_0 \sum_{l=1, l\neq j}^{N} \mathbf{T}^{(j)} \qquad\qquad j = 1, \ldots, N \tag{113}$$

où N est le nombre d'objets dans le système. Chaque $\mathbf{T}^{(j)}$ décrit le champ diffusé par un objet j en tenant compte des influences de tous les autres diffuseurs du système. Si nous pouvons résoudre ces équations, nous avons une solution complète des équations de diffusion multiple, puisque la fonction de Green du système s'écrit maintenant :

$$\mathbf{G} = \mathbf{G}_0 + \mathbf{G}_0 \sum_{j=1}^{N} \mathbf{T}^{(j)} \mathbf{G}_0 \tag{114}$$

Les équations (113) et (114) sont souvent connues sous le nom d'équations Foldy-Lax de la fonction de Green.

Résoudre les équations (113) s'annonce très difficile puisque $\mathbf{T}^{(j)}$, $\mathbf{t}^{(j)}$, et $\mathbf{G}_0$ sont tous des opérateurs. Il devient possible de les résoudre pourtant sur la base des ondes multipolaires. On commence par laisser les deux membres de l'équation opérer sur $\mathbf{G}_0 \left|\mathbf{J}\right\rangle$. Ensuite, on opère sur les deux cotés par $\mathbf{G}_0$ afin d'obtenir :

$$\mathbf{G}_0 \mathbf{T}^{(j)} \mathbf{G}_0 \left|\mathbf{J}\right\rangle \equiv \mathbf{G}_0 \mathbf{t}^{(j)} \mathbf{G}_0 \left|\mathbf{J}\right\rangle + \mathbf{G}_0 \mathbf{t}^{(j)} \mathbf{G}_0 \sum_{l=1, l\neq j}^{N} \mathbf{T}^{(l)} \mathbf{G}_0 \left|\mathbf{J}\right\rangle \tag{115}$$

Si les sources du champ restent à l'extérieur des objets, on peut récrire les équations de l'équation (113) sur la base des ondes multipolaires où elles prennent une forme matricielle. Après un certain nombre de calculs, on trouve que les équations (113) s'écrivent :

$$T^{(j)} J^{(j,0)} a = t^{(j)} J^{(j,0)} a + t^{(j)} \sum_{l=1, l\neq j}^{N} H^{(j,l)} T^{(l)} J^{(l,0)} a \tag{116}$$

Les matrices $H^{(j,l)} \equiv H(k_e (\mathbf{x}_j - \mathbf{x}_l))$ sont les matrices de translation irrégulière, et $J^{(j,0)} \equiv J(k_e \mathbf{x}_j)$ sont les matrices de translation régulières. Ces matrices analytiques sont un peu longues à écrire (voir l'appendice A) mais on peut actuellement les évaluer grâce à des sous-programmes efficaces.

Les «a» sont des matrices colonne contenant les coefficients de l'onde incidente sur la base des ondes multipolaires. Puisque les «a» sont arbitraires, on peut récrire l'équation (116) comme :

$$T^{(j)} J^{(j,0)} = t^{(j)} J^{(j,0)} + t^{(j)} \sum_{l=1, l\neq j}^{N} H^{(j,l)} T^{(l)} J^{(l,0)} \tag{117}$$

Cette équation a le désavantage de dépendre du choix de l'origine du système. On élimine ce problème en multipliant les deux membres de cette équation par les matrices $J^{(0,j)}$ afin d'obtenir :

$$T^{(j)} = t^{(j)} + t^{(j)} \sum_{l=1, l\neq j}^{N} H^{(j,l)} T^{(l)} J^{(l,j)} \qquad j = 1, \ldots, N \tag{118}$$

où nous avons utilisé les propriétés de groupe de la matrice de translation régulière J :

$$J^{(l,0)} J^{(0,j)} = J^{(l,j)} \tag{119}$$

$$J^{(j,0)} J^{(0,j)} = \mathbb{I} \tag{120}$$

On peut voir l'équation (118) comme une forme des équations de Foldy-Lax dans la représentation multipolaire.

8.9 Représentation multipolaire de la diffusion multiple

On peut en principe résoudre directement les équations (118), mais ce n'est pas évident en pratique du fait que les inconnues sont des matrices. Mackowski et Miscenko ont proposé néanmoins une solution de la diffusion multiple qui revient à une solution itérative des équations (118)[37]. Plutôt que de détailler l'obtention des équations (118) pour les $T^{(j)}$, à partir des fonctions de Green, on va maintenant les obtenir directement à partir du concept de champ d'excitation et du théorème de translation. Nous verrons que cette démarche nous inspire d'autres manières de résoudre le problème de diffusion multiple.

Le concept d'un champ d'excitation d'un objet est sous-jacent à la dérivation des équations de diffusion multiple de type Foldy-Lax, c'est-à-dire les équations (113) et (114). On part d'abord de l'idée que le

système tout entier, composé de plusieurs objets ou «diffuseurs», est soumis à un champ incident. Le champ d'excitation d'un diffuseur j du système est la somme du champ incident et du champ diffusé par les autres objets du système, le champ diffusé par l'objet j étant exclu :

$$\mathbf{E}_{\mathrm{e}}^{(j)}(\mathbf{r}) \equiv \mathbf{E}_{\mathrm{inc}}(\mathbf{r}) + \sum_{l=1,l\neq j}^{N} \mathbf{E}_{\mathrm{s}}^{(l)}(\mathbf{r})$$

$$= \mathcal{R}g\left\{\boldsymbol{\Psi}^t(\mathbf{r})\right\} a + \sum_{l=1,l\neq j}^{N} \boldsymbol{\Psi}^t(\mathbf{r}_l) f_{\mathrm{s}}^{(l)} \tag{121}$$

où nous avons développé l'onde diffusée par chaque diffuseur $\mathbf{E}_{\mathrm{s}}^{(l)}$ en termes d'un développement multipolaire centré sur le centre de la sphère circonscrite du diffuseur j. Le champ incident, $\mathbf{E}_{\mathrm{inc}}(\mathbf{r}) = \mathcal{R}g\left\{\boldsymbol{\Psi}^t(\mathbf{r})\right\} a$ est ici développé en ondes multipolaires centrées autour de l'origine arbitrairement choisie du système. On remarque que les $\mathbf{r}_l$ sont définis de $\mathbf{r}$ par rapport aux centres des sphères circonscrites des objets :

$$\mathbf{r}_l \equiv \mathbf{r} - \mathbf{x}_l \tag{122}$$

Grâce au théorème de translation, on peut récrire ces équations en termes de développements multipolaires

$$\mathbf{E}_{\mathrm{e}}^{(j)}(\mathbf{r}_j) = \mathcal{R}g\left\{\boldsymbol{\Psi}^t(\mathbf{r}_j)\right\} J^{(j,0)} a + \sum_{l=1,l\neq j}^{N} \mathcal{R}g\left\{\boldsymbol{\Psi}^t(\mathbf{r}_j)\right\} H^{(j,l)} f^{(l)} \tag{123}$$

où $H^{(j,l)} \equiv H(\mathbf{x}_j - \mathbf{x}_l)$ est la matrice de translation irrégulière (voir l'appendice A). Le champ d'excitation peut toujours être développé sur des coefficients inconnus d'une base d'ondes régulières :

$$\mathbf{E}_{\mathrm{e}}^{(j)}(\mathbf{r}_j) \equiv \mathcal{R}g\left\{\boldsymbol{\Psi}^t(\mathbf{r}_j)\right\} e^{(j)} \tag{124}$$

Avec cette définition, on peut éliminer la base des ondes multipolaires et l'on obtient une équation portant sur les coefficients seulement :

$$e^{(j)} = J^{(j,0)} a + \sum_{l=1,l\neq j}^{N} H^{(j,l)} f^{(l)}. \tag{125}$$

Invoquant la définition de la matrice T individuelle pour un diffuseur dans un milieu homogène, c'est-à-dire l'équation (53),

$$f^{(l)} = t^{(l)} e^{(l)} \tag{126}$$

on obtient un ensemble de N équations couplées où les matrices colonnes $e^{(j)}$ sont les inconnues :

$$e^{(j)} = J^{(j,0)} a + \sum_{l=1,l\neq j}^{N} H^{(j,l)} t^{(l)} e^{(l)} \qquad\qquad j = 1,...,N \tag{127}$$

On regarde les équations (127) et (126) comme les équations fondamentales de la diffusion multiple multipolaire. On peut voir ces équations, comme les équations de Foldy-Lax de base. Si l'on veut construire une solution de la diffusion multiple pour un champ incident donné, il suffit souvent de simplement résoudre ce système par itération. A partir de ces formules, on peut obtenir toutes les formulations des solutions de la diffusion multiple.

Si l'onde incidente est une onde plane, les équations (127) sont particulièrement faciles à résoudre puisque «$J^{(j,0)} a$» se remplace analytiquement par «$\exp(i\mathbf{k}\cdot\mathbf{x}_j) a$» dans ce cas :

$$e^{(j)} = \exp(i\mathbf{k}\cdot\mathbf{x}_j) a + \sum_{l=1,l\neq j}^{N} H^{(j,l)} t^{(l)} e^{(l)} \qquad\qquad j = 1,...,N \tag{128}$$

A condition que les objets ne soient pas trop grands par rapports à la longueur d'onde, on peut traiter des agrégats composés de centaines de sphères en simplement trouvant la solution des ces équations couplées.

8.9.1 Equations de Foldy-Lax de la diffusion multiple

Une solution des équations (127) ne constitue pas une solution complète du problème dans le sens que si on change l'onde incidente, il faut résoudre de nouveau le système d'équation (127) avec d'autres coefficients «a» du champ incident sur le système. Dans certaines applications, on peut vouloir obtenir des matrices-T à diffusion multiple du système tout entier. L'équation (127) peut servir à dériver toutes les formulations de matrice-T à diffusion multiple que j'ai vues dans la littérature.

Comme premier exemple, on va établir l'équation (118) en multipliant les deux membres de l'équation (127) par des matrices $t^{(j)}$ individuelles afin d'obtenir :

$$f^{(j)} = t^{(j)} J^{(j,0)} a + t^{(j)} \sum_{l=1, l\neq j}^{N} H^{(j,l)} f^{(l)} \tag{129}$$

où nous avons utilisé sur le membre de gauche, la relation $f^{(j)} = t^{(j)} e^{(j)}$. Ensuite, on définit $T^{(j)}$ par la relation :

$$f^{(j)} \equiv T^{(j)} J^{(j,0)} a \tag{130}$$

où l'on remarque que grâce à la présence de la matrice $J^{(j,0)}$, la matrice $T^{(j)}$ est indépendante du choix de l'origine arbitraire du système. Insérant cette relation dans l'équation (129), on obtient :

$$T^{(j)} J^{(j,0)} a = t^{(j)} J^{(j,0)} a + t^{(j)} \sum_{l=1, l\neq j}^{N} H^{(j,l)} T^{(l)} J^{(l,0)} a \tag{131}$$

Puisque la matrice a des coefficients de l'onde incidente est arbitraire, on obtient :

$$T^{(j)} J^{(j,0)} = t^{(j)} J^{(j,0)} + t^{(j)} \sum_{l=1, l\neq j}^{N} H^{(j,l)} T^{(l)} J^{(l,0)} \tag{132}$$

Multipliant les deux cotés de cette équation par $J^{(0,j)}$ et en utilisant les propriétés de groupe des $J^{(0,j)}$ (voir les éqs.(119)-(120)) on obtient :

$$T^{(j)} = t^{(j)} + t^{(j)} \sum_{l=1, l\neq j}^{N} H^{(j,l)} T^{(l)} J^{(l,j)} \tag{133}$$

qui est le même système d'équations correspondant aux équations de Foldy-Lax, éq.(118).

8.9.2 Solution de la diffusion multiple par inversion directe

Une autre solution semi-analytique de la diffusion multiple est de résoudre l'ensemble des équations (127) sous forme matricielle :

$$\begin{bmatrix} e^{(1)} \\ e^{(2)} \\ \vdots \\ e^{(N)} \end{bmatrix} = \begin{bmatrix} \mathbb{I} & -H^{(1,2)} t^{(2)} & \cdots & -H^{(1,N)} t^{(N)} \\ -H^{(2,1)} t^{(1)} & \mathbb{I} & \cdots & -H^{(2,N)} t^{(N)} \\ \vdots & \vdots & \ddots & \vdots \\ -H^{(N,1)} t^{(1)} & -H^{(N,2)} t^{(2)} & \cdots & \mathbb{I} \end{bmatrix}^{-1} \begin{bmatrix} J^{(1,0)} a \\ J^{(2,0)} a \\ \vdots \\ J^{(N,0)} a \end{bmatrix} \tag{134}$$

où $\mathbb{I}$ dénote la matrice d'identité. On peut obtenir une expression pour les coefficients de diffusion $f^{(j)}$ en multipliant les deux côtés de cette équation par une matrice diagonale par blocs où les matrices sur la diagonale sont des matrices $t^{(j)}$ d'objets isolés :

$$\begin{bmatrix} t^{(1)} & 0 & \cdots & 0 \\ 0 & t^{(2)} & \cdots & 0 \\ \vdots & \vdots & \ddots & \vdots \\ 0 & 0 & \cdots & t^{(N)} \end{bmatrix} \tag{135}$$

Après cette multiplication, l'éq.(134) prend la forme :

$$
\begin{bmatrix} f^{(1)} \\ f^{(2)} \\ \vdots \\ f^{(N)} \end{bmatrix} \equiv \begin{bmatrix} T^{(1,1)} & T^{(1,2)} & \dots & T^{(1,N)} \\ T^{(2,1)} & T^{(2,2)} & \dots & T^{(2,N)} \\ \vdots & \vdots & \ddots & \vdots \\ T^{(N,1)} & T^{(N,2)} & \dots & T^{(N,N)} \end{bmatrix} \begin{bmatrix} J^{(1,0)}\,a \\ J^{(2,0)}\,a \\ \vdots \\ J^{(N,0)}\,a \end{bmatrix}
\tag{136}
$$

où nous avons utilisée l'éq.(126) sur le membre de gauche de l'équation. Sur le membre de droite de l'équation nous avons définie les $N \times N$ blocs $T^{(j,k)}$:

$$
\begin{bmatrix} T^{(1,1)} & T^{(1,2)} & \dots & T^{(1,N)} \\ T^{(2,1)} & T^{(2,2)} & \dots & T^{(2,N)} \\ \vdots & \vdots & \ddots & \vdots \\ T^{(N,1)} & T^{(N,2)} & \dots & T^{(N,N)} \end{bmatrix} = \begin{bmatrix} t^{(1)} & 0 & \cdots & 0 \\ 0 & t^{(2)} & \cdots & 0 \\ \vdots & \vdots & \ddots & \vdots \\ 0 & 0 & \cdots & t^{(N)} \end{bmatrix}
$$

$$
\times \begin{bmatrix} \mathbb{I} & -H^{(1,2)}\,t^{(2)} & \cdots & -H^{(1,N)}\,t^{(N)} \\ -H^{(2,1)}\,t^{(1)} & \mathbb{I} & \cdots & -H^{(2,N)}\,t^{(N)} \\ \vdots & \vdots & \ddots & \vdots \\ -H^{(N,1)}\,t^{(1)} & -H^{(N,2)}\,t^{(2)} & \cdots & \mathbb{I} \end{bmatrix}^{-1}
$$

On peut écrire l'équation (136) de façon compacte comme N équations matricielles :

$$
f^{(j)} = \sum_{k=1}^{N} T^{(j,k)}\,J^{(k,0)}\,a \qquad\qquad j = 1,\dots,N
\tag{137}
$$

Nous avons donc présenté deux types de matrices-T qui nous permettent d'obtenir les coefficients $f^{(j)}$: soit à partir de l'éq.(137) en utilisant les matrices $T^{(j,k)}$, soit à partir des matrices $T_N^{(j)}$:

$$
f^{(j)} \equiv T^{(j)}\,J^{(j,0)}\,a
\tag{138}
$$

Une comparaison des équations (137) et (138) nous permet d'obtenir la matrice $T^{(j)}$ en fonction des $T^{(j,k)}$:

$$
T^{(j)} = \sum_{k=1}^{N} T^{(j,k)}\,J^{(k,j)}
\tag{139}
$$

On remarque néanmoins qu'il faut N matrices $T^{(j,k)}$ afin de construire une seule matrice $T^{(j)}$.

8.9.3 Troncature de la base des ondes partielles

Les matrices $T^{(j)}$ et $T^{(j,k)}$ sont toutes les deux des solutions complètes de l'équation de diffusion multiple. Néanmoins, formellement ces deux matrices sont de dimension infinie. Un calcul numérique de ces matrices doit forcément s'effectuer dans un espace tronqué. Les différents algorithmes de calcul que nous avons développés pour calculer les matrices $T^{(j,k)}$ sont numériquement stables puisqu'ils profitent de la troncature naturelle du problème lié à la taille finie des diffuseurs.

La troncature naturelle vient du fait que les matrices $t^{(j)}$ des diffuseurs isolés ne peuvent interagir qu'avec un nombre limité d'ondes multipolaires. En général, les éléments non-négligeables, d'une matrice $t^{(j)}$ sont contenus dans une matrice carrée contenant les premiers $n \lesssim k_e R^{(j)} + 3$ ordres multipolaires où $R^{(j)}$ est le rayon de la sphère circonscrite qui entoure chaque diffuseur. On peut montrer que toutes les matrices $T^{(j,k)}$ sont naturellement tronquées au même ordre multipolaire que les matrices $t^{(j)}$ (sur la gauche) et $t^{(k)}$ (sur la droite) des objets individuels. Cette troncature naturelle des matrices $T^{(j,k)}$ est particulièrement facile à démontrer dans un formalisme itératif comme illustré dans la section 9.2 ci-dessous. Néanmoins, il faut parfois agrandir la dimension de l'espace tronqué à des ordres multipolaires plus élevés si les objets sont fortement couplés, lors de l'excitation de plasmons par exemple.

Dans la littérature, certains auteurs préfèrent utiliser les algorithmes de calcul des N matrices $T^{(j)}$ plutôt que de calculer les N^2 matrices $T^{(j,k)}$. La difficulté est que les algorithmes de calcul pour les $T^{(j)}$ sont susceptibles d'entraîner des erreurs numériques, ce qui ressort de l'équation (139). Les matrices $T^{(j,k)}$ sont naturellement tronquées (voir section 9.2), mais les matrices $J^{(k,j)}$ opèrent en principe sur

un espace de dimension infinie et le fait de les tronquer dans un quelconque algorithme peut introduire des erreurs considérables. Certains algorithmes de calcul des matrices $T^{(j)}$ peuvent réussir parce que les matrices $J^{(k,j)} = J\left(k_{\mathrm{e}}\left(\mathbf{x}_k - \mathbf{x}_j\right)\right)$ peuvent en réalité être tronquées à des ordres multipolaires de l'ordre de $n \lesssim k_{\mathrm{e}} 2 R_{\mathrm{syt}}$ où R_{syt} est le rayon de la sphère circonscrite qui entoure le système tout entier. Néanmoins, le fait d'être obligé d'étendre la dimension de l'espace multipolaire à de telles dimensions nuit à l'utilité de ces algorithmes pour des systèmes de grande taille et rend certains algorithmes inutilisables, comme les algorithmes récursifs.

8.10   Forces optiques directes et induites

La manipulation mécanique d'atomes, molécules, et petits objets micrométriques en n'utilisant que la lumière est devenu monnaie courante dans de nombreux laboratoires à travers le monde. En dépit du fait qu'il s'agit de physique «classique», il existe bien des controverses au sujet de la formulation de la force optique sur une particule immergée dans un milieu diélectrique. Dans cette section, on essaie d'éclairer un peu ce débat en établissant l'expression du tenseur de contrainte d'un point de vue «microscopique».

8.10.1   Forces optiques et débat Minkowski - Abrahams

Pour un objet dans le vide, on définit la force électromagnétique ou simplement la force optique comme la force de Lorentz sur les charges de polarisation et les courants de polarisation dans l'objet qui sont donnés par :

$$\rho_{\mathrm{pol}} = \epsilon_0 \mathrm{div}\, \mathbf{E}$$
$$\mathbf{J}_{\mathrm{pol}} = \frac{1}{\mu_0} \mathrm{rot}\, \mathbf{B} - \epsilon_0 \frac{\partial \mathbf{E}}{\partial t} \tag{140}$$

$$\mathbf{F}_{\mathrm{o}} = \int_V d\mathbf{x}\, \left(\mathbf{E}\rho_{\mathrm{pol}} + \mathbf{J}_{\mathrm{pol}} \wedge \mathbf{B}\right) \tag{141}$$

où V est un volume qui contient l'objet. Après des manipulations sur les équations de Maxwell, on obtient :

$$\mathbf{F}_{\mathrm{o}} + \frac{d}{dt}\mathbf{p}_{\mathrm{champ}} = \oint_\Gamma \overleftrightarrow{\mathbf{T}} \cdot \hat{\mathbf{n}}\, ds \tag{142}$$

où $\mathbf{F}_{\mathrm{o}}$ est la force mécanique et Γ la surface du volume V. Le tenseur de contrainte de Maxwell, $\overleftrightarrow{\mathbf{T}}$, dans l'équation (142) s'écrit :

$$\overleftrightarrow{\mathbf{T}}_{ij} = \epsilon_0 E_i E_j + \frac{1}{\mu_0} B_i B_j - \delta_{ij} \left(\frac{\epsilon_0}{2}\mathbf{E}^2 + \frac{1}{\mu_0}\frac{1}{2}\mathbf{B}^2\right) \tag{143}$$

qui correspond au flux de quantité du mouvement à travers la surface Γ. Dans l'équation (142), on peut interpréter $\mathbf{p}_{\mathrm{champ}}$ comme la quantité de mouvement du champ dans le volume d'intégration V :

$$\mathbf{p}_{\mathrm{champ}} = \epsilon_0 \int_V \left(\mathbf{E} \wedge \mathbf{B}\right)\, d\mathbf{x} \tag{144}$$

donc la densité de la quantité du mouvement électromagnétique du champ électromagnétique, $\mathbf{g}_{\mathrm{c}}$, est :

$$\mathbf{g}_{\mathrm{c}} = \epsilon_0 \left(\mathbf{E} \wedge \mathbf{B}\right) = \epsilon_0 \mu_0 \mathbf{E} \wedge \mathbf{H}_{\mathrm{vide}} = \frac{1}{c^2} \mathbf{E} \wedge \mathbf{H}_{\mathrm{vide}} \tag{145}$$

Les difficultés commencent quand il faut déterminer la force optique sur un objet immergé dans un milieu diélectrique. Les choses se compliquent puisque sous l'action de l'onde, une quantité de mouvement est acquise par les électrons des dipôles moléculaires. Ces contributions moléculaires exerceront également des forces mécaniques sur l'objet.

Il semble néanmoins qu'on puisse faire des approximations raisonnables de la force optique si le milieu ambiant est transparent. Cette condition se traduit par le fait que les molécules dans un milieu transparent oscillent essentiellement en accord de phase avec l'onde incidente ce qui veut dire que la permittivité et la perméabilité relatives du milieu sont réels en première approximation. Quand cette condition est remplie, il semble qu'on puisse généraliser le tenseur de Maxwell au cas du milieu diélectrique liquide et transparent.

L'idée essentielle est que la force optique, à l'échelle de l'observation au moins, n'agit que sur les charges et courants de polarisation du milieu qui ne seraient pas présents si l'objet était remplacé par le milieu ambiant. Quand cette hypothèse de base est correcte à l'échelle microscopique, on peut écrire la force mécanique sur l'objet, $\mathbf{F}_{\mathrm{o}}$, comme :

$$\mathbf{F}_{\mathrm{o}} = \int_V d\mathbf{r} \left(\mathbf{E}\rho'_{\mathrm{pol}} + \left(\mathbf{J}'_{\mathrm{pol}} + \mathbf{J}'_{\mathrm{mag}} \right) \wedge \mathbf{B} \right) \tag{146}$$

où V est un volume qui contient l'objet et les primes signifient qu'il s'agit des charges et courants induits par la présence de l'objet à la place du milieu diélectrique ambiant.

Cette formulation de la force est analogue à la force d'Archimède. Pour un objet immergé dans un milieu liquide, la force de gravitation agit sur l'objet mais elle agit également sur l'eau. En conséquence, il y a également des forces moléculaires de l'eau qui agissent sur l'objet. La force mécanique totale sur l'objet est $\mathbf{F}_{\mathrm{t}} = (m_{\mathrm{obj}} - m_{\mathrm{eau}})\,\mathbf{g}$ où m_{eau} est la masse de l'eau déplacée par l'objet. Autrement dit, la force mécanique totale n'est que la force de gravitation agissant sur la masse supplémentaire qui est présente parce que l'objet remplace l'eau. Dans ce langage, la force de l'éq.(146) est la force sur les charges et courants de polarisation présents qui ne seraient pas là si l'objet était absent.

On commence avec des formules «microscopiques» de Maxwell sans sources :

$$\nabla \cdot \mathbf{E} = \rho_{\mathrm{pol}} \tag{147}$$

$$\frac{1}{\mu_0} \nabla \times \mathbf{B} = \epsilon_0 \frac{\partial \mathbf{E}}{\partial t} + \mathbf{J}_{\mathrm{pol}} + \mathbf{J}_{\mathrm{mag}} \tag{148}$$

où les densités et courants viennent des charges et courants de polarisation des milieux matériels. On fait l'hypothèse que les objets sont entièrement décrits par leurs densités de moment dipolaire électrique $\mathbf{P}_{\mathrm{s}}$ et de moment dipolaire magnétique $\mathbf{M}_{\mathrm{s}}$, où l'indice «s» indique qu'il s'agit du diffuseur, «scatterer». De même, le milieu externe est décrit par les densités $\mathbf{P}_{\mathrm{e}}$ et $\mathbf{M}_{\mathrm{e}}$.

L'objectif principal est d'écrire $\mathbf{F}_{\mathrm{o}}$ entièrement en fonction des champs $\mathbf{E}$, $\mathbf{B}$, $\mathbf{D}_{\mathrm{e}}$, et $\mathbf{H}_{\mathrm{e}}$. Si de plus, le milieu externe est non-absorbant, on peut écrire la force sur l'objet comme :

$$\mathbf{F}_{\mathrm{o}} = \int_V \nabla \cdot \overleftrightarrow{\mathbf{T}} \, d\mathbf{x} - \frac{d}{dt} \left(\mathbf{p}_{\mathrm{champ}} + \mathbf{p}_{\mathrm{milieu}} \right) \tag{149}$$

où $\overleftrightarrow{\mathbf{T}}$ est un tenseur de contrainte, et où $\mathbf{p}_{\mathrm{champ}}$ et $\mathbf{p}_{\mathrm{milieu}}$ représentent respectivement la quantité de mouvement du champ et la quantité du mouvement associée avec les polarisations du milieu externe dans le volume V d'intégration.

L'objectif est maintenant de montrer qu'on peut obtenir une relation du style de l'équation (149). On peut récrire l'équation (148) comme :

$$\mathbf{J}_{\mathrm{pol}} + \mathbf{J}_{\mathrm{mag}} = -\epsilon_0 \frac{\partial \mathbf{E}}{\partial t} + \frac{1}{\mu_0} \nabla \times \mathbf{B} \tag{150}$$

où les densités de charge et de courant ont les descriptions microscopiques habituelles :

$$\mathbf{J}_{\mathrm{pol}} = \frac{\partial}{\partial t} \mathbf{P}_{\mathrm{s}} \tag{151}$$

$$\mathbf{J}_{\mathrm{mag}} = \nabla \times \mathbf{M}_{\mathrm{s}} \tag{152}$$

Les relations avec les $\mathbf{J}'_{\mathrm{pol}}$ et $\mathbf{J}'_{\mathrm{mag}}$ sont données par :

$$\begin{aligned}
\mathbf{J}_{\mathrm{pol}}\left(\mathbf{r}, t\right) &= \frac{\partial}{\partial t} \left(\mathbf{P}_{\mathrm{s}} - \mathbf{P}_{\mathrm{e}} \right) + \frac{\partial}{\partial t} \mathbf{P}_{\mathrm{e}} = \mathbf{J}'_{\mathrm{pol}} + \frac{\partial}{\partial t} \mathbf{P}_{\mathrm{e}} \\
\mathbf{J}_{\mathrm{mag}}\left(\mathbf{r}, t\right) &= \nabla \times \left(\mathbf{M}_{\mathrm{s}} - \mathbf{M}_{\mathrm{e}} \right) + \nabla \times \mathbf{M}_{\mathrm{e}} = \mathbf{J}'_{\mathrm{mag}} + \nabla \times \mathbf{M}_{\mathrm{e}}
\end{aligned} \tag{153}$$

d'où l'on obtient :

$$\begin{aligned}
\mathbf{J}'_{\mathrm{pol}} + \mathbf{J}'_{\mathrm{mag}} &= -\frac{\partial}{\partial t} \left(\epsilon_0 \mathbf{E} + \mathbf{P}_{\mathrm{e}} \right) + \nabla \times \left(\frac{\mathbf{B}}{\mu_0} - \mathbf{M}_{\mathrm{e}} \right) \\
&= -\frac{\partial}{\partial t} \mathbf{D}_{\mathrm{e}} + \nabla \times \mathbf{H}_{\mathrm{e}}
\end{aligned} \tag{154}$$

Dans l'équation (154) nous avons fait appel aux champs «macroscopiques» du milieu externe :

$$\mathbf{H}_e \equiv \frac{\mathbf{B}}{\mu_0} - \mathbf{M}_e = \frac{\mathbf{B}}{\mu_e \mu_0}$$

$$\mathbf{D}_e \equiv \epsilon_0 \mathbf{E} + \mathbf{P}_e = \epsilon_0 \varepsilon_e \mathbf{E} \tag{155}$$

Les charges de polarisation s'écrivent :

$$\rho_{\text{pol}} = \epsilon_0 \nabla \cdot \mathbf{E} \tag{156}$$

La description microscopique des charges de polarisation est :

$$\rho_{\text{pol}} = -\nabla \cdot \mathbf{P} = -\nabla \cdot (\mathbf{P} - \mathbf{P}_e) - \nabla \cdot \mathbf{P}_e$$

$$= \rho'_{\text{pol}} - \nabla \cdot \mathbf{P}_e \tag{157}$$

On obtient donc :

$$\rho'_{\text{pol}} = \nabla \cdot (\epsilon_0 \mathbf{E} + \mathbf{P}_e) = \nabla \cdot \mathbf{D}_e \tag{158}$$

Grâce aux équations (154) et (158), la force optique s'écrit :

$$\mathbf{F}_o = \int_V d\mathbf{x} \left[\mathbf{E} \rho'_{\text{pol}} + \left(\mathbf{J}'_{\text{pol}} + \mathbf{J}'_{\text{mag}} \right) \wedge \mathbf{B} \right]$$

$$= \int_V d\mathbf{x} \left[\mathbf{E} \nabla \cdot \mathbf{D}_e - \left(\frac{\partial}{\partial t} \mathbf{D}_e \right) \wedge \mathbf{B} + (\nabla \times \mathbf{H}_e) \wedge \mathbf{B} \right] \tag{159}$$

On peut en principe calculer la force optique avec cette relation volumique. On peut manipuler cette équation et l'amener à la forme de l'équation (149) à condition que les paramètres constitutifs, ε_e et μ_e soient réels, autrement dit que les champs $\mathbf{D}_e$ et $\mathbf{H}_e$ ne soit pas déphasés par rapport aux champs $\mathbf{E}_e$ et $\mathbf{B}_e$. Sous cette condition, on peut écrire :

$$\mathbf{F}_o = \int_V d\mathbf{x} \left[\epsilon_0 \varepsilon_e \mathbf{E} \nabla \cdot \mathbf{E} + \frac{1}{\mu_e \mu_0} \mathbf{B} \nabla \cdot \mathbf{B} - \epsilon_0 \varepsilon_e \left(\frac{\partial}{\partial t} \mathbf{E} \right) \wedge \mathbf{B} + \frac{1}{\mu_e \mu_0} (\nabla \times \mathbf{B}) \wedge \mathbf{B} \right] \tag{160}$$

où nous avons utilisé le fait que $\nabla \cdot \mathbf{B} = 0$. Utilisant la relation :

$$\epsilon_0 \varepsilon_e \frac{\partial}{\partial t} (\mathbf{E} \wedge \mathbf{B}) = \epsilon_0 \varepsilon_e \left(\frac{\partial}{\partial t} \mathbf{E} \right) \wedge \mathbf{B} + \epsilon_0 \varepsilon_e \mathbf{E} \wedge \left(\frac{\partial}{\partial t} \mathbf{B} \right) \tag{161}$$

on obtient :

$$\mathbf{F}_o = \int_V d\mathbf{r} \left(\epsilon_0 \varepsilon_e \mathbf{E} \nabla \cdot \mathbf{E} + \frac{1}{\mu_e \mu_0} \mathbf{B} \nabla \cdot \mathbf{B} - \epsilon_0 \varepsilon_e \mathbf{E} \wedge (\nabla \times \mathbf{E}) + \frac{1}{\mu_e \mu_0} (\nabla \times \mathbf{B}) \wedge \mathbf{B} \right)$$

$$- \epsilon_0 \varepsilon_e \int_V d\mathbf{r} \frac{\partial}{\partial t} (\mathbf{E} \wedge \mathbf{B}) \tag{162}$$

où nous avons utilisé :

$$\frac{\partial}{\partial t} \mathbf{B} = -\nabla \times \mathbf{E} \tag{163}$$

Utilisant la formule :

$$\nabla (\mathbf{a} \cdot \mathbf{b}) = (\mathbf{a} \cdot \nabla) \mathbf{b} + (\mathbf{b} \cdot \nabla) \mathbf{a} + \mathbf{a} \wedge (\nabla \times \mathbf{b}) + \mathbf{b} \wedge (\nabla \times \mathbf{a}) \tag{164}$$

nous avons les relations :

$$\mathbf{E} \wedge (\nabla \times \mathbf{E}) = \frac{1}{2} \nabla \mathbf{E}^2 - (\mathbf{E} \cdot \nabla) \mathbf{E}$$

$$(\nabla \times \mathbf{B}) \wedge \mathbf{B} = -\frac{1}{2} \nabla \mathbf{B}^2 + (\mathbf{B} \cdot \nabla) \mathbf{B} \tag{165}$$

$$\mathbf{F}_o = \int_V d\mathbf{x} \nabla \cdot \overleftrightarrow{\mathbf{T}} - \frac{d}{dt} \int_V \mathbf{g}_e \, d\mathbf{x} \tag{166}$$

où le tenseur de contrainte s'écrit :

$$\overleftrightarrow{\mathbf{T}}_{ij} = \epsilon_0 \varepsilon_{\mathrm{e}} E_i E_j + \frac{1}{\mu_{\mathrm{e}} \mu_0} B_i B_j - \frac{1}{2} \delta_{ij} \left(\epsilon_0 \varepsilon_{\mathrm{e}} \mathbf{E}^2 + \frac{\mathbf{B}^2}{\mu_{\mathrm{e}} \mu_0} \right) \tag{167}$$

et $\mathbf{g}_{\mathrm{e}}$ est la densité de quantité du mouvement du champ plus la quantité de mouvement des dipôles moléculaires du milieu externe :

$$\mathbf{g}_{\mathrm{e}} = \epsilon_0 \varepsilon_{\mathrm{e}} \left(\mathbf{E} \wedge \mathbf{B} \right) = \epsilon_0 \mu_0 \varepsilon_{\mathrm{e}} \mu_{\mathrm{e}} \left(\mathbf{E} \wedge \mathbf{H}_{\mathrm{e}} \right) = \frac{1}{v_{\mathrm{e}}^2} \mathbf{E} \wedge \mathbf{H}_{\mathrm{e}} = \frac{\mathbf{S}_{\mathrm{e}}}{v_{\mathrm{e}}^2} \tag{168}$$

Cette relation connue comme relation de Minkowski pour la densité de quantité de mouvement a fait couler beaucoup d'encre. On remarque que $\mathbf{S}_{\mathrm{e}}$ est le flux d'énergie dans le milieu externe (même si $\mu_{\mathrm{e}} \neq 1$). La quantité $\mathbf{g}_{\mathrm{e}}$ est une densité de la quantité du mouvement. On obtient le flux de la quantité de mouvement en multipliant $\mathbf{g}_{\mathrm{e}}$ par la vitesse de la lumière dans le milieu, v_{e}. On obtient donc que le flux d'énergie égale v_{e} fois le flux de la quantité de mouvement. Dans le langage moderne, on aime parler des photons, et le flux de la «pseudo» quantité de mouvement satisfait $\frac{|\mathbf{S}_{\mathrm{e}}|}{v_{\mathrm{e}}} = N_{\mathrm{photon}} \widetilde{p}$, où N_{photon} est le nombre de photons et $\widetilde{p}$ leur «pseudo» quantité du mouvement. Le flux d'énergie satisfait $I = |\mathbf{S}_{\mathrm{e}}| = N_{\mathrm{photon}} \widetilde{E}$ où $\widetilde{E}$ est la «pseudo» énergie des photons. On obtient donc une relation entre la «pseudo» quantité de mouvement, $\widetilde{p}$, et la «pseudo» énergie, $\widetilde{E}$, des photons :

$$\widetilde{E} = v_{\mathrm{e}} p = \frac{c}{n_{\mathrm{e}}} \widetilde{p} \tag{169}$$

Les mots «pseudo» sont utilisés puisque $\widetilde{E}$ et $\widetilde{p}$ contiennent des contributions venant du milieu externe.

La controverse autour de ce sujet est due largement au fait qu'Abrahams et d'autres auteurs ont souligné que la «vraie» densité de quantité de mouvement du champ est, $\mathbf{g}_{\mathrm{c}} = \frac{1}{c^2} \mathbf{E} \wedge \mathbf{H}_{\mathrm{vide}}$, comme donnée par un traitement du tenseur de Maxwell dans le vide (voir l'éq.(145)). Si maintenant, on essayait d'obtenir le flux de la nouvelle quantité de mouvement du photon dans le milieu en multipliant $\mathbf{g}_{\mathrm{c}}$ par v_{e}, on obtiendrait que flux de la quantité de mouvement soit, $\frac{v_{\mathrm{e}}}{c^2} |\mathbf{E} \wedge \mathbf{H}_{\mathrm{vide}}|$. Puisque le flux d'énergie du champ est $|\mathbf{E} \wedge \mathbf{H}_{\mathrm{vide}}|$, on arriverait à la conclusion que les photons obéissent à la relation $E = n_{\mathrm{e}} c p$, cette fois-ci avec le facteur n_{e} dans le numérateur contrairement à l'équation (169). Une telle interprétation de la relation d'Abrahams n'est pourtant pas correcte puisqu'on n'a pas le droit de multiplier une densité de quantité de mouvement exclusivement du champ, $\mathbf{g}_{\mathrm{c}}$, par une vitesse de phase $v_{\mathrm{e}} = c/n_{\mathrm{e}}$ qui inclut les effets du milieu. La vitesse du champ «pur» est toujours c. Le «ralentissement» de la vitesse de la lumière dans le milieu est un effet apparent du aux rayonnements moléculaires.

En conséquence, si l'on veut adopter le point de vue d'Abrahams, le flux de la «vraie» quantité de mouvement est obtenu en multipliant $\mathbf{g}_{\mathrm{c}}$ par la vraie vitesse du champ c, et la quantité de mouvement des photons est donnée par $N_{\mathrm{photon}} p = |c \mathbf{g}_{\mathrm{c}}|$. Vu du fait que le «vrai» flux d'énergie est $|\mathbf{E} \wedge \mathbf{H}_{\mathrm{vide}}| = N_{\mathrm{photon}} E$, on obtient que les photons satisfont la relation :

$$E = cp \tag{170}$$

Les partisans d'Abrahams ont raison en ce qui concerne strictement l'énergie et la quantité du mouvement du champ. Néanmoins, c'est la quantité de mouvement du champ plus la quantité de mouvement moléculaire de la forme de Minkowski, (l'éq.(168)) qui donne la force optique *effective* qui agit sur l'objet.

8.10.2   Formulation harmonique du tenseur de Maxwell

Avec un traitement habituel, on trouve à partir des éqs.(166)-(168), que la force optique d'un champ harmonique moyennée sur une période dans le temps est donnée par un tenseur de Maxwell «harmonique», $\overleftrightarrow{\mathbf{T}}_{\mathrm{h}}$:

$$\langle \mathbf{F}_{\mathrm{o}} \rangle_T = \oint_S \overleftrightarrow{\mathbf{T}}_{\mathrm{h}} \cdot \widehat{\mathbf{n}} \, dS \tag{171}$$

où $\overleftrightarrow{\mathbf{T}}_{\mathrm{h}}$ est le tenseur de Maxwell moyenné dans le temps :

$$\overleftrightarrow{\mathbf{T}}_{\mathrm{h}} = \frac{1}{2} \mathrm{Re} \left\{ \epsilon_0 \varepsilon_{\mathrm{e}} E_i^* E_j + \frac{1}{\mu_{\mathrm{e}} \mu_0} B_i^* B_j - \frac{1}{2} \delta_{ij} \left(\epsilon_0 \varepsilon_{\mathrm{e}} \|\mathbf{E}\|^2 + \frac{\|\mathbf{B}\|^2}{\mu_{\mathrm{e}} \mu_0} \right) \right\} \tag{172}$$

Le débat d'Abrahams-Minkowski disparaît dans le cas harmonique puisque la moyenne temporelle des termes concernés disparaît pour des champs harmoniques :

$$\left\langle \frac{d}{dt} \int_V d\mathbf{r} \, (\mathbf{E} \wedge \mathbf{B}) \right\rangle_T = \left\langle \frac{d}{dt} \int_V d\mathbf{r} \, (\mathbf{E} \wedge \mathbf{H}) \right\rangle_T = 0 \tag{173}$$

Aussi longtemps que le milieu externe reste non-absorbant et qu'on évalue le tenseur de Maxwell sur une surface qui entoure l'objet, on n'aura pas de problèmes. Néanmoins, si l'on s'intéressait à ce qui se passe à l'intérieur de l'objet diélectrique, ce serait une erreur de penser qu'il faut évaluer le tenseur de Maxwell en remplaçant ε_e et μ_e par les constantes ε_s et μ_s de l'objet. Dans le calcul microscopique, il est explicite qu'il faut garder la forme de l'éq.(167) ou (172) du tenseur de Maxwell avec les constantes ε_e et μ_e, même à l'intérieur de l'objet. De plus, il ne faut pas oublier que le tenseur de Maxwell ne pouvait être obtenu que dans le cas d'un milieu externe non-absorbant, c'est-à-dire que ε_e et μ_e sont réels.

La discussion du paragraphe précédent peut sembler inutile, mais plusieurs résultats faux sont apparus récemment, y compris encore cette année, où des erreurs sur la force de radiation agissant sur les charges de polarisation à une interface étaient dues au fait que le tenseur de Maxwell pris à l'intérieur du milieu était incorrect.

8.10.3   Sections efficaces pour la force de radiation

Il est souhaitable de traduire les résultats d'un calcul du tenseur de Maxwell sous une forme qui soit plus pratique pour les comparaisons avec expérience. Afin de s'affranchir de la dépendance sur l'irradiance des champs, il est pratique, pour des faisceaux homogènes, de définir une section efficace «vectorielle», $\boldsymbol{\sigma}_f$, telle que :

$$\mathbf{F}_o \equiv \frac{I}{v_e} \boldsymbol{\sigma}_f \tag{174}$$

où $I = |\mathbf{S}_i|$ est l'irradiance et v_e la vitesse de phase de l'onde dans le milieu $v_e = c/n_e = \sqrt{\varepsilon_e \mu_e \epsilon_0 \mu_0}^{-1}$.

Souvent dans les expériences de force optique, le faisceau est inhomogène (faisceau laser par exemple). Si l'homogénéité du champ varie lentement par rapport à la taille de l'objet, on peut simplement écrire :

$$\mathbf{F}_o \simeq \frac{I(\mathbf{r})}{v_e} \boldsymbol{\sigma}_f \tag{175}$$

Pour une pincette optique, la variation spatiale du faisceau n'est souvent pas négligeable à l'échelle de l'objet et cette approximation n'est plus valable. Dans de telles situations, on peut généraliser la section efficace afin qu'elle dépende de la position de la particule :

$$\mathbf{F}_o \equiv \frac{I(\mathbf{0})}{v_e} \boldsymbol{\sigma}_f(\mathbf{r}) \tag{176}$$

où $I(\mathbf{0})$ est l'irradiance à un certain point judicieusement choisi du faisceau (choisi comme origine).

La difficulté avec cette formulation est que l'irradiance pour une position donnée d'une pincette optique est difficilement mesurable. Pour les faisceaux inhomogènes, la puissance du faisceau incidente, P_i, est la donnée expérimentale. Il est donc plus utile de formuler la force en fonction d'une efficacité $\mathbf{Q}_f$:

$$\mathbf{F}_o = \frac{P_i}{v_e} \frac{k^2 \varphi}{\pi} \boldsymbol{\sigma}_f(\mathbf{r})$$
$$\equiv \frac{P_i}{v_e} \mathbf{Q}_f(\mathbf{r}) \tag{177}$$

où $\mathbf{Q}_f(\mathbf{r})$ est une quantité sans dimensions. Le facteur φ que nous appelons la «*shape normalization parameter*» dépend de la forme du faisceau et est déterminé par la relation entre $I(\mathbf{0})$ et la puissance totale du faisceau :

$$I(\mathbf{0}) \equiv \varphi \frac{k^2 P_i}{\pi} \tag{178}$$

On détermine le facteur φ en intégrant le faisceau modèle afin de déterminer sa puissance totale. Pour un faisceau axisymétrique par exemple, la puissance du faisceau est donnée par l'intégrale :

$$P_i = \frac{2\pi}{k^2} \int_0^\infty I(\mathbf{r}) \, k\rho \, (k d\rho) \bigg|_{z=\text{cte}} \tag{179}$$

où l'irradiance $I(\mathbf{r})$ est donnée par :

$$I(\mathbf{r}) \equiv \frac{1}{2}\,\mathrm{Re}\left\{\mathbf{E}\wedge\mathbf{H}^*\right\}\cdot\widehat{\mathbf{z}} \tag{180}$$

et z est l'axe de symétrie du faisceau. Une comparaison avec l'éq.(178) montre que φ est donné par :

$$\varphi = \left(2\int_0^\infty \frac{I(\mathbf{r})}{I(\mathbf{0})}k\rho\,(kd\rho)\bigg|_{z=\mathrm{cte}}\right)^{-1} \tag{181}$$

On obtient une formule pour $\boldsymbol{\sigma}_\mathrm{f}$ en choisissant comme surface fermée dans l'éq.(171) une sphère à l'infini, invoquant les limites du champ lointain et comparant le résultat du calcul avec l'équation (177). On obtient que $\boldsymbol{\sigma}_\mathrm{f}$ s'exprime par :

$$\boldsymbol{\sigma}_\mathrm{f} = \boldsymbol{\sigma}_\mathrm{r} - \boldsymbol{\sigma}_\mathrm{a} \tag{182}$$

où $\boldsymbol{\sigma}_\mathrm{a}$ caractérise la contribution de la force due aux asymétries dans la diffusion par la particule :

$$\boldsymbol{\sigma}_\mathrm{a} = \frac{v_\mathrm{e}}{4I(\mathbf{0})}\int\widehat{\mathbf{r}}\left\{\varepsilon_\mathrm{e}\epsilon_0\mathbf{E}_\mathrm{s}^*\cdot\mathbf{E}_\mathrm{s} + \frac{1}{\mu_\mathrm{e}\mu_0}\mathbf{B}_\mathrm{s}^*\cdot\mathbf{B}_\mathrm{s}\right\}d\Omega_r$$

$$\underset{r\to\infty}{=} \frac{1}{2I(\mathbf{0})}r^2\left(\frac{\varepsilon_\mathrm{e}\epsilon_0}{\mu_\mathrm{e}\mu_0}\right)^{1/2}\int_\Omega\widehat{\mathbf{r}}\,\mathbf{E}_\mathrm{s}^*\cdot\mathbf{E}_\mathrm{s}\,d\Omega_r \tag{183}$$

Nous avons éliminé le champ magnétique de l'expression en utilisant l'identité vectorielle $(\mathbf{a}\times\mathbf{b})\cdot(\mathbf{c}\times\mathbf{d}) = (\mathbf{a}\cdot\mathbf{c})(\mathbf{b}\cdot\mathbf{d}) - (\mathbf{a}\cdot\mathbf{d})(\mathbf{b}\cdot\mathbf{c})$, et utilisé le comportement du champ lointain $\lim_{r\to\infty}\widehat{\mathbf{r}}\cdot\mathbf{E}_\mathrm{s} = 0$; nous avons en outre utilisé la relation [40] :

$$\mathbf{B}_\mathrm{s}(\mathbf{r})\underset{r\to\infty}{=}(\varepsilon_\mathrm{e}\epsilon_0\mu_\mathrm{e}\mu_0)^{\frac{1}{2}}\,\widehat{\mathbf{r}}\times\mathbf{E}_\mathrm{s} \tag{184}$$

L'autre contribution à la force optique $\boldsymbol{\sigma}_\mathrm{r}$ correspond au flux de la quantité de mouvement prélevé au champ incident :

$$\boldsymbol{\sigma}_\mathrm{r}\underset{r\to\infty}{=} -\frac{v_\mathrm{e}}{4I(\mathbf{0})}r^2\left\{\varepsilon_\mathrm{e}\epsilon_0\int\widehat{\mathbf{r}}\,\mathrm{Re}\left\{\mathbf{E}_\mathrm{s}^*\cdot\mathbf{E}_\mathrm{exc} + \mathbf{E}_\mathrm{exc}^*\cdot\mathbf{E}_\mathrm{s}\right\}d\Omega_r\right.$$

$$\left.+\frac{1}{\mu_\mathrm{e}\mu_0}\int_\Omega\widehat{\mathbf{r}}\,\mathrm{Re}\left\{\mathbf{B}_\mathrm{s}^*\cdot\mathbf{B}_\mathrm{exc} + \mathbf{B}_\mathrm{exc}^*\cdot\mathbf{B}_\mathrm{s}\right\}d\Omega_r\right\}$$

$$= -\frac{1}{2I(\mathbf{0})}\lim_{r\to\infty}r^2\left(\frac{\varepsilon_\mathrm{e}\epsilon_0}{\mu_\mathrm{e}\mu_0}\right)^{1/2}\int\widehat{\mathbf{r}}\,\mathrm{Re}\left\{\mathbf{E}_\mathrm{s}^*\cdot\mathbf{E}_\mathrm{exc} + \mathbf{E}_\mathrm{exc}^*\cdot\mathbf{E}_\mathrm{s}\right\}d\Omega_r \tag{185}$$

où nous avons de nouveau éliminé le champ magnétique en employant les mêmes techniques décrites après l'éq.(183) et utilisant $\lim_{r\to\infty}\mathbf{B}_\mathrm{e}(\mathbf{r})\underset{r\to\infty}{=}(\varepsilon_\mathrm{e}\epsilon_0\mu_\mathrm{e}\mu_0)^{\frac{1}{2}}\,\widehat{\mathbf{r}}\times\mathbf{E}_\mathrm{e}$.

9   Quelques résultats des travaux récents

Après avoir mis au point des techniques numériquement stables de calcul de diffusion multiple de sphères isotropes dans les années 1999-2000, j'ai travaillé à étendre ces techniques de calcul aux systèmes composés d'objets de composition plus compliquée. Notamment, j'ai mis au point des techniques de calcul des matrices-T de sphères enrobées concentriques et non-concentriques et ainsi que des matrices-T de sphères avec des inclusions sphériques.

La matrice-T d'un système composé d'un grand nombre d'objets contient une grande quantité d'information. Un autre axe de travail consiste à en extraire l'information qui nous intéresse. Parmi les différents types d'information que nous avons pu extraire, on trouve les matrices de diffusion ainsi que les sections efficaces totales et différentielles de diffusion. Pour des systèmes de géométrie aléatoire, les sections efficaces moyennées sur les orientations sont souvent plus significatives qu'une section efficace dans une orientation donnée. D'autres informations d'intérêt que nous avons explorées sont les sections efficaces d'absorption des objets individuels, et les forces optiques sur les différents objets du système.

Mes études les plus récentes concernent l'élaboration de nouvelles théories différentielles pour le calcul des matrices-T d'objets de forme non-sphériques et composés de matériaux isotropes ou anisotropes. Bien

que plusieurs techniques de calcul de matrice-T pour des objets tridimensionnels existent déjà, elles sont souvent limitées par la taille et/où la non-sphéricité des objets qu'elles peuvent décrire. L'espoir est que ces nouvelles techniques qui exploitent les récents progrès dans la théorie des réseaux de diffraction (FFF ou «Fast Fourier Factorization» et algorithmes de propagation de la matrice-S) puissent étendre le domaine de tels calculs. Mes derniers travaux dans ce domaine consistent en une technique et un code de calcul pour la matrice-T de sphères composées d'un matériau anisotrope. Une formulation théorique pour les objets de forme non-sphérique est déjà terminée, et la programmation est commencée.

9.1 Solutions récursives de la matrice T à diffusion multiple

La solution récursive des $T^{(j,k)}$ par inversion d'une matrice de dimension $N^2 \times 2p_{\max} \times 2p_{\max}$ rencontre souvent des problèmes d'inversion. Rien n'empêche de résoudre les N équations donnant les matrices $T^{(j)}$, mais ces matrices ne sont pas carrées mais de dimension $2p_{\max} \times 2p'_{\max}$. La taille de $p'_{\max}$ est relativement mal contrôlée et de l'ordre de $p'_{\max} = [n'_{\max}\,(n'_{\max}+1)]$ avec $n'_{\max} \simeq kD_{\mathrm{syst}}$ où D_{syst} est de l'ordre de la taille (diamètre) du système. Cette technique nécessite donc de calculer des ordres multipolaires élevés quand le système devient grand.

Afin de tenter de palier ces difficultés Chew[36] et d'autres auteurs[38] ont développé une méthode récursive pour calculer les $T^{(j)}$ dans les années 1990. L'idée est qu'on peut construire les matrices $T_N^{(j)}$ pour un système à N-objets à partir des matrices $T_{N-1}^{(j)}$. Chaque addition d'un objet serait accompagnée par une inversion de matrice décrivant un seul diffuseur et non pas tous les N objets à la fois. Commençant la méthode avec un seul objet, on répète le procédé jusqu'au nombre d'objets voulu.

Certains chercheurs qui ont tenté d'utiliser la formulation formellement correcte de Chew ont rapidement découvert de grandes instabilités numériques. Ils ont publié leurs difficultés dans le journal du IEEE en 2000, et il est maintenant «bien connu» que la méthode récursive «ne marche pas» pour résoudre les équations de diffusion multiple[39].

De notre côté, nous avons rencontré les mêmes problèmes en 1999 et développé une formulation récursive parfaitement stable basée sur les matrices-T en paires du système, $T_N^{(k,j)}$. Avant d'entamer le procédé récursif, il faut calculer les N matrices-T de chacun des objets isolés, $t^{(1)}$, $t^{(2)}$, ..., $t^{(N)}$. Dans la majorité des applications que nous avons traitées jusqu'ici, nous avons adopté le choix particulièrement simples des sphères isotropes puisque les matrices $t^{(j)}$ sont diagonales et particulièrement simples à calculer dans ce cas.

Notre procédé pour calculer les $T_N^{(j,k)}$ est d'ajouter les diffuseurs au système un à un dans un ordre arbitraire, en calculant les matrices $T_N^{(j,k)}$ à chaque étape. Si l'on a les matrices $T_{N-1}^{(k,j)}$ pour un système contenant $N-1$ objets, on peut calculer la matrice $T_N^{(N,N)}$ du N^e objet ajouté au système en effectuant une inversion de matrice effectuée dans un espace d'ondes partielles décrivant une seule particule [15, 20] :

$$T_N^{(N,N)} = t^{(N)} \left[\mathbb{I} - \sum_{j,k=1}^{N-1} H^{(N,k)}\, T_{N-1}^{(k,j)}\, H^{(j,N)}\, t^{(N)} \right]^{-1} \tag{186}$$

En général, la matrice qu'il faut inverser est de dimension $2p_{\max} \times 2p_{\max}$. Une fois que nous avons la matrice $T_N^{(N,N)}$, nous pouvons obtenir les matrices $T_N^{(N,k)}$ et $T_N^{(j,N)}$ par multiplications matricielles :

$$T_N^{(N,k)} = T_N^{(N,N)} \sum_{i=1}^{N-1} H^{(N,i)}\, T_{N-1}^{(i,k)} \qquad\qquad k \neq N \tag{187}$$

$$T_N^{(j,N)} = \sum_{i=1}^{N-1} T_{N-1}^{(j,i)}\, H^{(i,N)}\, T_N^{(N,N)} \qquad\qquad j \neq N \tag{188}$$

On peut également modifier les matrices $T_{N-1}^{(j,k)}$; avec $j \neq N, k \neq N$ afin qu'elles tiennent compte de la présence de la particule N :

$$T_N^{(j,k)} = T_{N-1}^{(j,k)} + \sum_{i=1}^{N-1} T_{N-1}^{(j,i)}\, H^{(i,N)}\, T_N^{(N,k)} \qquad\qquad j,k \neq N \tag{189}$$

Nous avons vérifié et utilisé notre méthode par de nombreuses études (refs : [2], [10]-[13] et [17]-[18]).

9.2   Solutions itératives de la matrice-T à diffusion multiple

On peut également montrer que les matrices $T^{(j,k)}$ doivent satisfaire les N^2 conditions[16] :

$$T^{(j,k)} = t^{(j)} \sum_{l=1, l \neq j}^{N} H^{(j,l)} T^{(l,k)} \qquad j \neq k$$

$$T^{(j,j)} = t^{(j)} + t^{(j)} \sum_{l=1, l \neq j}^{N} H^{(j,l)} T^{(l,j)} \tag{190}$$

Si on désigne par l'indice q un ordre d'itération, on peut formuler ces équations comme une solution itérative :

$$T_q^{(j,k)} = t^{(j)} \sum_{l=1, l \neq j}^{N} H^{(j,l)} T_{q-1}^{(l,k)} \qquad j \neq k$$

$$T_q^{(j,j)} = t^{(j)} + t^{(j)} \sum_{l=1, l \neq j}^{N} H^{(j,l)} T_{q-1}^{(l,j)} \tag{191}$$

où on initialise l'itération avec :

$$T_0^{(j,k)} = t^{(j)} H^{(j,k)} t^{(k)} \qquad\qquad j \neq k \qquad j,k = 1, ..., N$$
$$T_0^{(j,j)} = t^{(j)} \qquad\qquad\qquad\qquad j = 1, ..., N \tag{192}$$

Les diagrammes de Feynman qui correspondent à ces termes sont donnés sur la figure 6. Un trait plein correspond à un propagateur (ici une matrice H) et les cercles correspondent matrices $t^{(j)}$ des objets.
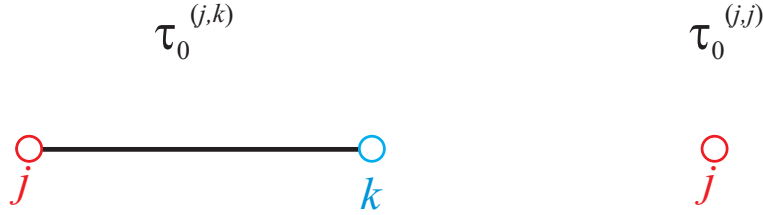
FIG. 6 – Diagrammes de Feynman à l'ordre zéro dans la formulation itérative de $T_0^{(j,k)}$ et de $T_0^{(j,j)}$

La première itération des équations (191) donne :

$$T_1^{(j,k)} = t^{(j)} \sum_{l \neq j}^{N} H^{(j,l)} T_0^{(l,k)} = t^{(j)} H^{(j,k)} T_0^{(k,k)} + t^{(j)} \sum_{l \neq j, l \neq k}^{N} H^{(j,l)} T_0^{(l,k)}$$

$$= t^{(j)} H^{(j,k)} t^{(k)} + t^{(j)} \sum_{l \neq j, l \neq k}^{N} H^{(j,l)} t^{(l)} H^{(l,k)} t^{(k)} \qquad j \neq k \qquad j,k = 1, ..., N$$

$$T_1^{(j,j)} = t^{(j)} + t^{(j)} \sum_{l \neq j}^{N} H^{(j,l)} T_0^{(l,j)}$$

$$= t^{(j)} + t^{(j)} \sum_{l \neq j}^{N} H^{(j,l)} t^{(l)} H^{(l,j)} t^{(j)} \qquad\qquad j = 1, ..., N \tag{193}$$

Les nouveaux diagrammes de Feynman introduits par cette itération sont présentés sur la figure 7. Dans ces diagrammes, le trait en pointillés entre deux matrices $t^{(j)}$ signifie qu'il s'agit du même diffuseur.

$$\tau_1^{(j,k)} \qquad\qquad\qquad \tau_1^{(j,j)}$$
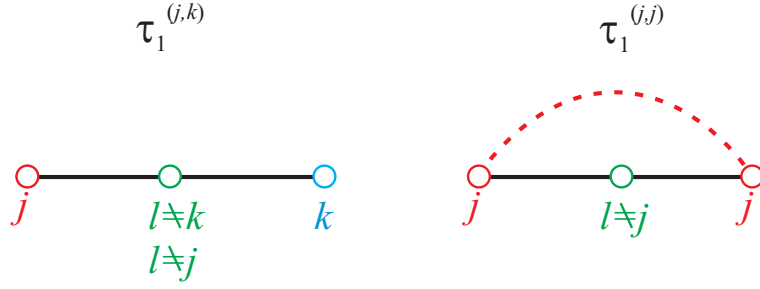
FIG. 7 – Diagrammes de Feynman ajoutés à $T^{(j,k)}$ et $T^{(j,j)}$ dans la première itération de $T_1^{(j,k)}$ et de $T_1^{(j,j)}$

La deuxième itération donne :

$$T_2^{(j,k)} = t^{(j)} \sum_{l \neq j}^{N} H^{(j,l)}\, T_1^{(l,k)} = t^{(j)}\, H^{(j,k)}\, T_1^{(k,k)} + t^{(j)} \sum_{l \neq j, l \neq k}^{N} H^{(j,l)}\, T_1^{(l,k)}$$

$$= t^{(j)}\, H^{(j,k)}\, t^{(k)} + \underbrace{t^{(j)}\, H^{(j,k)} t^{(k)} H^{(k,j)}\, t^{(j)}\, H^{(j,k)}\, t^{(k)}}_{a)} + t^{(j)}\, H^{(j,k)} t^{(k)} \underbrace{\sum_{l \neq k, l \neq j}^{N} H^{(k,l)}\, t^{(l)}\, H^{(l,k)}\, t^{(k)}}_{b)}$$

$$+ t^{(j)} \sum_{l \neq j, l \neq k}^{N} H^{(j,l)}\, t^{(l)}\, H^{(l,k)}\, t^{(k)} + t^{(j)} \underbrace{\sum_{l \neq j, l \neq k}^{N} H^{(j,l)}\, T_1^{(l,k)} t^{(l)}\, H^{(l,j)}\, t^{(j)}\, H^{(j,k)}\, t^{(k)}}_{c)}$$

$$+ t^{(j)} \underbrace{\sum_{l \neq j, l \neq k}^{N} \sum_{m \neq l, m \neq k, m \neq j}^{N} H^{(j,l)}\, t^{(l)}\, H^{(l,m)}\, t^{(m)}\, H^{(m,k)}\, t^{(k)}}_{d)} \qquad\qquad j \neq k$$

$$T_2^{(j,j)} = t^{(j)} + t^{(j)} \sum_{l \neq j}^{N} H^{(j,l)}\, T_1^{(l,j)}$$

$$= t^{(j)} + t^{(j)} \sum_{l \neq j}^{N} H^{(j,l)}\, t^{(l)}\, H^{(l,j)}\, t^{(j)} + t^{(j)} \underbrace{\sum_{l \neq j}^{N} \sum_{m \neq l, m \neq j}^{N} H^{(j,l)}\, t^{(l)}\, H^{(l,m)}\, t^{(m)}\, H^{(m,j)}\, t^{(j)}}_{e)} \qquad (194)$$

et leurs diagrammes de Feynman correspondants introduits par cette itération sont présentés sur la figure 8.

La méthode itérative a l'avantage de permettre de comprendre l'association entre les matrices $T^{(j,k)}$ et des développements diagrammatiques. On remarque au passage, que ces matrices $T^{(j,k)}$ permettent une séparation plus naturelle de certaines classes de diagrammes que ce qu'on obtiendrait en développant les matrices $T^{(j)}$ du genre Foldy Lax. L'analyse «diagrammatique» démontre également pourquoi les algorithmes de calcul des matrices $T^{(j,k)}$ sont généralement plus fiables que les algorithmes de calcul pour les matrices $T^{(j)}$. On voit sur les figures 6 -8 que les propagateurs dans une matrice $T^{(j,k)}$ se trouvent toujours entre deux matrices-T individuelles (on se rappelle que ces matrices $t^{(j)}$ sont naturellement tronquées). Les diagrammes qui correspondent aux matrices $T^{(l)} J^{(l,0)}$ où $T^{(l)} J^{(l,j)}$ des équations (117) ou (118) par contre ont des propagateurs «libres» (c'est-à-dire. qu'ils ne se terminent pas sur un coté sur des matrices-T). Puisqu'il n'y a pas de troncature naturelle pour les propagateurs, les algorithmes de calcul des matrices $T^{(j)}$ sont assez sensibles aux troncatures de l'espace multipolaire.

En exploitant les associations diagrammatiques comme celles des figures 6-8, on peut espérer élaborer de nouvelles techniques pour l'étude de milieux aléatoires.
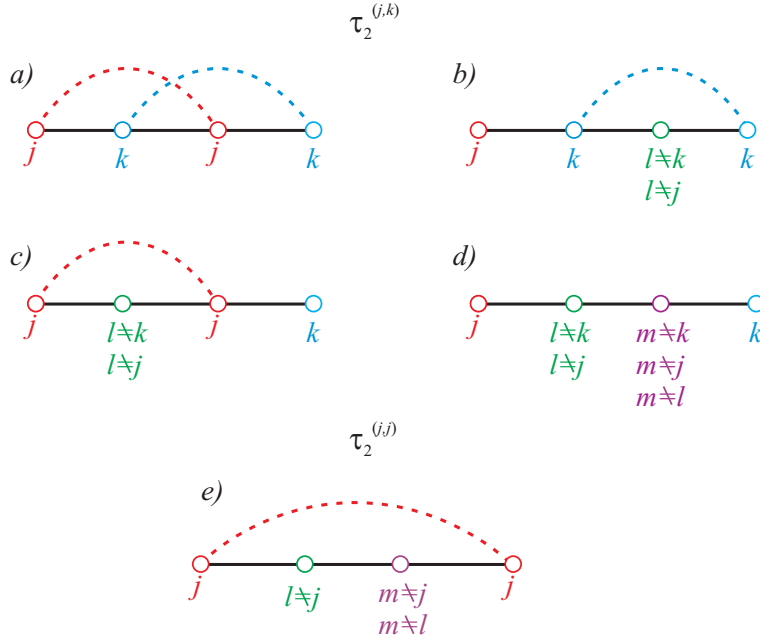
$$\tau_2^{(j,k)}$$

$$\tau_2^{(j,j)}$$

Fig. 8 – Diagrammes de Feynman ajoutés à $T^{(j,k)}$ et $T^{(j,j)}$ dans la première itération de $T_2^{(j,k)}$ et de $T_2^{(j,j)}$

9.3 Matrices de diffusion et sections efficaces

Une fois que nous avons calculé la matrice-T d'un système hétérogène, il nous reste à extraire les quantités d'intérêt physique. Souvent celles-ci peuvent être exprimées en termes de matrices de diffusion ou de sections efficaces. Ces quantités sont les plus utiles quand l'onde incidente sur tout le système est représentable en première approximation par une onde plane. On peut généraliser ces concepts à des champs incidents inhomogènes, mais l'analyse se complique. Nous avons déjà parlé d'une telle situation en section 8.10 pour les forces optiques et dans la Ref.[8]

Pour comparer les résultats numériques avec l'expérience, il est souvent pratique de décrire les états de polarisation par rapport au plan de diffusion (parfois appelé plan d'incidence). Le plan de diffusion est défini comme le plan qui contient la direction du détecteur, $\widehat{\mathbf{r}}$, et le vecteur d'onde de l'onde incidente, $\mathbf{k}_i$. On définit deux vecteurs orthogonaux à $\mathbf{k}_i$ qui sont respectivement parallèles et perpendiculaires au plan de diffusion $\hat{\mathbf{e}}_{\parallel,i}$ et $\hat{\mathbf{e}}_{\perp,i}$, tels que :

$$\hat{\mathbf{e}}_{\parallel,i} \wedge \hat{\mathbf{e}}_{\perp,i} = \mathbf{k}_i \tag{195}$$

On peut maintenant exprimer une onde plane incidente sur le système par :

$$\mathbf{E}_i = E \exp\left(i\mathbf{k}_i \cdot \mathbf{r}\right)\left(e_\parallel \hat{\mathbf{e}}_{\parallel,i} + e_\perp \hat{\mathbf{e}}_{\perp,i}\right) \tag{196}$$

Les coefficients sans dimension $e_\parallel$ et $e_\perp$ sont des nombres complexes qui déterminent la phase et la polarisation de l'onde. On impose que $\left|e_\parallel\right|^2 + \left|e_\perp\right|^2 = 1$, afin que $\|\mathbf{E}_i\|^2 = E^2$.

De même, on peut définir deux vecteurs unitaires $\hat{\mathbf{e}}_\parallel$ et $\hat{\mathbf{e}}_\perp$ transverses à $\widehat{\mathbf{r}}$ tels que :

$$\hat{\mathbf{e}}_\parallel \wedge \hat{\mathbf{e}}_\perp = \widehat{\mathbf{r}} \tag{197}$$

En champ lointain, on peut écrire le champ diffusé $\mathbf{E}_s$ comme :

$$\lim_{r \to \infty} \mathbf{E}_s\left(r, \theta, \phi\right) = \frac{\exp(ikr)}{ikr}\left[E_{s,\parallel}\hat{\mathbf{e}}_\parallel + E_{s,\perp}\hat{\mathbf{e}}_\perp\right] \tag{198}$$

La matrice de diffusion dans les coordonnées sphériques s'exprime en terme d'une matrice 2×2 :

$$\begin{pmatrix} E_{s,\parallel} \\ E_{s,\perp} \end{pmatrix} = E\,\frac{\exp(ikr)}{ikr}\begin{pmatrix} S_{\parallel\parallel} & S_{\parallel\perp} \\ S_{\perp\parallel} & S_{\perp\perp} \end{pmatrix}\begin{pmatrix} e_\parallel \\ e_\perp \end{pmatrix} \tag{199}$$

qui donne les coefficients $E_{s,\parallel}$ et $E_{s,\perp}$ en termes de $e_\parallel$ et $e_\perp$.

Il faut calculer les quatre éléments de la matrice de diffusion, $S_{\parallel\parallel}(\theta,\phi)$, $S_{\parallel\perp}(\theta,\phi)$, $S_{\perp\parallel}(\theta,\phi)$, et $S_{\perp\perp}(\theta,\phi)$ à partir de la matrice-T. Pour ce calcul, il faut faire une rotation de la matrice T afin que l'axe z soit confondu avec $\mathbf{k}_i$. L'angle ϕ est défini par rapport à l'axe x du système dans lequel est calculée la matrice-T. On peut calculer analytiquement les coefficients sur la base multipolaire (voir l'éq.(44)). Pour une polarisation parallèle au plan de diffusion les coefficients sont :

$$a_{\parallel,h,\nu\mu} = i^{\nu+1}\sqrt{\pi(2\nu+1)}\left[\delta_{\mu,1}e^{-i\phi} + \delta_{\mu,-1}e^{i\phi}\right]$$
$$a_{\parallel,e,\nu\mu} = i^{\nu+1}\sqrt{\pi(2\nu+1)}\left[\delta_{\mu,1}e^{-i\phi} - \delta_{\mu,-1}e^{i\phi}\right] \tag{200}$$

Pour une polarisation perpendiculaire au champ incident les coefficients sont :

$$a_{\perp,h,\nu\mu} = i^{\nu}\sqrt{\pi(2\nu+1)}\left[\delta_{\mu,1}e^{-i\phi} - \delta_{\mu,-1}e^{i\phi}\right]$$
$$a_{\perp,e,\nu\mu} = i^{\nu}\sqrt{\pi(2\nu+1)}\left[\delta_{\mu,1}e^{-i\phi} + \delta_{\mu,-1}e^{i\phi}\right] \tag{201}$$

On peut maintenant écrire les coefficients de l'onde diffusée par chaque objet dans un agrégat en utilisant les matrices T, $\tau^{(j,k)}$:

$$f_{\parallel,\perp}^{(j)} = \sum_k \exp\left(ik\widehat{\mathbf{z}}\cdot\mathbf{x}_k\right)T^{(j,k)}\,a_{\parallel,\perp} \tag{202}$$

On obtient ensuite les matrices S en termes des coefficients de diffusion $f^{(j)}$[2] :

$$S_{\parallel\parallel} = \sum_{j=1}^N \exp\left(-ik\widehat{\mathbf{r}}\cdot\mathbf{x}_j\right)\sum_{n,m}e^{im\phi}i^{-n+1}\left[\overline{u}_n^m(\cos\theta)f_{\parallel,h,nm}^{(j)} + \overline{s}_n^m(\cos\theta)f_{\parallel,e,nm}^{(j)}\right]$$

$$S_{\parallel\perp} = \sum_{j=1}^N \exp\left(-ik\widehat{\mathbf{r}}\cdot\mathbf{x}_j\right)\sum_{n,m}e^{im\phi}i^{-n+1}\left[\overline{u}_n^m(\cos\theta)f_{\perp,h,nm}^{(j)} + \overline{s}_n^m(\cos\theta)f_{\perp,e,nm}^{(j)}\right]$$

$$S_{\perp\perp} = -\sum_{j=1}^N \exp\left(-ik\widehat{\mathbf{r}}\cdot\mathbf{x}_j\right)\sum_{n,m}e^{im\phi}i^{-n}\left[\overline{s}_n^m(\cos\theta)f_{\perp,h,nm}^{(j)} + \overline{u}_n^m(\cos\theta)f_{\perp,e,nm}^{(j)}\right]$$

$$S_{\perp\parallel} = -\sum_{j=1}^N \exp\left(-ik\widehat{\mathbf{r}}\cdot\mathbf{x}_j\right)\sum_{n,m}e^{im\phi}i^{-n}\left[\overline{s}_n^m(\cos\theta)f_{\parallel,h,nm}^{(j)} + \overline{u}_n^m(\cos\theta)f_{\parallel,e,nm}^{(j)}\right] \tag{203}$$

On peut utiliser cette matrice S afin de prédire le champ diffusé par un agrégat de diffuseurs. Nous avons tout récemment trouvé un très bon accord entre les résultats prédits par cette technique et des mesures sur la diffusion effectuées dans le domaine micro-onde dans une chambre anéchoïque.[2] Nous venons d'obtenir un contrat de recherche ANR afin d'étudier l'absorption dans des agrégats de géométrie aléatoire du type «suie».

Les sections efficaces totales sont d'autres quantités d'intérêt physique, surtout quand nous sommes moins concernés par la polarisation du champ. Les sections efficaces sont définies en termes de vecteur de Poynting qui décrit le flux d'énergie électromagnétique. La section efficace différentielle est définie par :

$$\frac{d\sigma_{\text{scat}}^{\text{syst}}(\theta,\phi,\theta_i,\phi_i)}{d\Omega} \equiv \lim_{r\to\infty}r^2\frac{\widehat{\mathbf{r}}\cdot\mathbf{S}_{\text{scat}}^{\text{syst}}(\mathbf{r})}{\|\mathbf{S}_{\text{inc}}\|}$$
$$= \lim_{r\to\infty}r^2\frac{\left\|\sum_j^N\mathbf{E}_s^{(j)}(\mathbf{r})\right\|^2}{\|\mathbf{E}_{\text{inc}}\|^2} \tag{204}$$

où $\mathbf{S}_{\text{scat}}^{\text{syst}}$ est le vecteur de Poynting du champ diffusé par tous les N objets du système :

$$\mathbf{S}_{\text{scat}}^{\text{syst}} \equiv \frac{1}{2}\text{Re}\left\{\sum_{j,l}^N\mathbf{E}_s^{(j)}\wedge\mathbf{H}_s^{(l)*}\right\} \tag{205}$$

Puisque la section efficace différentielle est déterminée par le module du champ diffusé, on peut l'évaluer à partir de la matrice de diffusion de l'équation (199). La section efficace totale de diffusion

est en principe simplement obtenue par intégration sur tous les angles solides de la section efficace différentielle. Néanmoins, l'expression souvent assez compliquée de $d\sigma_{\text{scat}}/d\Omega$ peut rendre cette intégration assez fastidieuse. Il est plus efficace d'exploiter la présence d'harmoniques sphériques vectorielles afin d'intégrer numériquement $d\sigma_{\text{scat}}/d\Omega$ afin d'obtenir une formule analytique pour $\sigma_{\text{scat}}^{\text{syst}}$ directement en termes des coefficients de diffusion $f^{(j)}$:

$$\sigma_{\text{scat}}^{\text{syst}}(\theta_{\text{i}}, \phi_{\text{i}}) \equiv \int \frac{d\sigma_{\text{scat}}^{\text{syst}}(\theta, \phi, \theta_{\text{i}}, \phi_{\text{i}})}{d\Omega} d\Omega$$

$$= \frac{1}{k^2} \sum_{j,l}^{N} \text{Re}\left\{ f^{(j)\dagger} J^{(j,l)} f^{(l)} \right\}. \tag{206}$$

Pour d'autres types de sections efficaces comme la section efficace d'extinction, la forme différentielle n'a pas une signification physique particulière et il n'y a que la section efficace totale qui nous intéresse. La section efficace d'extinction s'écrit :

$$\sigma_{\text{ext}}^{\text{syst}}(\theta_{\text{i}}, \phi_{\text{i}}) \equiv \frac{1}{2} \lim_{r \to \infty} \frac{r^2}{\|\mathbf{S}_{\text{inc}}\|} \int \hat{\mathbf{r}} \cdot \sum_j \text{Re}\left\{ \mathbf{E}_{\text{i}} \wedge \mathbf{H}_{\text{s}}^{(j)*} + \mathbf{E}_{\text{s}}^{(j)} \wedge \mathbf{H}_{\text{i}}^* \right\} d\Omega$$

$$= -\frac{1}{k^2} \sum_j \text{Re}\left\{ a^\dagger f^{(j)} \right\} \tag{207}$$

Il est également possible de définir des sections efficaces d'absorption individuelles, $\sigma_{\text{abs}}^{(j)}$, pour chacun des objets j dans le système. Si le milieu externe est transparent, on obtient la formule :

$$\sigma_{\text{abs}}^{(j)} = -\frac{1}{k^2} \text{Re}\left\{ \left[f^{(j)} \right]^\dagger \left[\mathbb{I} + \left[t^{(j)} \right]^{-1} \right] f^{(j)} \right\} \tag{208}$$

et l'absorption totale est simplement la somme de toutes les sections efficaces individuelles :

$$\sigma_{\text{abs}}^{\text{syst}} = \sum_{j=1}^{N} \sigma_{\text{abs}}^{(j)} \tag{209}$$

Dans le cas d'un milieu extérieur transparent, la conservation de l'énergie donne une formule alternative pour l'absorption totale :

$$\sigma_{\text{abs}}^{\text{syst}} = \sigma_{\text{ext}}^{\text{syst}} - \sigma_{\text{scat}}^{\text{syst}} \tag{210}$$

ce qui nous donne un moyen de vérifier les calculs. Dans le projet ANR «suie», nous utiliserons ces formules afin d'étudier l'absorption dans des agrégats aléatoires.

Pour un système de géométrie aléatoire, des moyennes sur toutes les orientations du système ont souvent plus d'intérêt que les sections efficaces dans une orientation donnée. De nouveau, de telles moyennes peuvent en principe être effectuées de façon numérique, mais sont largement facilitées par des formules analytiques.

La moyenne sur les orientations de la section efficace d'extinction est donnée par exemple par la formule[16] :

$$\langle \sigma_{\text{ext}}^{\text{syst}} \rangle_o = -\frac{2\pi}{k^2} \sum_{j,k=1}^{N} \text{Re}\left[\text{Tr}\left\{ T_N^{(j,k)} J^{(k,j)} \right\} \right] \tag{211}$$

alors que la moyenne sur les orientations de la section efficace de diffusion est donnée par la formule[16] :

$$\langle \sigma_{\text{scat}}^{\text{syst}} \rangle_o = \frac{2\pi}{k^2} \text{Re}\left\{ \sum_{j,k,i,l}^{N} \text{Tr}\left\{ \left[T_N^{(j,l)} \right]^\dagger J^{(j,k)} T_N^{(k,i)} J^{(i,l)} \right\} \right\} \tag{212}$$

9.4 Forces optiques

On se rappelle que la force optique utilisant la forme de Minkowski du tenseur de Maxwell s'écrit :

$$\mathbf{F}_{\text{o}} \equiv \frac{I(\mathbf{0})}{v_{\text{b}}} \boldsymbol{\sigma}_{\text{f}}(\mathbf{x}) \equiv \varphi \frac{P_{\text{i}}}{v_{\text{b}}} \mathbf{Q}_{\text{f}}(\mathbf{x}) \tag{213}$$

où $I(\mathbf{0})$ est l'irradiance du faisceau à l'origine, P_{i} la puissance du faisceau, et $\boldsymbol{\sigma}_{\mathrm{f}}(\mathbf{x})$ dépend de la position $\mathbf{x}$ de la particule.[8]

On veut calculer la force sur une particule j du système. Afin de travailler sur un scalaire, on calcule la projection de cette force selon une direction $\widehat{\mathbf{c}}$ où l'orientation de $\widehat{\mathbf{c}}$ est spécifiée par des angles θ, et ϕ :

$$\mathbf{F}_{\mathrm{o}}^{(j)} \cdot \widehat{\mathbf{c}} \equiv \frac{I(\mathbf{0})}{v_{\mathrm{b}}} \sigma_{\mathrm{f}}^{(j)}(\theta, \phi, \mathbf{x}) \tag{214}$$

Comme nous avons vu en section 8.10.3, on peut décomposer σ_{f} en deux termes :

$$\sigma_{\mathrm{f}}^{(j)} = \sigma_{\mathrm{r}}^{(j)} - \sigma_{\mathrm{a}}^{(j)} \tag{215}$$

L'expression pour $\sigma_{\mathrm{a}}^{(j)}$ est :

$$\sigma_{\mathrm{a}}^{(j)}(\theta, \phi, \mathbf{x}) \equiv \hat{\mathbf{c}} \cdot \boldsymbol{\sigma}_{\mathrm{a}} = \frac{1}{2I(\mathbf{0})} \left(\frac{\varepsilon_{\mathrm{e}} \epsilon_0}{\mu_{\mathrm{e}} \mu_0} \right)^{1/2} \lim_{r \to \infty} r^2 \int_{\Omega} \widehat{\mathbf{c}} \cdot \widehat{\mathbf{r}} \, \mathbf{E}_{\mathrm{s}}^{(j),*} \cdot \mathbf{E}_{\mathrm{s}}^{(j)} \, d\Omega$$

$$= \frac{1}{k^2} f^{(j),\dagger}(\mathbf{x}) \, \Lambda(\theta, \phi) \, f^{(j)}(\mathbf{x}) \tag{216}$$

où la matrice analytique $\Lambda(\theta, \phi)$ est obtenue en décomposant le champ en ondes multipolaires et en effectuant une intégration sur l'angle solide. La matrice $\Lambda(\theta, \phi)$ s'écrit :

$$\Lambda(\theta, \phi) \equiv \mathrm{D}(\phi, \theta, 0) \, \Upsilon \, \mathrm{D}^{\dagger}(\phi, \theta, 0) \tag{217}$$

où $\mathrm{D}(\phi, \theta, 0)$ est la matrice de rotation et Υ une matrice qui s'écrit :

$$\Upsilon \equiv \left[\begin{array}{cc} \Xi & \Theta \\ \Theta & \Xi \end{array} \right] \tag{218}$$

où les blocs $\Theta_{nm,\nu\mu}$ et $\Xi_{nm,\nu\mu}$ s'écrivent :

$$\Theta_{nm,\nu\mu} = \frac{m}{n(n+1)} \delta_{m,\mu} \delta_{n,\nu}$$

$$\Xi_{nm,\nu\mu} = \delta_{m,\mu} \frac{i}{\sqrt{(2n+1)(2\nu+1)}} \left(\frac{\delta_{\nu,n-1}}{n} \sqrt{(n^2-1)(n^2-m^2)} \right.$$

$$\left. - \frac{\delta_{\nu,n+1}}{\nu} \sqrt{(\nu^2-1)(\nu^2-m^2)} \right) \tag{219}$$

La matrice de rotation $\mathrm{D}(\alpha, \beta, \gamma)$ s'écrit :

$$\mathrm{D}(\alpha, \beta, \gamma) \equiv \left[\begin{array}{cc} \mathcal{D}(\alpha, \beta, \gamma) & 0 \\ 0 & \mathcal{D}(\alpha, \beta, \gamma) \end{array} \right] \tag{220}$$

et les éléments du bloc $\mathcal{D}(\alpha, \beta, \gamma)$ sont donnés par :

$$[\mathcal{D}(\alpha, \beta, \gamma)]_{\nu\mu,nm} = \delta_{n,\nu} \exp(i\mu\alpha) \, d_{\mu m}^{(n)}(\beta) \exp(im\gamma) \tag{221}$$

Les éléments $d_{\mu m}^{(n)}$ sont standard[32].

Effectuant un calcul analogue pour σ_{r}, nous trouvons :

$$\sigma_{\mathrm{r}}^{(j)}(\theta, \phi, \mathbf{x}) \equiv \hat{\mathbf{c}} \cdot \boldsymbol{\sigma}_{\mathrm{r}} = -\frac{1}{2I(\mathbf{0})} \left(\frac{\varepsilon_{\mathrm{b}} \epsilon_0}{\mu_{\mathrm{b}} \mu_0} \right)^{1/2} \lim_{r \to \infty} r^2 \int_{\Omega} \hat{\mathbf{c}} \cdot \widehat{\mathbf{r}} \, \mathrm{Re} \left\{ \mathbf{E}_{\mathrm{s}}^* \cdot \mathbf{E}_{\mathrm{exc}} + \mathbf{E}_{\mathrm{exc}}^* \cdot \mathbf{E}_{\mathrm{s}} \right\} d\Omega$$

$$= -\frac{1}{k^2} \mathrm{Re} \left\{ f^{(j),\dagger}(\mathbf{x}) \, \Lambda(\theta, \phi) \left[t^{(j)} \right]^{-1} f^{(j)}(\mathbf{x}) \right\} \tag{222}$$

Nous avons utilisé ces formules pour calculer le piégeage d'une particule dans des pincettes optiques[8], ainsi que les forces optiquement induites entre particules ou «binding»[5].

9.5 Matrices-T des objets sans symétrie sphérique

De façon analogue à la décomposition du champ sur une base multipolaire (voir les éqs.(47)-(49)), nous pouvons mettre les fonctions d'un développement général d'un champ sur les harmoniques sphériques (voir l'équation (54)) dans une matrice colonne :

$$
\left.\begin{bmatrix} \overline{\vdots} \\ E_{Y,p} \\ \vdots \\ \hline \vdots \\ E_{X,p} \\ \vdots \\ \hline \vdots \\ E_{Z,p} \\ \vdots \end{bmatrix} \right\} (n_{\max} + 1)^2 \tag{223}
$$

La dimension de cette matrice est déterminée par la troncature de l'espace multipolaire où $n_{\max}$ est le plus grand nombre quantique multipolaire. Décomposant de la même manière le champ $\mathbf{D}$, la relation $\mathbf{D} = \epsilon_0 \varepsilon(\mathbf{r}) \mathbf{E}$ dans un milieu hétérogène devient :

$$
[\mathbf{D}] = \epsilon_0 Q_\varepsilon [\mathbf{E}] \tag{224}
$$

où Q_ε est une matrice composée de 9 blocs, chacune de dimension $(n_{\max} + 1)^2$:

$$
Q_\varepsilon = \begin{pmatrix} Q_{\varepsilon YY} & Q_{\varepsilon YX} & Q_{\varepsilon YZ} \\ Q_{\varepsilon XY} & Q_{\varepsilon XX} & Q_{\varepsilon XZ} \\ Q_{\varepsilon ZY} & Q_{\varepsilon ZX} & Q_{\varepsilon ZZ} \end{pmatrix} \tag{225}
$$

La matrice Q_ε dépend de la distance r et doit être construite d'une manière très spécifique afin d'éviter des instabilités numériques induites par la troncature de l'espace multipolaire. Ce procédé est tiré des progrès récents sur la théorie des réseaux et est expliqué en détail dans la référence [7].

La relation 224 et les équations de Maxwell sur les harmoniques sphériques vectorielles des équations (55) et (56) forment un système d'équations complètes pour déterminer le champ. On peut manipuler ces équations afin d'obtenir une seule équation différentielle ordinaire par rapport à la variable r :

$$
\frac{d[F]}{dr} = M(r)[F] \tag{226}
$$

La matrice colonne $[F]$ est constituée de fonctions multipliant les harmoniques vectorielles $\mathbf{X}$ et $\mathbf{Z}$ des champs $\mathbf{E}$ et $\mathbf{H}$ dans des développements du type (54)) :

$$
[F(r)] = \begin{bmatrix} [E_X] \\ [E_Z] \\ [\widetilde{H}_X] \\ [\widetilde{H}_Z] \end{bmatrix} \tag{227}
$$

où le champ $\widetilde{\mathbf{H}} \equiv Z_0 \mathbf{H} = \sqrt{\frac{\mu_0}{\epsilon_0}} \mathbf{H}$ a la même dimension que le champ $\mathbf{E}$. La matrice M est composée de

4×4 blocs qui s'écrivent :

$$M_{11} = -\frac{\mathbb{I}}{r} \quad , \quad M_{12} = M_{13} = 0 \quad , \quad M_{14} = i\mu\frac{\omega}{c}\mathbb{I}$$

$$M_{21} = -\frac{a}{r}Q_{\varepsilon YY}^{-1}Q_{\varepsilon YX} \quad , \quad M_{22} = -\frac{\mathbb{I}}{r} - \frac{a}{r}Q_{\varepsilon YY}^{-1}Q_{\varepsilon YZ}$$

$$M_{23} = i\frac{\omega}{c}\left(\left(\frac{c}{r\omega}\right)^2 aQ_{\varepsilon YY}^{-1}a - \mu\mathbb{I}\right) \quad , \quad M_{24} = 0$$

$$M_{31} = i\frac{\omega}{c}\left(Q_{\varepsilon ZY}Q_{\varepsilon YY}^{-1}Q_{\varepsilon YX} - Q_{\varepsilon ZX}\right) \quad , \quad M_{32} = i\frac{\omega}{c}\left(Q_{\varepsilon ZY}Q_{\varepsilon YY}^{-1}Q_{\varepsilon YZ} - Q_{\varepsilon ZZ}\right) \tag{228}$$

$$M_{33} = \frac{1}{r}\left(Q_{\varepsilon ZY}Q_{\varepsilon YY}^{-1}a - \mathbb{I}\right) \quad , \quad M_{34} = 0$$

$$M_{41} = i\frac{\omega}{c}\left(Q_{\varepsilon XX} - Q_{\varepsilon XY}Q_{\varepsilon YY}^{-1}Q_{\varepsilon YX} - \frac{1}{\mu}\left(\frac{ac}{\omega r}\right)^2\right) \quad , \quad M_{42} = i\frac{\omega}{c}\left(Q_{\varepsilon XZ} - Q_{\varepsilon XY}Q_{\varepsilon YY}^{-1}Q_{\varepsilon YZ}\right)$$

$$M_{43} = -Q_{\varepsilon XY}Q_{\varepsilon YY}^{-1}\frac{a}{r} \quad , \quad M_{44} = -\frac{\mathbb{I}}{r}$$

où $\mathbb{I}$ est la matrice unité et « a » est une matrice diagonale d'éléments $a_p\delta_{p,q}$ avec $a_p = \sqrt{n(n+1)}$.

On peut donc en principe construire une matrice-T d'un objet en intégrant l'équation différentielle de l'éq.(226) avec une méthode de tir. Le départ de la méthode de tir est la sphère inscrite isotrope (voir figure 4 : section 8.6), et l'on arrête l'intégration numérique à la sphère circonscrite. Si la région hétérogène entre ces deux sphères est suffisamment profonde, il faut compléter cette intégration par une technique de propagation de matrice-S afin d'éviter des instabilités numériques qui s'installent lors d'une intégration sur une grande longueur.

Par la suite, nous avons généralisé cette technique à des objets composés de matériaux anisotropes.[3, 4] Dans de tels matériaux, il faut commencer la méthode de tir à partir d'une sphère inscrite anisotrope. Nous avons constaté qu'une formulation d'une matrice-T d'une sphère anisotrope n'existait pas auparavant. Nous avons donc formulé une solution semi-analytique d'une matrice-T d'une sphère caractérisée par une anisotropie générale.[4] Nous avons commencé tout récemment à explorer les applications numériques de cette technique[1].

10   Orientation future des travaux

Actuellement, je continue des études sur les forces optiquement induites dans des systèmes composés de plusieurs diffuseurs. Dans le cadre d'un projet ANR concernant des agrégats de particules absorbantes du type «suie», je prépare des études sur l'absorption dans des grands agrégats ayant des géométries aléatoires. Les premières études vont traiter des agrégats de sphères, mais je prépare aussi la programmation sur des agrégats composés d'objets de forme non-sphérique.

En employant la théorie de type Mie sur les ordinateurs modernes, on peut traiter des sphères isolées homogènes de très grandes tailles par rapport à la longueur d'onde. Des raffinements concernant la théorie de Mie permettent de traiter également des sphères ayant des inhomogénéités radiales jusqu'à de très grandes tailles. Pourtant, à l'heure actuelle, il y a des limitations plutôt sévères sur les tailles et non-sphéricités qu'on peut traiter quand il s'agit d'objets de forme non-sphérique ou d'objets composés de matériaux anisotropes. Je compte porter un regard particulier sur les possibilités d'étendre les domaines de calcul aux objets et agrégats de grande taille.

Dans l'avenir, j'aimerais aussi explorer sur le plan théorique et numérique les possibilités de combiner les techniques de calcul analytique utilisant les ondes multipolaires avec les techniques diagrammatiques venant du formalisme de fonctions de Green. Un des objectifs de ces investigations serait d'améliorer la modélisation des milieux aléatoires étendus, du type peintures et revêtements. Un autre axe d'intérêt serait l'étude des effets des défauts dans des milieux ordonnés du genre cristaux photoniques. En particulier les structures de type opale semblent présenter un intérêt particulier. L'utilisation des fonctions de Green permet également de faire des études sur la densité d'états locaux dans ces structures compliquées.

11 Résumés d'études

11.1 Interactions effectives

[27, 31]

Dans mes premiers travaux, il s'agissait fréquemment de calculer les transitions, souvent exotiques, entre divers états d'excitation nucléaires et les états fondamentaux. Les noyaux nucléaires contiennent en général un grand nombre de composants nucléoniques (protons, neutrons ou autres). Souvent, les transitions concernent surtout les nucléons dans les couches «externes» des noyaux. On essayait donc de calculer les transitions dans un espace «tronqué» ou «effectif» qui ne contienne que les nucléons externes qui participent à la transition. Néanmoins, puisque les nucléons sont en interaction forte avec les autres composants du noyau, de tels calculs ne sont possibles que si l'on détermine des interactions effectives entre les nucléons des couches externes qui tiennent compte des interactions résiduelles avec les autres composants du noyau. Il fallait également déterminer une matrice G qui estime les effets dus aux états hautement énergétiques des noyaux qui ne sont pas contenus dans l'espace modèle.

Dans ce contexte, j'ai développé des logiciels pour les calculs suivants :
– Calcul des éléments de la matrice G de Brueckner sur une base d'oscillateurs harmoniques pour les potentiels de Paris, Bonn et de Reid. Ce logiciel est capable de calculer la matrice G pour un noyau de masse arbitraire (l'approximation courante dite de «angle average» n'a pas été employée).
– Calcul d'interactions effectives pour une région de masse quelconque (en utilisant les résultats de la matrice G décrits ci-dessus). Nous avons publié une communication rapide qui montre une amélioration des résultats pour le potentiel dit de Bonn-A dans la couche s-d.[31]

Nous avons également effectué des calculs fournissant les résultats dans la couche f-p et dans la région du plomb.[1**]

11.2 Opérateurs effectifs

[29]

Afin de calculer les amplitudes de transition entre différents états nucléaires, nous avons développé un formalisme qui permet la construction de ce qui est essentiellement une «formule de réduction» pour le problème à N-corps non-relativiste. Bien que les techniques de diagramme de Feynman aient été utilisées depuis longtemps dans la théorie à N-corps, ce travail définit rigoureusement la connexion entre le modèle des couches, les interactions effectives et les opérateurs effectifs.

11.3 Calcul du paramètre de densité des niveaux des noyaux chauds

[28]

Nous avons utilisé des interactions nucléon-nucléon réalistes (Paris et Bonn) pour calculer la dépendance en fonction de la température du paramètre de densité de niveaux, $a_{\text{eff}} = [E(T) - E(0)]/T^2$. On sait que a_{eff} décroît dans les collisions d'ions lourds de $\approx A/8$ à $\approx A/13$ quand la température croît de 2 à 5 Mev. Nos résultats sont qualitativement satisfaisants. Cependant, l'énergie d'excitation est plus élevée que la valeur attendue ; ce résultat mériterait une étude plus détaillée.

11.4 Capture d'électrons et décroissance dans les étoiles présupernovae

[30]

En collaboration avec M. Aufderheide, G.E. Brown, P. Vogel, nous avons étudié le rôle des interactions faibles (capture d'électrons et décroissances bêta) dans l'évolution des étoiles en fin de vie. Pour les coeurs riches en neutrons ($Y_e = Z/A$ compris entre 0.42 et 0.43), nous montrons que les noyaux avec $A > 60$, négligés jusqu'à présent dans les calculs de l'évolution stellaire, peuvent contribuer de façon significative au taux de capture d'électrons et au taux de décroissance bêta dans les dernières étapes de l'évolution stellaire.

11.5 Décroissance double bêta :

[26, 29],[2**]

Nous avons calculé la réduction du taux de décroissance double bêta, avec et sans neutrinos, pour les noyaux ^{76}Ge, ^{82}Se et ^{100}Mo. Pour cela, nous avons utilisé les interactions effectives obtenues par les potentiels nucléon-nucléon dits de Paris et de Bonn. Contrairement à d'autres auteurs, qui, pour des raisons de simplification, avaient supprimé les corrections de self-énergie dans le calcul du spectre d'énergie de 1-particule, nous avons inclus ces corrections. Ainsi, nous avons pu éviter le problème souvent rencontré de l'instabilité de QRPA (quasi-particle random phase approximation) au voisinage de $g_{pp} = 1$. La correspondance entre nos résultats (obtenus sans paramètre phénoménologique) et l'expérience est encourageante.

11.6 Brisure spontanée de symétrie

[25]

Pour mieux comprendre l'application des techniques du potentiel effectif dans les théories quantiques des champs comme la théorie ϕ^4, le modèle de Gross-Neveu, et le modèle de Nambu Jona-Lassinio, nous avons démontré que les techniques non-perturbatives du potentiel effectif donnent une solution exacte d'un modèle résolvable dans la limite $1/N \to 0$. Les résultats du modèle, dans le cas où N serait fini, nous permettent de faire des observations intéressantes sur l'effet tunnel entre dégénérescences de Goldstone. Notre traitement est aussi intéressant du point de vue des calculs de problèmes à N-corps. En effet, il évite l'apparition de l'instabilité RPA, «Random Phase Approximation» , pour des interactions fortes ; il montre tout au moins que «l'instabilité» RPA est la signature d'une transition de phase dans la limite $N \to \infty$.

11.7 Propagation des ondes et dispersion spatiale dans un milieu hétérogène

[24]

Ici, nous résolvons en priorité la dispersion spatiale d'une onde dans un milieu hétérogène. Après nous être intéressé à tous les domaines de fréquence, nous avons acquis des résultats intéressants quand la longueur d'onde se rapproche de la taille des micro-hétérogénéités. Physiquement, l'onde entre alors en résonance avec des diffuseurs. Nous utilisons une approximation quasi cristalline appliquée à la diffusion multiple. Dans les calculs, nous utilisons un modèle «ponctuel» de la matrice T complète des diffuseurs. Nous trouvons que la dispersion spatiale a pour conséquence de remplacer le seul mode de propagation d'un milieu homogène par une multitude de modes dans un milieu micro-hétérogène. A condition que la concentration des diffuseurs ne soit pas trop élevée, un seul mode peut se propager ; les autres modes ont des indices effectifs complexes, donc ils s'amortissent rapidement dans le milieu. Pour des fréquences voisines de la résonance, les parties imaginaires de ces indices diminuent de façon notable. Il existe alors une possibilité d'existence de nouveaux modes de propagation.

11.8 Approximation en champ moyen pour la construction de matrices-T complètes de sphères de taille finie et de diffuseurs flous

[23]

Notre but est d'insérer des modèles de matrices T complètes dans des formalismes de diffusion multiple. Dans cette optique, nous introduisons une méthode de construction de matrices T complètes extrêmement simplifiées, mais vérifiant la conservation d'énergie et le principe de causalité. Cette méthode fait approximation en remplaçant les champs à l'intérieur d'un diffuseur individuel par un champ moyen. De ce fait, elle permet une évaluation facile de la diffusion par des diffuseurs sphériques, irréguliers, et même flous (par exemple des agrégats fractals). Dans la limite quasi-statique de diffuseurs sphériques, nous retrouvons la limite «ponctuelle» introduite par «M. Nieuwenhuizen et co-auteurs» en 1992[*]. Contrairement au modèle ponctuel, nos modèles contiennent une dépendance en fonction du vecteur d'onde et donc font intervenir la dispersion spatiale. Cette propriété les rend légèrement plus compliqués que le modèle ponctuel mais, de ce fait, plus riches. En particulier, nos modèles satisfont la relation de Kramers-Krönig de causalité, contrairement au modèle ponctuel qui la viole. Actuellement, nous appliquons ce modèle à des théories de diffusion multiple. Dans les formalismes où nous l'avons employé jusqu'ici, nous trou-

vons un comportement physique bien supérieur à celui du modèle ponctuel et les instabilités de solution rencontrées dans le modèle ponctuel n'apparaissent pas.

[*] M.Nieuwenhuizen A. Lagendijk and B. van Tiggelen, Phys.Lett. A 169,191(1992).

11.9 Matrice-T électromagnétique et propriétés dynamiques effectives d'un milieu aléatoire

[22, 23]

Il s'agit ici d'étudier la réponse des paramètres constitutifs effectifs (permittivité et perméabilité magnétique) d'un matériau composite dans le domaine dynamique, c'est à dire pour tous les domaines de fréquence. Nous apportons des précisions et des réévaluations sur la notion de paramètre effectif. De nouvelles définitions sont proposées pour ces derniers. Nous appliquons ces formules de définition en effectuant une approximation dite approximation de potentiel cohérent (CPA), et nous résolvons les équations de dispersion afin d'extraire les observables physiques.

Afin de disposer de résultats exacts, nous calculons pour la première fois la matrice-T complète pour une sphère ayant à la fois une permittivité et une perméabilité magnétique qui diffèrent de celles du milieu ambiant. Nous trouvons que la condition d'unitarité, devant être vérifiée par toute matrice-T d'un système sans pertes, restreint sévèrement les formes que peuvent prendre les matrices T.

11.10 Facteurs de phase des ondes incidentes et sortantes dans la diffusion par des agrégats

[19, 21]

Nous étudions en détail les facteurs de phase associés aux ondes entrantes et sortantes lors de la diffusion multiple. Nous montrons que ces facteurs peuvent être traités de la même façon, et nous discutons en détail leur relation avec les matrices de translation-addition. Nous établissons également bon nombre de formules utiles dans les problèmes de diffusion multiple. Nous montrons le rôle important joué par les facteurs de phase dans les quantités contenant des interférences. Dans plusieurs cas, nous avons pu généraliser les résultats publiés. Nous avons également développé de nouvelles relations imposées par la réciprocité dans la diffusion par un agrégat. Nos résultats se simplifient de façon considérable en adoptant une convention où les matrices de translation-addition sont unitaires.

11.11 Modélisation de fibres optiques structurées avec un modèle unidimensionnel

[20]

Nous avons développé un modèle unidimensionnel pour le problème des fibres optiques structurées avec guidage dans un cœur d'air enrobé d'un cristal photonique, dites «holy fibers» . Le but est d'examiner la possibilité de guidage de faisceaux lasers de haute puissance. Nous utilisons pour cela une méthode numérique rapide et stable, et calculons les caractéristiques des modes de propagation dans de telles fibres. Nous avons mis en évidence la propriété «mono-mode» de ces fibres et l'importance du choix des propriétés du cœur afin d'éviter les «fuites» de lumière induites par diffraction.

11.12 Calculs des champs locaux par des techniques de matrices de transition

[2, 13, 15, 16, 17, 18]

Nous avons développé de nouvelles méthodes de calcul dans le cadre des matrices de transition afin de calculer les champs locaux dans des systèmes tridimensionnels fortement diffusants. Afin de garder toute l'information sur les champs locaux, et d'éviter les problèmes résultants des dimensions des matrices de translation, nous calculons les matrices de transition centrées sur les diffuseurs. Ces techniques ont l'avantage de faciliter des analyses systématiques des champs locaux pour toutes les directions incidentes possibles (des calculs sur les moyennes sur les orientations sont également effectués). De plus, nos méthodes réduisent le temps de calcul en exploitant une approche récursive.

11.13 Relations d'auto-consistance des matrices de transition et calculs de champs de diffusion

[16]

Dans cette étude nous avons obtenu des relations d'auto-consistance devant être satisfaites par les matrices de transition d'un système de diffuseurs. De telles relations servent à vérifier la stabilité numérique de notre méthode de calcul des matrices. Nous trouvons que notre méthode est fiable jusqu'à la précision des machines, dans tous les cas que nous avons testés. Dans cet article nous démontrons également l'utilité des matrices de transition dans le calcul des modifications du champ causé par la diffusion dépendante.

11.14 Absorption dans des systèmes de diffusion multiple et cohérente

[9, 10, 11, 19]

A l'Institut Fresnel et ailleurs, il est devenu possible de fabriquer de petits diffuseurs recouverts d'une couche d'un deuxième matériau. Si de tels diffuseurs sont distribués dans une matrice en densité suffisante, le milieu va fortement diffuser la lumière. On sait qu'une des conséquences de cette diffusion est de prolonger le chemin parcouru par lumière. En conséquence, un milieu chargé de petits diffuseurs recouverts d'une couche de matériau absorbant peut voir son absorption augmenter d'une façon considérable. Nous traitons de façon exacte la diffusion d'ondes électromagnétique par un système de plusieurs particules absorbantes. Nous sommes donc amenés à tenir compte de la diffusion multiple et cohérente puisque chaque onde «d'excitation» sur un diffuseur contient l'onde incidente sur le système mais aussi les ondes diffusées par chacun des autres diffuseurs. Dans cette étude, nous établissons des formules de calcul rigoureux de la matrice de transition d'un système où les diffuseurs sont des sphères avec plusieurs enrobages (pas nécessairement concentriques). Cette étude nous a amenés à définir une nouvelle quantité, la longueur d'absorption effective, $l_{\text{abs}}^{\text{eff}}$, qui permet d'estimer l'absorptivité d'un milieu présentant à la fois de l'absorption et de la diffusion. Le calcul de $l_{\text{abs}}^{\text{eff}}$ nous a amenés à mettre au point de nouvelles méthodes qui permettent la séparation des effets de diffusion cohérente de ceux de diffusion multiple. Cette technique s'avérera utile dans l'extrapolation des effets macroscopiques à partir des calculs sur les interactions microscopiques.

11.15 Calcul des forces optiques dans des faisceaux arbitraires en utilisant le théorème de translation-addition

[5, 8]

On établit des méthodes quasi-analytiques pour le calcul des forces optiques sur des particules micrométriques piégées dans des «pincettes» et pièges optiques. La décomposition du faisceau incident sur une base permet la description d'une grande variété de faisceaux incidents. L'utilité de cette étude se trouve dans le fait que les approximations les plus couramment utilisées dans le calcul des forces optiques ne sont que rarement valables dans la pratique. On démontre notamment que les résonances ont une influence considérable sur les amplitudes des forces optiques et même sur la position d'équilibre dans une pincette optique. Nous discutons aussi l'importance de la forme du faisceau d'une pincette optique afin d'établir le lien entre la forme et la puissance totale du faisceau.

11.16 Théorie différentielle de la diffusion de la lumière par un objet tri-dimensionnel

[7]

On développe la théorie différentielle de la diffraction de la lumière par un objet de forme quelconque décrit en coordonnées sphériques. Le champ est développé sur une base d'harmoniques sphériques vectorielles.

On réduit les équations de Maxwell à un système différentiel du premier ordre. On étend la technique dite «Fast Fourier Factorization» à des bases de fonctions vectorielles. On utilise l'algorithme de propagation de la matrice S afin d'éviter les instabilités numériques autrefois rencontrées dans de la théorie différentielle des réseaux de diffraction.

11.17 Théorie différentielle de la diffraction par des objets anisotropes de forme sphérique

[5]

Nous avons établi un développement en harmoniques sphériques vectorielles du champ à l'intérieur d'une sphère homogène composé d'un matériau anisotrope arbitraire. Ce développement nous permet d'étendre à ce problème une analyse du type de la théorie de Mie pour écrire les conditions aux limites à la surface de la sphère. Cette solution permet d'établir la première étape dans la formulation d'une théorie différentielle de diffraction pour un objet anisotrope de forme quelconque. Des applications sont actuellement en cours afin de mieux comprendre la diffusion par des poussières interstellaires anisotropes.[1]

11.18 Théorie différentielle de la diffraction par des objets anisotropes de forme arbitraire

[1, 3, 4]

Commencent avec une sphère inscrite à l'intérieur d'un objet anisotrope quelconque, on étend la théorie de la diffraction par un objet isotrope tri-dimensionnel de forme quelconque[7] aux objets anisotropes de forme quelconque. La théorie utilise la technique de «Fast Fourier Factorization» étendue à des bases de fonctions vectorielles et à des bases de fonctions scalaires arbitraires. Elle utilise l'algorithme de propagation de la matrice S afin d'éviter les instabilités numériques.

11.19 Méthode de la matrice T appliquée aux cristaux photoniques tridimensionnels

Généralement, les théories développées pour étudier les cristaux photoniques les supposent parfaitement périodiques et donc de dimensions infinies. Néanmoins, de nombreuses études ont récemment démontré que les effets de bord et les défauts dans les cristaux photoniques sont très importants, en pratique, sur les systèmes réels.

Une solution possible pour traiter des cristaux photoniques de taille finie est d'évaluer la matrice T pour chaque élément (diffuseur) d'un système et, ensuite, de construire la matrice-T du système tout entier à travers une théorie de diffusion multiple.

Comme beaucoup d'autres méthodes, on peut utiliser la matrice-T du système afin de calculer la carte de champ dans un cristal photonique, mais, plus important encore la formulation par matrice-T se prête à une extraction rapide d'un grand nombre de quantités physiques d'intérêt expérimental comme les sections efficaces et la matrice de (l'amplitude de) diffusion. Cette utilité s'est déjà avérée fructueuse lors de la comparaison avec l'expérience effectuée sur la diffusion par des agrégats (en amplitude et en phase) dans le domaine micro-ondes.[2]

12 Publications dans des journaux avec comité de lecture

Références

[1] *The T-matrix of the homogeneous anisotropic sphere : applications to orientation averaged resonant scattering*, B.Stout, M. Nevière, E. Popov, JOSA A **24**, pp. 1120-1130 (2007).

[2] *Amplitude and phase of light scattered by micro-scale aggregates of dielectric spheres : Comparison between theory and microwave analogy experiments*, P. Sabouroux, B. Stout, J-M. Geffrin, C. Eyraud, I. Ayranci, R. Vaillon, N. Selçuk, "Journal of Quantitative Spectroscopy & Radiative Transfer" **103**, pp.156-167 (2007).

[3] *Mie scattering by an anisotropic object. Part II : Arbitrary-shaped object – differential theory,* B.Stout, M. Nevière, E. Popov, JOSA A **23**, pp. 1124-1134 (2006).

[4] *Mie scattering by an anisotropic object. Part I : Homogeneous sphere*, B.Stout, M. Nevière, E. Popov, JOSA A, **23** , pp. 1111-1123 (2006).

[5] *Longitudinal optical binding of high optical contrast microdroplets in air*, M.Guillon, Olivier Moine, Brian Stout, Physical Review Letters 96 143902-(1-4) (2006)

[6] *Scattering efficiency of aggregated clusters of spheres : dependence on configuration and composition*, J.C. Auger, B.Stout, V. Martinez, JOSA A, **22** , pp. 2700-2708 (2005).

[7] *Light diffraction by a three-dimensional object : differential theory*, B.Stout, M. Nevière, E. Popov, JOSA A, **22** , pp. 2385-2404, (2005).

[8] *Optical force calculations in arbitrary beams by use of the vector addition theorem*, Olivier Moine and B.Stout, JOSA B, **22** , pp. 1620-1631, (2005).

[9] *Optical properties of an eccentrically located pigment within an air bubble*, J.C.Auger, Ruben G. Barrera, B.Stout, Progress in Organic Coatings, **49** , pp. 74-83, (2004).

[10] *Absorption in Multiple Scattering Systems of Coated Spheres*, B. Stout, C. Andraud, S.Stout, J.Lafait, J. Opt Soc. Am. A, **20**, pp. 1050-1059, (2003).

[11] *Absorption in Multiple Scattering Systems of Coated Spheres : Design applications,* B. Stout, C. Andraud, S.Stout, J.Lafait, Physica B, **338**, pp.121-125, (2003).

[12] *Multiple light scattering in multistratified media : model, experiment*, A. da Silva, C. Andraud, E.Charron, B.Stout, J.Lafait, Physica B, **338**, pp. 74-78, (2003).

[13] *A recursive centered T-Matrix algorithm to solve the multiple scattering equation : numerical validation*, J C Auger, B Stout, Journal of Quantitative Spectroscopy & Radiative Transfer, **79-80**, pp. 533-547, (2003).

[14] *Scattering efficiencies of aggregates of spherical particles*, J C Auger, R G Barrera, B Stout, Journal of Quantitative Spectroscopy & Radiative Transfer, **79-80**, pp. 521-531 (2003).

[15] *A Transfer Matrix Approach to Local Field Calculations in Multiple Scattering Problems*, B. Stout, J.C. Auger, Jacques Lafait, Journal of Modern Optics, **49**, pp. 2129-2152, (2002).

[16] *Complete field descriptions in three-dimensional multiple scattering problems : a transfer-matrix approach*, B Stout, C Andraud, D Prot, J Lafait, J C Auger and S Stout, J. Opt. A : Pure Appl. Opt. **4** S182-S187, (2002).

[17] *Local electric field enhancements and large third-order optical nonlinearity in nanocomposite materials*, D. Prot, B. Stout, K.Lafait, N.Pinçon,B Palpant and S Debrus, J. Opt. A : Pure Appl. Opt. **4** S99-S102, (2002).

[18] *Individual and Aggregate Scattering Matrices and Cross Sections : Conservation Laws and Reciprocity*, B.Stout, J.C.Auger, J.Lafait, Journal of Modern Optics, **48**, 2105-2128, (2001).

[19] *Scattering Properties of Rutile Pigments Located Eccentrically Within Microvoids*, J.C. Auger B. Stout, R.G. Barrera, F.Curiel, Journal of Quant Spect. & Rad. Transfer, **70**, 675-695, (2001).

[20] *Photonic Crystal Waveguides : A One Dimensional Model Theory*, B.Stout, S.Stout, M.Nevière, Journal of Electromagnetic Waves and Applications, **15**, pp. 961-988, (2001).

[21] *Observations and Calculations of Light Scattering from Clusters of Spheres*, S. Holler, J.C. Auger, B. Stout, Y. Pan, J.R. Bottiger, R.K. Chang, G. Videen, Applied Optics, **39**, pp. 6873-6887, (2000).

[22] *Dependent light scattering in dense heterogeneous media*, J.C. Auger, B. Stout, Jacques Lafait, Physica B **279**, pp. 21-24, (2000).

[23] *Momentum Dependent Electromagnetic T-matrix and Dynamic Effective Properties of Random Media*, Y.P. Pellegrini, D.B. Stout and P.Thibaudeau, Physica A, **241**, pp. 72-76, (1997).

[24] *Off-Shell Mean-Field Electromagnetic T-matrix of Finite Size Spheres and Fuzzy Scatterers*, Y.P. Pellegrini, D.B. Stout and P.Thibaudeau, Journal of Physics : Condensed Matter, **9** (1), pp. 177-191, (1997).

[25] *Spontaneous Symmetry Breaking in a Solvable Model*, D.B. Stout, Nuclear Physics A567 553-575 North Holland, (1994).

[26] *Two Neutrino Double Beta Decay and Self-Consistent Self-Energies*, D.B.Stout and T.T.S. Kuo, Physical Review Letters, **69** (13), (1992).

[27] *Bonn Potential and s-d Shell Effective Interaction*, M.F. Jiang and R. Machleidt D.B. Stout and T.T.S. Kuo, Phys. Rev. C46, 910, (1992).

[28] *Level Density Parameter of Nuclei at Finite Temperature*, D.B. Stout, C. Grégoire, T.T.S. Kuo, Nuclear Physics A530 94-110 North Holland, (1991).

[29] *Linked Diagram Expansions for the Transition Matrix and the Normalization of Model-Space Wave Functions*, D.B. Stout and T.T.S. Kuo, Nuclear Physics A526 90-108 North Holland, (1991).

[30] *Electron Capture and β-Decay in Presupernova stars*, M.B. Aufderheide and G.E. Brown, T.T.S. Kuo and D.B. Stout and P. Vogel, The Astrophysical Journal **362** 241, (1990).

[31] *Strength of Tensor Force and s-d-Shell Effective Interactions*, M.F. Jiang and R. Machleidt D.B. Stout and T.T.S. Kuo, Physical. Review. C Rapid Communications 40 R1857, 1989.

Autres Publications

[1**] Shell Model Interactions from Modern NN Potentials for Nuclei in the Pb Region, D.B. Stout and T.T.S. Kuo and Dan Strottman, (publication interne, Los Alamos National Laboratory)

[2**] Zero Neutrino Double Beta Decay with Self-Consistent Self-Energies, D.B.Stout (thèse)

[3**] Wave Propagation and Spatial Dispersion in Random Media, Y.P. Pellegrini, D.B. Stout and P.Thibaudeau (Proceedings Journées Maxwell 95, June 6-9, Bordeaux-Lac, CEA-CESTA BP2, F-33114, Le Barp, France (1995)).

Reférences générales

[32] A.R. Edmonds, *Angular Momentum in Quantum Mechanics*, Princeton University Press, Princeton New Jersey (1960).

[33] C. Cohen-Tannoudji, *Photons & Atomes - Introduction à l'électrodynamique quantique*, (InterEdition/ Editions du CNRS 1987).

[34] J.D. Jackson, *Classical Electrodynamics*, (John Wiley & Sons 1965).

[35] Leung Tsang, Jin Au Kong, Robert T. Shin, "Theory of Microwave Remote Sensing, Wiley Series in Remote Sensing", John Wiley & Sons, (1985).

[36] Weng Cho Chew, *Waves and Fields in Inhomogeneous Media* ; IEEE Press Series on Electromagnetic Waves, IEE Press, New York (1994).

[37] D. W. Mackowski, *Calculation of the T matrix and the scattering matrix for ensembles of spheres*, J. Opt. Soc. Am. **13**, 2266-2278, (1996).

[38] Y.C. Tzeng and A.K.Fung, *T-matrix approach to multiple scattering of EM waves from N-spheres*, Journal of Electr. Waves and Appl., **8**, (1994).

[39] P.R. Siqueira and K. Sarabandi *T-matrix Determination of Effective Permittivity for Three-Dimensional Dense Random Media*, IEEE Transactions on Antennas and Propagation, Vol 48, Febuary 2000.

[40] C. F. Bohren, D. R. Huffman, *Absorption and Scattering of Light by Small Particles* (Wiley-Interscience, New-York, 1983).

13   Appendices

A   Théorème de translation pour ondes partielles vectorielles

On prend un point M dans un système de coordonnées sphériques. On considère un second système de coordonnées sphériques centré sur la position $\mathbf{r}_0$. La position de M dans ce deuxième système centré sur $\mathbf{r}_0$ est :

$$\mathbf{r}' = \mathbf{r} - \mathbf{r}_0 \tag{A1}$$

Le théorème de translation exprime les ondes multipolaires du système d'origine en termes des ondes multipolaires centrées sur $\mathbf{r}_0$:

$$\boldsymbol{\Psi}^t\left(k\mathbf{r}\right) = \boldsymbol{\Psi}^t\left(k\mathbf{r}'\right) J(k\mathbf{r}_0) \qquad\qquad r' > r_0$$
$$\boldsymbol{\Psi}^t\left(k\mathbf{r}\right) = \mathcal{R}g\left\{\boldsymbol{\Psi}^t\left(k\mathbf{r}'\right)\right\} H(k\mathbf{r}_0) \qquad\qquad r' < r_0$$
$$\mathcal{R}g\left\{\boldsymbol{\Psi}^t\left(\mathbf{r}\right)\right\} = \mathcal{R}g\left\{\boldsymbol{\Psi}^t\left(\mathbf{r}'\right)\right\} J(k\mathbf{r}_0) \qquad\qquad \forall |r_0| \tag{A2}$$

où la matrice $J(k\mathbf{r}_0)$ est définie comme la partie régulière de $H(k\mathbf{r}_0)$, $J(k\mathbf{r}_0) \equiv \mathcal{R}g\left\{H(k\mathbf{r}_0)\right\}$, et $H(k\mathbf{r}_0)$ est la matrice de translation irrégulière. De façon explicite, $H(k\mathbf{r}_0)$ s'exprime :

$$H(k\mathbf{r}_0) = \left[\begin{array}{cc} A_{\nu\mu,nm}\left(kr_0, \theta_0, \phi_0\right) & B_{\nu\mu,nm}\left(kr_0, \theta_0, \phi_0\right) \\ B_{\nu\mu,nm}\left(kr_0, \theta_0, \phi_0\right) & A_{\nu\mu,nm}\left(kr_0, \theta_0, \phi_0\right) \end{array}\right]. \tag{A3}$$

On peut exprimer les éléments du bloc A en suivant le traitement de Tsang and Kong :

$$A_{\nu\mu,nm}(kr_0, \theta_0, \phi_0) = \frac{\gamma_{nm}}{\gamma_{\nu\mu}}\left(-1\right)^{\mu} \sum_{p=|n-\nu|}^{n+\nu} a\left(m, n| - \mu, \nu|p\right) a\left(n, \nu, p\right) h_p\left(kr_0\right) P_p^{m-\mu}\left(\cos\theta_0\right) e^{i(m-\mu)\phi_0} \tag{A4}$$

où les coefficients de normalisation sont définies :

$$\gamma_{nm} \equiv \sqrt{\frac{(2n+1)(n-m)!}{4\pi n(n+1)(n+m)!}} \tag{A5}$$

Les quantités $a\left(m, n|\mu, \nu|p\right)$ sont les coefficients de Gaunt et sont exprimées en termes des coefficients de Wigner $3j$:

$$a\left(m, n|\mu, \nu|p\right) = (-1)^{m+\mu}(2p+1)\left[\frac{(n+m)!\,(\nu+\mu)!\,(p-m-\mu)!}{(n-m)!\,(\nu-\mu)!\,(p+m+\mu)!}\right]^{1/2}$$
$$\times \left(\begin{array}{ccc} n & \nu & p \\ 0 & 0 & 0 \end{array}\right)\left(\begin{array}{ccc} n & \nu & p \\ m & \mu & -(m+\mu) \end{array}\right) \tag{A6}$$

Le facteur multiplicatif, $a\left(n, \nu, p\right)$, dans (A4), est défini par :

$$a\left(n, \nu, p\right) \equiv \frac{i^{\nu+p-n}}{2\nu(v+1)}\left[2\nu(\nu+1)(2\nu+1) + (\nu+1)(n-\nu+p+1)(n+\nu-p)\right.$$
$$\left. -\nu(\nu-n+p+1)(n+\nu+p+2)\right]$$
$$= i^{\nu+p-n}\frac{2\nu+1}{2\nu(v+1)}\left[\nu(\nu+1) + n(n+1) - p(p+1)\right] \tag{A7}$$

Les éléments du bloc matrice B s'écrivent :

$$B_{\nu\mu,nm}(kr_0, \theta_0, \phi_0) = \frac{\gamma_{nm}}{\gamma_{\nu\mu}}\left(-1\right)^{\mu+1} \sum_{p=|n-\nu|+1}^{n+\nu-1} a\left(m, n| - \mu, \nu|p, p-1\right) b\left(n, \nu, p\right)$$
$$h_p\left(kr_0\right) P_p^{m-\mu}\left(\cos\theta_0\right) e^{i(m-\mu)\phi_0} \tag{A8}$$

où $a\left(m, n|\mu, \nu|p, q\right)$ est un coefficient très similaire au coefficient de Gaunt :

$$a\left(m, n|\mu, \nu|p, q\right) = (-1)^{m+\mu}(2p+1)\left[\frac{(n+m)!\,(\nu+\mu)!\,(p-m-\mu)!}{(n-m)!\,(\nu-\mu)!\,(p+m+\mu)!}\right]^{1/2}$$
$$\times \left(\begin{array}{ccc} n & \nu & q \\ 0 & 0 & 0 \end{array}\right)\left(\begin{array}{ccc} n & \nu & p \\ m & \mu & -m-\mu \end{array}\right) \tag{A9}$$

et où

$$b\left(n,\nu,p\right) \equiv -i^{\nu+p-n}\frac{2\nu+1}{2\nu\left(\nu+1\right)}\left[\left(n+\nu+p+1\right)\left(\nu-n+p\right)\left(n-\nu+p\right)\left(n+\nu-p+1\right)\right]^{1/2}.$$

T matrix of the homogeneous anisotropic sphere: applications to orientation-averaged resonant scattering

Brian Stout, Michel Nevière, and Evgeny Popov

Institut Fresnel, Unité Mixte de Recherche 6133 associée au Centre National de la Recherche Scientifique, Case 161, Faculté des Sciences et Techniques, Centre de Saint Jérôme, 13397 Marseille Cedex 20, France

We illustrate some numerical applications of a recently derived semianalytic method for calculating the *T* matrix of a sphere composed of an arbitrary anisotropic medium with or without losses. This theory is essentially an extension of Mie theory of the diffraction by an isotropic sphere. We use this theory to verify a long-standing conjecture by Bohren and Huffman that the extinction cross section of an orientation-averaged anisotropic sphere is not simply the average of the extinction cross sections of three isotropic spheres, each having a refractive index equal to that of one of the principal axes. © 2007 Optical Society of America

OCIS codes: 290.5850, 050.1940, 000.3860, 000.4430.

1. INTRODUCTION

We recently formulated a semianalytic solution to the problem of diffraction (scattering) by a sphere composed of a material with a uniform anisotropic dielectric tensor $\bar{\bar{\varepsilon}}$ immersed in a homogeneous isotropic medium.[1] Due to the length of the detailed derivation, no numerical applications were presented at that time. One of the goals of this paper is to present some previously absent details necessary to the construction of numerical algorithms for generating the *T* matrix of an anisotropic sphere using this method and to provide some modified derivations of some of the formulas in the interest of improved clarity in numerical applications. Since our method can generate the *T* matrix for arbitrary anisotropic scatterers, we also begin to explore possible applications to multiple scattering, notably by calculating orientation averaged cross sections for use in independent scattering approximations.

Due to the previous lack of solutions for anisotropic scatterers, it has been commonplace in the literature to approximate the orientation average of the extinction cross section of an anisotropic sphere (denoted $\langle \sigma_{a,\text{ext}} \rangle_o$) by the "one-third rule" of averaging in which one simply averages the extinction cross sections of three isotropic spheres, i.e.,

$$\langle \sigma_{a,\text{ext}} \rangle_o \simeq \langle \sigma_{a,\text{ext}1/3} \rangle \equiv \tfrac{1}{3}\sigma_{1,\text{ext}} + \tfrac{1}{3}\sigma_{2,\text{ext}} + \tfrac{1}{3}\sigma_{3,\text{ext}}, \qquad (1)$$

where each of these extinction cross sections $\sigma_{i,\text{ext}}$ is the extinction cross section of a homogeneous sphere composed of a material of dielectric constant ε_i, $i=1,2,3$ corresponding to the dielectric constant of each of the three principal axes. Although one can demonstrate that this formula holds true for anisotropic scatterers in the dipole approximation,[2,3] in practice, it has, in fact, been extrapolated considerably beyond this domain. Bohren and Huffman conjectured in their book that this relation, in fact, does not hold true outside of the dipole approximation.[2]

We will demonstrate that they were correct in this regard as far as precise geometric resonant structures in the cross sections are concerned. Nevertheless, we find that in certain situations at least, the $\tfrac{1}{3}$ averaging rule frequently yields a reasonable approximation to overall trends in cross sections, and in certain circumstances, even quantitatively reproduces low-frequency resonance structures well beyond the regime in which the dipole approximation is valid. On the other hand, the $\tfrac{1}{3}$ averaging rule is much less reliable when applied to metallic or semiconductor materials.

Sections 2 and 3 review how to obtain general vector spherical harmonic expansions of both the external fields and the fields inside the anisotropic medium. In Section 3, we arrange for the internal and scattered fields to depend on the same number of independent expansion parameters through a Fourier-space discretization procedure that is somewhat different than that presented in our previous paper.[1] In Section 4, we show that the satisfaction of the boundary conditions can be obtained by inverting a matrix whose elements are given by analytical expressions. Finally, some numerical applications are presented in Section 5, together with a summary of the algorithm for determining the anisotropic sphere *T* matrix. We find that one can quite routinely calculate up to size parameters of the order of $2\pi R/\lambda \approx 5$. One can go to even higher size parameters provided that one invokes sufficiently sophisticated linear equation solvers (results for size parameters of $2\pi R/\lambda \approx 12$ appear in Fig. 2 and Table 2). All calculations are carried out in SI units, in the time-harmonic domain with an $\exp(-i\omega t)$ time dependence.

2. PLANE-WAVE SOLUTIONS IN A HOMOGENOUS ANISOTROPIC MEDIUM

We assume a sphere composed of a uniform anisotropic, nonmagnetic media ($\mu = \mu_0$), and allow the relative dielec-

tric tensor, $\bar{\bar{\varepsilon}}$, expressed in Cartesian coordinates, to have the most general possible form,

$$\bar{\bar{\varepsilon}} = \begin{bmatrix} \varepsilon_{xx} & \varepsilon_{xy} & \varepsilon_{xz} \\ \varepsilon_{yx} & \varepsilon_{yy} & \varepsilon_{yz} \\ \varepsilon_{zx} & \varepsilon_{zy} & \varepsilon_{zz} \end{bmatrix}, \tag{2}$$

where no special symmetry relations are assumed and the various tensor elements may be complex numbers.

Inside a homogenous anisotropic medium, the Maxwell equations result in the propagation equation,

$$\mathbf{curl}(\mathbf{curl\,E}) - k_0^2 \bar{\bar{\varepsilon}} \mathbf{E} = \mathbf{0}, \tag{3}$$

where $k_0 = \omega/c$ is the vacuum wavenumber with c as the speed of light in vacuum. It is well known that this equation allows solutions in the form of plane waves,

$$\mathbf{E(r)} = \mathbf{A(k)}\exp(i\mathbf{k}\cdot\mathbf{r}), \tag{4}$$

where $\mathbf{r} \equiv \mathbf{OM}$ is the radius vector of an arbitrary observation point M and $\mathbf{k}$ is the wave vector. Any solution to Eq. (3) can then be expressed as a superposition of plane waves.

Putting the plane-wave form of Eq. (4) into Eq. (3) imposes that

$$(k^2\mathbb{I} - (\mathbf{kk}) - k_0^2\bar{\bar{\varepsilon}})\mathbf{A} = \mathbf{0}, \tag{5}$$

where we introduced a tensor $(\mathbf{kk})$, with elements $(\mathbf{kk})_{i,j} \equiv k_i k_j$, defined $k^2 \equiv |\mathbf{k}|^2 = \mathrm{Tr}(\mathbf{kk})$, and represented the unit matrix as $\mathbb{I}$. We showed in detail in Ref. 1 how to solve this equation in a spherical coordinate system. Summarizing the principal results, we saw that the dielectric tensor in spherical coordinates, $\tilde{\bar{\varepsilon}}$,

$$\tilde{\bar{\varepsilon}} = \mathfrak{R}\bar{\bar{\varepsilon}}\mathfrak{R}^t \equiv \begin{bmatrix} \varepsilon_{rr} & \varepsilon_{r\theta} & \varepsilon_{r\phi} \\ \varepsilon_{\theta r} & \varepsilon_{\theta\theta} & \varepsilon_{\theta\phi} \\ \varepsilon_{\phi r} & \varepsilon_{\phi\theta} & \varepsilon_{\phi\phi} \end{bmatrix}, \tag{6}$$

was obtained using the Cartesian to spherical transformation matrix, $\mathfrak{R}$,

$$\mathfrak{R} = \begin{bmatrix} \sin\theta_k\cos\phi_k & \sin\theta_k\sin\phi_k & \cos\theta_k \\ \cos\theta_k\cos\phi_k & \cos\theta_k\sin\phi_k & -\sin\theta_k \\ -\sin\phi_k & \cos\phi_k & 0 \end{bmatrix}, \tag{7}$$

where θ_k and ϕ_k designate the spherical coordinate angles that define the direction of the vector $\mathbf{k}$ and $\mathfrak{R}^t$ is the transpose of this matrix.

We then showed that the four eigenvalues of the propagation equation in spherical coordinates, k_j $(j=1,4)$, were given by

$$\frac{k_1}{k_0} \equiv \tilde{k}_1 \equiv \sqrt{(\tilde{k}^2)'} = -\tilde{k}_3 = -\frac{k_3}{k_0},$$

$$\frac{k_2}{k_0} \equiv \tilde{k}_2 \equiv \sqrt{(\tilde{k}^2)''} = -\tilde{k}_4 = -\frac{k_4}{k_0}, \tag{8}$$

where

$$(\tilde{k}^2)' = \frac{\beta + \sqrt{\Delta}}{2\alpha}, \quad (\tilde{k}^2)'' = \frac{\beta - \sqrt{\Delta}}{2\alpha}, \tag{9}$$

with

$$\Delta \equiv \beta^2 - 4\alpha\gamma, \quad \alpha = \varepsilon_{rr},$$

$$\beta = \alpha(\varepsilon_{\theta\theta} + \varepsilon_{\phi\phi}) - \varepsilon_{r\theta}\varepsilon_{\theta r} - \varepsilon_{r\phi}\varepsilon_{\phi r}, \quad \gamma = \det(\tilde{\bar{\varepsilon}}) = \det(\bar{\bar{\varepsilon}}). \tag{10}$$

For lossy materials, $\tilde{\bar{\varepsilon}}$ is necessarily non-Hermitian, and the classical theory of crystal optics no longer holds. Nevertheless, Eqs. (8)–(10) remain valid, the only difference being that $\tilde{k}_1, \tilde{k}_2,$ and $\sqrt{\Delta}$ are now complex and are chosen to have positive imaginary parts. Taking $\mathbf{A}(k_j\hat{\mathbf{r}}_k)$ to yield the eigenvector $\mathbf{A}^{(j)}$ corresponding to an eigenvalue k_j, we saw in Ref. 1 that $\mathbf{A}(k_3\hat{\mathbf{r}}_k) = \mathbf{A}(-k_1\hat{\mathbf{r}}_k)$ and $\mathbf{A}(k_4\hat{\mathbf{r}}_k) = \mathbf{A}(-k_2\hat{\mathbf{r}}_k)$. Since our goal is to represent arbitrary field solutions on a set of independent eigenvectors, in plane-wave representations, such as those of Eq. (31) below, we will consequently integrate over the full $\mathbf{k}$-space, keeping only the $j=1,2$ eigenvectors.

Since the eigenvectors are solutions of a system of linear homogenous equations, they are determined by the interrelations of their components. Denoting the projections of an eigenvector $\mathbf{A}^{(j)}$ on the unit vectors $\hat{\mathbf{r}}_k$, $\hat{\boldsymbol{\theta}}_k$, and $\hat{\boldsymbol{\phi}}_k$, respectively, by $A_r^{(j)}$, $A_\theta^{(j)}$ and $A_\phi^{(j)}$, Eq. (5) in spherical coordinates leads to

$$\varepsilon_{rr}A_r^{(j)} + \varepsilon_{r\theta}A_\theta^{(j)} + \varepsilon_{r\phi}A_\phi^{(j)} = 0,$$

$$\varepsilon_{\theta r}A_r^{(j)} + (\varepsilon_{\theta\theta} - \tilde{k}_j^2)A_\theta^{(j)} + \varepsilon_{\theta\phi}A_\phi^{(j)} = 0,$$

$$\varepsilon_{\phi r}A_r^{(j)} + \varepsilon_{\phi\theta}A_\theta^{(j)} + (\varepsilon_{\phi\phi} - \tilde{k}_j^2)A_\phi^{(j)} = 0. \tag{11}$$

A. Eigenvector Algorithm

The solutions to Eqs. (11) for arbitrary anisotropy and propagation directions can be broken up into three principal cases.

Case 1: The condition

$$\begin{vmatrix} \varepsilon_{r\phi} & \varepsilon_{r\theta} \\ \varepsilon_{\theta\phi} & \varepsilon_{\theta\theta} - \tilde{k}_j^2 \end{vmatrix} \neq 0 \tag{12}$$

is satisfied for both $\tilde{k}_1$ and $\tilde{k}_2$. Both eigenvectors then contain radial components and can be expressed as

$$\mathbf{A}^{(j)} = \tilde{A}^{(j)}\boldsymbol{\Gamma}^{(j)}, \quad \boldsymbol{\Gamma}^{(j)} \equiv (\hat{\mathbf{r}}_k + \Gamma_\theta^{(j)}\hat{\boldsymbol{\theta}}_k + \Gamma_\phi^{(j)}\hat{\boldsymbol{\phi}}_k), \tag{13}$$

with

$$\Gamma_\theta^{(j)} = \frac{\begin{vmatrix} \varepsilon_{rr} & \varepsilon_{r\phi} \\ \varepsilon_{\theta r} & \varepsilon_{\theta\phi} \end{vmatrix}}{\begin{vmatrix} \varepsilon_{r\phi} & \varepsilon_{r\theta} \\ \varepsilon_{\theta\phi} & \varepsilon_{\theta\theta} - \tilde{k}_j^2 \end{vmatrix}}, \quad \Gamma_\phi^{(j)} = -\frac{\begin{vmatrix} \varepsilon_{rr} & \varepsilon_{r\theta} \\ \varepsilon_{\theta r} & \varepsilon_{\theta\theta} - \tilde{k}_j^2 \end{vmatrix}}{\begin{vmatrix} \varepsilon_{r\phi} & \varepsilon_{r\theta} \\ \varepsilon_{\theta\phi} & \varepsilon_{\theta\theta} - \tilde{k}_j^2 \end{vmatrix}}. \tag{14}$$

Case 2: There is one and only one of the eigenvalues k_1 or k_2 for which

$$\begin{vmatrix} \varepsilon_{r\phi} & \varepsilon_{r\theta} \\ \varepsilon_{\theta\phi} & \varepsilon_{\theta\theta} - \tilde{k}_j^2 \end{vmatrix} \neq 0. \tag{15}$$

When this case presents itself, we rename the eigenvalues if necessary so that k_1 is associated with the nonzero determinant.

If the following additional condition is satisfied,

$$\begin{vmatrix} \varepsilon_{rr} & \varepsilon_{r\phi} \\ \varepsilon_{\theta r} & \varepsilon_{\theta\phi} \end{vmatrix} = 0, \tag{16}$$

then the eigenvectors are

$$\mathbf{A}^{(1)} = \tilde{A}^{(1)}\mathbf{\Gamma}^{(1)}, \quad \mathbf{\Gamma}^{(1)} = -\frac{\varepsilon_{r\phi}}{\varepsilon_{rr}}\hat{\mathbf{r}}_k + \hat{\boldsymbol{\phi}}_k,$$

$$\mathbf{A}^{(2)} = \tilde{A}^{(2)}\mathbf{\Gamma}^{(2)}, \quad \mathbf{\Gamma}^{(2)} = \hat{\boldsymbol{\theta}}_k. \tag{17}$$

If, on the other hand,

$$\begin{vmatrix} \varepsilon_{rr} & \varepsilon_{r\phi} \\ \varepsilon_{\theta r} & \varepsilon_{\theta\phi} \end{vmatrix} \neq 0, \tag{18}$$

then $\mathbf{\Gamma}_1$ is determined from Eqs. (13) and (14), while $\mathbf{A}^{(2)}$ is given by

$$\mathbf{A}^{(2)} = \tilde{A}^{(2)}\mathbf{\Gamma}^{(2)}, \quad \mathbf{\Gamma}^{(2)} = \hat{\boldsymbol{\theta}}_k - \frac{\varepsilon_{r\theta}}{\varepsilon_{r\phi}}\hat{\boldsymbol{\phi}}_k. \tag{19}$$

Case 3: The condition

$$\begin{vmatrix} \varepsilon_{r\phi} & \varepsilon_{r\theta} \\ \varepsilon_{\theta\phi} & \varepsilon_{\theta\theta} - \tilde{k}_j^2 \end{vmatrix} = 0 \tag{20}$$

is satisfied for both $\tilde{k}_1$ and $\tilde{k}_2$. The eigenvectors are given by

$$\mathbf{A}^{(1)} = \tilde{A}^{(1)}\mathbf{\Gamma}^{(1)}, \quad \mathbf{\Gamma}^{(1)} = \hat{\boldsymbol{\phi}}_k,$$

$$\mathbf{A}^{(2)} = \tilde{A}^{(2)}\mathbf{\Gamma}^{(2)}, \quad \mathbf{\Gamma}^{(2)} = -\frac{\varepsilon_{r\theta}}{\varepsilon_{rr}}\hat{\mathbf{r}}_k + \hat{\boldsymbol{\theta}}_k. \tag{21}$$

Uniaxial and isotropic materials correspond to Case 3 of the above general procedure, and were already discussed in Ref. 1.

3. FIELD DEVELOPMENTS IN A VECTOR SPHERICAL HARMONIC BASIS

Any general vector field can be developed by radial functions multiplying a spherical harmonic basis:

$$\mathbf{E}(\mathbf{r}) = \sum_{n=0}^{\infty} \sum_{m=-n}^{m=n} [E_{nm}^{(Y)}(r)\mathbf{Y}_{nm}(\theta,\phi)$$

$$+ E_{nm}^{(X)}(r)\mathbf{X}_{nm}(\theta,\phi) + E_{nm}^{(Z)}(r)\mathbf{Z}_{nm}(\theta,\phi)]$$

$$= \sum_{p=0}^{\infty} [E_p^{(Y)}(r)\mathbf{Y}_p(\theta,\phi)$$

$$+ E_p^{(X)}(r)\mathbf{X}_p(\theta,\phi) + E_p^{(Z)}(r)\mathbf{Z}_p(\theta,\phi)], \tag{22}$$

where we have denoted by $\mathbf{Y}_{nm}$, $\mathbf{X}_{nm}$, and $\mathbf{Z}_{nm}$, the *nor-*

malized vector spherical harmonics[4] (see Appendix A). The last line of Eq. (22) introduces the now common procedure of reducing to a single summation by defining a generalized index p for which any integer value of p corresponds to a unique n, m pair[5]: $p = n(n+1) + m$. The inverse relations between a value of p and the corresponding n, m are given by

$$n(p) = \text{Int}\sqrt{p},$$

$$m(p) = p - n(p)[n(p) + 1]. \tag{23}$$

One should remark that the summation begins in Eq. (22) with $n = m = 0$ since the vector spherical harmonic $\mathbf{Y}_{00}$ is nonzero even though $\mathbf{X}_{00}$ and $\mathbf{Z}_{00}$ are identically zero (cf. Appendix A).

The scattering problem for any spherical scatterer can be readily solved provided that we can determine the $E_p^{(Y)}$, $E_p^{(X)}$, $E_p^{(Z)}$ functions and their magnetic field counterparts $H_p^{(Y)}$, $H_p^{(X)}$, $H_p^{(Z)}$ for all p both inside and outside the scatterer. This is the objective of the remainder of this section.

A. Partial Wave Expansions of the External Fields
The dielectric behavior of the isotropic and homogenous external medium is not described by a tensor, but by a (possibly complex) scalar, ε_e, and the propagation equation in the external medium is

$$\mathbf{curl}(\mathbf{curl}\ \mathbf{E}) - k_e^2\mathbf{E} = \mathbf{0}, \tag{24}$$

where $k_e \equiv k_0\sqrt{\varepsilon_e}$ is the wavenumber in the external medium. The vector partial waves, conventionally denoted $\mathbf{M}_{n,m}$ and $\mathbf{N}_{n,m}$ are solutions of this equation that obey outgoing wave conditions and are defined only starting with $n = 1$. In terms of the vector spherical harmonics, the normalized partial waves, $\mathbf{M}_{n,m}(k_e\mathbf{r})$ and $\mathbf{N}_{n,m}(k_e\mathbf{r})$ can be expressed as[4]

$$\mathbf{M}_{nm}(k_e\mathbf{r}) \equiv h_n^+(k_er)\mathbf{X}_{nm}(\theta,\phi),$$

$$\mathbf{N}_{nm}(k_e\mathbf{r}) \equiv \frac{1}{k_er}\{\sqrt{n(n+1)}h_n^+(k_er)\mathbf{Y}_{nm}(\theta,\phi)$$

$$+ [k_er h_n^+(k_er)]'\mathbf{Z}_{nm}(\theta,\phi)\}, \tag{25}$$

where $h_n^+(\rho)$ is the outgoing spherical Hankel function defined by $h_n^+(\rho) \equiv j_n(\rho) + iy_n(\rho)$.

Since $\mathbf{M}_{nm}$ and $\mathbf{N}_{nm}$ form a complete basis set for outgoing electromagnetic waves in an isotropic medium, the scattered field, $\mathbf{E}_{\text{scat}}$, can be expressed as

$$\mathbf{E}_{\text{scat}}(\mathbf{r}) = E\sum_{p=1}^{\infty} [\mathbf{M}_p(k_e\mathbf{r})f_p^{(h)} + \mathbf{N}_p(k_e\mathbf{r})f_p^{(e)}], \tag{26}$$

where $f_p^{(h)}$ and $f_p^{(e)}$ are dimensionless expansion coefficients of the field and E is a real coefficient with the dimension of the electric field and whose value will be fixed by the incident field strength [see Eq. (27)].

The nondivergent (i.e., regular) incident field can be expressed in terms of the regular partial waves $Rg\{\mathbf{M}_{nm}\}$, $Rg\{\mathbf{N}_{nm}\}$, which are obtained by replacing the spherical Hankel $h_n^+(\rho)$ function in the outgoing partial waves of Eq. (25) by spherical Bessel functions $j_n(\rho)$. An arbitrary inci-

dent field can, in turn, be expressed in terms of these regular vector partial waves:

$$\mathbf{E}_{\text{inc}}(\mathbf{r}) = E \sum_{p=1}^{\infty} [Rg\{\mathbf{M}_p(k_e\mathbf{r})\}e_p^{(h)} + Rg\{\mathbf{N}_p(k_e\mathbf{r})\}e_p^{(e)}],$$

(27)

where $e_p^{(h)}$ and $e_p^{(e)}$ are dimensionless expansion coefficients of the locally incident or excitation field on the particle. If the incident field is a plane wave, then the constant E with the dimension of an electric field is typically chosen such that $\|\mathbf{E}_{\text{inc}}\|^2 = E^2$ (for more general incident fields see Ref. 6).

Since the field in the external medium is $\mathbf{E}_{\text{inc}} + \mathbf{E}_{\text{scat}}$, the field developments in Eqs. (26) and (27) taken together with the partial-wave expression of $\mathbf{M}_{nm}$ and $\mathbf{N}_{n,m}$ [see Eq. (25)], shows that the radial functions $E_p^{(X)}$, $E_p^{(Z)}$, and $E_p^{(Y)}$ of a general electric field [cf. Eq. (22)] must have the form

$$E_p^{(Y)}(r) = \frac{E}{k_e r} \sqrt{n(n+1)}[j_n(k_e r)e_p^{(e)} + h_n^+(k_e r)f_p^{(e)}], \quad p \geq 1,$$

$$E_p^{(X)}(r) = \frac{E}{k_e r}[\psi_n(k_e r)e_p^{(h)} + \xi_n(k_e r)f_p^{(h)}], \quad p \geq 1,$$

$$E_p^{(Z)}(r) = \frac{E}{k_e r}[\psi_n'(k_e r)e_p^{(e)} + \xi_n'(k_e r)f_p^{(e)}], \quad p \geq 1, \quad (28)$$

where the functions are determined by the known coefficients of the incident field, $e_p^{(h)}$ and $e_p^{(e)}$, and the unknown coefficients $f_p^{(h)}$ and $f_p^{(e)}$ of the scattered field. In Eq. (28), we have invoked the Riccati–Bessel functions, $\psi_n(x) = xj_n(x)$ and $\xi_n(x) \equiv xh_n^+(x)$ and taken the prime to express a derivative with respect to the argument, i.e., $\psi_n'(x) = j_n(x) + xj_n'(x)$, etc.

We recall at this point that the goal is to obtain the T matrix in the partial wave basis, which by definition is expressed as the linear relationship between the incident and scattering coefficients:

$$f \equiv Te. \quad (29)$$

To obtain this T matrix, we need, in addition to the general external field development of Eq. (28), the general electromagnetic field development [i.e., of the form of Eq. (22)] within the anisotropic material. The remainder of this section is devoted to this goal, and the result is given in Eq. (44) below.

Before embarking on the development of the internal field, we remark that the utility in numerical applications of the field expansions of the type encountered in Eqs. (22), (26), and (27) arises from the fact the field at any finite $|\mathbf{r}|$ can be described to essentially arbitrary accuracy by keeping only a finite number of terms in the multipole expansion:

$$\sum_{n=0}^{n_{\text{max}}} \sum_{m=-n}^{m=n} \rightarrow \sum_{p=0}^{p_{\text{max}}=n_{\text{max}}^2+2n_{\text{max}}} . \quad (30)$$

The value of n_{max} will determine the accuracy of the field developments at the surface of the sphere, $|\mathbf{r}| = R$, where the boundary conditions have to be imposed.

B. Field Development in the Anisotropic Medium

In our previous paper, we showed that one can approximate the radial functions $E_p^{(Y)}, E_p^{(X)}, E_p^{(Z)}$ in a finite domain as a superposition of appropriately defined Bessel functions. This development is determined by appealing to the fact that the regular field in the interior of a homogenous spherical domain can be developed on a plane-wave basis (i.e., by a three-dimensional Fourier transform). Explicitly, the electric field inside a homogenous region can be developed as

$$\mathbf{E}_{\text{int}}(\mathbf{r}) = E \sum_{j=1}^{2} \int_0^{4\pi} d\Omega_k \mathbf{A}^{(j)} \exp(ik_j \hat{\mathbf{r}}_k \cdot \mathbf{r})$$

$$= E \sum_{j=1}^{2} \int_0^{\pi} \sin \theta_k d\theta_k \int_0^{2\pi} d\phi_k \widetilde{A}^{(j)} \mathbf{\Gamma}^{(j)}(\theta_k, \phi_k)$$

$$\times \exp(ik_j(\theta_k, \phi_k)\hat{\mathbf{r}}_k \cdot \mathbf{r}). \quad (31)$$

Although the continuum basis is necessary to develop the electric field in the full three-dimensional space, we only need to describe the electric field within a finite-sized spherical region. As will be demonstrated in our treatment below, an arbitrary field in such a finite region may be described by a discrete subset of the full plane-wave continuum. A satisfactory phase-space discretization procedure is outlined below (this discretization is similar to that which we proposed previously,[1] but it appears more practical for numerical applications).

1. Fourier Space Discretization Index

The following discretization procedure was designed so that the discretized directions are relatively evenly distributed throughout the full 4π space of solid angles. A simple discretization in θ_k and ϕ_k would have clustered the discretized angles around the poles. Furthermore, since the discretization of the Fourier integral is intimately related to the size of the spherical region under study (i.e., the size of the scatterer) and thereby n_{max}, we determine the Fourier space discretization scheme such that it will automatically adjust itself to the choice of a given n_{max} necessary for describing the external fields at the boundary surface [see Eq. (30)].

We discretize the Fourier integral over a half-space by defining a generalized Fourier space discretization index $\nu \in [1, \ldots, p_{\text{max}}]$, where p_{max} is the p index truncation determined by the multipolar truncation, n_{max}, via Eq. (30). Each value of ν will specify a unique direction in k space associated with a unique pair of indices n_θ and n_ϕ. The polar index n_θ goes over a range

$$n_\theta = 0, 1, \ldots, 2n_{\text{max}}^{-1}, \quad (32)$$

with the Fourier polar angle θ_ν associated with the discretization index n_θ given by

Table 1. Fourier Space Discretization Index, ν, and the Associated Angular Discretization Numbers (n_θ, n_ϕ) and Angles (θ_ν, ϕ_ν) for Different Values of the Multipole Space Cutoff, n_{max}

$n_{max}=1$			
ν	1	2	3
(n_θ, n_ϕ)	$(0,0)$	$(1,0)$	$(1,1)$
(θ_ν, ϕ_ν)	$(0,\pi)$	$(\frac{\pi}{2},\frac{\pi}{2})$	$(\frac{\pi}{2},\frac{3\pi}{2})$

$n_{max}=2$							
ν	1	2	3	4	5	6	7	8
(n_θ, n_ϕ)	$(0,0)$	$(1,0)$	$(1,1)$	$(2,0)$	$(2,1)$	$(2,2)$	$(3,0)$	$(3,1)$
(θ_ν, ϕ_ν)	$(0,\pi)$	$(\frac{\pi}{4},\frac{\pi}{2})$	$(\frac{\pi}{4},\frac{3\pi}{2})$	$(\frac{\pi}{2},\frac{\pi}{3})$	$(\frac{\pi}{2},\pi)$	$(\frac{\pi}{2},\frac{5\pi}{3})$	$(\frac{3\pi}{4},\frac{\pi}{2})$	$(\frac{3\pi}{4},\frac{3\pi}{2})$

$$\theta_\nu = \frac{\pi n_\theta}{2 n_{max}},$$

i.e.,

$$\theta_\nu = 0, \frac{\pi}{2n_{max}}, \frac{2\pi}{2n_{max}}, \ldots, \pi - \frac{\pi}{2n_{max}}, \tag{33}$$

thus evenly spacing θ_ν in the interval $\theta \in [0,\pi]$. Provided that the polar index, n_θ, is in the range $n_\theta \leq n_{max}$, the azimuthal index n_ϕ covers the range

$$n_\phi = 0, \ldots, n_\theta,$$

with

$$\phi_\nu = \pi \frac{2n_\phi + 1}{n_\theta + 1}. \tag{34}$$

The generalized index ν for $n_\theta \leq n_{max}$ is given by

$$\nu = \frac{n_\theta(n_\theta + 1)}{2} + n_\phi + 1, \quad n_\theta \leq n_{max}. \tag{35}$$

The inverse relations for going from the generalized index ν to (n_θ, n_ϕ) provided that the index ν is in the range $\nu \leq (n_{max}+1)(n_{max}+2)/2$ are

$$n_\theta = \mathrm{Int}\left(\sqrt{2\nu - 1} - \frac{1}{2}\right), \quad n_\phi = \nu - \frac{n_\theta(n_\theta + 1)}{2} - 1. \tag{36}$$

For $n_\theta > n_{max}$, the azimuthal index, n_ϕ, covers the range

$$n_\phi = 0, \ldots, 2n_{max} - n_\theta,$$

with

$$\phi_\nu = \pi \frac{2n_\phi + 1}{2n_{max} - n_\theta + 1}. \tag{37}$$

The generalized index ν for $n_\theta > n_{max}$ is given by the expression

$$\nu = (n_{max}+1)^2 - \frac{(2n_{max} - n_\theta)(2n_{max} - n_\theta + 3)}{2} + n_\phi. \tag{38}$$

The inverse relations for $\nu > (n_{max}+1)(n_{max}+2)/2$ are

$$n_\theta = 2n_{max} - \mathrm{Int}\left(\sqrt{2(n_{max}+1)^2 - 2\nu + 1} - \frac{1}{2}\right),$$

$$n_\phi = \nu + \frac{(2n_{max} - n_\theta)(2n_{max} - n_\theta + 3)}{2} - (n_{max}+1)^2. \tag{39}$$

One can appreciate the rather symmetric sampling of the phase-space integral of this discretization by explicitly writing out the p_{max} values of the ν index and its corresponding n_θ and n_ϕ values as illustrated in Table 1.

2. Discretized Internal Field Expansion
Using the above index notation, the internal field in a finite region can be described by

$$\mathbf{E}_{int}(\mathbf{r}) \cong E \sum_{j=1}^{2} \sum_{\nu=1}^{p_{max}} \widetilde{A}_\nu^{(j)} \mathbf{\Gamma}_\nu^{(j)} \exp(ik_\nu^{(j)} \hat{\mathbf{r}}_\nu \cdot \mathbf{r}), \tag{40}$$

where

$$\widetilde{A}_\nu^{(j)} \equiv \widetilde{A}^{(j)}(\theta_\nu, \phi_\nu)\sin\theta_\nu, \quad \mathbf{\Gamma}_\nu^{(j)} \equiv \mathbf{\Gamma}^{(j)}(\theta_\nu, \phi_\nu),$$

$$k_\nu^{(j)} \equiv k_j(\theta_\nu, \phi_\nu), \quad \hat{\mathbf{r}}_\nu \equiv \hat{\mathbf{r}}(\theta_\nu, \phi_\nu). \tag{41}$$

We remark in the field development of Eq. (40) that there are $2p_{max}$ basis functions, $\mathbf{\Gamma}_\nu^{(j)} \exp(ik_\nu^{(j)} \hat{\mathbf{r}}_\nu \cdot \mathbf{r})$, which are weighted by their corresponding expansion coefficients $\widetilde{A}_\nu^{(j)}$. It is important to note that the number of discretized directions, $p_{max} = n_{max}^2 + 2n_{max}$ is the same as that adopted in the multipole cutoff for the external fields. We will see below that this choice naturally leads to a unique solution.

3. Projection onto the Vector Spherical Harmonic Basis
One can produce exactly satisfied boundary conditions by transforming Eq. (40) into a form involving vector spherical harmonics. This is accomplished by the formula[1]

$$\exp(ik_\nu^{(j)}\hat{\mathbf{r}}_\nu \cdot \mathbf{r})\Gamma_{j,\nu} = \sum_{p=0}^{\infty} \left\{ a_{p,\nu}^{(h,j)} j_n(k_\nu^{(j)} r)\mathbf{X}_p(\hat{\mathbf{r}}) \right.$$

$$+ \left[a_p a_{p,\nu}^{(e,j)} \frac{j_n(k_\nu^{(j)} r)}{k_\nu^{(j)} r} + a_{p,\nu}^{(o,j)} j_n'(k_\nu^{(j)} r) \right]\mathbf{Y}_p(\hat{\mathbf{r}})$$

$$+ \left[a_{p,\nu}^{(e,j)} \frac{\psi_n'(k_\nu^{(j)} r)}{k_\nu^{(j)} r} + a_p a_{p,\nu}^{(o,j)} \frac{j_n(k_\nu^{(j)} r)}{k_\nu^{(j)} r} \right]\mathbf{Z}_p(\hat{\mathbf{r}}),$$

$$(42)$$

where we have defined $a_p \equiv \sqrt{n(p)(n(p)+1)}$ and the coefficients $a_{p,\nu}^{(e,j)}$, $a_{p,\nu}^{(h,j)}$, and $a_{p,\nu}^{(o,j)}$ are given by

$$a_{p,\nu}^{(h,j)} = 4\pi i^n \mathbf{X}_p^*(\hat{\mathbf{r}}_\nu) \cdot \Gamma_\nu^{(j)}, \quad a_{p,\nu}^{(e,j)} = 4\pi i^{n-1}\mathbf{Z}_p^*(\hat{\mathbf{r}}_\nu) \cdot \Gamma_\nu^{(j)},$$

$$a_{p,\nu}^{(o,j)} = 4\pi i^{n-1}\mathbf{Y}_p^*(\hat{\mathbf{r}}_\nu) \cdot \Gamma_\nu^{(j).} \quad (43)$$

Inserting Eq. (42) into Eq. (40), we find that the expressions for the radial functions for the internal field, $\mathbf{E}_{\text{int}}(\mathbf{r})$, are

$$E_p^{(Y)}(r) = E\sum_{j=1}^{2}\sum_{\nu=1}^{p_{\max}} \left[a_p a_{p,\nu}^{(e,j)} \frac{j_n(k_\nu^{(j)} r)}{k_\nu^{(j)} r} + a_{p,\nu}^{(o,j)} j_n'(k_\nu^{(j)} r) \right]\tilde{A}_\nu^{(j)},$$

$$p \ge 0,$$

$$E_p^{(X)}(r) = E\sum_{j=1}^{2}\sum_{\nu=1}^{p_{\max}} a_{p,\nu}^{(h,j)} \frac{\psi_n(k_\nu^{(j)} r)}{k_\nu^{(j)} r}\tilde{A}_\nu^{(j)}, \quad p \ge 1,$$

$$E_p^{(Z)}(r) = E\sum_{j=1}^{2}\sum_{\nu=1}^{p_{\max}} \left[a_{p,\nu}^{(e,j)} \frac{\psi_n'(k_\nu^{(j)} r)}{k_\nu^{(j)} r} + a_p a_{p,\nu}^{(o,j)} \frac{\psi_n(k_\nu^{(j)} r)}{(k_\nu^{(j)} r)^2} \right]\tilde{A}_\nu^{(j)},$$

$$p \ge 1. \quad (44)$$

C. Magnetic Field
Until now, we have concentrated our attention on the electric field. Just as in isotropic Mie theory, the boundary conditions that we will impose are the continuity of the tangential components of the electric field and the $\mathbf{H} = \mathbf{B}/\mu_0$ field. Like the electric field, any $\mathbf{H}$ field can be developed in terms of a vector spherical harmonic decomposition:

$$\mathbf{H}(\mathbf{r}) = \sum_{p=0}^{\infty} [H_p^{(Y)}(r)\mathbf{Y}_p(\theta,\phi) + H_p^{(X)}(r)\mathbf{X}_p(\theta,\phi)$$

$$+ H_p^{(Z)}(r)\mathbf{Z}_p(\theta,\phi)]. \quad (45)$$

The $\mathbf{H}$ field is deduced from the electric field via the Maxwell–Faraday relation:

$$\mathbf{H} = \frac{1}{i\omega\mu_0}\mathbf{curl}\,\mathbf{E}. \quad (46)$$

Inserting the partial wave developments of Eqs. (26) and (27) into this equation and using the relations **curl M** $=k_e\mathbf{N}$ and **curl N**$=k_e\mathbf{M}$, we find that the functions in Eq. (45) for the external $\mathbf{H}$ field must be of the form

$$H_p^{(Y)}(r) = \frac{a_p}{i\omega\mu_0}\frac{E}{r}[j_n(k_e r)e_p^{(h)} + h_n(k_e r)f_p^{(h)}], \quad p \ge 1,$$

$$H_p^{(X)}(r) = \frac{1}{i\omega\mu_0}\frac{E}{r}[\psi_n(k_e r)e_p^{(e)} + \xi_n(k_e r)f_p^{(e)}], \quad p \ge 1,$$

$$H_p^{(Z)}(r) = \frac{1}{i\omega\mu_0}\frac{E}{r}[\psi_n'(k_e r)e_p^{(h)} + \xi_n'(k_e r)f_p^{(h)}], \quad p \ge 1.$$

$$(47)$$

For the internal magnetic field, $\mathbf{H}_{\text{int}}$, we appeal to the projection of Eq. (46) onto the vector spherical harmonic basis [see Ref. 4 and Eqs. (37)–(39) therein for a detailed derivation]:

$$H_p^{(Y)} = \frac{a_p}{i\omega\mu_0}\frac{E_p^{(X)}}{r},$$

$$H_p^{(X)} = \frac{1}{i\omega\mu_0}\left(a_p \frac{E_p^{(Y)}}{r} - \frac{E_p^{(Z)}}{r} - \frac{\mathrm{d}E_p^{(Z)}}{\mathrm{d}r} \right),$$

$$H_p^{(Z)} = \frac{1}{i\omega\mu_0}\left(\frac{E_p^{(X)}}{r} + \frac{\mathrm{d}E_p^{(X)}}{\mathrm{d}r} \right). \quad (48)$$

Inserting the developments of the internal electric field, Eq. (44), into equations (48), we find, after some manipulation,

$$H_p^{(Y)}(r) = \frac{a_p E}{i\omega\mu_0}\sum_{j=1}^{2}\sum_{\nu=1}^{p_{\max}} \tilde{A}_\nu^{(j)} a_{p,\nu}^{(h,j)} \frac{j_n(k_\nu^{(j)} r)}{r}, \quad p \ge 1,$$

$$H_p^{(X)}(r) = \frac{E}{i\omega\mu_0}\sum_{j=1}^{2}\sum_{\nu=1}^{p_{\max}} \tilde{A}_\nu^{(j)} a_{p,\nu}^{(e,j)} \frac{\psi_n(k_\nu^{(j)} r)}{r}, \quad p \ge 1,$$

$$H_p^{(Z)}(r) = \frac{E}{i\omega\mu_0}\sum_{j=1}^{2}\sum_{\nu=1}^{p_{\max}} \tilde{A}_\nu^{(j)} a_{p,\nu}^{(h,j)} \frac{\psi_n'(k_\nu^{(j)} r)}{r}, \quad p \ge 1. \quad (49)$$

4. BOUNDARY CONDITIONS AND *T*-MATRIX FORMULATION

We recall from Eqs. (28) and (47) above that the external field depends on the unknown scattering coefficients, labeled $f_p^{(e)}$ and $f_p^{(h)}$, for $p=1,\ldots,p_{\max}$. The internal fields in Eqs. (44) and (49), on the other hand, depend on the unknown coefficients, $\tilde{A}_\nu^{(1)}$ and $\tilde{A}_\nu^{(2)}$ for $\nu=1,\ldots,p_{\max}$. The internal and external fields are, respectively, described by $2p_{\max}$ unknowns.

From the orthogonality of the vector spherical harmonics and Eqs. (28), (44), (47), and (49), the continuity of the independent transverse field components, $E_p^{(X)}$, $E_p^{(Z)}$, $H_p^{(X)}$, and $H_p^{(Z)}$ at the $r=R$ spherical interface results in four sets of equations for each $p \in [1,\ldots,p_{\max}]$:

$$\psi_n(k_eR)e_p^{(h)} + \xi_n(k_eR)f_p^{(h)} = \sum_{j=1}^{2} \sum_{\nu=1}^{p_{max}} a_{p,\nu}^{(h,j)} \frac{k_e}{k_\nu^{(j)}} \psi_n(k_\nu^{(j)}R)\widetilde{A}_\nu^{(j)},$$

$$(50)$$

$$\psi_n'(k_eR)e_p^{(e)} + \xi_n'(k_eR)f_p^{(e)} = \sum_{j=1}^{2} \sum_{\nu=1}^{p_{max}} \left[a_{p,\nu}^{(e,j)} \frac{k_e}{k_\nu^{(j)}} \psi_n'(k_\nu^{(j)}R) + a_p a_{p,\nu}^{(o,j)} \right.$$
$$\left. \times \left(\frac{k_e}{k_\nu^{(j)}} \right)^2 \frac{\psi_n(k_\nu^{(j)}R)}{k_eR} \right] \widetilde{A}_\nu^{(j)}, \qquad (51)$$

$$\psi_n(k_eR)e_p^{(e)} + \xi_n(k_eR)f_p^{(e)} = \sum_{j=1}^{2} \sum_{\nu=1}^{p_{max}} a_{p,\nu}^{(e,j)} \psi_n(k_\nu^{(j)}R)\widetilde{A}_\nu^{(j)},$$

$$(52)$$

$$\psi_n'(k_eR)e_p^{(h)} + \xi_n'(k_eR)f_p^{(h)} = \sum_{j=1}^{2} \sum_{\nu=1}^{p_{max}} a_{p,\nu}^{(h,j)} \psi_n'(k_\nu^{(j)}R)\widetilde{A}_\nu^{(j)}.$$

$$(53)$$

Eliminating the scattering coefficients $f_p^{(h)}$ in Eqs. (50) and (53), we obtain

$$ie_p^{(h)} = \sum_{\nu=1}^{p_{max}} \sum_{j=1}^{2} a_{p,\nu}^{(h,j)} \left[\frac{k_e}{k_\nu^{(j)}} \psi_n(k_\nu^{(j)}R)\xi_n'(k_eR) \right.$$
$$\left. - \psi_n'(k_\nu^{(j)}R)\xi_n(k_eR) \right] \widetilde{A}_\nu^{(j)}, \qquad (54)$$

where we invoked the Wronskian identity:

$$\psi_n(x)\xi_n'(x) - \psi_n'(x)\xi_n(x) = i. \qquad (55)$$

Similarly eliminating $f_p^{(e)}$ from Eqs. (51) and (52), and again invoking the Wronskian identity yields

$$ie_p^{(e)} = \sum_{\nu=1}^{p_{max}} \sum_{j=1}^{2} \left\{ a_{p,\nu}^{(e,j)} \left[\psi_n(k_\nu^{(j)}R)\xi_n'(k_eR) \right. \right.$$
$$\left. - \frac{k_e}{k_\nu^{(j)}} \psi_n'(k_\nu^{(j)}R)\xi_n(k_eR) \right] - a_p a_{p,\nu}^{(o,j)}$$
$$\times \left(\frac{k_e}{k_\nu^{(j)}} \right)^2 \psi_n(k_\nu^{(j)}R)\frac{\xi_n(k_eR)}{k_eR} \right\} \widetilde{A}_\nu^{(j)}. \qquad (56)$$

The full set of equations (54) and (56) can be expressed in a matrix form,

$$\begin{bmatrix} [e^{(h)}] \\ [e^{(e)}] \end{bmatrix} = i \begin{bmatrix} V^{(h,1)} & V^{(h,2)} \\ V^{(e,1)} & V^{(e,2)} \end{bmatrix} \begin{bmatrix} [\widetilde{A}^{(1)}] \\ [\widetilde{A}^{(2)}] \end{bmatrix}, \qquad (57)$$

with the blocks given by

$$[V^{(h,j)}]_{p,\nu} = a_{p,\nu}^{(h,j)} \left[\psi_n'(k_\nu^{(j)}R)\xi_n(k_eR) - \frac{k_e}{k_\nu^{(j)}} \psi_n(k_\nu^{(j)}R)\xi_n'(k_eR) \right],$$

$$[V^{(e,j)}]_{p,\nu} = a_{p,\nu}^{(e,j)} \left[\frac{k_e}{k_\nu^{(j)}} \psi_n'(k_\nu^{(j)}R)\xi_n(k_eR) - \psi_n(k_\nu^{(j)}R)\xi_n'(k_eR) \right]$$
$$+ a_p a_{p,\nu}^{(o,j)} \left(\frac{k_e}{k_\nu^{(j)}} \right)^2 \psi_n(k_\nu^{(j)}R)\frac{\xi_n(k_eR)}{k_eR}. \qquad (58)$$

The solution for the internal field in terms of the incident field coefficients can in principal be found by a unique matrix inversion:

$$i \begin{bmatrix} [\widetilde{A}^{(1)}] \\ [\widetilde{A}^{(2)}] \end{bmatrix} = V^{-1} \begin{bmatrix} [e^{(h)}] \\ [e^{(e)}] \end{bmatrix}. \qquad (59)$$

To derive a T matrix, it suffices to obtain a relation between the internal coefficients and the scattering coefficients. Eliminating $e_p^{(h)}$ from Eqs. (50) and (53), we obtain

$$f_p^{(h)} = i \sum_{\nu=1}^{p_{max}} \sum_{j=1}^{2} a_{p,\nu}^{(h,j)} \left[\frac{k_e}{k_\nu^{(j)}} \psi_n(k_\nu^{(j)}R)\psi_n'(k_eR) \right.$$
$$\left. - \psi_n'(k_\nu^{(j)}R)\psi_n(k_eR) \right] \widetilde{A}_\nu^{(j)}. \qquad (60)$$

Similarly eliminating $e_p^{(e)}$ from Eqs. (51) and (52) yields

$$f_p^{(e)} = i \sum_{\nu=1}^{p_{max}} \sum_{j=1}^{2} \left\{ a_{p,\nu}^{(e,j)} \left[\psi_n(k_\nu^{(j)}R)\psi_n'(k_eR) \right. \right.$$
$$\left. - \frac{k_e}{k_\nu^{(j)}} \psi_n'(k_\nu^{(j)}R)\psi_n(k_eR) \right]$$
$$- \left(\frac{k_e}{k_\nu^{(j)}} \right)^2 a_p a_{p,\nu}^{(o,j)} \psi_n(k_\nu^{(j)}R)\frac{\psi_n(k_eR)}{k_eR} \right\} \widetilde{A}_\nu^{(j)}. \qquad (61)$$

We can write Eqs. (60) and (61) in matrix form by defining the matrix U such that

$$\begin{bmatrix} [f_p^{(h)}] \\ [f_p^{(e)}] \end{bmatrix} = \begin{bmatrix} U^{(h,1)} & U^{(h,2)} \\ U^{(e,1)} & U^{(e,2)} \end{bmatrix} i \begin{bmatrix} [\widetilde{A}^{(1)}] \\ [\widetilde{A}^{(2)}] \end{bmatrix}, \qquad (62)$$

with blocks of the U matrix given by

$$[U^{(h,j)}]_{p,\nu} = a_{p,\nu}^{(h,j)} \left[\frac{k_e}{k_\nu^{(j)}} \psi_n(k_\nu^{(j)}R)\psi_n'(k_eR) - \psi_n'(k_\nu^{(j)}R)\psi_n(k_eR) \right],$$

$$[U^{(e,j)}]_{p,\nu} = a_{p,\nu}^{(e,j)} \left[\psi_n(k_\nu^{(j)}R)\psi_n'(k_eR) - \frac{k_e}{k_\nu^{(j)}} \psi_n'(k_\nu^{(j)}R)\psi_n(k_eR) \right]$$
$$- \left(\frac{k_e}{k_\nu^{(j)}} \right)^2 a_p a_{p,\nu}^{(o,j)} \psi_n(k_\nu^{(j)}R)\frac{\psi_n(k_eR)}{k_eR}. \qquad (63)$$

Combining Eqs. (59) and (62), we obtain the T matrix of the anisotropic sphere,

$$\begin{bmatrix} [f_p^{(h)}] \\ [f_p^{(e)}] \end{bmatrix} = UV^{-1} \begin{bmatrix} [e^{(h)}] \\ [e^{(e)}] \end{bmatrix} \equiv \begin{bmatrix} T^{(h,h)} & T^{(h,e)} \\ T^{(e,h)} & T^{(e,e)} \end{bmatrix} \begin{bmatrix} [e^{(h)}] \\ [e^{(e)}] \end{bmatrix},$$

(64)

where each of the $T^{(h,h)}$, $T^{(h,e)}$, $T^{(e,h)}$, and $T^{(e,e)}$ blocks of the T matrix are $p_{max} \times p_{max}$ matrices.

This procedure closely imitates a derivation of Mie theory except that in Mie theory, all the matrices are diagonal and the corresponding matrix inversion is trivial. In fact, the Mie theory for isotropic spheres emerges analytically from the above formulas.

5. APPLICATIONS

The final algorithm for calculating the T matrix of a homogenous anisotropic sphere is relatively simple. We resume the essential steps below.

A. *T*-matrix Computation Algorithm

• The first step is to select a multipole cutoff for n_{max}. We generally found that n_{max} needs to be larger than that required to obtain similar accuracy for an isotropic sphere of the same size and comparable refractive index.
• We then discretize the 4π solid angle directions in the Fourier **k** space with an index $1 \le \nu \le p_{max} = n_{max}^2 + 2n_{max}$ as explained in Subsection 3.B.1.
• For each discretized **k**-space direction (θ_ν, ϕ_ν) specified by the ν index [see Eqs. (33), (34), and (37)], we determine the two eigenvalues, $\tilde{k}_\nu^{(1)}$ and $\tilde{k}_\nu^{(2)}$ from Eq. (8), and their corresponding eigenvectors following the procedure in Subsection 2.A.
• The coefficients $a_{p,\nu}^{(e,j)}$, $a_{p,\nu}^{(h,j)}$, $a_{p,\nu}^{(o,j)}$ are obtained from Eq. (43) via scalar products of the $\Gamma^{(1)}$, $\Gamma^{(2)}$ eigenvectors, and the vector spherical harmonics [see Eqs. (A3)–(A5) of Appendix A].
• The elements of the V and U matrices are then obtained, respectively, from Eqs. (58) and (63) using the $k_\nu^{(1)}$ and $k_\nu^{(2)}$, eigenvalues, the known $a_{p,\nu}^{(e,j)}$, $a_{p,\nu}^{(h,j)}$, $a_{p,\nu}^{(o,j)}$, a_p coefficients, and the evaluation of Riccati–Bessel functions $\psi_n(x)$ and $\xi_n(x)$.
• The T matrix is obtained by matrix inversion followed by matrix multiplication, Eq. (64). If one only requires the scattering coefficients for a single given incident field, or if the V matrix is difficult to invert, one can solve the set of linear equations in Eq. (57) for the $\tilde{A}$ vector and then multiply this solution by the U matrix [see Eq. (62)] in order to obtain the scattering coefficients, f.

B. Conservation Laws and Reciprocity

Although our theory ensures the satisfaction of the boundary conditions at the surface of the sphere, the description of the internal fields is correct only if enough terms are included in the multipole development. Consequently, underlying physical constraints like energy conservation and reciprocity will only be satisfied provided that n_{max} is sufficiently high. Although this could be looked upon as a handicap from a general theoretical point of view, the nonsatisfaction of these laws when the truncation is too severe provides quite useful tests for the choice of n_{max}.

In scattering from a lossless medium, energy conservation implies that $\sigma_{ext} = \sigma_{scat}$, and one can deduce that the T matrix consequently satisfies[5,7]:

$$-\tfrac{1}{2}(T + T^\dagger) = T^\dagger T.$$

(65)

Reciprocity is another restriction on the form of the T matrix, which is particularly useful in systems containing losses for which Eq. (65) no longer holds true. The satisfaction of reciprocity implies that the T matrix must satisfy[5]:

$$T_{-m'n',(-m)n}^{(i,j)} = (-1)^{m+m'} T_{mn,m'n'}^{(i,j)}.$$

(66)

In all our numerical calculations carried out so far, the satisfaction of energy conservation and/or reciprocity constraints was accompanied by numerically stable T-matrix determinations.

C. Numerical Verifications

We remark that our code for evaluating the T matrix following the procedure described in Subsection 5.A generally works with no problem as long as the sphere diameter is not too much larger than a wavelength. For larger spheres, the coupling to higher-order multipole elements tends to render the V matrix ill conditioned for the required large multipole spaces. For such large spheres, it was usually sufficient to solve the linear equations in Eq. (57) for the unknown $\tilde{A}$ coefficients and then obtain the scattering coefficients from Eq. (62).

The T matrix itself contains too much information to report, so instead we use the T matrix to calculate cross sections and orientation averaged cross sections. For differential cross sections, we will follow Geng *et al.* and use the radar cross section, σ_{radar},[8] which is 4π times the ordinary differential scattering cross section, $d\sigma_{scat}/d\Omega$:

$$\sigma_{radar}(\theta_{inc}, \phi_{inc}, \gamma_{inc}; \theta_{scat}, \phi_{scat}) \equiv 4\pi \frac{d\sigma_{scat}}{d\Omega} = 4\pi \lim_{r \to \infty} r^2 \frac{\|\mathbf{E}_{scat}\|^2}{\|\mathbf{E}_{inc}\|^2}.$$

(67)

We will also give values for the dimensionless scattering and extinction efficiencies, (Q_{ext}, Q_{scat}), which are the total cross sections[5,7] divided by the corresponding geometric cross section, πR^2 where R is the sphere radius.

We will compare our results for radar cross sections[5] with the published results of Geng *et al.*,[8] who formulated a theory for calculating the radar cross sections from a uniaxial sphere by parameterizing the amplitude functions in a plane-wave expansion of the internal field but without calculating the T matrix. Our radar cross sections are calculated from the T matrix (i.e., the scattering coefficients, f) using the formulas developed in Refs. 5, 7, and 9 and are displayed in Fig. 1. Following Geng *et al.*,[8] we adopt a uniaxial material in which the ordinary or transverse relative dielectric constant is $\varepsilon_t = 5.3495$ while the optic axis dielectric constant is $\varepsilon_{o.a.} = 4.9284$. The radar cross sections in Fig. 1 correspond to that of a plane wave propagating along the optic axis, while the E plane denotes the plane where the scattered radiation is measured in the plane parallel to the plane containing the incident polarization. The H plane refers to the plane perpendicular to the incident field polarization. For the

Stout *et al.*

sphere radius of $k_eR = \pi$ (i.e., $R = \lambda/2$), we obtained $Q_{\text{ext}} = Q_{\text{scat}} = 1.094$ for an optic axis-oriented incident wave, and $\langle Q_{\text{ext}}\rangle_o = \langle Q_{\text{scat}}\rangle_o = 1.183$ for the orientation-averaged efficiencies [the $\frac{1}{3}$ averaging of Eq. (1) yields $\langle Q_{\text{ext}}\rangle_{1/3} = \langle Q_{\text{scat}}\rangle_{1/3} = 1.243$]. Geng *et al.*[8] reported that their results had converged for $n_{\max} = 6$, and our calculations for the total cross section had indeed converged to better than 1% accuracy at $n_{\max} = 6$. Nevertheless, it was necessary to raise the cutoff to $n_{\max} = 9$ in order to obtain an $(Q_{\text{ext}} - Q_{\text{scat}}) \simeq 10^{-6}$ accuracy in energy conservation and obtain five significant digits in the cross section.

Geng *et al.*[8] also reported radar cross sections for $k_eR = 2\pi$ spheres of the same composition and incident field direction, reporting a convergence at $n_{\max} = 10$. Although for this particular incident field direction, the radar cross section is relatively well reproduced at $n_{\max} = 10$, we found that the cutoff for the T-matrix algorithm must be pushed to $n_{\max} = 14$ before it begins to converge, but that at this model-space size, the V matrix in Eq. (57) begins to become ill conditioned and difficult to invert. Solving the set of linear equations and pushing $n_{\max}$ to 16 allowed us to
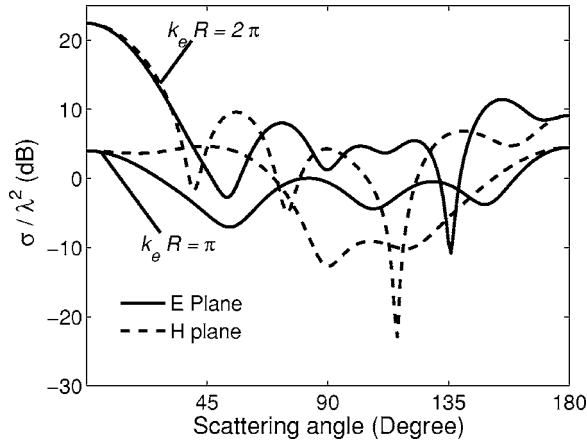
Fig. 1. Radar cross sections versus scattering angle θ (in degrees) in the E plane (solid curve) and in the H plane (dashed curve). The size parameters are $k_eR = \pi$ and $k_eR = 2\pi$, while the uniaxial permittivity tensor elements are taken as $\varepsilon_t = 5.3495$ and $\varepsilon_{\text{o.a.}} = 4.9284$.
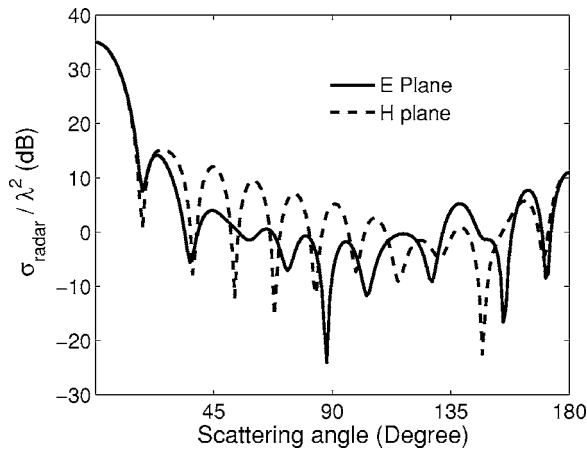
Fig. 2. Radar cross sections versus scattering angle θ (in degrees), in the E plane (solid curve) and in the H plane (dashed curve) for an absorbing uniaxial sphere with $k_eR = 4\pi$, $\varepsilon_t = 2 + 0.1i$ and $\varepsilon_{\text{o.a.}} = 4 + 0.2i$.

Table 2. Total Efficiencies (Cross Sections) for a Uniaxial Sphere with $\varepsilon_t = 2 + 0.1i$ and $\varepsilon_{\text{o.a.}} = 4 + 0.2i$ [a]

k_eR	$\langle Q_{\text{scat}}\rangle$	$\langle Q_{\text{ext}}\rangle$	$\langle Q_{\text{ext}}\rangle_{1/3}$	Q_{scat}	Q_{ext}	$\langle Q_{\text{abs}}\rangle$	Q_{abs}
π	2.578	3.118	2.71	2.156	2.556	0.539	0.40
2π	2.08	2.94	3.03	2.27	3.15	0.86	0.88
4π	2.45	1.53	2.50	1.46	2.52	0.92	1.05

[a]The unaveraged efficiencies are calculated for a plane wave incident along the optic axis while the averaged efficiencies average over all possible incident field directions and polarizations.

obtain $Q_{\text{ext}} = Q_{\text{scat}} = 2.379$ for the incident-field direction parallel to the optic axis, and $\langle Q_{\text{ext}}\rangle_o = \langle Q_{\text{scat}}\rangle_o = 2.567$. As far as we can tell at this scale, our plotted on-axis results for the radar cross section are essentially identical to those obtained by Geng *et al.*[8]

One can also apply this theory when absorption is present. Again following Geng *et al.*,[8] we take an absorbing model uniaxial sphere with $\varepsilon_t = 2 + 0.1i$ and $\varepsilon_{\text{o.a.}} = 4 + 0.2i$. Energy is no longer conserved in this system, but one can still test the calculations with reciprocity. Although Geng *et al.*[8] reported that the radar cross section had converged at $n_{\max} = 20$ for on optic axis illumination, we found that we had to go to $n_{\max} \simeq 30$ to obtain the 10^{-3} to 10^{-4} error in the total cross sections. We illustrate in Fig. 2, the radar cross section with an on-optic axis illumination for a $k_eR = 4\pi$ sphere. These results are visibly the same as those obtained by Geng *et al.*[8] The total scattering efficiencies for the on-optic axis incidence and the average total efficiencies are given in Table 2 for $k_eR = \pi$, $k_eR = 2\pi$, and $k_eR = 4\pi$ spheres.

D. Orientation Averaging and the Bohren–Huffman Conjecture
In the dipole approximation, if the incident field is parallel to a principal axis of a small lossless sphere, then the scattering and extinction efficiencies of a lossless sphere are given by[2,3]

$$Q_{\text{ext}} = Q_{\text{scat}} \underset{\text{dipole}}{\simeq} \frac{8}{3}\left|\frac{\varepsilon_i - \varepsilon_e}{\varepsilon_i + 2\varepsilon_e}\right|^2 (k_eR)^4, \qquad (68)$$

where ε_i is the dielectric constant along the corresponding principal axis. The $(k_eR)^4$ factor in this equation yields the famous Rayleigh inverse fourth power dependence on wavelength, $\sigma \propto 1/\lambda^4$.

An orientation average of the extinction efficiency in the dipole approximation immediately yields the formula

$$\langle Q_{\text{ext}}\rangle_o \simeq \langle Q_{\text{ext}}\rangle_{1/3} = \tfrac{1}{3}Q_{\text{ext},1} + \tfrac{1}{3}Q_{\text{ext},2} + \tfrac{1}{3}Q_{\text{ext},3}, \qquad (69)$$

where $Q_{\text{ext},1}, Q_{\text{ext},2}$, and $Q_{\text{ext},3}$, refer to extinction efficiencies for isotropic spheres composed of a material with each of the three principal dielectric constants. Bohren and Huffman however, rightly presumed that Eq. (69) does not strictly apply outside of the dipole approximation.

Since we can now calculate the true $\langle Q_{\text{ext}}\rangle_o$, from the trace of the T matrix,[10] one can test Eq. (69) and see to what extent this formula remains valid beyond the dipole approximation. In the three graphs in Fig. 3, we compare the true extinction average efficiency with that given by the simple $\frac{1}{3}$ averaging rule in the size range $k_eR \in [0,5]$

for three different sets of principal dielectric constants of ε_1, ε_2, and ε_3. The results for the dipole approximation of the cross section, i.e., results obtained from Eq. (68) and the $\frac{1}{3}$ rule are illustrated for comparison. It is immediately obvious in all three graphs of Fig. 3 that the $\frac{1}{3}$ rule approximation gives reasonable results well beyond the domain of validity of dipole approximation.

In Fig. 3(a), we compare the $\frac{1}{3}$ rule with both the dipole approximation and the correct orientation average of the total extinction (scattering efficiency) for the weakly anisotropic medium studied in Fig. 1. We remark that the $\frac{1}{3}$ rule reproduces very well the angle averaged (extinction) scattering efficiency section for the resonances at low, $k_eR \lesssim 3$ values, and that differences only begin to appear at $k_eR \gtrsim 3$ resonances involving high multipole orders. We see in Fig. 3(b) that even for quite large anisotropies the $\frac{1}{3}$ averaging rule tends to follow the general amplitude of the extinction (scattering) efficiencies even though it does not do as well in reproducing the resonance peaks.

To find a notable failing of the $\frac{1}{3}$ averaging rule, we invoked a scenario in which one of the principal dielectric constants has gone to plasmon-type values, for example, $\varepsilon_3 = -2.2$ as shown in Fig. 3(c). Of course, there should be at least some absorption as well as strong dispersion associated with such negative dielectric functions, but a small absorption proved to be of little consequence in the simulations, so we preferred to use real dielectric constants in our example in order to preserve energy conser-

vation. Dispersion is of course important for frequency measurements but would complicate our simply demonstrative calculations by eliminating scale invariance. In the simulation of Fig. 3(c), we allowed the strong plasmon resonance at $k_eR \simeq 0.28$ to go off the scale (the maximum is $Q_{ext} \simeq 25$) since this simple resonance is well described by the $\frac{1}{3}$ rule.

6. CONCLUSIONS

There is a temptation at this point to conclude that weak and even relatively strong anisotropy can usually be treated with simple $\frac{1}{3}$ averaging procedures. This may be true for transparent anisotropic materials in some situations at least, although more studies concerning the angular distribution of the scattered radiation should be carried out before making this assertion. In physical situations where orientation averaging is not appropriate, the semianalytic solution is useful in light of the fact that the cross sections can vary considerably as a function of the relative orientation between the principal axes and the incident radiation. We also feel that the existence of semianalytic solutions is likely to be valuable when treating exotic materials and phenomena. Another point to keep in mind is that anisotropic particles in nature are not spherical, and that anisotropic optical properties may couple significantly to geometric nonsphericities. This problem is largely unexplored, and one should keep in mind that much of the interest of an anisotropic sphere was as a starting point for more sophisticated theories treating arbitrarily shaped anisotropic objects.[11]
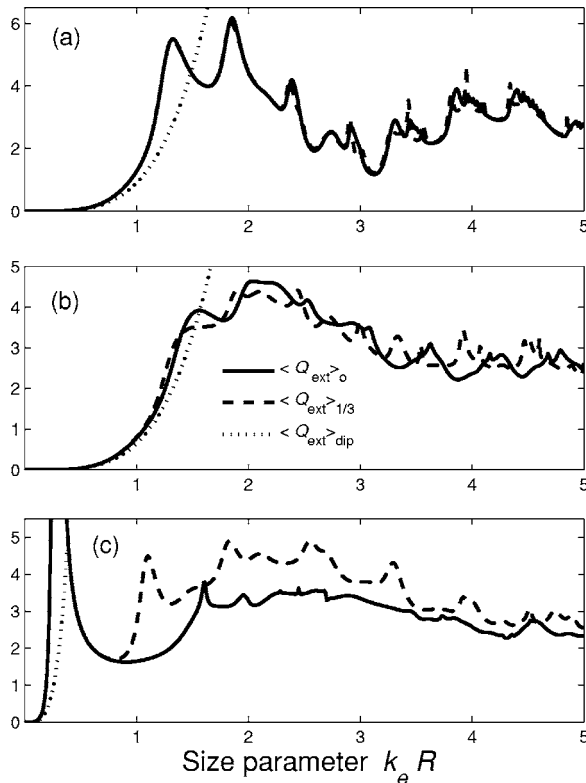

Fig. 3. Orientation-averaged extinction efficiencies of anisotropic spheres, $\langle Q_{ext} \rangle_o$ (solid curve) are compared with the $\frac{1}{3}$ average approximation, $\langle Q_{ext} \rangle_{1/3}$ (dashed curve) and the orientation averaged dipole approximation, $\langle Q_{ext} \rangle_{dip}$ (dotted curve). In (a), the principal dielectric constants are $\varepsilon_1 = \varepsilon_2 = 5.3495$, $\varepsilon_3 = 4.9284$. In (b), $\varepsilon_1 = 3$, $\varepsilon_2 = 4$, and $\varepsilon_3 = 5$. In (c), $\varepsilon_1 = 3$, $\varepsilon_2 = 4$, and $\varepsilon_3 = -2.2$.

APPENDIX A: VECTOR SPHERICAL HARMONICS

The scalar spherical harmonics $Y_{nm}(\theta, \phi)$ are expressed in terms of associated Legendre functions $P_n^m(\cos \theta)$ as[12,13]

$$Y_{nm}(\theta,\phi) = \left[\frac{2n+1}{4\pi} \frac{(n-m)!}{(n+m)!} \right]^{1/2} P_n^m(\cos\theta)\exp(im\phi),$$

$$(A1)$$

where the $P_n^m(\cos\theta)$ has a $(-)^m$ factor in its definition.[13] It is convenient to define normalized associated Legendre functions, $\bar{P}_n^m$ so that Eq. (A1) reads

$$Y_{nm}(\theta,\phi) \equiv \bar{P}_n^m(\cos\theta)\exp(im\phi). \qquad (A2)$$

Vector spherical harmonics are described in several reference books and papers,[4,5,12–14] although their definitions and notations vary with the authors. Our vector harmonics $\mathbf{Y}_{nm}$, $\mathbf{X}_{nm}$, and $\mathbf{Z}_{nm}$ have the numerically convenient expressions

$$\mathbf{Y}_{nm}(\theta,\phi) = \hat{\mathbf{r}}\bar{P}_n^m(\cos\theta), \qquad (A3)$$

$$\mathbf{X}_{nm}(\theta,\phi) = i\bar{u}_n^m(\cos\theta)\exp(im\phi)\hat{\boldsymbol{\theta}} - \bar{s}_n^m(\cos\theta)\exp(im\phi)\hat{\boldsymbol{\phi}},$$

$$(A4)$$

Stout *et al.*

$$\mathbf{Z}_{nm}(\theta, \phi) = \bar{s}_n^m(\cos \theta)\exp(im\phi)\hat{\boldsymbol{\theta}} + i\bar{u}_n^m(\cos \theta)\exp(im\phi)\hat{\boldsymbol{\phi}},$$

$$(A5)$$

where normalized functions $\bar{u}_n^m$ and $\bar{s}_n^m$ are defined by

$$\bar{u}_n^m(\cos \theta) \equiv \frac{1}{\sqrt{n(n+1)}}\frac{m}{\sin \theta}\bar{P}_n^m(\cos \theta), \qquad (A6)$$

$$\bar{s}_n^m(\cos \theta) \equiv \frac{1}{\sqrt{n(n+1)}}\frac{d}{d\theta}\bar{P}_n^m(\cos \theta), \qquad (A7)$$

which like the $\bar{P}_n^m$ can readily be evaluated from recursive algorithms.[5]

The authors may be contacted at brian.stout@fresnel.fr, michel.neviere@fresnel.fr, and evgueni.popov@fresnel.fr.

REFERENCES

1. B. Stout, M. Nevière, and E. Popov, "Mie scattering by an anisotropic object. Part I: Homogeneous sphere," J. Opt. Soc. Am. A **23**, 1111–1123 (2006).
2. C. F. Bohren and D. R. Huffman, *Absorption and Scattering of Light by Small Particles* (Wiley-Interscience, 1983).
3. H. C. Van de Hulst, *Light Scattering by Small Particles* (Dover, 1957).
4. B. Stout, M. Nevière, and E. Popov, "Light diffraction by a three-dimensional object: differential theory," J. Opt. Soc. Am. A **22**, 2385–2404 (2005).
5. L. Tsang, J. A. Kong, and R. T. Shin, *Theory of Microwave Remote Sensing* (Wiley, 1985).
6. O. Moine and B. Stout, "Optical force calculations in arbitrary beams by use of the vector addition theorem," J. Opt. Soc. Am. B **22**, 1620–1631 (2005).
7. B. Stout, J. C. Auger, and J. Lafait, "Individual and aggregate scattering matrices and cross sections: conservation laws and reciprocity," J. Mod. Opt. **48**, 2105–2128 (2001).
8. Y. L. Geng, X.-B. Wu, L. W. Li, and B. R. Guan, "Mie scattering by a uniaxial anisotropic sphere," Phys. Rev. E **70**, 056609 (2004).
9. P. Sabouroux, B. Stout, J.-M. Geffrin, C. Eyraud, I. Ayranci, R. Vaillon, and N. Selçuk, "Amplitude and phase of light scattered by micro-scale aggregates of dielectric spheres: comparison between theory and microwave analogy experiments," J. Quant. Spectrosc. Radiat. Transf. **103**, 156–167 (2007).
10. B. Stout, J. C. Auger, and J. Lafait, "A transfer matrix approach to local field calculations in multiple scattering problems," J. Mod. Opt. **49**, 2129–2152 (2002).
11. B. Stout, M. Nevière, and E. Popov, "Mie scattering by an anisotropic object. Part II: Arbitrary-shaped object—differential theory," J. Opt. Soc. Am. A **23**, 1124–1134 (2006).
12. A. R. Edmonds, *Angular Momentum in Quantum Mechanics* (Princeton U. Press, 1960).
13. J. D. Jackson, *Classical Electrodynamics* (Wiley, 1965).
14. C. Cohen-Tannoudji, *Photons & Atomes—Introduction à l'Électrodynamique Quantique* (InterEdition/Editions du CNRS, 1987).

Amplitude and phase of light scattered by micro-scale aggregates of dielectric spheres: Comparison between theory and microwave analogy experiments

Pierre Sabouroux[a,b,*], Brian Stout[a,b], Jean Michel Geffrin[a,b], Christelle Eyraud[a,b], Isil Ayranci[c,d], Rodolphe Vaillon[c], Nevin Selçuk[d]

[a]*Institut Fresnel, UMRCNRS 6133, Université de Provence, Aix-Marseille 1, France*
[b]*Université Paul Cézanne, Aix-Marseille 3, Ecole Généraliste d'Ingénieurs de Marseille, Campus de Saint Jérôme, Case 162, 13397 Marseille Cedex 20, France*
[c]*Centre de Thermique de Lyon (CETHIL CNRS-INSA Lyon-UCBL), INSA de Lyon, 69621 Villeurbanne, France*
[d]*Chemical Engineering Department, Middle East Technical University, 06531 Ankara, Turkey*

Abstract

Light scattering is a useful diagnostic tool for characterization of particles. Direct scattering measurements for arbitrarily shaped micro-scale particles is difficult due to small-scale limitations. Microwave analogy is a convenient approach to realize such measurements as it enables realization of analogous experiments with larger model particles in a spectral domain where wavelengths are on centimeter scale. In the present study a test model analogous to light scattering by a micro-scale aggregate of dielectric spheres was constructed and experimentally characterized in the microwave regime. Measured amplitude and phase of the scattered field were compared with theoretical predictions obtained from quasi-exact multiple-scattering T-matrix method and discrete dipole approximation (DDA). Excellent agreement demonstrates the validities of both the experiment and the models.

0. Introduction

For a long time now the interaction between electromagnetic waves and small solid aggregate-forming particles (dust, flakes, grains pollens, etc.) has generated a number of questions due to the complexity of the problem. Despite considerable efforts and progress, the difficulty of the problem is underlined by the comparatively small number and quality of quantitative experimental results.

The majority of experimental studies on such aggregates involves optical diagnostics. However, in order to validate the theoretical modeling of these light–particle interactions, it is essential to have a precise knowledge

*Corresponding author. Tel.: +33 4 91 28 83 53; fax: +33 4 91 67 67 44 28.
E-mail address: pierre.sabouroux@fresnel.fr (P. Sabouroux).

of the geometry and constitution of the aggregates. Since the characteristic dimensions of such particles in the optical domain is often of the same order of magnitude as the wavelength of light, the particles are too small to conveniently allow the fabrication of aggregates with precisely controlled geometries. Given these obstacles to such studies, one practical solution is to simultaneously scale both the characteristic dimensions of the aggregate and the wavelength of the incident radiation so that they are both on the centimeter scale. This method was employed in the 1970s for determination of the radar equivalent surface of aeronautical vehicles [1] and characterization of interplanetary dust grains [2].

In this work, we propose to use such techniques to study the interaction of electromagnetic waves with a complex shape particle such as a small size aggregate of spheres. Indeed, micro-scale aggregates constitute a class of particles, which are of interest in astrophysics (interstellar grains) and in mechanical and chemical engineering (soot particles) to cite a few examples. In the particular case of combustion products such as soot, characterization from optical diagnostics can permit a better understanding of their formation processes and then enable proposals of methods to reduce their production and thereby limit pollution. In any case, non-intrusive or remote sensing optical techniques based on the measurement and analysis of light scattered by these micro-sized particles are classically employed. However, to better understand the results of optical measurements new methods using electromagnetic waves with much larger wavelengths and scaling allows comparative studies to be carried out on model aggregates of considerably larger size. The characteristic particle dimensions in the present study are on the centimeter scale. Gustafson and his co-workers [3–8] employed a similar methodology. However, use was made of millimetric wavelengths (about 3 mm), which can hinder a precise characterization and/or the fabrication of certain test aggregates. The utilization of lower frequencies allows measurements to be carried out on rigorously controlled geometries.

On the other hand, a scattered field is completely characterized by its intensity, polarization state and phase and hence complete validation of electromagnetic scattering models necessitates experimental data on both amplitude and phase of the scattered field at two orthogonal polarization states. To the authors' knowledge such complete data was not previously published for dielectric agglomerates. Experimental data presented in this study is expected to be useful for validation of scattering models in terms of all primary variables.

This article is presented in three distinct parts. In the first part, the measurement apparatus and the model aggregate employed here are presented. In the second part, two models are presented for calculating the light scattered by the aggregate when subject to an incident electromagnetic field. In the third part, model predictions are compared with experimental results and conclusive remarks are made. Then, we present our conclusions and future works.

1. Description of the model aggregate and the experimental apparatus.

This first part presents the model dielectric aggregate and the microwave frequency experimental apparatus used in this study.

1.1. Model aggregate

As pointed out in the introduction, the characteristic size of the test aggregate (Fig. 1) is linked to the wavelength characterizing the incident electromagnetic wave so that the target (i.e. the aggregate) is of comparable size. The wavelength of the incident radiation can vary between 1.7 cm (18 GHz) and 15 cm (2 GHz). The apparatus making up the measurement chain determines this frequency range. The chosen material is an optically transparent dielectric, which aids in optimizing the alignments of the experimental configuration thanks to the utilization of laser beam. At the present time, the precision of the target position is inferior to 1 mm or in other words $\lambda/20$ for the highest encountered frequencies which is the most extreme case.

The global geometry of the aggregate is cubic. The aggregate is composed of a collection of 27 dielectric spheres each having a diameter of $D = 15.90 \pm 0.05$ mm. The edge of a cube is therefore 47.7 mm long. The spheres are composed of a PMMA (Altuglass, Fig. 2) with a relative permittivity of 2.5. This value was measured with the aid of a device developed in our laboratory: *EpsiMu* [9].
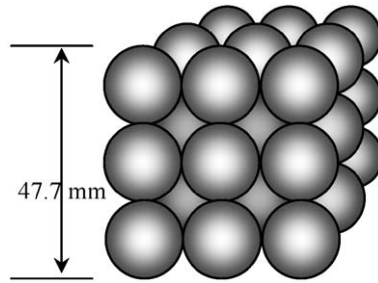
Fig. 1. Aggregate schematic.

Fig. 2. Photo of the test aggregate.

The wavelength utilized has to be compared to the dimension of an edge of the cube containing the 27 dielectric spheres. We choose then as a geometric parameter for comparison, kw where $w = 3 \times D$ represents the edge of the cube, i.e. 47.7 mm. In this manner $kw = 2\pi w/\lambda$.

1.2. Experimental apparatus

The experimental system is composed of a collection of mechanical positioners set within an anechoic chamber. Absorbers are HYFRAL APM66 and the reflectivity is less than –50 dB from 3 to 20 GHz. The internal dimensions of the chamber are 14.50 m long, 6.50 m wide and 6.50 m high. The mechanical positioners enable the emission and reception antennas follow circular trajectories centered on target to be analyzed. In the present case, the target aggregate is positioned at the center of these circular trajectories with an expanded polystyrene mast. The rigourous alignment of the target in the middle of the chamber is realised with a laser beam. The distance between the origin and the antennas is 173.50 cm for the emitting antenna and 175 cm for the receiving antenna.

The trajectories of the emission and reception antennas are contained in a horizontal plane passing through the center of the spherical coordinate system describing the setup. Two incident field directions are studied: a "face incidence" for which the propagation direction is perpendicular to one of the faces of the cube (case 0°), and an "edge incidence" for which the beam is oriented at an angle of 45° with respect to the normal (case 45°) as shown in Figs. 3 and 4. Furthermore, two incident field polarizations are studied with respect to the bistatic plane, i.e. the plane containing both the incident wave vector $\mathbf{k}_i$, and the scattered wave vector $\mathbf{k}_r \equiv k\hat{\mathbf{r}}$ where $\hat{\mathbf{r}}$ is the detector direction). "Vertical polarization" represents the case where electric field is normal to the bistatic plane, and "horizontal polarization" is used when the electric field lies within the bistatic plane (sometimes referred to as "parallel" to the bistatic plane).
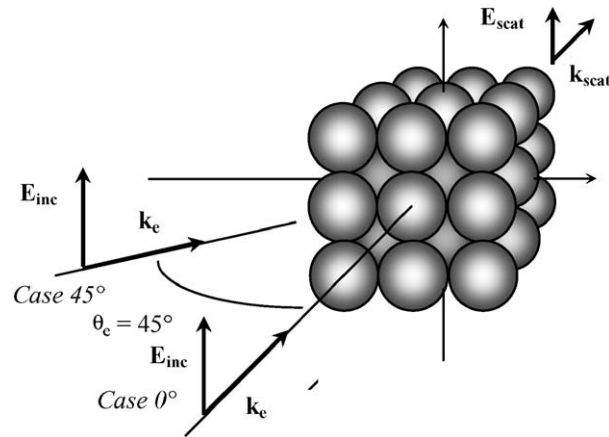
Fig. 3. Studied geometries.
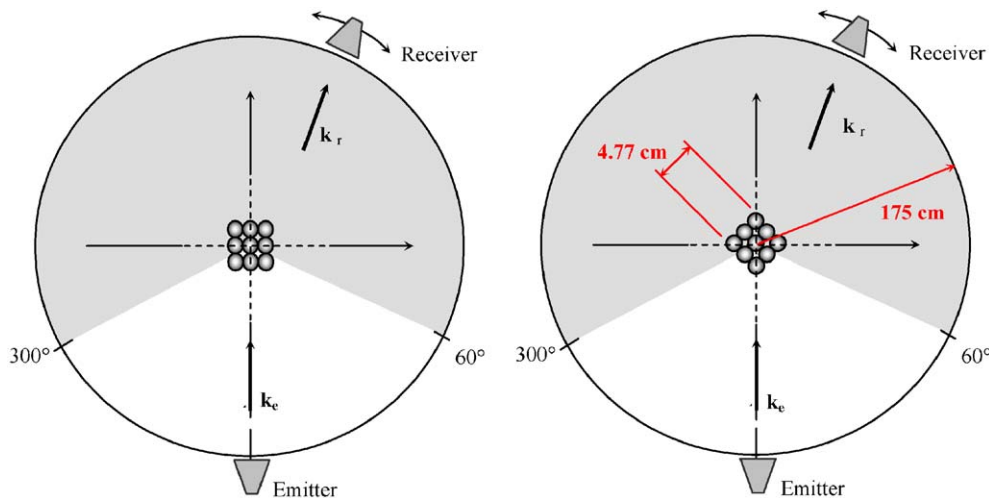
Fig. 4. Geometric disposition of the two positions of the aggregate with respect to the incident field. Case 0° on the left and Case 45° on the right.

The experimental setup has already been described in the reference papers [10–11]. The electromagnetic wave is emitted by a large band horn type antenna, designated as *double ridged antenna linearly polarized* (ARA DRG 118A). The incident polarization is fixed by the orientation of the emission antenna. The reception antenna is oriented such that the principal polarization is measured. The domain of angular detection covers 60–300° with the direction of forward scattering being designated by 180°. The angular step size is fixed to 1°. The microwave detection setup employs a vector network analyzer (HP8510C) working with multiple sources and mixers displaced and brought to the level of the antennas in order to limit the measurement uncertainties arising from the considerable length of the coaxial cables.

The measurement protocol, as described in Refs. [10–11], allows us to obtain both the amplitude and phase of the electric field scattered by the target (i.e. the aggregate). The scattered field is obtained by vector subtraction of the electromagnetic field with and without the presence of the target. The first of these two measurements corresponds to the total field measured with the target in place, which corresponds to a superposition of the incident and scattered fields. The second measurement is simply that of the incident field measured with the target removed. Under these conditions, for each frequency, and for each angular position,

the value of the complex diffracted field is the result of the vector subtraction of incident field (without the target) from the total field (with the target).

2. Theoretical calculations

2.1. Amplitude scattering matrix or S-matrix

We begin by defining a scattering plane as the plane containing the incident wave vector and the direction vector of the detector. If the incident field can be approximated by a plane wave in the region of the target, then it can be expressed as

$$\mathbf{E}_i = (E_{0//,i}\hat{\mathbf{e}}_{//,i} + E_{0\perp,i}\hat{\mathbf{e}}_{\perp,i})\exp(ikz - i\omega t)$$
$$= E_{//,i}\hat{\mathbf{e}}_{//,i} + E_{\perp,i}\hat{\mathbf{e}}_{\perp,i}, \tag{1}$$

where $k \equiv 2\pi/\lambda$, $E_{0//,i}$, $E_{0\perp,i}$ are complex constants, and $\hat{\mathbf{e}}_{//,i}$ and $\hat{\mathbf{e}}_{\perp,i}$ are unit vectors which are, respectively, parallel and perpendicular to the scattering plane, and chosen so that $(\hat{\mathbf{e}}_{//,i}, \hat{\mathbf{e}}_{\perp,i}, \hat{\mathbf{k}}_i)$ form a right-handed coordinate system.

Denoting the detector direction $\hat{\mathbf{k}}_s$, the far-field limit of the scattered field will have a spherical wave-type behavior in the neighborhood of the detector

$$\mathbf{E}_s \cong (E_{0//,s}\hat{\mathbf{e}}_{//,s} + E_{0\perp,s}\hat{\mathbf{e}}_{\perp,s})\frac{\exp(ikr - i\omega t)}{-ikr}$$
$$= (E_{//,s}\hat{\mathbf{e}}_{//,s} + E_{\perp,s}\hat{\mathbf{e}}_{\perp,s}), \tag{2}$$

where the $-ik$ factor in the denominator is a (non-universal) historical convention. The complex amplitudes $E_{0//,s}$ and $E_{0//,s}$ are functions of the detector angle, and the unit vectors $(\hat{\mathbf{e}}_{//,s}, \hat{\mathbf{e}}_{\perp,s}, \hat{\mathbf{k}}_s)$ form a right-handed coordinate system.

Adopting a coordinate system in which the $\hat{\mathbf{k}}_i$ direction defines the $\hat{\mathbf{z}}$ axis, the $\exp(i\mathbf{k}_i \cdot \mathbf{r})$ becomes simply $\exp(ikz)$, and the relationship between the $E_{//,s}, E_{\perp,s}$ and the incident field components, $E_{//,i}, E_{\perp,i}$ can be expressed via a 2×2 amplitude scattering matrix S [12]:

$$\lim_{r\to\infty}\begin{bmatrix} E_{//,s} \\ E_{\perp,s} \end{bmatrix} = \frac{\exp(ik(r-z))}{-ikr}\begin{bmatrix} S_2 & S_3 \\ S_4 & S_1 \end{bmatrix}\begin{bmatrix} E_{//,i} \\ E_{\perp,i} \end{bmatrix}, \tag{3}$$

where r and z are the length of the detector arm and the emitter to target distance, respectively and are equivalent in the present configuration. Each of the four scattering matrix elements in (S_1, S_2, S_3, S_4), are functions of the "scattering angle" θ, and the "azimuthal angle" ϕ [12].

Amplitude and phase of the scattered field, which are the parameters of interest, can be obtained from the elements of the amplitude scattering matrix. Complex constants of the incident and scattered electric fields in (1) and (2) can be represented in phasor notation as

$$E_{//,i} = a_{//,i}.\exp(i\delta_{//,i}), \quad E_{\perp,i} = a_{\perp,i}.\exp(i\delta_{\perp,i}), \tag{4}$$

$$E_{//,s} = a_{//,s}.\exp(i\delta_{//,s}), \quad E_{\perp,s} = a_{\perp,s}.\exp(i\delta_{\perp,s}). \tag{5}$$

Amplitude scattering matrix elements are complex numbers that can also be expressed in the form

$$S_n = |S_n|.e^{i\delta_n} \quad n = 1, 2, 3, 4. \tag{6}$$

The ratio of amplitude of scattered wave in the far field to that of incident wave can be obtained by substituting Eqs. (4–6) in Eq. (3) and rearranging:

$$M_{//,//} = \frac{a_{//,s}}{a_{//,i}} = \frac{|S_2|}{kr}, \tag{7}$$

$$M_{\perp,\perp} = \frac{a_{\perp,s}}{a_{\perp,i}} = \frac{|S_1|}{kr}. \tag{8}$$

Similarly, the phase difference between the scattered and incident fields can be obtained as

$$\Delta\phi_{//,//} = -\left[\delta_2 - \frac{\pi}{2}\right], \tag{9}$$

$$\Delta\phi_{\perp,\perp} = -\left[\delta_1 - \frac{\pi}{2}\right]. \tag{10}$$

2.2. T-Matrix calculations

When an object (aggregate) is composed of a number of components, one can obtain an essentially exact solution to the scattering fields by coupling a multiple-scattering theory of finite clusters with the T-matrices of the component objects [13–15]. When the components of the aggregate are spheres, the T-matrices of the individual spheres have analytic expressions obtained through generalizations of Mie theory [16]. Although any near or far-field information can be obtained from the T-matrix formulation that we employ, we are concerned herein only with far-field applications.

The principal difficulties encountered in the past for such T-matrix treatments were in the formulation of numerically reliable T-matrix computation schemes. Nowadays, numerical stability is no longer an obstacle since it can be overcome in a variety of ways (stable recursive algorithms, fast iterative schemes, sparse matrix inversions, etc.). In particular, numerical instabilities in the *stable* recursive RCTMA algorithm [13,14] employed here (*not* to be confused with earlier *unstable* recursive algorithms [17]) have not been observed to date [13–15,19–21]. The only other difficulty encountered is the necessity of generating the required special functions in efficient computer codes, but this problem has been successfully addressed in recent decades.

2.2.1. Extraction of the amplitude scattering matrix from the T-matrix

One requires the derivation of appropriate formulas in order to pass from the more complete scattering information residing within a system T-matrix [13–15] to the more limited scattering information described by the amplitude scattering matrix S. The comparison with experiment is facilitated by fixing the $\hat{x}$-axis to be some readily identifiable direction in the experimental setup (we chose the $\hat{x}$-axis to define the "vertical" direction in the experimental setup).

With the above coordinate system choices one can analytically calculate a set of incident field coefficients for each of the possible polarizations $a_{//}$ and $a_{\perp}$ [14,15]:

$$a_{//,q,v,\mu} = i^{v+1}\sqrt{\pi(2v+1)}[\delta_{\mu,1}e^{-i\phi} - (-)^q\delta_{\mu,-1}e^{-i\phi}],$$
$$a_{\perp,q,v,\mu} = i^{v}\sqrt{\pi(2v+1)}[\delta_{\mu,1}e^{-i\phi} + (-)^q\delta_{\mu,-1}e^{-i\phi}], \tag{11}$$

where $0 \leqslant \phi \leqslant (\pi/2)$ is the azimuthal angle between the scattering plane and the $\hat{x}$-axis (for e.g. $\phi = \pi/2$ for all comparisons with experiments illustrated in this work).

The indices in Eq. (11) are associated with the fact that these coefficients correspond to different types of electromagnetic partial waves composing the incident field. The $v = 1, \ldots, N_{max}$ are a multipole index with N_{max} being a truncation parameter which usually determines the precision of the calculation to about the same order as the Mie theory of a single spherical particle. In Eq. (11), we also remark an angular momentum projection index $\mu = -n, \ldots, n$ and a wave-type index $q = 1, 2$ where $q = 1$ designates waves generated from magnetic "sources" and $q = 2$ from electric sources [15,18]. The physical meaning of the indices can however be ignored at this point, however, since the physics of the electromagnetic waves has already been addressed when deriving Eqs. (3) and (11–14).

The next step in calculating the S-matrix is to construct a set of scattering coefficients $f_{//,p,n,m}^{(j)}$ and $f_{\perp,p,n,m}^{(j)}$ for each of the $j = 1, \ldots, N$ particles in the aggregate by matrix multiplication of the block matrices, $\tau_N^{(j,k)}$, composing the full body-centered T-matrix, τ_N, and the incident coefficients $a_{//}$, $a_{\perp}$ given above [13–15]:

$$f_{//,p,n,m}^{(j)} = \sum_{k=1}^{N} \sum_{q=1,2} \sum_{v,\mu} \exp(ik\hat{z} \cdot \mathbf{x}_k)[\tau_N^{(j,k)}]_{p,n,m;q,v,\mu} a_{//,q,v,\mu} \tag{12}$$

and idem for the perpendicular polarization, $\perp$. Once these calculations have been carried out, one can readily calculate the S-matrix components from the following analytical formulae:

$$S_1 = \sum_{j=1}^{N} \exp(-i\mathbf{k}_s \cdot \mathbf{x}_j) \sum_{n,m} \exp(im\phi)i^{-n}$$
$$\times [\bar{s}_n^m(\cos\theta)f_{\perp,1,n,m}^{(j)} + \bar{u}_n^m(\cos\theta)f_{\perp,2,n,m}^{(j)}],$$

$$S_4 = \sum_{j=1}^{N} \exp(-i\mathbf{k}_s \cdot \mathbf{x}_j) \sum_{n,m} \exp(im\phi)i^{-n}$$
$$\times [\bar{s}_n^m(\cos\theta)f_{//,1,n,m}^{(j)} + \bar{u}_n^m(\cos\theta)f_{//,2,n,m}^{(j)}],$$

$$S_2 = -\sum_{j=1}^{N} \exp(-i\mathbf{k}_s \cdot \mathbf{x}_j) \sum_{n,m} \exp(im\phi)i^{-n+1}$$
$$\times [\bar{u}_n^m(\cos\theta)f_{//,1,n,m}^{(j)} + \bar{s}_n^m(\cos\theta)f_{//,2,n,m}^{(j)}],$$

$$S_3 = -\sum_{j=1}^{N} \exp(-i\mathbf{k}_s \cdot \mathbf{x}_j) \sum_{n,m} \exp(im\phi)i^{-n+1}$$
$$\times [\bar{u}_n^m(\cos\theta)f_{\perp,1,n,m}^{(j)} + \bar{s}_n^m(\cos\theta)f_{\perp,2,n,m}^{(j)}], \tag{13}$$

where $\mathbf{k}_s = (\omega/c)\hat{\mathbf{k}}_s$. The $\cos\theta$-dependent functions, $\bar{u}_n^m$ and $\bar{s}_n^m$, in Eq. (13) are obtained from the associated Legendre functions:

$$\bar{u}_n^m(\cos\theta) \equiv \gamma_{nm}\frac{im}{\sin\theta}P_n^m(\cos\theta),$$

$$\bar{s}_n^m(\cos\theta) \equiv \gamma_{nm}\frac{d}{d\theta}P_n^m(\cos\theta),$$

$$\gamma_{nm} \equiv \left(\frac{(2n+1)(n-m)!}{4\pi n(n+1)(n+m)!}\right)^{1/2}. \tag{14}$$

2.3. Discrete Dipole Approximation

Discrete Dipole Approximation (DDA) is a well-established approach for estimation of scattering and absorption of electromagnetic radiation by arbitrarily shaped particles of size comparable to incident wavelength. This approach is categorized as one of the volume-integral equation methods for numerical modeling of electromagnetic scattering [22]. Pioneered by Purcell and Pennypacker [23], DDA has been improved to its present state mostly by Draine and Flatau [24,25]. The approximation is based on replacement of a continuum real scatterer by a finite array of interacting discrete dipoles positioned at the sites of a lattice such that the lattice spacing is small compared to wavelength. The oscillating polarizations (dipole moments) induced on each dipole due to the incident wave and the electric fields of the other oscillating dipoles in the system can be expressed by linear relations depending on polarizability of the dipole, incident electric field, positions and polarizations of other dipoles. The resulting system of $3N$ coupled linear equations, N being the total number of dipoles, represents a discrete analog of the integral equation that governs the scattering problem. Once the system of complex linear equations is solved for polarizations, the scattered electric fields at desired scattering planes and directions can be readily evaluated. The associated formulations for evaluation of polarizations, forward scattering amplitude matrix elements, amplitude scattering matrix elements, absorption emission and scattering cross sections were extensively documented previously [24].

Publicly available DDSCAT code [26] developed by Draine and Flatau provides a flexible means for application of DDA methodology. The code was previously developed and validated for estimation of scattering and absorption by irregular targets in terms of radiative properties such as scattering and

absorption cross sections, some of the 4×4 scattering matrix elements, etc. ([27] and references cited therein) which are parameters that characterize polarization state and intensity of the scattered field and are eventually related to the magnitudes of the amplitude scattering matrix elements. However, for prediction of phase, some modifications related to the position of dipoles with respect to origin of the scattering plane needs to be incorporated into the most recent code (v.6.1) so that the arguments of the complex scattering matrix elements can be predicted correctly. Details of prediction of amplitude and phase of the scattered field by using DDSCAT can be found in [28] where the accuracy of the modified code was demonstrated on single sphere targets of various sizes and materials by validating both the magnitudes and phases of the predicted complex amplitude scattering matrix elements against Mie theory solutions.

The target of 27-sphere cubic agglomerate under consideration was framed in a $48 \times 48 \times 48$ cubic lattice in which the number of occupied lattice sites amount to 56781 dipoles. This discretization with $|m|kd = 0.27$ for 8 GHz case and $|m|kd = 0.47$ for 14 GHz case was checked to satisfy the applicability criterion of DDSCAT, reported as $|m|kd < 0.5$, where m represents the complex index of refraction and d stands for the lattice spacing [26,27]. DDSCAT code modified for phase computations [28] was run by using the target shape module for multisphere targets (NSPHER), generalized prime factor algorithm for fast Fourier transform (GPFAFT), preconditioned biconjugate gradient method with stabilization (PBCGST) for iterative solution of the system of complex linear equations and corrected lattice dispersion relation by Gutkowitcz–Krusin and Draine (GKDLDR) for determination of dipole polarizabilities. Error tolerance used in conjugate gradients method was 10^{-5}. Resulting amplitude scattering matrix elements were substituted in Eqs. (6–10) to obtain amplitude and phase of scattered field relative to the incident field.

3. Results, comparison between theory and experiment

Due to the large volume of experimental data gathered from our test aggregate composed of 27 spheres in a cubic arrangement, we choose two representative frequencies and compare the results: 8 GHz ($\lambda = 3.75$ cm) and 14 GHz ($\lambda = 2.14$ cm). We have then two values for the kw parameter, $w = 3 \times D$ indicative of aggregates whose total size are far from being small with respect to the wavelength:

For $f = 8$ GHz, $\lambda = 3.75$ cm $\rightarrow kw = 8$,

For $f = 14$ GHz, $\lambda = 2.14$ cm $\rightarrow kw = 14$.

In order to compare results between theory and experiment, a normalization is performed. For the amplitudes, we simply normalize with respect to the scattering maximum of forward scattering. The phase is similarly normalized by taking forward scattering to define the origin of the phase shift.

Comparison between experimental and theoretical results for the cases of polarization parallel and perpendicular to the scattering plane when the incident wave vector was normal to the face of an aggregate (case 0°) are illustrated in Figs. 5a–d. Analogous results obtained for an incident wave vector oriented along an edge of the cube are grouped in Figs. 6a–d. In both figures, the experimental results are embodied by a solid black curve. The theoretical results generated by the multiple scattering T-matrix method are represented by a solid gray curve. Finally, the results obtained from the DDSCAT method are illustrated by using black crosses. As can be seen from the figures, theoretical and experimental results are in excellent agreement.

We observe some slight differences in the phase curves at the two frequencies for the case of incidence on the face of the target (case 0°). This is apparently due to a slight misalignment of the target in the experimental reference frame.

In view of the excellent agreements, we can now consider our experimental protocols to be validated as well as our means for carrying out theoretical modeling via the T-matrix or DDA. Under these conditions, we are currently planning the characterizations of more realistic aggregates containing larger number of particles in more complex configurations where absorption is present.
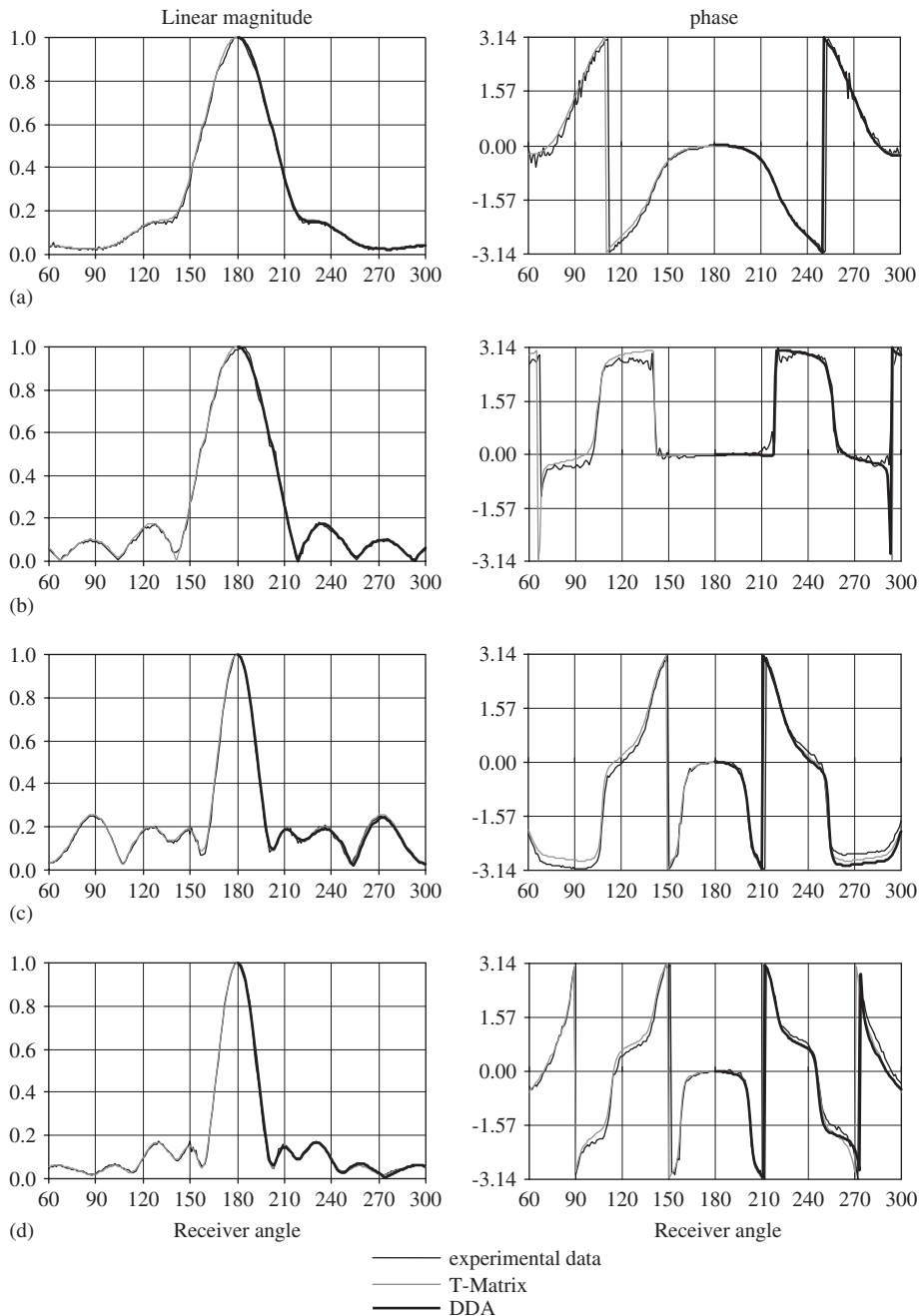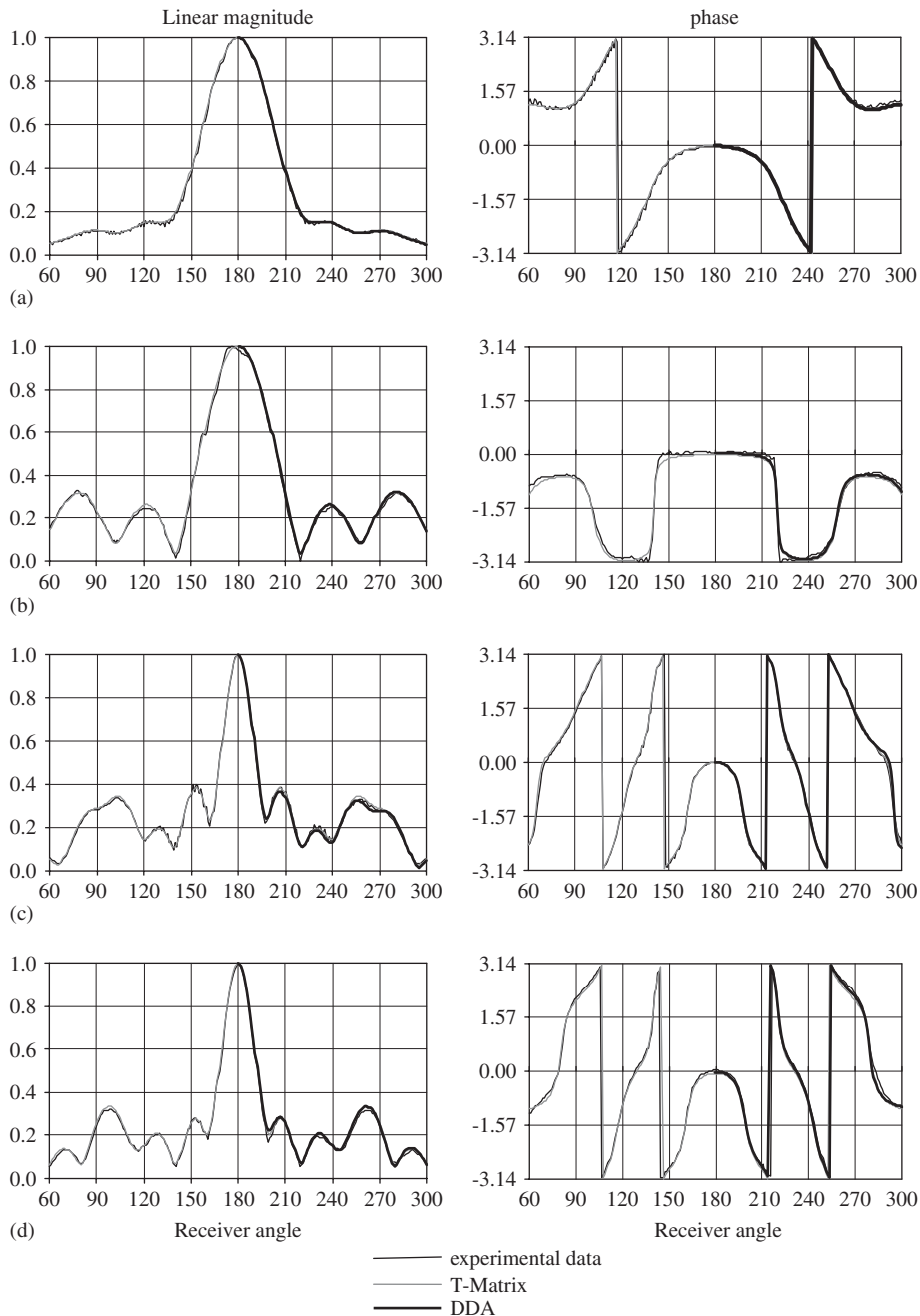
Fig. 5. (a) Case 0°: polarisation //, 8 GHz; (b) Case 0°: polarisation ⊥, 8 GHz (c) Case 0°: polarisation //, 14 GHz; (d) Case 0°: polarisation ⊥, 14 GHz.

4. Conclusions

Electromagnetic scattering of light by microscale aggregates of dielectric spheres has been investigated both theoretically and experimentally. Magnitude and phase of scattered field measured by microwave analogy principle were compared with predictions of T-Matrix and DDA models. The originality of those measurements is that both magnitude and phase are measured.

Fig. 6. (a) Case 45°: polarisation //, 8 GHz; (b) Case 45°: polarisation ⊥, 8 GHz; (c) Case 45°: polarisation //, 14 GHz; (d) Case 45°: polarisation ⊥, 14 GHz.

Excellent agreements between the model predictions and measurements reveal the validity of both the experimental approach and the models for analysis of electromagnetic scattering in similar situation. The experimental data presented here provide reference solutions against which light scattering models can be tested for accurate prediction of both amplitude and phase of scattered fields.

As future work, it is planned to extend the analysis to chain-like aggregates of absorbing spheres. Morphology and optical properties will be selected so as to be representative of soot particles produced by

reactive media. The interest of this work, associating experimental measurements and different types of theoretical modeling calculations on aggregates of spheres, should also manifest itself in the astrophysical community for studies concerning interstellar dust. Indeed, some stellar dust grains are also assumed to have the shape of aggregates.

Experimental data are available electronically on request to the corresponding author.

Acknowledgments

References

[1] Crispin JW, Siegel KM. Method of radar cross-section analysis. Electrical science series. New York: Academic Press; 1968.
[2] Greenberg JM, Pedersen NE, Pedersen JC. Microwave analog to the scattering of light by nonspherical particles. J Appl Phys 1961;32:233–42.
[3] Gustafson B. Microwave analog to light scattering measurements: a modern implementation of a proven method to achieve precise control. JQSRT 1996;55(5):663–72.
[4] Xu Y, Gustafson BÅS. A generalized multiparticle Mie-solution: further experimental verification. JQSRT 2001;70(4–6):395–419.
[5] Gustafson BÅS. Scattering by simple and complex systems I: methods. In: Greenberg JM, Li A, editors. Formation and evolution of solids in space, vol. 523. Dordrecht: Kluwer Academic Publishers; 1999. p. 535–48.
[6] Gustafson BÅS, Kolokolova L, Thomas-Osip JE, Waldemarsson KWT, Loesel J, Xu Y-l. Scattering by simple and complex systems II: microwave measurements. In: Greenberg JM, Li A, editors. Formation and evolution of solids in space. Dordrecht: Kluwer Academic Publishers; 1999. p. 549–63.
[7] Gustafson BS. Microwave analog to light scattering measurements. In: Mishchenko MI, Hovenier JW, Travis LD, editors. Light scattering by nonspherical particles: theory, measurements, and geophysical applications. New York: Academic Press; 1999. p. 367–90 [ISBN 0-12-498660-9, Chapter 13].
[8] Xu Y-l. Electromagnetic scattering by an aggregate of spheres: far field. Appl Opt 1997;36:9496–508.
[9] Sabouroux P, Boschi P. EpsiMu un nouvel outil pour déterminer les caractéristiques électromagnétiques de matériaux dans le domaine des hyperfréquences. Rev Electr Electron 2005;10:58–62.
[10] Belkebir K, Bonnard S, Pezin F, Sabouroux P, Saillard M. Validation of 2D inverse scattering algorithms from multi-frequency experimental data. J Electromagn Waves Appl 2000;14:1637–67.
[11] Geffrin JM, Sabouroux P, Eyraud C. Free space experimental scattering database continuation: experimental set-up and measurement precision. Inverse Probl 2005;21:S117–30.
[12] Bohren CF, Huffmann ER. Absorption and scattering of light by small particles. New York: Wiley; 1983.
[13] Stout B, Auger JC, Lafait J. A transfer matrix approach to local field calculations in multiple scattering problems. J Mod Opt 2002;49:2129–52.
[14] Auger JC, Stout B. A recursive T-matrix algorithm to solve the multiple scattering equation: numerical validation. JQSRT 2003;79–80:533–47.
[15] Stout B, Auger JC, Lafait J. Individual and aggregate scattering matrices and cross sections: conservation laws and reciprocity. J Mod Opt 2001;48(14):2105–28.
[16] Tsang L, Kong J, Shin R. Theory of microwave remote sensing, Wiley series in remote sensing. New York: Wiley; 1985.
[17] Siqueira PR, Sarabandi K. T-matrix determination of effective permittivity for three-dimensional dense random media. IEEE Trans Antennas Propagat 2000;48.
[18] Jackson JD. Classical electrodynamics, 3rd ed. New York: Wiley; 1999.
[19] Auger JC, Stout B, Martinez V. Scattering efficiency of aggregated clusters of spheres: dependence on configuration and composition. JOSA A 2005;22:2700–8.
[20] Stout B, Andraud C, Stout S, Lafait J. Absorption in multiple scattering systems of coated spheres. JOSA A 2003;20:1050–9.
[21] de Silva A, Andraud C, Charron E, Stout B, Lafait J. Multiple light scattering in multistratified media: model experiment. Physica B 2003;338:74–8.
[22] Kahnert FM. Numerical methods in electromagnetic scattering theory. JQSRT 2003;79:775–824.
[23] Purcell EM, Pennypacker CR. Scattering and absorption of light by nonspherical dielectric grains. Astrophys J 1973;186:705–14.
[24] Draine BT. The discrete-dipole approximation and its application to interstellar graphite grains. Astrophys J 1988;333:848–72.

[25] Draine BT, Flatau PJ. Discrete-dipole approximation for scattering calculations. J Opt Soc Am A—Opt Image Sci Vis 1994;11: 1491–9.

[26] Draine BT, Flatau PJ. User guide for the discrete dipole approximation code DDSCAT.6.1, 2004. 〈http://arxiv.org/abs/astro-ph/0409262〉.

[27] Draine BT. The discrete dipole approximation for light scattering by irregular targets. In: Mishchenko MI, Hovenier JW, Travis LD, editors. Light scattering by nonspherical particles: theory, measurements and applications. San Diego: Academic Press; 2000. p. 131–45.

[28] Ayranci I, Vaillon R, Selçuk N. Performance of discrete dipole approximation for prediction of amplitude and phase of electromagnetic scattering by particles. JQSRT 2006, in press, doi:10.1016/j.jqsrt.2006.06.006.

Longitudinal Optical Binding of High Optical Contrast Microdroplets in Air

Marc Guillon,[1,*] Olivier Moine,[2,†] and Brian Stout[2,‡]

[1]*Laboratoire d'Interférométrie Stellaire et Exoplanétaire, Observatoire de Haute Provence,*
04870 Saint Michel l'Observatoire, France

[2]*Institut Fresnel, UMR 6133 Université Aix-Marseille I, Case 161 Faculté des Sciences et Techniques, Centre de Saint Jérome,*
13397 Marseille Cedex 20, France

Binding along the beam axis (which we shall call "longitudinal optical binding") has been observed between micron-sized oil droplets in a three dimensional optical trap in air. We argue that it is the high optical contrast which is responsible for the exceptionally stable doublet structures observed experimentally. It was also observed that optically bound doublets tend to cling to interference fringes created by the two counterpropagating beams. Our observations are qualitatively discussed in the context of both the ray model (optics) approximation, and in the Rayleigh (dipolar) range. Our observations were consistent with calculations of binding and trapping forces which we carried out by employing an exact multiple-scattering theory.

PACS numbers: 42.25.Fx, 42.25.Gy, 42.25.Hz, 42.25.Kb

Since the pioneering work of Ashkin [1], optical trapping and manipulation of single microparticles has become a commonplace experimental tool. Moreover, in multiple-particle traps, optical interactions between scattering microspheres have been repeatedly demonstrated and have begun to find applications in their own right [2–4]. These optically induced interactions, (commonly known as "binding forces") can be attractive or repulsive, and indicate intriguing perspectives in multiple-particle manipulations and spontaneous optical organization [2].

Optical trapping of mesoscopic particles has predominately been studied for particles suspended in liquids. Manipulation of micron-sized particles in rarefied media is notoriously more difficult due to the existence of strong van der Waals sticking forces, and viscosities approximately a thousand times smaller in air than those present in liquids. Nevertheless, air [1,5,6] and vacuum [5,7,8] trapping and levitation experiments have been performed and exhibited strong single-particle trapping efficiencies. The two main solutions to overcome van der Waals forces are, usually, the use of aerosols like oil [8] or water droplets [1,9] and, for solid particles, strongly focused high power laser beams [5,6] and ultrasonic vibrations to free the particles from the solid surfaces on which they tend to cling.

Although optical binding studies in liquid media offer numerous advantages such as heavy damping, the weak optical contrasts between the trapped particles and the liquid in the experimental configurations studied so far tends to weaken these interactions and may limit their applications. In more rarefied media such as air with less damping, the high optical index contrasts can induce higher trapping efficiencies as well allow for a better confinement of whispering gallery modes [10,11] which can, in turn, induce nonlinear scattering studies such as lasing [12] and stimulated Raman spectroscopy [9]. The possibility of creating stable optically bound clusters of

particles in air could open up new domains of study in the aforementioned phenomena, as well as introducing others such as the formation of secondary optical traps for nano-scale or molecular particles [13].

In this Letter, we report on the apparently first experimental and theoretical studies of strong longitudinal binding (i.e., binding along the direction of the beam axis) in two and three droplet systems of oil microdroplets in air (see Figs. 1 and 2). These droplets are much smaller than those previously studied in air or vacuum (from 1 to 2.5 μm in diameter), and considerably smaller than those
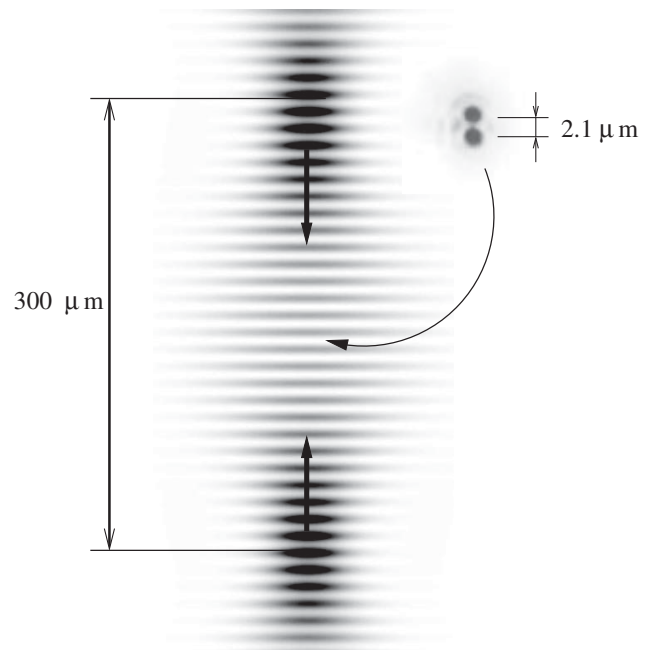

FIG. 1. Principle of the experimental setup for coherent and counterpropagating circularly polarized laser beams. The screen shot of the oil-droplet doublet (most stable observed structure from far) is out of scale.
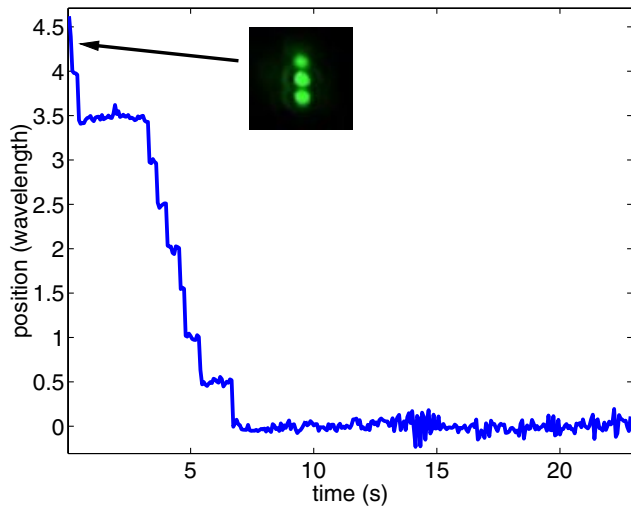
FIG. 2 (color online). Mean position (in units of λ) of a trapped doublet returning to its equilibrium position, taken for reference as zero, after the smaller third droplet (on top) escaped. The droplets are roughly 2.1 μm apart from one another.

studied in simulations of trapping and/or binding before now [11]. We have found that they exhibit behavior [14] quite different from that previously observed in water [4,15,16]. We also report on our preliminary exact multipolar calculations invoking the Maxwell stress tensor in the resonant or "Mie" regime [17] which corroborate our observations.

The experimental configurations for observing longitudinal binding in both air and liquid consist essentially of optical traps formed by two counterpropagating and diverging laser beams (see Fig. 1: not to scale). In our air experiment, the laser beam we use is circularly polarized ($\lambda = 532$ nm, $P \simeq 30$ mW). The counterpropagating beam is generated by a cat's eye retroreflector. The so-built two counterpropagating beams are focused 300 μm apart with a weak numerical aperture (1/15). Trapping occurs in the region where the upward and downward beam have near equal irradiance. The trap is ~ 20 μm wide and over 300 μm high. Trapping in the direction transverse to the beam propagation is achieved by forces associated with the intensity gradient. Trapped doublets in such an arrangement are exceptionally stable (on the order of hours) and are quite resistant to physical and optical perturbations as well.

Optical trapping of microspheres (of radius R, and refraction index n_s) imbedded in a lower index homogenous medium n_m, has been studied for a long time in the geometric optics (ray model) regime ($kR \gg 1$: $k = n_m \frac{\omega}{c}$) [18], but the particles under study here clearly fall outside of this domain. Nevertheless, one might be tempted to argue based on geometric optics intuition that the optical binding observed here may be due to each sphere acting as a lens which creates an optical trap for the other sphere. This could be a first approximate explanation for the

stability of the doublet, as well as explaining why similar phenomenon are not observed in liquid media.

On the other extreme, when the radius of the spheres is such that $kR < 1$, the dipole or "Rayleigh" approximation becomes reasonable (also depending on the relative refractive index). For multiple-particle traps in which the particle separations are orthogonal to both the beam axis and the beam polarization, it has been experimentally observed and theoretically corroborated in the Rayleigh approximation that spheres experience optical potential minima every λ (wavelength in the medium) [3]. When the particle separation is along the beam axis, similar calculations indicate (longitudinal) potential wells roughly every $\lambda/2$. Both of these periodic phenomena are essentially of a wave-interference origin, and one can expect analogous behavior (in the far-field at least) even when the scattering is essentially of a resonant nature ($R \sim \lambda$).

In our experiment, the trapping beams cross a glass cell filled with a sunflower oil-droplet cloud. The glass cell protects droplets from convection currents in the room. Scattered irradiance is projected onto a video camera. The most commonly trapped structure was a doublet, being observed more frequently than even a single droplet. The observation of interference of their respective Airy rings tells us that the droplets in a doublet are phase locked despite sometimes considerable perturbations arising from Brownian motion, intensity fluctuations between the counterpropagating beams, and the speckle pattern (mainly due to the surrounding droplet cloud and dirt on the optics).

It also appears clear that the droplets are not in contact as capillary forces are much larger than optical forces. Droplets coming into physical contact would coalesce rapidly into a single droplet. Despite all of the aforementioned perturbations, trapped doublets were typically stable for hours, implying a deep optical potential barrier separating the particles.

After a doublet has been trapped, many other droplets coming from the cloud continue to enter the trap, and interact with the trapped doublet. These interactions sometimes lead to trapped triplet structures (see Fig. 2). These structures have a much more limited stability than doublets and typically finish their existence with the third droplet either collapsing onto the doublet or escaping. The newly trapped droplet of a triplet structure is always observed to be smaller than the two previously trapped particles. This is due to the fact that a stable, readily imaged, doublet is the end result of the merging of several particles initially present in the cloud. We also remark that the center to center separation distance of the doublet increases as particles grow in such a manner that the particles never touch. The increase in the doublet size finishes when the entire oil cloud in the cell has descended to the floor of the chamber. The radii of the droplets initially present in the cloud can be estimated from a Stokes model and the observed terminal velocities to lie within the range of 0.5 μm to 0.8 μm.

When a small third droplet hangs on the doublet, the equilibrium position in the trap is different from that of a doublet. Although we do not analyze this effect quantitatively here, we believe that geometric dissymmetry and optically induced interactions between the particles leads to a dissymmetry in the radiation pressure. In Fig. 2, we illustrate the time evolution of the mean position of a doublet returning to its equilibrium position. The previous structure was a bound triplet for which the third droplet finally escaped. Taking a mean of the images (which cover several pixels) allows us to determine the position of the doublet to subpixel precision. The doublet is seen to cling to fringes created by the two counterpropagating coherent beams. We conclude that the interference fringes are capable of creating shallow $\lambda/2$ traps for the doublet as a whole which lead to a measurable dwell time for the doublet with thermal energy being sufficient to make transitions to more stable minima, henceforth ensuring that the doublet as a whole attains a potential energy minimum.

Up until this point in our observations, one could imagine that the binding effect could be described purely as a lens effect in the geometric optics approximation. From time to time, we observed rapid changes in the doublet appearance. This phenomenon may be due to a collision with an nonvisible droplet coming from the descending cloud. The low resolving power of the imaging microscope objective ($0.25 N.A.$) creates an interference pattern between particles' images preventing a precise measurement of the distance separation. However, the difference of distance separation could be estimated to be of the order of 200 nm. The observed phenomenon might alternatively correspond to a switching between two longitudinal optical potential wells, separated by $\approx \lambda/2$. This second hypothesis is further supported by the observations of the interference of Airy rings (see Fig. 3). We can observe that in the first picture, the Airy rings interfere in a manner as to give a dark fringe between the droplets while on the other, bright dots can be seen on the symmetry plane. This tends to confirm that in one case, the nonresolved particles are emitting in phase and in the other case, they are emitting in phase opposition. This interpretation, inspired by the Rayleigh approximation is also consistent with the rigorous calculations presented further.

In our case, the radii of the spheres are comparable in size to the wavelength of the trapping radiation (typically referred to as the resonant or Mie regime), so that neither Rayleigh nor geometric optics approximations are valid, and one must invoke full electromagnetic calculations in order to obtain quantitative force predictions. An advantage of our quasiexact calculations is that they describe not only the direct wave-particle interactions, but all of the multiple-scattering effects as well. Our calculations were performed by coupling an analytic calculation of the optical force [17] with analytic multiple-scattering calculations (formulated in terms of a multiple-scattering T matrix [19,20]).

We present here results of simulations concerning initial doublet formation and stability (force simulations for the larger doublets will be presented elsewhere). We define the binding force, $F_{b,\parallel} \equiv \frac{1}{2}\hat{z} \cdot (\mathbf{F}_2 - \mathbf{F}_1)$, where $\mathbf{F}_1$ and $\mathbf{F}_2$ are the optical forces on droplets 1 and 2 labeled such that $z_2 > z_1$ so that $F_{b,\parallel} < 0$ corresponds to attraction. In Fig. 4, we show the results of our calculations of $F_{b,\parallel}$ on a pair of $1.2\lambda \simeq 0.6$ μm in radius oil droplets ($n_s = 1.48$). The force is calculated as a function of particle separation, d/λ. The curve (a) corresponds to $F_{b,\parallel}$ for a single plane wave. For curves (b) and (c) the binding force is calculated when a circularly polarized plane wave is coherently reflected back onto itself. The curve (b) corresponds to the case where one particle is artificially "frozen" to be centered on one of the interference maxima, while for curve (c), one particle is frozen to be centered on an intensity minimum. The force is calculated in picoNewtons for an incident beam irradiance of 1 mW per μm^2. The beam irradiance used in the experiment being ~ 0.3 mW μm^{-2}, forces should simply be multiplied by this factor, the doublet geometry is irradiance independent as long as optical forces dominates thermal forces.

FIG. 3. Two consecutive pictures of a doublet. The quick change ($<1/15$ s) is attributed to a switching between two different equilibrium positions which is corroborated by the qualitatively distinct interference patterns. Droplets are ~ 2 μm in diameter.
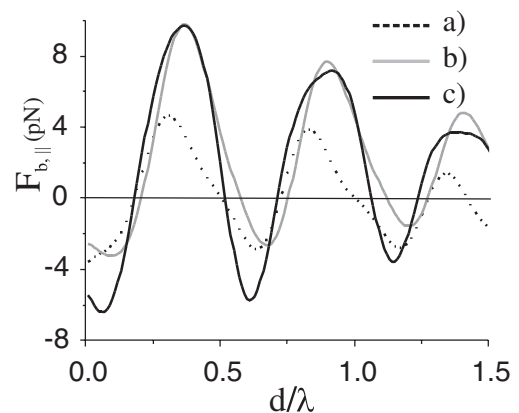

FIG. 4. Binding force: (a) $F_{b,\parallel}$ for a single plane wave, (b) $F_{b,\parallel}$ for counterpropagating circularly polarized plane waves with one particle on an interference maxima, (c) $F_{b,\parallel}$ in the same situation as for (b) except that one particle lies on an interference minima.
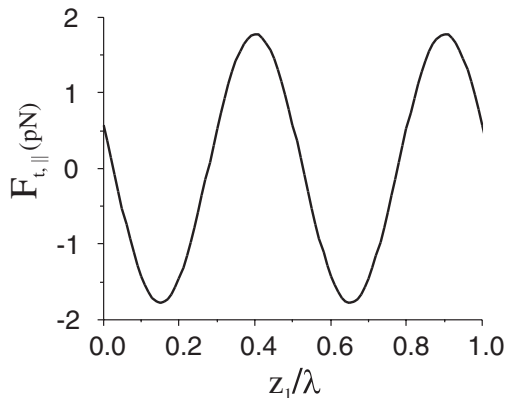
FIG. 5. Total longitudinal force, $F_{t,\parallel}$, on a doublet with a separation distance of $d = 0.55\lambda$ as a function of the position, z_1/λ, of the "first" particle.

An important observation of the force in Fig. 4 is the existence of a local stable equilibrium position ($F_{b,\parallel} = 0$ and $dF_{b,\parallel}/dz < 0$) which occur every $\sim\lambda/2$, even for a single plane wave, which can explain the high stability of the doublet despite strong speckle perturbations. It is also important to remark that the calculations indicate that the optical forces in this experiment are on the order of several picoNewtons and should consequently dominate other forces present (gravitational and electrostatic) on the doublet to yield rather deep optical potential wells (which are centered on the equilibrium positions) in agreement with our experimental observations. We also remark that the positions of the local equilibrium positions vary only slightly when the position of the frozen particle is moved with respect to the interference fringes.

The total longitudinal force on the doublet, $F_{t,\parallel} \equiv \hat{\mathbf{z}} \cdot (\mathbf{F}_1 + \mathbf{F}_2)$, is plotted in Fig. 5. Although this plot is the result of our full multipole calculations, the total force on the doublet can be qualitatively understood in terms of the "gradient" force and the intensity maxima and minima of the interference fringes. This figure indicates that the total trapping forces on a doublet originating from interference fringe effects are comparatively weak with respect to the forces associated with binding. This observation is consistent with experimental observations where the mean remaining time in fringes is much smaller than the doublet lifetime. More precise comparisons between theory and experiment could be made by modeling the longitudinal variations in the beam irradiance.

In conclusion, binding effects have been studied both experimentally and theoretically in air for particles in the resonant or Mie domain. The strong relative index contrast is the main difference between these experiments and those carried out in water. Potential minima separated by $\lambda/2$ may have been observed in longitudinal binding in analogy with the λ periodicity observed in optical binding transverse to the beam propagation [3]. It also seems likely that

there is an analogy between our observations and the recent longitudinal bistability observed in liquid media experiments [21]. The strong binding behavior that we have observed in air opens opportunities to build self-structured photonic crystals or opals. It can also be a useful tool to study mode coupling between microcavities and the creation of secondary, high gradient optical traps.

We would like to particularly thank Professor A. Labeyrie for fruitful discussions and advice for the experimental setup.

[1] A. Ashkin, Phys. Rev. Lett. **24,** 156 (1970).
[2] M. Burns, J.-M. Fournier, and J. Golovchenko, Science **249,** 749 (1990).
[3] M. Burns, J.-M. Fournier, and J. Golovchenko, Phys. Rev. Lett. **63,** 1233 (1989).
[4] S. Tatarkova, A. Carruthers, and K. Dholakia, Phys. Rev. Lett. **89,** 283901 (2002).
[5] A. Ashkin and J. Dziedzic, Appl. Phys. Lett. **19,** 283 (1971).
[6] R. Omori, T. Kobayashi, and A. Suzuki, Opt. Lett. **22,** 816 (1997).
[7] G. Roosen, Can. J. Phys. **57,** 1260 (1979).
[8] A. Ashkin and J. Dziedzic, Appl. Phys. Lett. **28,** 333 (1976).
[9] R. Hopkins, L. Mitchem, A. Ward, and J. Reid, Phys. Chem. Chem. Phys. **6,** 4924 (2004).
[10] A. Ashkin and J. Dziedzic, Phys. Rev. Lett. **38,** 1351 (1977).
[11] M. Povinelli, S. Johnson, M. Loncar, M. Ibanescu, E. Smythe, F. Capasso, and J. Joannopoulos, Opt. Express **13,** 8286 (2005).
[12] H.-M. Tzeng, K. Wall, M. Long, and R. Chang, Opt. Lett. **9,** 499 (1984).
[13] H. Xu and M. Kall, Phys. Rev. Lett. **89,** 246802 (2002).
[14] M. Guillon, Proc. SPIE Int. Soc. Opt. Eng. **5930,** 461 (2005).
[15] V. Garcés-Chávez, D. Roskey, M. Summers, H. Melville, D. McGloin, E. Wright, and K. Dholakia, Appl. Phys. Lett. **85,** 4001 (2004).
[16] W. Singer, M. Frick, S. Bernet, and M. Ritsch-Marte, J. Opt. Soc. Am. B **20,** 1568 (2003).
[17] O. Moine and B. Stout, J. Opt. Soc. Am. B **22,** 1620 (2005).
[18] R. Gussgard, T. Lindmo, and I. Brevik, J. Opt. Soc. Am. B **9,** 1922 (1991).
[19] J.C. Auger and B. Stout, J. Quant. Spectrosc. Radiat. Transfer **79–80,** 533 (2003).
[20] B. Stout, J. Auger, and J. Lafait, J. Mod. Opt. **49,** 2129 (2002).
[21] N. Metzger, K. Dholakia, and E. Wright, Phys. Rev. Lett. **96,** 068102 (2006).

Mie scattering by an anisotropic object. Part I. Homogeneous sphere

Brian Stout, Michel Nevière, and Evgeny Popov

*Institut Fresnel, Unité mixte de Recherche 6133, Case 161 Faculté des Sciences et Techniques,
Centre de Saint Jérôme, 13397 Marseille Cedex 20, France*

Establishing a vector spherical harmonic expansion of the electromagnetic field propagating inside an arbitrary anisotropic medium, we extend Mie theory to the diffraction by an anisotropic sphere, with or without losses. The particular case of a uniaxial material leads to a simpler analysis. This work opens the way to the construction of a differential theory of diffraction by a three-dimensional object with arbitrary shape, filled by an arbitrary anisotropic material. © 2006 Optical Society of America

OCIS codes: 290.5850, 050.1940, 000.3860, 000.4430.

1. INTRODUCTION

Resonant scattering from anisotropic particles is a field of growing interest due to an increasing number of technological and biological applications. By "resonant scattering" we mean particles comparable in size to the wavelength of the incident radiation. By "comparable in size," we mean any particle size approaching an order of magnitude smaller than the wavelength and within a few orders of magnitude larger than the wavelength. Scattering from anisotropic particles much smaller than the wavelength is well understood from dipolar considerations,[1] while one generally considers that particles a few orders of magnitude larger than the wavelength can be reasonably well treated with geometric optics[2] (despite some notable exceptions already known from scattering by large isotropic scatterers.[3]) Scattering of electromagnetic radiation from a homogeneous isotropic sphere as originally addressed by Lorenz[4,5] and later by Mie[6] has been the source of a vast quantity of scientific and technological studies over the last 50 years (at least). The Lorenz–Mie solution is expressed analytically as an infinite series involving spherical Bessel functions. The complexity involved in evaluating these special functions largely prevented detailed studies from being performed before the availability of electronic calculators.

In view of the wide popularity and success of studies based on Mie theory and the numerous questions posed by anisotropic scattering, a number of attempts have been made in the literature to extend Mie theory to the problem of scattering by a sphere composed of anisotropic media. Studies involving analytical calculations have usually chosen to simplify the problem by addressing some particular geometries and/or anisotropic configurations in order to facilitate analytic or near analytic calculations (anisotropy in a spherical layer,[7] radial or uniform,[8] radial anisotropy in a sphere.[9]) A notable exception is the recent paper by Geng *et al.*,[10] who presented an analytic solution for the uniaxial anisotropic sphere and of which we became aware during the preparation of this paper. Concerning general homogeneous anisotropy, however, the recent work of Ref. 10 declares it to be not "exactly soluble," while the well-known book of Bohren and Huffman[11] says only that no exact solution has been published and concentrates on the Rayleigh–Gans approximation. In this paper, we solve the problem of scattering by a sphere composed of an *arbitrary* homogeneous anisotropic medium. By arbitrary, we mean that the sphere is composed of a medium described by an arbitrary permittivity tensor, including the possibility of absorption. This solution, like the Mie solution, is analytic in the sense that it involves only mathematical formulas that can be readily evaluated on a computer so that the only source of error comes from selection of a finite partial wave cutoff (as in ordinary Mie theory), as well as machine errors.

2. ELECTRIC PERMITTIVITY IN SPHERICAL COORDINATES

In Cartesian coordinates, the tensor of relative permittivity has the most general form:

$$\bar{\bar{\epsilon}} = \begin{bmatrix} \epsilon_{xx} & \epsilon_{xy} & \epsilon_{xz} \\ \epsilon_{yx} & \epsilon_{yy} & \epsilon_{yz} \\ \epsilon_{zx} & \epsilon_{zy} & \epsilon_{zz} \end{bmatrix}, \tag{1}$$

where no restricted symmetry properties are assigned and the elements may be complex numbers. The sphere is assumed to be homogeneous, which means that the elements of the permittivity tensor are independent of the spatial position. In spherical coordinates, its expression $\tilde{\epsilon}$ can be derived through the Cartesian-to-spherical transformation matrix $\mathfrak{R}$ using the formula

$$\tilde{\epsilon} = \mathfrak{R}\bar{\bar{\epsilon}}\mathfrak{R}^{\mathrm{T}} \tag{2}$$

where T stands for transpose.

We denote with a circumflex the unit vectors along the coordinate axis. The transformation matrix $\mathfrak{R}$ is expressed using the scalar products of these unit vectors:

$$\Re = \begin{pmatrix} \hat{\mathbf{r}} \cdot \hat{\mathbf{x}} & \hat{\mathbf{r}} \cdot \hat{\mathbf{y}} & \hat{\mathbf{r}} \cdot \hat{\mathbf{z}} \\ \hat{\boldsymbol{\theta}} \cdot \hat{\mathbf{x}} & \hat{\boldsymbol{\theta}} \cdot \hat{\mathbf{y}} & \hat{\boldsymbol{\theta}} \cdot \hat{\mathbf{z}} \\ \hat{\boldsymbol{\varphi}} \cdot \hat{\mathbf{x}} & \hat{\boldsymbol{\varphi}} \cdot \hat{\mathbf{y}} & \hat{\boldsymbol{\varphi}} \cdot \hat{\mathbf{z}} \end{pmatrix}. \tag{3}$$

The unit vectors are linked by the relations

$$\hat{\mathbf{r}} = \hat{\mathbf{x}} \cos \varphi \sin \theta + \hat{\mathbf{y}} \sin \varphi \sin \theta + \hat{\mathbf{z}} \cos \theta,$$

$$\hat{\boldsymbol{\varphi}} = - \hat{\mathbf{x}} \sin \varphi + \hat{\mathbf{y}} \cos \varphi,$$

$$\hat{\boldsymbol{\theta}} = - \hat{\mathbf{r}} \times \hat{\boldsymbol{\varphi}} = \hat{\mathbf{x}} \cos \varphi \cos \theta + \hat{\mathbf{y}} \sin \varphi \cos \theta - \hat{\mathbf{z}} \sin \theta, \tag{4}$$

and thus the matrix $\Re$ takes the form

$$\Re = \begin{pmatrix} \cos \varphi \sin \theta & \sin \varphi \sin \theta & \cos \theta \\ \cos \varphi \cos \theta & \sin \varphi \cos \theta & - \sin \theta \\ - \sin \varphi & \cos \varphi & 0 \end{pmatrix}. \tag{5}$$

Equations (1), (2), and (5) give the elements $\tilde{\tilde{\epsilon}}_{ij}, i,j = r, \theta, \varphi$ of $\tilde{\epsilon}$. Since the spherical coordinate system is orthogonal, it is not necessary to distinguish between covariant and contravariant components, and all vector and tensor components will be denoted by subscripts. It is worth noticing that the elements of $\tilde{\epsilon}$ depend on (θ, φ), contrary to Ref. 9, but do not depend on (x, y, z), as already mentioned.

3. PROPAGATION EQUATION OF PLANE WAVES

The monochromatic propagation equation has the form

$$\text{curl curl } \mathbf{E} - k_0^2 \tilde{\tilde{\epsilon}} \mathbf{E} = 0, \tag{6}$$

where $k_0 = \omega/c$ is the vacuum wavenumber, ω is the angular frequency, and c the speed of light in vacuum. As is well known, this equation permits solutions in the form of plane waves,

$$\mathbf{E}(\mathbf{k}, \mathbf{r}_{OM}) = \mathbf{A}(\mathbf{k}) \exp(i \mathbf{k} \cdot \mathbf{r}_{OM}) \tag{7}$$

where $\mathbf{r}_{OM}$ is the radius vector of an arbitrary point M and $\mathbf{k}$ is the wave vector of this wave with $\mathbf{k} = |\mathbf{k}| \hat{\mathbf{r}}$. In the case of isotropic media, $\mathbf{E}$ is a solution of the Helmholtz equation, and the wave vector $\mathbf{k}$ becomes isotropic, its norm being independent of the direction of propagation. Anisotropy complicates the form of the solution, since $|\mathbf{k}|$ then depends on the direction of propagation. Nevertheless $|\mathbf{k}|$ can be determined analytically from the elements of the permittivity tensor. Noting that

$$\text{curl}[\mathbf{A} \exp(i \mathbf{k} \cdot \mathbf{r}_{OM})] = i \mathbf{k} \times \mathbf{A} \exp(i \mathbf{k} \cdot \mathbf{r}_{OM}), \tag{8}$$

one obtains from Eq. (6) that $\mathbf{A}$ must satisfy

$$\mathbf{k} \times (\mathbf{k} \times \mathbf{A}) + k_0^2 \tilde{\tilde{\epsilon}} \mathbf{A} = 0. \tag{9}$$

Introducing the tensor $(\mathbf{kk})$ whose (i, j) element is equal to $k_i k_j$, Eq. (9) can be written in the form

$$[k^2 \mathbb{I} - (\mathbf{kk}) - k_0^2 \tilde{\tilde{\epsilon}}] \mathbf{A}(\mathbf{k}) = 0, \tag{10}$$

where $k^2 = |\mathbf{k}|^2 = \text{Tr}(\mathbf{kk})$ and $\mathbb{I}$ is the unit matrix. Equation (10) shows that k^2 must be a nonlinear eigenvalue of the

operator $(\mathbf{kk}) + k_0^2 \tilde{\tilde{\epsilon}}$ and that $\mathbf{A}(\mathbf{k})$ is the corresponding eigenvector. The eigenvalue equation reads

$$\det[k^2 \mathbb{I} - (\mathbf{kk}) - k_0^2 \tilde{\tilde{\epsilon}}] = 0. \tag{11}$$

4. SOLUTION OF THE EIGENPROBLEM

A. Eigenvalues

Following the work of Papadakis *et al.*,[12] we express Eq. (11) in spherical coordinates. As the wave vector $\mathbf{k}$ of the plane wave is invariant with respect to translation, its only nonzero component is along $\hat{\mathbf{r}}$; however, in anisotropic media $k_r = k_r(\theta, \varphi)$ depends only on the direction of propagation, as already discussed. This fact considerably simplifies the form of the tensor $(\mathbf{kk})$ in spherical coordinates:

$$(\mathbf{kk}) = k^2 \mathbb{I}_{1/3} \tag{12}$$

with

$$\mathbb{I}_{1/3} = \begin{pmatrix} 1 & 0 & 0 \\ 0 & 0 & 0 \\ 0 & 0 & 0 \end{pmatrix}, \tag{13}$$

and Eq. (11) then reads

$$\det \left[\frac{k^2}{k_0^2} (\mathbb{I} - \mathbb{I}_{1/3}) - \tilde{\tilde{\epsilon}} \right] = 0 \Leftrightarrow \begin{vmatrix} \epsilon_{rr} & \epsilon_{r\theta} & \epsilon_{r\varphi} \\ \epsilon_{\theta r} & \epsilon_{\theta\theta} - \hat{k}^2 & \epsilon_{\theta\varphi} \\ \epsilon_{\varphi r} & \epsilon_{\varphi\theta} & \epsilon_{\varphi\varphi} - \hat{k}^2 \end{vmatrix} = 0, \tag{14}$$

where $\hat{k} \equiv k/k_0$.

Equation (14) represents a biquadratic algebraic equation for $\hat{k}$, which can be written in the form

$$\alpha \hat{k}^4 - \beta \hat{k}^2 + \gamma = 0, \tag{15}$$

where

$$\alpha = \epsilon_{rr},$$

$$\beta = \epsilon_{rr}(\epsilon_{\theta\theta} + \epsilon_{\varphi\varphi}) - \epsilon_{r\theta}\epsilon_{\theta r} - \epsilon_{r\varphi}\epsilon_{\varphi r},$$

$$\gamma = \det(\tilde{\tilde{\epsilon}}). \tag{16}$$

Defining $\Delta = \beta^2 - 4\alpha\gamma$, Eq. (15) has two roots for $\hat{k}^2$, $(\hat{k}^2)' = (\beta + \sqrt{\Delta})/2\alpha$ and $(\hat{k}^2)'' = (\beta - \sqrt{\Delta})/2\alpha$. From there, we obtain four eigenvalues of $\hat{k}$ noted $\hat{k}_j$ ($j = 1-4$), which give four values of k_j:

$$k_1/k_0 = \hat{k}_1 = \sqrt{(\hat{k}^2)'} = - \hat{k}_3 = - k_3/k_0,$$

$$k_2/k_0 = \hat{k}_2 = \sqrt{(\hat{k}^2)''} = - \hat{k}_4 = - k_4/k_0. \tag{17}$$

For lossless materials, energy conservation requires that the tensor $\tilde{\tilde{\epsilon}}$ (and thus $\tilde{\epsilon}$) is real and symmetric. It can be shown that for each real direction of propagation (θ, φ), two real positive values k_1 and k_2 exist, which, in general, depend on (θ, φ). The other two values correspond to waves propagating in the opposite direction.

For lossy materials, $\bar{\bar{\epsilon}}$ and $\tilde{\bar{\epsilon}}$ have complex elements, and their real and imaginary parts cannot in general be diagonalized in the same basis. However, the analysis of this subsection can be directly generalized to lossy media by searching for complex solutions of Eq. (11). This could be done numerically, but by applying a simple procedure, one can directly use Eqs. (17). To that end, it is necessary to define a complex spherical coordinate system in the following manner. A complex unit vector $\hat{\mathbf{r}}_C = \mathbf{k}/|k|$ is introduced, from which two complex angles θ_C and φ_C are derived using the simple trigonometric relations:

$$\cos(\theta_C) = \hat{\mathbf{r}}_C \cdot \hat{\mathbf{z}}$$

$$\cos(\varphi_C) = \hat{\mathbf{r}}_C \cdot \hat{\mathbf{x}}/\sin(\theta_C) \qquad (18)$$

A complex orthogonal basis is then constructed by extending the second and the third of Eqs. (4) to complex angles. Using this coordinate system, Eqs. (12)–(14), (5), and (16) are still valid and Eq. (17) holds for lossy media as well, taking $\sqrt{\Delta}$, k_1, and k_2 with nonnegative imaginary parts.

B. Eigenvectors

1. Arbitrary Anisotropy
As solutions of a linear homogeneous equation, all eigenvector are determined through interrelations among their components. Let us take as an independent component $A_{j,r} = \mathbf{A}(k_j\hat{\mathbf{r}}) \cdot \hat{\mathbf{r}}$, $j=1,2$ (the case when this component is zero is discussed further on). Due to the fact that $\mathbf{A}(k_j\hat{\mathbf{r}})$ depends on k^2 only, Eq. (10), the eigenvectors can be separated into two pairs, each corresponding to $+k_j$ and $-k_j$ and having the same vector components. However, these vector components are expressed in two opposite local trihedrals (r, θ, φ), so that $\mathbf{A}(k_3\hat{\mathbf{r}}) = -\mathbf{A}(k_1\hat{\mathbf{r}})$ and $\mathbf{A}(k_4\hat{\mathbf{r}}) = -\mathbf{A}(k_2\hat{\mathbf{r}})$. Equation (10) reads

$$\left|\begin{array}{l} \epsilon_{rr}A_{j,r} + \epsilon_{r\theta}A_{j,\theta} + \epsilon_{r\varphi}A_{j,\varphi} = 0, \\ \epsilon_{\theta r}A_{j,r} + (\epsilon_{\theta\theta} - \hat{k}_j^2)A_{j,\theta} + \epsilon_{\theta\varphi}A_{j,\varphi} = 0, \\ \epsilon_{\varphi r}A_{j,r} + \epsilon_{\varphi\theta}A_{j,\theta} + (\epsilon_{\varphi\varphi} - \hat{k}_j^2)A_{j,\varphi} = 0. \end{array}\right. \qquad (19)$$

The first two equations give the relations

$$A_{j,\theta} = \frac{\begin{vmatrix} -\epsilon_{rr} & \epsilon_{r\varphi} \\ -\epsilon_{\theta r} & \epsilon_{\theta\varphi} \end{vmatrix}}{\begin{vmatrix} \epsilon_{r\theta} & \epsilon_{r\varphi} \\ \epsilon_{\theta\theta} - \hat{k}_j^2 & \epsilon_{\theta\varphi} \end{vmatrix}} A_{j,r}, \qquad (20)$$

$$A_{j,\varphi} = \frac{\begin{vmatrix} \epsilon_{rr} & -\epsilon_{r\theta} \\ \epsilon_{\theta r} & \hat{k}_j^2 - \epsilon_{\theta\theta} \end{vmatrix}}{\begin{vmatrix} \epsilon_{r\theta} & \epsilon_{r\varphi} \\ \epsilon_{\theta\theta} - \hat{k}_j^2 & \epsilon_{\theta\varphi} \end{vmatrix}} A_{j,r}. \qquad (21)$$

Denoting $A_{j,r}$ by $A_{j,r} = \tilde{A}_j$, Eqs. (20) and (21) provide the components of the eigenvectors $\mathbf{A}(k_j\hat{\mathbf{r}})$ as functions of $\tilde{A}_j$. Moreover, all the particular cases discussed in the next subsections enable us to define known vectors $\mathbf{\Gamma}_j$, which allow the eigenvector components to be expressed in terms of one free parameter $\tilde{A}_j$:

$$\mathbf{A}_j = \tilde{A}_j\mathbf{\Gamma}_j. \qquad (22)$$

As mentioned before, this analysis excludes the possibility of having $A_{j,r} = 0$. However, this is a quite common situation, since it corresponds to a transverse wave, when the electric field vector has no component along the direction of propagation. This concerns all waves in isotropic homogeneous media, ordinary waves in uniaxial materials, and extraordinary waves traveling along the optic axis of uniaxial materials. These cases require a special analysis.

2. Uniaxial Materials
If the z axis is chosen to be parallel to the optic axis, the permittivity tensor of a uniaxial material has a diagonal form in Cartesian coordinates:

$$\bar{\bar{\epsilon}} = \begin{pmatrix} \epsilon_x & 0 & 0 \\ 0 & \epsilon_x & 0 \\ 0 & 0 & \epsilon_z \end{pmatrix}. \qquad (23)$$

Its form in spherical coordinates is obtained by applying the transformation defined by Eqs. (2) and (3):

$$\tilde{\bar{\epsilon}} = \begin{pmatrix} \epsilon_x \sin^2\theta + \epsilon_z \cos^2\theta & (\epsilon_x - \epsilon_z)\sin\theta\cos\theta & 0 \\ (\epsilon_x - \epsilon_z)\sin\theta\cos\theta & \epsilon_z \sin^2\theta + \epsilon_x \cos^2\theta & 0 \\ 0 & 0 & \epsilon_x \end{pmatrix}, \qquad (24)$$

i.e., $\epsilon_{r\varphi} = \epsilon_{\varphi r} = \epsilon_{\varphi\theta} = \epsilon_{\theta\varphi} = 0$. The set of equations (19) then reduces to

$$\epsilon_{rr}A_{j,r} + \epsilon_{r\theta}A_{j,\theta} = 0, \qquad (25)$$

$$\epsilon_{\theta r}A_{j,r} + (\epsilon_{\theta\theta} - \hat{k}_j^2)A_{j,\theta} = 0, \qquad (26)$$

$$(\epsilon_{\varphi\varphi} - \hat{k}_j^2)A_{j,\varphi} = 0. \qquad (27)$$

There are two possible classes of solutions. The ordinary wave is characterized by refractive index $\hat{k}_1 = \sqrt{\epsilon_x} \equiv \sqrt{\epsilon_{\varphi\varphi}}$ and eigenvalue $k_1 = k_0\hat{k}_1$; i.e., the coefficient in Eq. (27) vanishes for the ordinary wave:

$$\epsilon_{\varphi\varphi} = \hat{k}_1^2 = 0, \qquad (28)$$

and it is then possible to have

$$A_{1,\varphi} \neq 0. \qquad (29)$$

If we take into account that for uniaxial materials $\epsilon_x \neq \epsilon_z$, then it can be shown that Eqs. (25) and (26) are incompatible under condition (28), leading to $A_{1,r} = A_{1,\theta} = 0$, and thus the ordinary eigenvector has the form

$$\mathbf{A}_1 = \tilde{A}_1\mathbf{\Gamma}_1, \quad \text{with } \mathbf{\Gamma}_1 = \hat{\boldsymbol{\varphi}} \text{ and } \tilde{A}_1 = A_{1,\varphi}. \qquad (30)$$

The extraordinary wave is described by the second solution of Eqs. (25)–(27), characterized by

$$A_{j,\varphi} \equiv A_{2,\varphi} = 0. \qquad (31)$$

The corresponding eigenvalue $(k_2 = k_0\hat{k}_2)$ is obtained provided that there exists a nontrivial solution of Eqs. (25) and (26), i.e., provided that

$$\begin{vmatrix} \epsilon_{rr} & \epsilon_{r\theta} \\ \epsilon_{\theta r} & \epsilon_{\theta\theta} - \hat{k}_2^2 \end{vmatrix} = 0, \tag{32}$$

which provides the value of the extraordinary refractive index $\hat{k}_2$ (Ref. 13), which depends on the polar angle:

$$\frac{1}{\hat{k}_2^2(\theta)} = \frac{\sin^2\theta}{\epsilon_z} + \frac{\cos^2\theta}{\epsilon_x}. \tag{33}$$

The extraordinary eigenvector $\mathbf{A}_2$ can then be obtained within a multiplicative constant $A_{2,\theta} \equiv \tilde{A}_2$. We get from Eq. (25)

$$A_{2,r} = -\frac{\epsilon_{r\theta}}{\epsilon_{rr}} A_{2,\theta} \equiv \frac{(\epsilon_z - \epsilon_x)\sin\theta\cos\theta}{\epsilon_x \sin^2\theta + \epsilon_z \cos^2\theta} \tilde{A}_2 \Rightarrow \mathbf{A}_2 = \tilde{A}_2 \mathbf{\Gamma}_2,$$

with $\mathbf{\Gamma}_2 = \dfrac{(\epsilon_z - \epsilon_x)\sin\theta\cos\theta}{\epsilon_x \sin^2\theta + \epsilon_z \cos^2\theta}\hat{\mathbf{r}} + \hat{\boldsymbol{\theta}}, \qquad \tilde{A}_2 = A_{2,\theta}. \tag{34}$

Along the optic axis ($\theta=0$), $\Gamma_{2,r}=0$ and the extraordinary solution becomes a transverse wave like the ordinary one, since then $\mathbf{\Gamma}_2 = \hat{\boldsymbol{\theta}}$. However, the polarizations of the ordinary and extraordinary waves are orthogonal.

3. Isotropic Medium

The isotropic case is obtained from the uniaxial one by stating that $\epsilon_x = \epsilon_z$. The tensor of permittivity is proportional to the unit tensor, and from Eq. (25) it is evident that the wave has a transversal character with $A_{1,r} = A_{2,r} = 0$. The eigensystem is degenerate, i.e., the eigenvalues are equal with $k_1 = k_2 = k_0\sqrt{\epsilon_x}$, as obtained from Eqs. (15) and (16) or, more directly, from Eqs. (26) and (27). Equations (30) and (34), respectively, provide two independent eigenvectors, transverse to the direction of the wave vector:

$$\mathbf{A}_1 = \tilde{A}_1 \hat{\boldsymbol{\varphi}},$$

$$\mathbf{A}_2 = \tilde{A}_2 \hat{\boldsymbol{\theta}}. \tag{35}$$

5. GENERAL FORM OF THE PLANE WAVE EXPANSION

At an arbitrary point M in space with radius vector $\mathbf{r}_{OM}$, the nondiverging electric field vector can be expressed as a superposition of plane waves propagating in each direction. For each given direction, the wave vector can take two possible values; thus the general form of the field is given by a three-dimensional Fourier transform (having only two Fourier components along $\mathbf{k}$),

$$\mathbf{E}(\mathbf{r}_{OM}) = \sum_{j=1}^{2} \int_0^\pi \sin\theta\, d\theta \int_0^{2\pi} d\varphi \mathbf{A}_j(\theta,\varphi)$$

$$\times \exp[ik_j(\theta,\varphi)\hat{\mathbf{r}} \cdot \mathbf{r}_{OM}], \tag{36}$$

where the different components of $\mathbf{A}_j$ are interrelated as discussed in Section 4, each vector being determined within a multiplicative factor. During the numerical treatment of the problem, this double integral has to be

discretized into N_θ values along θ and N_φ values along φ. In Section 6 we introduce a multipole expansion of the field. Let n_{Max} be the cutoff associated with the multipole cutoff of the n index [see Eq. (52) below]. We shall discretize the Fourier integral by defining a generalized Fourier space discretization index $\nu \in [1, \dots, N_\nu]$. As we demonstrate in what follows, the two cutoffs have to be linked by the relation $N_\nu = (n_{\text{Max}} + 1)^2$ to obtain a well-determined system of equations for the unknown field amplitudes $\mathbf{A}_j$. Each value of ν will specify a unique direction in k space associated with a unique pair of indices n_θ and n_φ. The polar index goes over a range

$$n_\theta = 1, 2, \dots, 2n_{\text{Max}} + 1, \tag{37}$$

with the Fourier polar angle θ_ν associated with its discretization index given by

$$\theta_\nu = \pi \frac{n_\theta - 1}{2n_{\text{Max}}}. \tag{38}$$

We thus realize that this yields values for θ_ν that are evenly spaced over the interval $\theta \in [0, \pi]$:

$$\theta_\nu = 0, \frac{\pi}{2n_{\text{Max}}}, \frac{2\pi}{2n_{\text{Max}}}, \dots, \pi \tag{39}$$

and that when $n_\theta = n_{\text{Max}} + 1$, then $\theta = \pi/2$.

For the same density of discretization directions to be preserved, the number of discretization points along φ must depend on θ. In the upper half-space, the polar index n_θ is in the range $n_\theta \le n_{\max} + 1$ and the azimuthal index n_φ covers the range

$$n_\varphi = 1, \dots, n_\theta, \tag{40}$$

while the azimuthal angle φ_ν is given by

$$\varphi_\nu = 2\pi \frac{n_\varphi}{n_\theta + 1} \tag{41}$$

and the generalized index ν in the range $n_\theta \le n_{\text{Max}} + 1$, $n_\varphi \le n_\theta$, is given by

$$\nu = n_\varphi + \frac{n_\theta(n_\theta - 1)}{2}. \tag{42}$$

The inverse relations for going from the generalized index ν to n_θ and n_φ provided that the index ν is in the range

$$\nu = \le \frac{(n_{\text{Max}} + 1)(n_{\text{Max}} + 2)}{2} \tag{43}$$

are

$$n_\theta = \text{Int}\left(\frac{1 + \sqrt{8\nu - 7}}{2}\right),$$

$$n_\varphi = \nu - \frac{n_\theta(n_\theta - 1)}{2}. \tag{44}$$

In the lower half-space where $n_\theta > n_{\text{Max}} + 1$, to obtain the same density of discretized directions as in the upper half-space, the azimuthal index covers the range

$$n_\varphi = 1, \ldots, 2(n_{\text{Max}} + 1) - n_\theta \qquad (45)$$

and the associated azimuthal angle φ_ν is given by

$$\varphi_\nu = \frac{2\pi n_\varphi}{2(n_{\text{Max}} + 1) - n_\theta + 1}, \qquad (46)$$

while the generalized index ν in this range is given by the expression

$$\nu = (n_{\text{Max}} + 1)^2 + n_\varphi - \frac{(2n_{\text{Max}} - n_\theta + 3)(2n_{\text{Max}} - n_\theta + 2)}{2},$$

$$n_\theta > n_{\text{Max}} + 1, \qquad n_\varphi \leq 2(n_{\text{Max}} + 1) - n_\theta. \qquad (47)$$

The inverse relations are

$$n_\theta = 2(n_{\text{Max}} + 1) - \text{Int}\left(\frac{1 + \sqrt{8(n_{\text{Max}} + 1)^2 - 8\nu + 1}}{2} \right),$$

$$n_\varphi = \nu + \frac{(2n_{\text{Max}} - n_\theta + 3)(2n_{\text{Max}} - n_\theta + 2)}{2} - (n_{\text{Max}} + 1)^2. \qquad (48)$$

These rules might seem a bit complicated at first, but they are easy to program. The total number N_ν of discretized values of ν can be obtained by taking into account that the maximum value taken by n_φ is equal to n_θ in the upper half-space, Eq. (40), where n_θ varies from 1 to n_{Max}. Thus the number of discretized directions in the upper half-space is equal to $N_{\text{up}} = \sum_1^{n_{\text{Max}}} n_\theta = (n_{\text{Max}}/2)(n_{\text{Max}} + 1)$. In the lower half-space, as already explained, we preserve the same number of discretized directions as in the upper half. In the equatorial plane the number of discretizations is equal to $(n_{\text{Max}} + 1)$. Thus the total number N_ν is the sum of the numbers in the upper and lower half-spaces and in the equatorial plane:

$$N_\nu = 2N_{\text{up}} + (n_{\text{Max}} + 1) = (n_{\text{Max}} + 1)^2. \qquad (49)$$

By explicitly writing out the values of ν and its corresponding n_θ and n_φ values as illustrated in Tables 1 and 2, we can easily see that the rules of discretization create a rather symmetric sampling of the phase space integral.

In its discretized form, Eq. (36) can be written as

$$\mathbf{E}(\mathbf{r}_{OM}) = \sum_{j=1}^{2} \sum_{\nu=1}^{N_\nu} \mathbf{A}_{j,\nu} \exp(ik_{j,\nu} \hat{\mathbf{r}}_\nu \cdot \mathbf{r}_{OM})$$

$$= \sum_{j=1}^{2} \sum_{\nu=1}^{N_\nu} \tilde{A}_{j,\nu} \mathbf{\Gamma}_{j,\nu} \exp(ik_{j,\nu} \hat{\mathbf{r}}_\nu \cdot \mathbf{r}_{OM}), \qquad (50)$$

with

Table 1. Discretization Corresponding to a Dipolar Representation ($n_{\text{Max}} = 1$)

ν	1	2	3	4
n_θ, n_φ	1, 1	2, 1	2, 2	3, 1
θ_ν, φ_ν	$0, \pi$	$\dfrac{\pi}{2}, \dfrac{2\pi}{3}$	$\dfrac{\pi}{2}, \dfrac{4\pi}{3}$	π, π

$$\tilde{A}_{j,\nu} = \tilde{A}_j(\theta_\nu, \varphi_\nu)\sin \theta_\nu,$$

$$\mathbf{\Gamma}_{j,\nu} = \mathbf{\Gamma}_j(\theta_\nu, \varphi_\nu),$$

$$k_{j,\nu} = k_j(\theta_\nu, \varphi_\nu),$$

$$\hat{\mathbf{r}}_\nu = \hat{\mathbf{r}}(\theta_\nu, \varphi_\nu). \qquad (51)$$

Thus, the general form of the field in Eq. (50) depends on $2N_\nu$ coefficients $\tilde{A}_{j,\nu}$, which determine the norm of each eigenvector. These unknown field amplitudes could be obtained by matching the tangential field components on the boundaries between different physical regions, in particular on the surface of the optically anisotropic sphere under study. However, this standard procedure requires separation between incident (known) and diffracted (unknown) waves. While it is evident how to do this in Cartesian coordinates and isotropic media, anisotropy and spherical geometry complicate considerably the separation into incident and diffracted waves, in particular inside the sphere. To this aim, we first project the field onto the basis of vector spherical harmonic functions $\mathbf{Y}_{nm}(\theta, \varphi)$, $\mathbf{X}_{nm}(\theta, \varphi)$, and $\mathbf{Z}_{nm}(\theta, \varphi)$. This enables us to explicitly separate the field into two parts, proportional to the spherical Bessel functions j_n and h_n^+. The second part, which diverges at the origin of coordinates has to be eliminated inside the sphere.

6. FIELD EXPANSION ON VECTOR SPHERICAL HARMONICS

In spherical coordinates, several different bases are available to represent the electromagnetic field in any isotropic or anisotropic material. We shall use the basis of vector spherical harmonic functions $\mathbf{Y}_{nm}(\theta, \varphi)$, $\mathbf{X}_{nm}(\theta, \varphi)$, and $\mathbf{Z}_{nm}(\theta, \varphi)$ (Ref. 14), in which basis the electric field takes the form

$$\mathbf{E}(r, \theta, \varphi) = \sum_{n=0}^{n_{\text{Max}}} \sum_{m=-n}^{n} [E_{Ynm}(r)\mathbf{Y}_{nm}(\theta, \varphi) + E_{Xnm}(r)\mathbf{X}_{nm}(\theta, \varphi)$$

$$+ E_{Znm}(r)\mathbf{Z}_{nm}(\theta, \varphi)]. \qquad (52)$$

Appendix A establishes the development of the field of a single plane wave on the basis of vector spherical harmonic functions. Each term in Eq. (50) can then be represented by an expansion having the form of Eq. (A20). As it was done in Section 5, we simplify the notation by introducing a single summation index p defined in terms of the two integers n and m through the relations

$$p = n(n + 1) + m + 1,$$

$$p_{\text{Max}} = (n_{\text{Max}} + 1)^2, \qquad (53)$$

or vice versa:

$$n(p) = \text{Int}\sqrt{p - 1},$$

$$m(p) = p - 1 - n(p)[n(p) + 1], \qquad (54)$$

with $\text{Int}(x)$ standing for the integer part of x.

Table 2. Discretization Corresponding to a Quadrupolar Representation for $n_{\mathrm{Max}}=2$

ν	1	2	3	4	5	6	7	8	9
n_θ, n_φ	1, 1	2, 1	2, 2	3, 1	3, 2	3, 3	4, 1	4, 2	5, 1
θ_ν, φ_ν	$0, \pi$	$\dfrac{\pi}{4}, \dfrac{2\pi}{3}$	$\dfrac{\pi}{4}, \dfrac{4\pi}{3}$	$\dfrac{\pi}{2}, \dfrac{\pi}{2}$	$\dfrac{\pi}{2}, \pi$	$\dfrac{\pi}{2}, \dfrac{3\pi}{2}$	$\dfrac{3\pi}{4}, \dfrac{2\pi}{3}$	$\dfrac{3\pi}{4}, \dfrac{4\pi}{3}$	π, π

Thus, each term in Eq. (50) takes the form of Eq. (A20) with a summation with respect to the simple subscript p:

$$\boldsymbol{\Gamma}_{j,\nu} \exp(ik_{j,\nu}\hat{\mathbf{r}}_{j,\nu}\cdot\mathbf{r}_{OM})$$

$$= \sum_{p=1}^{p_{\mathrm{Max}}} \left\{ a_{h,p,j,\nu}(k_{j,\nu}r_{OM})\mathbf{X}_p(\theta_{OM},\varphi_{OM}) \right.$$

$$+ \left[a_p a_{e,p,j,\nu}\frac{j_n(k_{j,\nu}r_{OM})}{k_{j,\nu}r_{OM}} + a_{o,p,j,\nu}j'_n(k_{j,\nu}r_{OM}) \right]$$

$$\times \mathbf{Y}_p(\theta_{OM},\varphi_{OM}) + \left[a_{e,p,j,\nu}\frac{(k_{j,\nu}r_{OM}j_n(k_{j,\nu}r_{OM}))'}{k_{j,\nu}r_{OM}} \right.$$

$$\left. \left. + a_p a_{o,p,j,\nu}\frac{j_n(k_{j,\nu}r_{OM})}{k_{j,\nu}r_{OM}} \right]\mathbf{Z}_p(\theta_{OM},\varphi_{OM}) \right\}, \qquad (55)$$

where r_{OM}, θ_{OM}, φ_{OM} are the spherical coordinates of M, $a_p = \sqrt{n(p)[n(p)-1]}$, and

$$a_{h,p,j,\nu} = 4\pi i^n \mathbf{X}_p^*(\hat{\mathbf{r}}_\nu)\cdot\boldsymbol{\Gamma}_{j,\nu}, \qquad a_{e,p,j,\nu} = 4\pi i^{n-1}\mathbf{Z}_p^*(\hat{\mathbf{r}}_\nu)\cdot\boldsymbol{\Gamma}_{j,\nu},$$

$$a_{o,p,j,\nu} = 4\pi i^{n-1}\mathbf{Y}_p^*(\hat{\mathbf{r}}_\nu)\cdot\boldsymbol{\Gamma}_{j,\nu}. \qquad (56)$$

In a region that does not contain the origin (for example, outside the sphere or in an additional separate layer covering the sphere), there exist other solutions of the Maxwell equations, containing terms that would diverge at the origin. These solutions represent fields radiated from the origin and propagating outward in the direction $r \rightarrow \infty$. They can be described in terms of h_n^+, another set of spherical Bessel functions, as mentioned at the end of Section 5. These solutions can be obtained as a linear combination with amplitudes $\tilde{A}_{j,\nu}^{(d)}$ of the terms participating in the expansion given on the right-hand side of Eq. (55) by substituting j_n with h_n^+. Inside the inner region, these amplitudes are null in order to avoid field divergence at the origin. Outside the sphere, they represent the outgoing (scattered, diffracted) solutions; thus the use of superscript (d). The bounded part, containing j_n, plays the role of incident waves in the outermost region and will have amplitudes $\tilde{A}_{j,\nu}^{(i)}$, the superscript (i) standing for incident, which are known outside the sphere from the amplitude and polarization of the incident wave. If the sphere is covered by a layer(s), both $\tilde{A}_{j,\nu}^{(i)}$ and $\tilde{A}_{j,\nu}^{(d)}$ will be unknown constants. Thus the most general form of the electric field vector will contain two terms:

$$\mathbf{E} = \mathbf{E}^{(i)} + \mathbf{E}^{(d)}, \qquad (57)$$

The incident (bounded) part has the form, resulting from Eqs. (50) and (55),

$$\mathbf{E}^{(i)}(\mathbf{r}_{OM}) = \sum_{p=1}^{p_{\mathrm{Max}}}\sum_{\nu=1}^{N_\nu-1}\sum_{j=1}^{2}\tilde{A}_{j,\nu}^{(i)}\left\{ a_{h,p,j,\nu}j_n(k_{j,\nu}r_{OM})\mathbf{X}_p(\theta_{OM},\varphi_{OM}) + \left[a_p a_{e,p,j,\nu}\frac{j_n(k_{j,\nu}r_{OM})}{k_{j,\nu}r_{OM}} + a_{o,p,j,\nu}j'_n(k_{j,\nu}r_{OM}) \right]\mathbf{Y}_p(\theta_{OM},\varphi_{OM}) \right.$$

$$\left. + \left[a_{e,p,j,\nu}\frac{(k_{j,\nu}r_{OM}j_n(k_{j,\nu}r_{OM}))'}{k_{j,\nu}r_{OM}} + a_p a_{o,p,j,\nu}\frac{j_n(k_{j,\nu}r_{OM})}{k_{j,\nu}r_{OM}} \right]\mathbf{Z}_p(\theta_{OM},\varphi_{OM}) \right\}, \qquad (58)$$

while the scattered (diverging at the origin) part can be obtained by replacing (i) by (d), and j_n by h_n^+:

$$\mathbf{E}^{(d)}(\mathbf{r}_{OM}) = \sum_{p=1}^{p_{\mathrm{Max}}}\sum_{\nu=1}^{N_\nu-1}\sum_{j=1}^{2}\tilde{A}_{j,\nu}^{(d)}\left\{ a_{h,p,j,\nu}h_n^+(k_{j,\nu}r_{OM})\mathbf{X}_p(\theta_{OM},\varphi_{OM}) + \left[a_p a_{e,p,j,\nu}\frac{h_n^+(k_{j,\nu}r_{OM})}{k_{j,\nu}r_{OM}} + a_{o,p,j,\nu}h_n^{+\prime}(k_{j,\nu}r_{OM}) \right]\mathbf{Y}_p(\theta_{OM},\varphi_{OM}) \right.$$

$$\left. + \left[a_{e,p,j,\nu}\frac{(k_{j,\nu}r_{OM}h_n^+(k_{j,\nu}r_{OM}))'}{k_{j,\nu}r_{OM}} + a_p a_{o,p,j,\nu}\frac{h_n^+(k_{j,\nu}r_{OM})}{k_{j,\nu}r_{OM}} \right]\mathbf{Z}_p(\theta_{OM},\varphi_{OM}) \right\}. \qquad (59)$$

Given the definition of vector spherical harmonics (Appendix A), it can be observed that $\mathbf{X}_1=\mathbf{Z}_1=0$, while $\mathbf{Y}_1 \neq 0$. In isotropic media the longitudinal field components are null, so the sum in p starts from 2 instead of 1. If we consider that the outside medium is isotropic (having refractive index n_{out}), the eigenvalues are equal to $k_1=k_2 =n_{\mathrm{out}}k_0$, and the incident and the diffracted eigenvectors are given by Eq. (35). The orthogonality between $\mathbf{Y}_{nm}(\theta,\varphi)$ (parallel to $\mathbf{r}$) and $\boldsymbol{\Gamma}_{j,\nu}$ [Eq. (35)] leads to $a_{o,nm,j,\nu}^{(i)}=a_{o,nm,j,\nu}^{(d)}=0$.

7. RESOLUTION OF THE BOUNDARY-VALUE PROBLEM

The unknown field amplitudes $\tilde{A}_{j,\nu}^{(d)}$ and $\tilde{A}_{j,\nu}$ can be found as functions of the incident field amplitudes $\tilde{A}_{j,\nu}^{(i)}$ by apply-

ing the boundary conditions on the surface of the sphere. They imply the continuity of the tangential field components. Here we can take advantage of the orthogonality of the basis functions. First, we observe that $\mathbf{Y}_p(\theta_{OM}, \varphi_{OM})$ is parallel to $\mathbf{r}_{OM}$, while $\mathbf{X}_p(\theta_{OM}, \varphi_{OM})$ and $\mathbf{Z}_p(\theta_{OM}, \varphi_{OM})$ are perpendicular to it. Second, the latter functions are mutually orthogonal for different values of their indices n and m and thus of p. Consequently, it suffices, for each value of p, to consider the continuity of $E_{X,p}$, $E_{Z,p}$, $H_{X,p}$, and $H_{Z,p}$ at $|\mathbf{r}_{OM}| = R$, radius of the sphere.

The continuity of $E_{X,p}$ gives

$$
\sum_{\nu=1}^{N_\nu-1} \sum_{j=1}^{2} \widetilde{A}_{j,\nu}^{(i)} a_{h,p,j,\nu} j_n(n_{out}k_0 R)
$$
$$
+ \sum_{\nu=1}^{N_\nu-1} \sum_{j=1}^{2} \widetilde{A}_{j,\nu}^{(d)} a_{h,p,j,\nu} h_n^+(n_{out}k_0 R)
$$
$$
= \sum_{\nu=1}^{N_\nu-1} \sum_{j=1}^{2} \widetilde{A}_{j,\nu} a_{h,p,j,\nu} j_n(k_{j,\nu} R), \qquad \forall \, p = 2, \ldots, p_{Max}.
$$
(60)

Since $\mathbf{X}_1 = 0$, it is evident from Eq. (56) that for $p = 1$, Eq. (60) is written $0 = 0$ and thus has to be excluded from the set. The requirement to preserve an equal number of unknowns and equations leads to disregarding one term in the sum in ν, too. However, we are not losing information concerning the longitudinal field components carried by the terms proportional to $a_{o,l,j,\nu}$ in Eqs. (58) and (59), because the amplitudes $\widetilde{A}_{j,\nu}$ are independent of the subscript p and once determined can be used to obtain the longitudinal terms corresponding to $p = 1$.

Equation (60) can be further simplified by using the fact that the argument of the spherical Bessel functions j_n and h_n^+ in the isotropic medium does not depend on the direction of propagation, i.e., on ν. We can thus introduce new amplitudes of the field in the isotropic region outside the sphere, which amplitudes contain the sum over j and ν:

$$
A_{h,p}^{(i)} = \sum_{\nu=1}^{N_\nu-1} \sum_{j=1}^{2} \widetilde{A}_{j,\nu}^{(i)} a_{h,p,j,\nu} \equiv \sum_{\nu=1}^{N_\nu-1} \sum_{j=1}^{2} \widetilde{A}_{j,\nu}^{(i)} 4\pi i^n \mathbf{X}_p^*(\hat{\mathbf{r}}_\nu) \cdot \mathbf{\Gamma}_{j,\nu},
$$

$$
A_{e,p}^{(i)} = \sum_{\nu=1}^{N_\nu-1} \sum_{j=1}^{2} \widetilde{A}_{j,\nu}^{(i)} a_{e,p,j,\nu} \equiv \sum_{\nu=1}^{N_\nu-1} \sum_{j=1}^{2} \widetilde{A}_{j,\nu}^{(i)} 4\pi i^{n-1} \mathbf{Z}_p^*(\hat{\mathbf{r}}_\nu) \cdot \mathbf{\Gamma}_{j,\nu},
$$

$$
B_{h,p} = \sum_{\nu=1}^{N_\nu-1} \sum_{j=1}^{2} \widetilde{A}_{j,\nu}^{(d)} a_{h,p,j,\nu} \equiv \sum_{\nu=1}^{N_\nu-1} \sum_{j=1}^{2} \widetilde{A}_{j,\nu}^{(d)} 4\pi i^n \mathbf{X}_p^*(\hat{\mathbf{r}}_\nu) \cdot \mathbf{\Gamma}_{j,\nu},
$$

$$
B_{e,p} = \sum_{\nu=1}^{N_\nu-1} \sum_{j=1}^{2} \widetilde{A}_{j,\nu}^{(d)} a_{e,p,j,\nu} \equiv \sum_{\nu=1}^{N_\nu-1} \sum_{j=1}^{2} \widetilde{A}_{j,\nu}^{(d)} 4\pi i^{n-1} \mathbf{Z}_p^*(\hat{\mathbf{r}}_\nu) \cdot \mathbf{\Gamma}_{j,\nu}.
$$
(61)

Here, $\widetilde{A}_{j,\nu}^{(i)}$ are derived from the amplitude and the polarization of the incident wave. For example, a plane incident wave has a non-null amplitude $\widetilde{A}^{(i)}$ only in its direction of propagation (θ_i, φ_i). Denoting its polarization vector by $\hat{\mathbf{e}}^{(i)}$, the first two of Eqs. (61) simply give $A_{h,p}^{(i)}$

$= 4\pi i^n \mathbf{X}_p^*(\theta_i, \varphi_i) \cdot \hat{\mathbf{e}}^{(i)} \widetilde{A}^{(i)}$ and $A_{e,p}^{(i)} = 4\pi i^{n-1} \mathbf{Z}_p^*(\theta_i, \varphi_i) \cdot \hat{\mathbf{e}}^{(i)} \widetilde{A}^{(i)}$, as seen in Eqs. (134) and (135) of Ref. 14.

Finally, the field inside the isotropic medium takes the same form as in Ref. 14, and Eq. (60) takes the form

$$
A_{h,p}^{(i)} j_n(n_{out}k_0 R) + B_{h,p} h_n^+(n_{out}k_0 R)
$$
$$
= \sum_{\nu=1}^{N_\nu-1} \sum_{j=1}^{2} \widetilde{A}_{j,\nu} a_{h,p,j,\nu} j_n(k_{j,\nu} R), \qquad \forall \, p = 2, \ldots p_{Max}.
$$
(62)

The continuity of $E_{Z,nm}$ gives

$$
A_{e,p}^{(i)} \frac{[n_{out}k_0 R j_n(n_{out}k_0 R)]'}{n_{out}k_0 R} + B_{e,p} \frac{[n_{out}k_0 R h_n^+(n_{out}k_0 R)]'}{n_{out}k_0 R}
$$
$$
= \sum_{\nu=1}^{N_\nu-1} \sum_{j=1}^{2} \widetilde{A}_{j,\nu} \left\{ a_{e,p,j,\nu} \frac{[k_{j,\nu} R j_n(k_{j,\nu} R)]'}{k_{j,\nu} R} \right.
$$
$$
\left. + a_p a_{o,p,j,\nu} \frac{j_n(k_{j,\nu} R)}{k_{j,\nu} R} \right\}, \qquad \forall \, p = 2, \ldots p_{Max}. \quad (63)
$$

Equation (63) can be expressed in a different form, more common in the studies using spherical coordinates:

$$
A_{e,p}^{(i)} \frac{\psi_n'(n_{out}k_0 R)}{n_{out}k_0 R} + B_{e,p} \frac{\xi_n'(n_{out}k_0 R)}{n_{out}k_0 R}
$$
$$
= \sum_{\nu=1}^{N_\nu-1} \sum_{j=1}^{2} \widetilde{A}_{j,\nu} \left[a_{e,p,j,\nu} \frac{\psi_n'(k_{j,\nu} R)}{k_{j,\nu} R} + a_p a_{o,p,j,\nu} \frac{j_n(k_{j,\nu} R)}{k_{j,\nu} R} \right],
$$
(64)

where ψ_n and ξ_n are Ricatti–Bessel functions,[14] which are linked, respectively, with j_n and h_n^+ by

$$
\psi_n(z) = z j_n(z), \qquad \xi_n(z) = z h_n^+(z). \quad (65)
$$

The second two sets of equations are obtained from Maxwell equations projected onto the vector spherical harmonic basis:

$$
a_p \frac{E_{X,p}}{r} = i\omega\mu_0 H_{Y,p}, \quad (66)
$$

$$
a_p \frac{E_{Y,p}}{r} - \frac{E_{Z,p}}{r} - \frac{dE_{Z,p}}{dr} = i\omega\mu_0 H_{X,p}, \quad (67)
$$

$$
\frac{E_{X,p}}{r} + \frac{dE_{X,p}}{dr} = i\omega\mu_0 H_{Z,p}, \quad (68)
$$

$$
a_p \frac{H_{X,p}}{r} = -i\omega D_{Y,p}, \quad (69)
$$

$$
a_p \frac{H_{Y,p}}{r} - \frac{H_{Z,p}}{r} - \frac{dH_{Z,p}}{dr} = -i\omega D_{X,p}, \quad (70)
$$

$$\frac{H_{X,p}}{r} + \frac{dH_{X,p}}{dr} = -i\omega D_{Z,p}. \qquad (71)$$

Equations (67), (58) and (59) enable us to express $H_{X,p}$ as a function of $E_{Z,p}$. After some transformations using the properties of j_n, h_n^+, ξ_n, and ψ_n (described in detail in Ref. 14), the continuity of $H_{X,nm}$ gives the third relation:

$$n_{out}k_0[A_{e,p}^{(i)}j_n(n_{out}k_0R) + B_{e,p}h_n^+(n_{out}k_0R)]$$
$$= \sum_{\nu=1}^{N_\nu-1} \sum_{j=1}^{2} \tilde{A}_{j,\nu} a_{e,p,j,\nu} k_{j,\nu} j_n(k_{j,\nu}R). \qquad (72)$$

Equation (68) represents $H_{Z,p}$ as a function of $E_{X,p}$, and its continuity gives

$$A_{h,p}^{(i)}\psi_n'(n_{out}k_0R) + B_{h,p}\xi_n'(n_{out}k_0R)$$
$$= \sum_{\nu=1}^{N_\nu-1} \sum_{j=1}^{2} \tilde{A}_{j,\nu} a_{h,p,j,\nu}\psi_n'(k_{j,\nu}R). \qquad (73)$$

Equations (62), (64), (72), and (73) form a set of equations sufficient to find the unknown diffracted amplitudes $\tilde{A}_{j,\nu}$, $B_{e,p}$, and $B_{h,p}$ when the incident field amplitudes $A_{e,p}^{(i)}$ and $A_{h,p}^{(i)}$ are given, a set that contains $4p_{Max}-4$ equations. In order that the number of unknowns be equal to the number of equations, it is necessary to impose that $N_\nu = p_{Max}$; i.e., the number of unknowns in the outside medium must be equal to the number of unknowns inside the sphere. It is worth noticing that the system of $4p_{Max}-4$ equations is decoupled with respect to the subscript p, i.e., with respect to the angular coordinates of the observation point M. For each value of p, it is possible to eliminate half of the unknowns, $B_{e,p}$ and $B_{h,p}$, and to obtain a linear system for $\tilde{A}_{j,\nu}$. In order to simplify the formulas and to obtain relations similar in form to Mie coefficients, let us introduce the symbolic notation. First, we define four diagonal matrices with elements given by

$$(\Psi_0)_{pq} = \delta_{pq}\psi_n(n_{out}k_0R), \qquad (\Psi_0')_{pq} = \delta_{pq}\psi_n'(n_{out}k_0R),$$

$$(\xi_0)_{pq} = \delta_{pq}\xi_n(n_{out}k_0R), \qquad (\xi_0')_{pq} = \delta_{pq}\xi_n'(n_{out}k_0R),$$
$$(74)$$

Second, we introduce five matrices,

$$\Psi_{h,a} = (\Psi_{h,a_1}, \Psi_{h,a_2}), \quad \text{with } (\Psi_{h,a_j})_{p\nu} = a_{h,p,j,\nu}\psi_n(k_{j,\nu}R),$$

$$\Psi_{h,a}' = (\Psi_{h,a_1}', \Psi_{h,a_2}'), \quad \text{with } (\Psi_{h,a_j}')_{p\nu} = a_{h,p,j,\nu}\psi_n'(k_{j,\nu}R),$$

$$\xi_{h,a} = (\xi_{h,a_1}, \xi_{h,a_2}), \quad \text{with } (\xi_{h,a_j})_{p\nu} = a_{h,p,j,\nu}\xi_n(k_{j,\nu}R),$$

$$\xi_{h,a}' = (\xi_{h,a_1}', \xi_{h,a_2}'), \quad \text{with } (\xi_{h,a_j}')_{p\nu} = a_{h,p,j,\nu}\xi_n'(k_{j,\nu}R),$$

$$J_{o,a} = (J_{o,a_1}, J_{o,a_2}), \quad \text{with } (J_{o,a_j})_{p\nu} = a_p a_{o,p,j,\nu} j_n(k_{j,\nu}R),$$
$$(75)$$

and similar definitions by exchanging the subscript h with e and o. Third, the wavenumbers of different waves are grouped in a diagonal matrix:

$$\left(\frac{k_{out}}{k_{in}}\right) = \begin{pmatrix} \left(\dfrac{k_{out}}{k_{in,1}}\right) & 0 \\ 0 & \left(\dfrac{k_{out}}{k_{in,2}}\right) \end{pmatrix} \quad \text{with } \left(\frac{k_{out}}{k_{in,j}}\right)_{\tau\nu} = \delta_{\tau\nu}\frac{n_{out}k_0}{k_{j,\nu}}.$$
$$(76)$$

With this notation, the four equations (62), (73), (64), and (72) take the matrix form

$$\Psi_0[A_h^{(i)}] + \xi_0[B_h] = \Psi_{h,a}\left(\frac{k_{out}}{k_{in}}\right)[\tilde{A}], \qquad (77)$$

$$\Psi_0'[A_h^{(i)}] + \xi_0'[B_h] = \Psi_{h,a}'[\tilde{A}], \qquad (78)$$

$$\Psi_0'[A_e^{(i)}] + \xi_0'[B_e] = (\Psi_{e,a}' + J_{o,a})\left(\frac{k_{out}}{k_{in}}\right)[\tilde{A}], \quad (79)$$

$$\Psi_0[A_e^{(i)}] + \xi_0[B_e] = \Psi_{e,a}[\tilde{A}], \qquad (80)$$

where the columns in the square brackets contain the corresponding field amplitudes, for example $[B_e]_p = B_{e,p}$.

Let us at first eliminate the amplitudes $B_{h,p}$ and $B_{e,p}$. To this end, Eqs. (77) and (78) are multiplied, respectively, by ξ_0' and ξ_0 and the results subtracted. With the Wronskian identity,

$$\psi_n(x)\xi_n'(x) - \psi_n'(x)\xi_n(x) = i, \qquad \forall n, \qquad (81)$$

the resulting equation takes the form

$$i[A_h^{(i)}] = \left[\xi_0'\Psi_{h,a}\left(\frac{k_{out}}{k_{in}}\right) - \xi_0\Psi_{h,a}'\right][\tilde{A}]. \qquad (82)$$

By multiplying Eqs. (79) and (80) by ξ_0 and ξ_0' and subtracting them, we can eliminate $B_{e,p}$, and the result has a similar form:

$$i[A_e^{(i)}] = \left[\xi_0'\Psi_{e,a} - \xi_0(\Psi_{e,a}' + J_{o,a})\left(\frac{k_{out}}{k_{in}}\right)\right][\tilde{A}]. \qquad (83)$$

Equations (82) and (83) form a set of $2(N_\nu-1)$ equations that can be solved by a unique matrix inversion,

$$[\tilde{A}] = iU^{-1}\begin{pmatrix} [A_h^{(i)}] \\ [A_e^{(i)}] \end{pmatrix}, \qquad (84)$$

where

$$U = \begin{pmatrix} \xi_0'\Psi_{h,a}\left(\dfrac{k_{out}}{k_{in}}\right) - \xi_0\Psi_{h,a}' \\ \xi_0'\Psi_{e,a} - \xi_0(\Psi_{e,a}' + J_{o,a})\left(\dfrac{k_{out}}{k_{in}}\right) \end{pmatrix}. \qquad (85)$$

Multiplying Eqs. (77) and (78) respectively by Ψ_0' and Ψ_0 and subtracting the results permits the elimination of $[A_h^{(i)}]$:

$$i[B_h] = \left[\Psi_0 \Psi'_{h,a} - \Psi'_0 \Psi_{h,a} \left(\frac{k_{\text{out}}}{k_{\text{in}}} \right) \right] [\tilde{A}]. \qquad (86)$$

By multiplying Eqs. (79) and (80) by Ψ_0 and Ψ'_0 and subtracting them we can eliminate $[A_e^{(i)}]$:

$$i[B_e] = \left[\Psi_0 (\Psi'_{e,a} + J_{o,a}) \left(\frac{k_{\text{out}}}{k_{\text{in}}} \right) - \Psi'_0 \Psi_{e,a} \right] [\tilde{A}]. \qquad (87)$$

Combining Eqs. (84), (86), and (87) gives the link between $B_{h,p}$ $B_{e,p}$ and $A_{h,p}^{(i)}$, $A_{e,p}^{(i)}$ in a matrix form,

$$\begin{pmatrix} [B_h] \\ [B_e] \end{pmatrix} = \begin{pmatrix} T_{hh} & T_{he} \\ T_{eh} & T_{ee} \end{pmatrix} \begin{pmatrix} [A_h^{(i)}] \\ [A_e^{(i)}] \end{pmatrix}, \qquad (88)$$

where the T matrix is equal to

$$T = \begin{pmatrix} T_{hh} & T_{he} \\ T_{eh} & T_{ee} \end{pmatrix} = \begin{pmatrix} \Psi_0 \Psi'_{h,a} - \Psi'_0 \Psi_{h,a} \left(\dfrac{k_{\text{out}}}{k_{\text{in}}} \right) \\[2em] \Psi_0 (\Psi'_{e,a} + J_{o,a}) \left(\dfrac{k_{\text{out}}}{k_{\text{in}}} \right) - \Psi'_0 \Psi_{e,a} \end{pmatrix}$$

$$\times \begin{pmatrix} \xi'_0 \Psi_{h,a} \left(\dfrac{k_{\text{out}}}{k_{\text{in}}} \right) - \xi_0 \Psi'_{h,a} \\[2em] \xi'_0 \Psi_{e,a} - \xi_0 (\Psi'_{e,a} + J_{o,a}) \left(\dfrac{k_{\text{out}}}{k_{\text{in}}} \right) \end{pmatrix}^{-1}. \qquad (89)$$

Thus the field is determined everywhere. The amplitudes $B_{e,p}$ and $B_{h,p}$ serve to obtain the physical quantities, such as total scattering, extinction and absorption cross section, and radar and differential cross section, using classical formulas, as recalled in Ref. 14.

In the case when the sphere is optically isotropic, the wavenumber does not depend on the direction of propagation, and it is possible to make the same change of unknowns inside the sphere as was done in the outer region using Eq. (61). We thus introduce the amplitudes $A_{h,p}^{(1)}$ and $A_{e,p}^{(1)}$ given by

$$A_{h,p}^{(1)} = \sum_{\nu=1}^{N_\nu - 1} \sum_{j=1}^{2} \tilde{A}_{j,\nu} a_{h,p,j,\nu},$$

$$A_{e,p}^{(1)} = \sum_{\nu=1}^{N_\nu - 1} \sum_{j=1}^{2} \tilde{A}_{j,\nu} a_{e,p,j,\nu}. \qquad (90)$$

Moreover, as $a_{o,p,j,\nu} = 0$, the matrix $J_{o,a}$ becomes null. The product of matrices $\Psi_{h,a}$ and $\Psi_{e,a}$ with $[\tilde{A}]$ gives diagonal matrices equal to

$$(\Psi_{h,a}[\tilde{A}])_p = \psi_n(n_1 k_0 R) A_{h,p}^{(1)},$$

$$(\Psi_{e,a}[\tilde{A}])_p = \psi_n(n_1 k_0 R) A_{e,p}^{(1)}, \qquad (91)$$

and similar expressions for $\Psi'_{h,a}$ and $\Psi'_{e,a}$. Equations (82) and (83) become diagonal and yield

$$iA_{h,p}^{(i)} = \left[\xi'_n(n_{\text{out}} k_0 R) \psi_n(n_1 k_0 R) \frac{n_{\text{out}}}{n_1} \right.$$

$$\left. - \xi_n(n_{\text{out}} k_0 R) \psi'_n(n_1 k_0 R) \right] A_{h,p}^{(1)},$$

$$iA_{e,p}^{(i)} = \left[\xi'_n(n_{\text{out}} k_0 R) \psi_n(n_1 k_0 R) \right.$$

$$\left. - \xi_n(n_{\text{out}} k_0 R) \psi'_n(n_1 k_0 R) \frac{n_{\text{out}}}{n_1} \right] A_{e,p}^{(1)}. \qquad (92)$$

The same is valid for Eqs. (86) and (87):

$$iB_{h,p} = \left[\psi_n(n_{\text{out}} k_0 R) \psi'_n(n_1 k_0 R) \right.$$

$$\left. - \psi'_n(n_{\text{out}} k_0 R) \psi_n(n_1 k_0 R) \frac{n_{\text{out}}}{n_1} \right] A_{h,p}^{(1)},$$

$$iB_{e,p} = \left[\psi_n(n_{\text{out}} k_0 R) \psi'_n(n_1 k_0 R) \frac{n_{\text{out}}}{n_1} \right.$$

$$\left. - \psi'_n(n_{\text{out}} k_0 R) \psi_n(n_1 k_0 R) \right] A_{e,p}^{(1)}. \qquad (93)$$

Matrix **U** becomes diagonal, and thus the T matrix takes a diagonal form with elements generally referred to as Mie coefficients:

$$(T_{hh})_{pq}$$

$$= \frac{\psi_n(n_{\text{out}} k_0 R) \psi'_n(n_1 k_0 R) - \psi'_n(n_{\text{out}} k_0 R) \psi_n(n_1 k_0 R) \dfrac{n_{\text{out}}}{n_1}}{\xi'_n(n_{\text{out}} k_0 R) \psi_n(n_1 k_0 R) \dfrac{n_{\text{out}}}{n_1} - \xi_n(n_{\text{out}} k_0 R) \psi'_n(n_1 k_0 R)} \delta_{pq},$$

$$(T_{ee})_{pq}$$

$$= \frac{\psi_n(n_{\text{out}} k_0 R) \psi'_n(n_1 k_0 R) \dfrac{n_{\text{out}}}{n_1} - \psi'_n(n_{\text{out}} k_0 R) \psi_n(n_1 k_0 R)}{\xi'_n(n_{\text{out}} k_0 R) \psi_n(n_1 k_0 R) - \xi_n(n_{\text{out}} k_0 R) \psi'_n(n_1 k_0 R) \dfrac{n_{\text{out}}}{n_1}} \delta_{pq}.$$

$$T_{eh} = T_{he} = 0. \qquad (94)$$

In that case, there is no coupling between the two fundamental polarizations nor between different p components. In other words, scattering by an isotropic sphere does not mix electric and magnetic degrees of freedom, nor does it mix multipole orders. On the other hand, anisotropy can mix multipole orders as well as electric and magnetic degrees of freedom.

8. UNIAXIAL MATERIALS

As already observed in Subsection 4.B.2, the equations are simplified for a uniaxial material. First, the wavenumber of the ordinary wave does not depend on the di-

rection of propagation, $k_{1,\nu}=k_0\sqrt{\epsilon_x}$, $\forall\,\nu$. Second, the ordinary wave is transverse, and thus $a_{o,p,l,\nu}=0$. Third, the ordinary-wave eigenvector does not depend on θ, $\mathbf{\Gamma}_{1,\nu}=\hat{\boldsymbol{\varphi}}$. The fourth simplification concerns the extraordinary wave. Its eigenvalue and eigenvector are independent of φ, as obtained from Eqs. (33) and (34). As a result, the φ dependence in Eqs. (58) and (59) remains only in the unknown amplitudes $\widetilde{A}_{j,\nu}=\widetilde{A}_j(\theta,\varphi_\nu)\sin\theta_\nu$ and in the coeffi-

cients $a_{h,p,j,\nu}$, $a_{e,p,j,\nu}$, and $a_{o,p,j,\nu}$. However, the φ dependence of these coefficients has a very simple form when the eigenvectors $\mathbf{\Gamma}_{j,\nu}$ do not depend on φ. This can be observed in Eqs. (7)–(10) and (13)–(17) of Ref. 14, summarized here in Eq. (A22). Taking them into account, as well as the above-mentioned arguments, it is possible to separate the variables in the coefficients defined in Eq. (56):

$$a_{h,p,1,\nu}=4\pi i^n\mathbf{X}_p^*(\hat{\mathbf{r}}_\nu)\cdot\mathbf{\Gamma}_{1,\nu}=4\pi i^n\mathbf{X}_p^*(\theta_\nu,\varphi_\nu)\cdot\hat{\boldsymbol{\varphi}}_\nu=2\pi\alpha_{h,p,1}(\theta_\nu)\exp[im(p)\varphi_\nu],$$

$$a_{e,p,1,\nu}=4\pi i^{n-1}\mathbf{Z}_p^*(\hat{\mathbf{r}}_\nu)\cdot\mathbf{\Gamma}_{1,\nu}=4\pi i^{n-1}\mathbf{Z}_p^*(\theta_\nu,\varphi_\nu)\cdot\hat{\boldsymbol{\varphi}}_\nu=2\pi\alpha_{e,p,1}(\theta_\nu)\exp[im(p)\varphi_\nu],$$

$$a_{o,p,1,\nu}=4\pi i^{n-1}\mathbf{Y}_p^*(\hat{\mathbf{r}}_\nu)\cdot\mathbf{\Gamma}_{1,\nu}=4\pi i^{n-1}\mathbf{Y}_p^*(\theta_\nu,\varphi_\nu)\cdot\hat{\boldsymbol{\varphi}}_\nu=0,$$

$$a_{h,p,2,\nu}=4\pi i^n\mathbf{X}_p^*(\hat{\mathbf{r}}_\nu)\cdot\mathbf{\Gamma}_{2,\nu}=4\pi i^n\mathbf{X}_p^*(\theta_{n_\theta},\varphi_\nu)\cdot\hat{\boldsymbol{\theta}}_\nu=2\pi\alpha_{h,p,2}(\theta_\nu)\exp[im(p)\varphi_\nu],$$

$$a_{e,p,2,\nu}=4\pi i^{n-1}\mathbf{Z}_p^*(\hat{\mathbf{r}}_\nu)\cdot\mathbf{\Gamma}_{2,\nu}=4\pi i^{n-1}\mathbf{Z}_p^*(\theta_\nu,\varphi_\nu)\cdot\hat{\boldsymbol{\theta}}_\nu=2\pi\alpha_{e,p,2}(\theta_\nu)\exp[im(p)\varphi_\nu],$$

$$a_{o,p,2,\nu}=4\pi i^{n-1}\mathbf{Y}_p^*(\hat{\mathbf{r}}_\nu)\cdot\mathbf{\Gamma}_{2,\nu}=4\pi i^{n-1}Y_p^*(\theta_\nu,\varphi_\nu)\Gamma_{2,\nu,r}=2\pi\alpha_{o,p,2}(\theta_\nu)\exp[im(p)\varphi_\nu].\qquad(95)$$

The new coefficients α can be obtained by using Eqs. (A22) and are expressed by using the normalized associated Legendre functions $\bar{P}_n^m(\cos\theta_\nu)$:

$$\alpha_{h,p,1}(\theta_\nu)=-\frac{2i^n}{a_p}\frac{\mathrm{d}\bar{P}_n^m(\cos\theta_\nu)}{\mathrm{d}\theta_\nu},$$

$$\alpha_{e,p,1}(\theta_\nu)=-\frac{2i^n m}{a_p\sin\theta_\nu}\bar{P}_n^m(\cos\theta_\nu),$$

$$\alpha_{h,p,2}(\theta_\nu)=-\frac{2i^{n+1}}{a_p\sin\theta_\nu}\bar{P}_n^m(\cos\theta_\nu),$$

$$\alpha_{e,p,2}(\theta_\nu)=-\frac{2i^{n-1}}{a_p}\frac{\mathrm{d}\bar{P}_n^m(\cos\theta_\nu)}{\mathrm{d}\theta_\nu},$$

$$\alpha_{o,p,2}(\theta_\nu)=2i^{n-1}\bar{P}_n^m(\cos\theta_\nu)\frac{(\epsilon_z-\epsilon_x)\sin\theta_\nu\cos\theta_\nu}{\epsilon_x\sin^2\theta_\nu+\epsilon_z\cos^2\theta_\nu},\quad(96)$$

where n and m are determined from p through Eq. (54). Quite important is that the new coefficients α depend on θ_ν but not on φ_ν. This fact enables us to reduce significantly the size of the set of equations to solve by introducing new amplitudes in a manner similar to the way they are used in Eqs. (61), which are, in fact, Fourier transforms of $\widetilde{A}_{j,\nu}$ with respect to φ:

$$\widetilde{A}_{j,p,n_\theta}=\frac{1}{2\pi}\sum_{n_\varphi=1}^{n_\theta}\widetilde{A}_{j,\nu(n_\theta,n_\varphi)}\exp[im(p)\varphi_{n_\varphi}].\qquad(97)$$

With this substitution, the set of Eqs. (82) and (83) changes into a set having a much smaller number of un-

knowns. When explicitly written, it takes the form

$$iA_{h,p}^{(i)}=\sum_{n_\theta=1}^{2n_{\mathrm{Max}}}\sum_{j=1}^{2}\widetilde{A}_{j,p,n_\theta}\alpha_{h,p,j,n_\theta}\left[\xi_n'(n_{\mathrm{out}}k_0R)\psi_n(k_{j,n_\theta}R)\frac{n_{\mathrm{out}}k_0}{k_{j,n_\theta}}\right.$$
$$\left.-\xi_n(n_{\mathrm{out}}k_0R)\psi_n'(k_{j,n_\theta}R)\right],$$

$$iA_{e,p}^{(i)}=\sum_{n_\theta=1}^{2n_{\mathrm{Max}}}\sum_{j=1}^{2}\widetilde{A}_{j,p,n_\theta}\left\{\alpha_{e,p,j,n_\theta}\xi_n'(n_{\mathrm{out}}k_0R)\psi_n(k_{j,n_\theta}R)\right.$$
$$-\xi_n(n_{\mathrm{out}}k_0R)[\alpha_{e,p,j,n_\theta}\psi_n'(k_{j,n_\theta}R)$$
$$\left.+a_p\alpha_{o,p,j,n_\theta}j_n(k_{j,n_\theta}R)]\frac{n_{\mathrm{out}}k_0}{k_{j,n_\theta}}\right\}.\qquad(98)$$

In addition to the change of the coefficients $a\to\alpha$, much more important is to notice that the summation in ν generally containing $N_\nu-1=n_{\mathrm{Max}}(n_{\mathrm{Max}}+2)$ terms has been reduced to only $2n_{\mathrm{Max}}$ terms for each p, i.e., almost n_{Max} times. Since $p_{\mathrm{Max}}=N_\nu$, a significant reduction of the required number of vector spherical harmonics is achieved.

After the amplitudes $\widetilde{A}_{j,p,n_\theta}$ are determined by solving the linear system of algebraic equations, the diffracted amplitudes in the outermost medium, $B_{e,p}$ and $B_{h,p}$, are found by using Eqs. (72) and (73). In addition, the inverse Fourier transform of Eq. (97) gives the amplitudes of each plane wave $\widetilde{A}_{j,p,\nu(n_\theta,n_\varphi)}$ inside the uniaxial material.

9. CONCLUSIONS

Using vector spherical harmonic functions as a basis, we succeeded in obtaining the general form of the electro-

magnetic field in an arbitrary anisotropic homogeneous medium. Applying the boundary conditions across the surface of a sphere allows us to find the components of the diffracted field from those of the incident field through a matrix inversion. This semianalytical method reduces, of course, to the analytic Mie theory when the sphere is filled with isotropic medium. The case of uniaxial material, characterized by a φ-independent permittivity tensor, leads to some simplifications and to a significant reduction of the size of the matrix to be inverted.

This work presents the first step toward resolving the problem of diffraction by an arbitrary-shaped anisotropic object or an inhomogeneous anisotropic sphere, for which the permittivity tensor is a function of the Cartesian coordinates. This problem is treated in detail in Part II (this issue):[16] its solution is based on this work and extends the differential theory, published in Ref. 14 to anisotropic bodies.

APPENDIX A: VECTOR SPHERICAL HARMONICS DEVELOPMENT OF AN ARBITRARY PLANE WAVE

In order to establish the development of an arbitrary vector plane wave, let us recall that it is well known that an arbitrary scalar plane wave can be represented in terms of Legendre polynomials,

$$\exp(i\mathbf{k}\cdot\mathbf{r}) = \sum_{q=0}^{\infty}(2q+1)i^q j_q(kr)P_q(\hat{\mathbf{r}}_k\cdot\hat{\mathbf{r}}), \quad (A1)$$

where P_q are the Legendre polynomials, $\hat{\mathbf{r}}=\mathbf{r}/r$, and $\hat{\mathbf{r}}_k \equiv \hat{\mathbf{k}}=\mathbf{k}/k$.

The addition theorem for Legendre polynomials represents them in terms of scalar spherical harmonics $Y_{qm}(\theta,\varphi)$:

$$P_q(\hat{\mathbf{r}}_k\cdot\hat{\mathbf{r}}) = \frac{4\pi}{2q+1}\sum_{m=-q}^{q}Y_{qm}^*(\hat{\mathbf{r}}_k)Y_{qm}(\hat{\mathbf{r}}). \quad (A2)$$

The scalar spherical harmonics are expressed in terms of associated Legendre functions P_q^m or of normalized associated Legendre functions $\bar{P}_q^m$:

$$Y_{qm}(\theta,\varphi) = \left[\frac{2m+1}{4\pi}\frac{(q-m)!}{(q+m)!}\right]^{1/2}P_q^m(\cos\theta)\exp(im\varphi)$$

$$= \bar{P}_q^m(\cos\theta)\exp(im\varphi). \quad (A3)$$

Equation (A2) allows us to write the expansion of a scalar plane wave in terms of the scalar spherical harmonics:

$$\exp(i\mathbf{k}\cdot\mathbf{r}) = 4\pi\sum_{q=0}^{\infty}\sum_{m=-q}^{q}i^q j_q(kr)Y_{qm}(\hat{\mathbf{r}})Y_{qm}^*(\mathbf{r}_k). \quad (A4)$$

The next step is to generalize these expressions to a vector plane wave with arbitrary vector amplitude. To this end we invoke a set of vector spherical harmonics. The first set, denoted $\mathbf{Y}_{n,n+1}^m$, $\mathbf{Y}_{n,n}^m$, $\mathbf{Y}_{n,n-1}^m$ is obtained through the so-called angular coupling formalism [15] by using the Cartesian spherical unit vectors:

$$\hat{\boldsymbol{\chi}}_1 = -\frac{1}{\sqrt{2}}(\hat{\mathbf{x}}+i\hat{\mathbf{y}}),$$

$$\hat{\boldsymbol{\chi}}_0 = \hat{\mathbf{z}},$$

$$\hat{\boldsymbol{\chi}}_{-1} = \frac{1}{\sqrt{2}}(\hat{\mathbf{x}}-i\hat{\mathbf{y}}). \quad (A5)$$

They form a complete orthogonal basis for the three-dimensional vectors:

$$\sum_{\mu=-1}^{1}\hat{\boldsymbol{\chi}}_\mu^*\hat{\boldsymbol{\chi}}_\mu = \mathbb{I}, \qquad \hat{\boldsymbol{\chi}}_\mu^*\cdot\hat{\boldsymbol{\chi}}_\tau = \delta_{\mu\tau}. \quad (A6)$$

Making use of Clebsch–Gordon coefficients, we define the first set of vector spherical harmonics in terms of the scalar spherical harmonics:

$$\mathbf{Y}_{n,q}^m = \sum_{\mu=-1}^{1}(q,m-\mu;1,\mu|n,m)Y_{q,m-\mu}\hat{\boldsymbol{\chi}}_\mu,$$

$$q = n-1, n, n+1. \quad (A7)$$

These vectors form a complete and orthogonal basis for functions depending on angular variables:

$$\int_0^{4\pi}\mathrm{d}\Omega\, Y_{n,q}^{*m}(\hat{\mathbf{r}})\cdot Y_{n',q'}^{m'}(\hat{\mathbf{r}}) = \delta_{nn'}\delta_{mm'}\delta_{qq'},$$

$$\sum_{n,m,q}Y_{n,q}^{*m}(\hat{\mathbf{r}})Y_{n,q}^{*m}(\hat{\mathbf{r}}') = \mathbb{I}\delta_\Omega(\hat{\mathbf{r}},\hat{\mathbf{r}}'). \quad (A8)$$

The vector analog of the scalar addition theorem, Eq. (A2) is

$$\mathbb{I}P_q(\hat{\mathbf{r}}_k\cdot\hat{\mathbf{r}}) = \frac{4\pi}{2q+1}\sum_{n,m}\mathbf{Y}_{nq}^{*m}(\hat{\mathbf{r}}_k)\mathbf{Y}_{nq}^m(\hat{\mathbf{r}}), \quad (A9)$$

which allows us to write the vector analog of Eq. (A4):

$$\mathbb{I}\exp(i\mathbf{k}\cdot\mathbf{r}) = 4\pi\sum_{n,m,q}i^q j_q(kr)\mathbf{Y}_{nq}^{*m}(\hat{\mathbf{r}}_k)\mathbf{Y}_{nq}^m(\hat{\mathbf{r}}). \quad (A10)$$

This expression can be used to express the vector plane wave polarized in direction $\boldsymbol{\Gamma}$ in the following form:

$$\boldsymbol{\Gamma}\exp(i\mathbf{k}\cdot\mathbf{r}) = \mathbb{I}\cdot\boldsymbol{\Gamma}\exp(i\mathbf{k}\cdot\mathbf{r})$$

$$= 4\pi\sum_{n,m,q}i^q j_q(kr)\mathbf{Y}_{nq}^{*m}(\hat{\mathbf{r}}_k)\mathbf{Y}_{nq}^m(\hat{\mathbf{r}})\cdot\boldsymbol{\Gamma}. \quad (A11)$$

When working in spherical coordinates, it is convenient to define a second set of vector spherical harmonics $\mathbf{Y}_{nm}$, $\mathbf{X}_{nm}$, $\mathbf{Z}_{nm}$, sometimes known as $\mathbf{Y}_{n,m}^{(o)}$, $\mathbf{Y}_{n,m}^{(m)}$, $\mathbf{Y}_{n,m}^{(e)}$. These are related to $\mathbf{Y}_{n,n+1}^m$, $\mathbf{Y}_{n,n}^m$, $\mathbf{Y}_{n,n-1}^m$ via the relations

$$\mathbf{X}_{nm} \equiv \mathbf{Y}_{n,m}^{(m)} \equiv \frac{1}{i}\mathbf{Y}_{n,n}^m,$$

$$\mathbf{Z}_{nm} \equiv \mathbf{Y}_{n,m}^{(e)} \equiv \left(\frac{n+1}{2n+1}\right)^{1/2}\mathbf{Y}_{n,n-1}^m + \left(\frac{n}{2n+1}\right)^{1/2}\mathbf{Y}_{n,n+1}^m,$$

$$\mathbf{Y}_{nm} \equiv \mathbf{Y}_{n,m}^{(o)} \equiv \left(\frac{n}{2n+1}\right)^{1/2}\mathbf{Y}_{n,n-1}^m - \left(\frac{n+1}{2n+1}\right)^{1/2}\mathbf{Y}_{n,n+1}^m,$$

$$\text{(A12)}$$

with inverse relations

$$\frac{1}{i}\mathbf{Y}_{n,n}^m = i\mathbf{X}_{nm},$$

$$\mathbf{Y}_{n,n-1}^m = \left(\frac{n+1}{2n+1}\right)^{1/2}\mathbf{Z}_{nm} + \left(\frac{n}{2n+1}\right)^{1/2}\mathbf{Y}_{nm},$$

$$\mathbf{Y}_{n,n+1}^m = \left(\frac{n}{2n+1}\right)^{1/2}\mathbf{Z}_{nm} - \left(\frac{n+1}{2n+1}\right)^{1/2}\mathbf{Y}_{nm}. \quad \text{(A13)}$$

With these new vector spherical harmonics, the three terms in the sum in $q = n-1, n, n+1$ in Eq. (A10) become

$q = n-1$

$$4\pi\sum_{n,m} i^{n-1}j_{n-1}(kr)\mathbf{Y}_{n,n-1}^{*m}(\hat{\mathbf{k}})\mathbf{Y}_{n,n-1}^m(\hat{\mathbf{r}})$$

$$= 4\pi\sum_{n,m} i^{n-1}j_{n-1}(kr)$$

$$\times\left\{\frac{n+1}{2n+1}\mathbf{Z}_{nm}(\hat{\mathbf{r}})\mathbf{Z}_{nm}^*(\hat{\mathbf{k}}) + \frac{n}{2n+1}\hat{\mathbf{Y}}_{nm}(\hat{\mathbf{r}})\hat{\mathbf{Y}}_{nm}^*(\hat{\mathbf{k}})\right.$$

$$\left. + \frac{\sqrt{n(n+1)}}{2n+1}[\hat{\mathbf{Y}}_{nm}(\hat{\mathbf{r}})\mathbf{Z}_{nm}^*(\hat{\mathbf{k}}) + \mathbf{Z}_{nm}(\hat{\mathbf{r}})\hat{\mathbf{Y}}_{nm}^*(\hat{\mathbf{k}})]\right\},$$

$$\text{(A14)}$$

$q = n$

$$4\pi\sum_{n,m} i^n j_n(kr)\mathbf{Y}_{n,n}^{*m}(\hat{\mathbf{k}})\mathbf{Y}_{n,n}^m(\hat{\mathbf{r}})$$

$$= 4\pi\sum_{n,m} i^n j_n(kr)\mathbf{X}_{nm}(\hat{\mathbf{r}})\mathbf{X}_{nm}^*(\hat{\mathbf{k}}), \quad \text{(A15)}$$

$q = n+1$

$$4\pi\sum_{n,m} i^{n+1}j_{n+1}(kr)\mathbf{Y}_{n,n+1}^{*m}(\hat{\mathbf{k}})\mathbf{Y}_{n,n+1}^m(\hat{\mathbf{r}})$$

$$= 4\pi\sum_{n,m} i^{n+1}j_{n+1}(kr)$$

$$\times\left\{\frac{n}{2n+1}\mathbf{Z}_{nm}(\hat{\mathbf{r}})\mathbf{Z}_{nm}^*(\hat{\mathbf{k}}) + \frac{n+1}{2n+1}\mathbf{Y}_{nm}(\hat{\mathbf{r}})\mathbf{Y}_{nm}^*(\hat{\mathbf{k}})\right.$$

$$\left. - \frac{\sqrt{n(n+1)}}{2n+1}[\mathbf{Y}_{nm}(\hat{\mathbf{r}})\mathbf{Z}_{nm}^*(\hat{\mathbf{k}}) + \mathbf{Z}_{nm}(\hat{\mathbf{r}})\mathbf{Y}_{nm}^*(\hat{\mathbf{k}})]\right\}.$$

$$\text{(A16)}$$

We thus obtain

$$\mathbb{I}\exp(i\mathbf{k}\cdot\mathbf{r}) = 4\pi\sum_{n,m} i^n j_n(kr)\mathbf{X}_{nm}(\hat{\mathbf{r}})\mathbf{X}_{nm}^*(\hat{\mathbf{k}})$$

$$+ 4\pi\sum_{n,m} \frac{i^{n-1}}{2n+1}[(n+1)j_{n-1}(kr)$$

$$- nj_{n+1}(kr)]\mathbf{Z}_{nm}(\hat{\mathbf{r}})\mathbf{Z}_{nm}^*(\hat{\mathbf{k}})$$

$$+ 4\pi\sum_{n,m} \frac{i^{n-1}}{2n+1}[nj_{n-1}(kr) - (n$$

$$+ 1)j_{n+1}(kr)]\mathbf{Y}_{nm}(\hat{\mathbf{r}})\mathbf{Y}_{nm}^*(\hat{\mathbf{k}})$$

$$+ 4\pi\sum_{n,m} \frac{i^{n-1}}{2n+1}\sqrt{n(n+1)}[j_{n-1}(kr) + j_{n+1}(kr)]$$

$$\times[\mathbf{Y}_{nm}(\hat{\mathbf{r}})\mathbf{Z}_{nm}^*(\hat{\mathbf{k}}) + \mathbf{Z}_{nm}(\hat{\mathbf{r}})\mathbf{Y}_{nm}^*(\hat{\mathbf{k}})]. \quad \text{(A17)}$$

This formula can be simplified by invoking the spherical Bessel function recursion formulas,

$$j_{n-1}(x) + j_{n+1}(x) = \frac{2n+1}{x}j_n(x),$$

$$nj_{n-1}(x) - (n+1)j_{n+1}(x) = (2n+1)j_n'(x),$$

$$(n+1)j_{n-1}(x) - nj_{n+1}(x) = \frac{2n+1}{x}[xj_n(x)]', \quad \text{(A18)}$$

to obtain

$$\mathbb{I}\exp(i\mathbf{k}\cdot\mathbf{r}) = 4\pi\sum_{n,m}\left\{i^n j_n(kr)\mathbf{X}_{nm}(\hat{\mathbf{r}})\mathbf{X}_{nm}^*(\hat{\mathbf{k}})\right.$$

$$+ i^{n-1}\frac{[krj_n(kr)]'}{kr}\mathbf{Z}_{nm}(\hat{\mathbf{r}})\mathbf{Z}_{nm}^*(\hat{\mathbf{k}})$$

$$+ i^{n-1}j_n'(kr)\mathbf{Y}_{nm}(\hat{\mathbf{r}})\mathbf{Y}_{nm}^*(\hat{\mathbf{k}})$$

$$+ i^{n-1}\sqrt{n(n+1)}\frac{j_n(kr)}{kr}[\mathbf{Y}_{nm}(\hat{\mathbf{r}})\mathbf{Z}_{nm}^*(\hat{\mathbf{k}})$$

$$\left. + \mathbf{Z}_{nm}(\hat{\mathbf{r}})\mathbf{Y}_{nm}^*(\hat{\mathbf{k}})]\right\}. \quad \text{(A19)}$$

Equation (A11) is then written in the basis of $\mathbf{Y}_{nm}$, $\mathbf{X}_{nm}$, $\mathbf{Z}_{nm}$,

$$\exp(i\mathbf{k}\cdot\mathbf{r})\Gamma = \sum_{n,m}\left\{a_{h,nm}j_n(kr)\mathbf{X}_{nm}(\hat{\mathbf{r}})\right.$$

$$+ \left[a_{e,nm}\frac{j_n(kr)}{kr}\sqrt{n(n+1)} + a_{o,nm}j_n'(kr)\right]\mathbf{Y}_{nm}(\hat{\mathbf{r}})$$

$$+ \left[a_{e,nm}\frac{[krj_n(kr)]'}{kr}\right.$$

$$\left.\left. + \sqrt{n(n+1)}a_{o,nm}\frac{j_n(kr)}{kr}\right]\mathbf{Z}_{nm}(\hat{\mathbf{r}})\right\}, \quad \text{(A20)}$$

where

$$a_{h,nm} = 4\pi i^n \mathbf{X}_{nm}^*(\hat{\mathbf{k}}) \cdot \mathbf{\Gamma}, \qquad a_{e,nm} = 4\pi i^{n-1} \mathbf{Z}_{nm}^*(\hat{\mathbf{k}}) \cdot \mathbf{\Gamma},$$

$$a_{o,nm} = 4\pi i^{n-1} \mathbf{Y}_{nm}^*(\hat{\mathbf{k}}) \cdot \mathbf{\Gamma}. \tag{A21}$$

It is useful to recall the additional relations between the vector spherical harmonics and the normalized associated Legendre functions $\bar{P}_q^m$ established in Ref. 14:

$$\mathbf{Y}_{nm}(\theta,\varphi) = \hat{\mathbf{r}}\bar{P}_n^m(\cos\theta)\exp(im\varphi)$$

$$\mathbf{Z}_{nm}(\theta,\varphi) = \frac{r}{\sqrt{n(n+1)}}\mathrm{grad}[\bar{P}_n^m(\cos\theta)\exp(im\varphi)]$$

$$= \frac{\exp(im\varphi)}{\sqrt{n(n+1)}}\left[\hat{\boldsymbol{\varphi}}\frac{im}{\sin\theta} + \hat{\boldsymbol{\theta}}\frac{\mathrm{d}}{\mathrm{d}\theta}\right]\bar{P}_n^m(\cos\theta)$$

$$\mathbf{X}_{nm}(\theta,\varphi) = \mathbf{Z}_{nm}(\theta,\varphi) \times \hat{\mathbf{r}}$$

$$= \frac{\exp(im\varphi)}{\sqrt{n(n+1)}}\left[\hat{\boldsymbol{\theta}}\frac{im}{\sin\theta} - \hat{\boldsymbol{\varphi}}\frac{\mathrm{d}}{\mathrm{d}\theta}\right]\bar{P}_n^m(\cos\theta). \tag{A22}$$

The corresponding author's e-mail address is brian.stout@fresnel.fr.

REFERENCES

1. C. F. Bohren and D. R. Huffman, *Absorption and Scattering of Light by Small Particles* (Wiley-Interscience, 1998), Chaps. 5 and 6.
2. Ref. 1, Chap. 7.
3. H. C. Van de Hulst, *Light Scattering by Small Particles* (Dover, 1957, 1981).
4. L. Lorenz, "Lysbevaegelsen i og uden for en af plane Lysbølger belyst Kulge," Vidensk Selk. Skr. **6**, 1–62 (1890).
5. L. Lorenz, "Sur la lumière réfléchie et réfractée par une sphère transparente," Oeuvres scientifiques de L. Lorenz, revues et annotées par H. Valentiner (Librairie Lehmann et Stage, 1898).
6. G. Mie, "Beiträge zur Optik Trüben Mefien speziell kolloidoaled Metallosungen," Ann. Phys. **25**, 377–452 (1908).
7. J. Roth and M. J. Dignam, "Scattering and extinction cross sections for a spherical particle with an oriented molecular layer," J. Opt. Soc. Am. **63**, 308–311 (1973).
8. A. D. Kiselev, V. Yu. Reshetnyak, and T. J. Sluckin, "Light scattering by optically anisotropic scatterers: T-matrix theory for radial and uniform anisotropies," Phys. Rev. E **65**, 056609-1–056609-16 (2002).
9. J. C. Monzon, "Three-dimensional field expansion in the most general rotationally symmetric anisotropic material: application to the scattering by a sphere," IEEE Trans. Antennas Propag. **37**, 728–735 (1989).
10. Y. L. Geng, Xin-Bao Wu, L. W. Li, and B. R. Guan, "Mie scattering by a uniaxial anisotropic sphere," Phys. Rev. E **70**, 056609-1–056609-6 (2004).
11. Ref. 1, Chap. 8.2.
12. S. N. Papadakis, N. K. Uzunoglu, and C. N. Capsalis, "Scattering of a plane wave by a general anisotropic dielectric ellipsoid," J. Opt. Soc. Am. A **7**, 991–997 (1990).
13. M. Born and E. Wolf, *Principles of Optics: Electromagnetic Theory of Propagation Interference and Diffraction of Light*, 7th ed. (Cambridge U. Press, Cambridge, 2002).
14. B. Stout, M. Nevière, and E. Popov, "Light diffraction by a three-dimensional object: differential theory," J. Opt. Soc. Am. A **22**, 2385–2404 (2005).
15. A. R. Edmonds, *Angular Momentum in Quantum Mechanics* (Princeton U. Press, 1960).
16. B. Stout, M. Nevière, and E. Popov, "Mie scattering by an anisotropic object. Part II. Arbitrary-shaped object: differential theory," J. Opt. Soc. Am. A **23**, 1124–1134 (2006).

Stout *et al.*

Mie scattering by an anisotropic object. Part II. Arbitrary-shaped object: differential theory

Brian Stout, Michel Nevière, and Evgeny Popov

*Institut Fresnel, Unité mixte de Recherche 6133, Case 161 Faculté des Sciences et Techniques,
Centre de Saint Jérôme, 13397 Marseille Cedex 20, France*

The differential theory of diffraction by an arbitrary-shaped body made of arbitrary anisotropic material is developed. The electromagnetic field is expanded on the basis of vector spherical harmonics, and the Maxwell equations in spherical coordinates are reduced to a first-order differential set. When discontinuities of permittivity exist, we apply the fast numerical factorization to find the link between the electric field vector and the vector of electric induction, developed in a truncated basis. The diffraction problem is reduced to a boundary-value problem by using a shooting method combined with the S-matrix propagation algorithm, formulated for the field components instead of the amplitudes. © 2006 Optical Society of America

OCIS codes: 290.5850, 050.1940, 000.3860, 000.4430.

1. INTRODUCTION

Light diffraction and scattering by arbitrary three-dimensional (3D) objects is a problem of interest in many domains of science and technology, such as astrophysics, atmospheric physics, remote detection, radar scattering, and photonics. In a previous paper[1] we developed a differential theory to analyze the problem in the case of isotropic materials. However, in both nature and technology, diffracting particles are more complicated. Two examples are that interstellar dust can include crystalline particles[2] and that high-frequency light modulation can be performed by using electro-optical effects in anisotropic crystals such as $LiNbO_3$.[3]

Although a great amount of work has been devoted to the problem during the past 15 years, it seems that a general theory that could handle arbitrary shaped objects made of arbitrary anisotropic lossless or lossy material needs to be formulated. Published studies address particular shapes or kinds of anisotropy. For example, Ref. 4 deals with dielectric ellipsoids, and Ref. 5 considers rotationally symmetric anisotropy with geometries conformal to spherical coordinates; Ref. 6 deals with perfectly conducting cylinders coated with an anisotropic layer, while Ref. 7 is restricted to spherical scatterers including an annular layer of anisotropic material.

The aim of this paper is to take advantage of the flexibility of the differential theory of light diffraction,[8] recently extended to 3D optically isotropic objects described in spherical coordinates,[1] in order to develop the theory for an arbitrary anisotropy. This has become possible thanks to the possibility of representing the field in an anisotropic material in the basis of vector spherical harmonics, described in Part I.[9]

2. PRESENTATION OF THE PROBLEM

The diffracting object is represented schematically in Fig. 1. It has an arbitrary shape limited by a surface S, described in spherical coordinates by the equation

$$f(r, \theta, \varphi) = 0, \tag{1}$$

or by

$$r = g(\theta, \varphi), \qquad \theta \in [0, \pi]. \tag{2}$$

The tensor of relative permittivity in Cartesian coordinates has the form

$$\bar{\bar{\epsilon}} = \begin{bmatrix} \epsilon_{xx} & \epsilon_{xy} & \epsilon_{xz} \\ \epsilon_{yx} & \epsilon_{yy} & \epsilon_{yz} \\ \epsilon_{zx} & \epsilon_{zy} & \epsilon_{zz} \end{bmatrix}, \tag{3}$$

and we assume that its elements do not depend on (x, y, z). Its elements in any coordinate system with unit vectors $(\hat{\mathbf{i}}, \hat{\mathbf{j}}, \hat{\mathbf{l}})$ can be obtained using the formula $\tilde{\bar{\epsilon}} = \mathfrak{R} \bar{\bar{\epsilon}} \mathfrak{R}^{\mathrm{T}}$, where T stands for transpose and $\mathfrak{R}$ is the corresponding transformation matrix:

$$\mathfrak{R} = \begin{bmatrix} \hat{\mathbf{i}} \cdot \hat{\mathbf{x}} & \hat{\mathbf{i}} \cdot \hat{\mathbf{y}} & \hat{\mathbf{i}} \cdot \hat{\mathbf{z}} \\ \hat{\mathbf{j}} \cdot \hat{\mathbf{x}} & \hat{\mathbf{j}} \cdot \hat{\mathbf{y}} & \hat{\mathbf{j}} \cdot \hat{\mathbf{z}} \\ \hat{\mathbf{l}} \cdot \hat{\mathbf{x}} & \hat{\mathbf{l}} \cdot \hat{\mathbf{y}} & \hat{\mathbf{l}} \cdot \hat{\mathbf{z}} \end{bmatrix}. \tag{4}$$

We divide the space into three regions by introducing two spheres S_1 and S_2 with radii R_1 and R_2, respectively. The first sphere S_1 is inscribed in the object, and the second sphere S_2 is circumscribed around the object (Fig. 1). Regions inside S_1 and outside S_2 are homogeneous. The intermediate region is inhomogeneous and will be called the modulated region. In this region, for any value of r ($R_1 < r < R_2$) each tensorial component $\tilde{\bar{\epsilon}}_{ij}$, $i, j = (r, \theta, \varphi)$, of the permittivity is a periodic function of φ with period 2π and can furthermore be expressed on the basis of scalar spherical harmonics:

$$\tilde{\bar{\epsilon}}_{ij}(r, \theta, \varphi) = \sum_{n=0}^{\infty} \sum_{m=-n}^{n} \epsilon_{ij,nm}(r) Y_{nm}(\theta, \varphi), \tag{5}$$

where
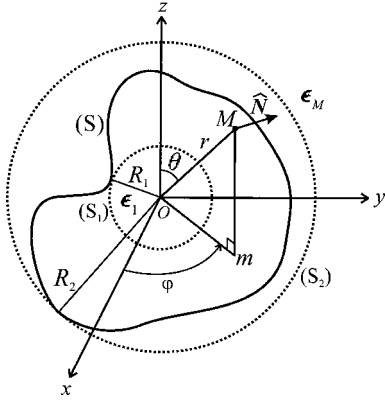
Fig. 1. Depiction of the diffracting object and notation.

$$\epsilon_{ij,nm}(r) = \int_0^{2\pi} d\varphi \int_0^\pi \tilde{\bar{\epsilon}}_{ij}(r,\theta,\varphi) Y_{nm}^*(\theta,\varphi)\sin\theta d\theta$$

$$\equiv \int_0^{4\pi} \tilde{\bar{\epsilon}}_{ij}(r,\theta,\varphi) Y_{nm}^*(\theta,\varphi) d\Omega. \tag{6}$$

It is important to notice that the elements of $\bar{\bar{\epsilon}}$ in Cartesian coordinates are piecewise-constant with respect to φ and θ.

3. FIELD EXPANSION ON VECTOR SPHERICAL HARMONICS

In spherical coordinates, several different basis sets are available to represent the electromagnetic field in any isotropic or anisotropic material. As already discussed in detail in Ref. 1, we shall use the basis of vector spherical harmonic functions $\mathbf{Y}_{nm}(\theta,\varphi)$, $\mathbf{X}_{nm}(\theta,\varphi)$, and $\mathbf{Z}_{nm}(\theta,\varphi)$, which allows the electric field to be expressed as

$$\mathbf{E}(r,\theta,\varphi) = \sum_{n=0}^\infty \sum_{m=-n}^n [E_{Ynm}(r)\mathbf{Y}_{nm}(\theta,\varphi) + E_{Xnm}(r)\mathbf{X}_{nm}(\theta,\varphi)$$

$$+ E_{Znm}(r)\mathbf{Z}_{nm}(\theta,\varphi)]. \tag{7}$$

A numerical treatment requires truncation of the infinite sum in n, Eq. (7), to a value denoted by n_{Max}. We define a single summation index p to replace the two integers n and m through the relation $p=n(n+1)+m+1$ so that $p_{\text{Max}}=(n_{\text{Max}}+1)^2$. The inverse relations permit the determination of n and m from the values of p:

$$n = \text{Int}\sqrt{p-1},$$

$$m = p - 1 - n(n+1). \tag{8}$$

In addition, we introduce a generic notation for the vector spherical harmonic functions, using a Greek letter superscript:

$$\mathbf{W}_p^{(\eta)} = \begin{cases} \mathbf{Y}_p, & \eta=1 \\ \mathbf{X}_p, & \eta=2 \\ \mathbf{Z}_p, & \eta=3 \end{cases}. \tag{9}$$

Using Eqs. (8) and (9), we can represent the electric field in a form more compact than Eq. (7):

$$\mathbf{E}(r,\theta,\varphi) = \sum_{p=1}^{p_{\text{Max}}} \sum_{\eta=1}^3 E_{\eta p}(r)\mathbf{W}_p^{(\eta)}(\theta,\varphi). \tag{10}$$

Similar expansions will be used for the magnetic field $\mathbf{H}$ and electric induction $\mathbf{D}$. In addition, Eq. (5) takes the form

$$\tilde{\bar{\epsilon}}_{ij}(r,\theta,\varphi) = \sum_{p=1}^{p_{\text{Max}}} \epsilon_{ij,p}(r)Y_p(\theta,\varphi). \tag{11}$$

One of the advantages of using vector spherical harmonics is that the Maxwell equations take a simple form[1]:

$$a_p\frac{E_{X,p}}{r} = i\omega\mu_0 H_{Y,p}, \tag{12}$$

$$a_p\frac{E_{Y,p}}{r} - \frac{E_{Z,p}}{r} - \frac{dE_{Z,p}}{dr} = i\omega\mu_0 H_{X,p}, \tag{13}$$

$$\frac{E_{X,p}}{r} + \frac{dE_{X,p}}{dr} = i\omega\mu_0 H_{Z,p}, \tag{14}$$

$$a_p\frac{H_{X,p}}{r} = -i\omega D_{Y,p}, \tag{15}$$

$$a_p\frac{H_{Y,p}}{r} - \frac{H_{Z,p}}{r} - \frac{dH_{Z,p}}{dr} = -i\omega D_{X,p}, \tag{16}$$

$$\frac{H_{X,p}}{r} + \frac{dH_{X,p}}{dr} = -i\omega D_{Z,p}, \tag{17}$$

where $a_p=\sqrt{n(n+1)}$ and n is given in Eq. (8).

As we have done in the isotropic case,[1] we introduce a matrix Q_ϵ that links the components of $\mathbf{E}$ and $\mathbf{D}$:

$$\begin{pmatrix} [D_Y] \\ [D_X] \\ [D_Z] \end{pmatrix} = \epsilon_0 Q_\epsilon \begin{pmatrix} [E_Y] \\ [E_X] \\ [E_Z] \end{pmatrix}, \tag{18}$$

where each column denoted by square brackets contains the $p_{\text{Max}}-1$ elements of each vector component. For example,

$$[E_X] = \begin{pmatrix} E_{X,2} \\ \vdots \\ E_{X,p_{\text{Max}}} \end{pmatrix}. \tag{19}$$

Then the set of Eqs. (12)–(17) can be written in the form of a first-order differential set,

$$\frac{d}{dr}[F] = M(r)[F], \tag{20}$$

where the column $[F]$ has four blocks:

$$[F] = \begin{pmatrix} [E_X] \\ [E_Z] \\ [\tilde{H}_X] \\ [\tilde{H}_Z] \end{pmatrix} \tag{21}$$

with $\tilde{\mathbf{H}} = \sqrt{\mu_0/\epsilon_0}\mathbf{H}$, and the matrix M is a square matrix having 16 blocks, each having dimension $p_{Max}-1$ and equal to

$$M_{11} = -\frac{\mathbb{I}}{r}, \qquad M_{12} = M_{13} = 0, \qquad M_{14} = i\mu k_0 \mathbb{I},$$

$$M_{21} = -\frac{a}{r}Q_{\epsilon,YY}^{-1}Q_{\epsilon,YX}, \qquad M_{22} = -\frac{\mathbb{I}}{r} - \frac{a}{r}Q_{\epsilon,YY}^{-1}Q_{\epsilon,YZ},$$

$$M_{23} = i\left(\frac{aQ_{\epsilon,YY}^{-1}a}{k_0 r^2} - \mu k_0 \mathbb{I}\right), \qquad M_{24} = 0,$$

$$M_{31} = ik_0(Q_{\epsilon,ZY}Q_{\epsilon,YY}^{-1}Q_{\epsilon,YX} - Q_{\epsilon,ZX}),$$

$$M_{32} = ik_0(Q_{\epsilon,ZY}Q_{\epsilon,YY}^{-1}Q_{\epsilon,YZ} - Q_{\epsilon,ZZ}),$$

$$M_{33} = \frac{1}{r}(Q_{\epsilon,ZY}Q_{\epsilon,YY}^{-1}a - \mathbb{I}), \qquad M_{34} = 0,$$

$$M_{41} = i\left(k_0 Q_{\epsilon,XX} - k_0 Q_{\epsilon,XY}Q_{\epsilon,YY}^{-1}Q_{\epsilon,YX} - \frac{a^2}{\mu k_0 r^2}\right),$$

$$M_{42} = ik_0(Q_{\epsilon,XZ} - Q_{\epsilon,XY}Q_{\epsilon,YY}^{-1}Q_{\epsilon,YZ}),$$

$$M_{43} = -Q_{\epsilon,XY}Q_{\epsilon,YY}^{-1}\frac{a}{r}, \qquad M_{44} = -\frac{\mathbb{I}}{r}. \tag{22}$$

Here $\mathbb{I}$ is a unit matrix and a is a diagonal matrix with diagonal elements equal to a_p.

These equations are valid for both isotropic and anisotropic materials. The difference between isotropic and anisotropic cases is contained in the form of both the matrix Q_ϵ and the field expansion inside the homogeneous anisotropic region $(r<R_1)$. In the following sections we deal consecutively with these two topics.

4. DETERMINATION OF THE Q_ϵ MATRIX USING THE FAST NUMERICAL FACTORIZATION

As in the isotropic case, the components of Q_ϵ are determined by obtaining the link between $\mathbf{E}$ and $\mathbf{D}$, projected onto the same truncated basis. The truncation requires applying special factorization rules, one for the tangential (subscript T) components, the other for the normal (subscript N) ones.[10,11] However, in contrast to the isotropic case,[1] the tensorial character of $\tilde{\tilde{\epsilon}}$ complicates the relation

between $\mathbf{E}$ and $\mathbf{D}$, so D_N depends on both E_N and E_T, and likewise for D_T. This requires applying an approach quite different from the one used in Ref. 1 but similar to that followed in Cartesian coordinates to analyze anisotropic diffraction gratings.[8]

Let us consider the unit vector $\hat{\mathbf{N}}$, normal to the surface S of the object, defined on the surface:

$$\hat{\mathbf{N}}(\theta,\varphi) = \mathbf{grad}\,f/|\mathbf{grad}\,f|_{f=0}. \tag{23}$$

We need to extend the definition of $\hat{\mathbf{N}}$ to the entire modulated region; we state

$$\hat{\mathbf{N}}(r,\theta,\varphi) \equiv \hat{\mathbf{N}}(\theta,\varphi), \qquad \forall\, r \in [R_1, R_2]. \tag{24}$$

As previously stated, the circumflex denotes unit vectors. We then construct two unit tangential vectors $\hat{\mathbf{T}}_1$ and $\hat{\mathbf{T}}_2$, defined by

$$\hat{\mathbf{T}}_1 = \frac{\hat{\mathbf{N}} \times \hat{\boldsymbol{\varphi}}}{|\hat{\mathbf{N}} \times \hat{\boldsymbol{\varphi}}|} \equiv \frac{N_\theta}{\sqrt{N_r^2 + N_\theta^2}}\hat{\mathbf{r}} - \frac{N_r}{\sqrt{N_r^2 + N_\theta^2}}\hat{\boldsymbol{\theta}}, \tag{25}$$

$$\hat{\mathbf{T}}_2 = \hat{\mathbf{T}}_1 \times \hat{\mathbf{N}} \equiv -\frac{N_r N_\theta}{\sqrt{N_r^2 + N_\theta^2}}\hat{\mathbf{r}} - \frac{N_\theta N_\varphi}{\sqrt{N_r^2 + N_\theta^2}}\hat{\boldsymbol{\theta}}$$
$$+ \frac{1 - N_\varphi^2}{\sqrt{N_r^2 + N_\theta^2}}\hat{\boldsymbol{\varphi}}, \tag{26}$$

if $\hat{\mathbf{N}}$ is not parallel to $\hat{\boldsymbol{\varphi}}$. If they are parallel, then

$$\hat{\mathbf{T}}_1 = \hat{\mathbf{r}}, \tag{27}$$

$$\hat{\mathbf{T}}_2 = \hat{\mathbf{T}}_1 \times \hat{\mathbf{N}} \equiv -\hat{\boldsymbol{\theta}}. \tag{28}$$

The column

$$F_\epsilon \equiv \begin{pmatrix} F_{\epsilon,1} \\ F_{\epsilon,2} \\ F_{\epsilon,3} \end{pmatrix} = \begin{pmatrix} E_{T_1} \\ \dfrac{1}{\epsilon_0}D_N \\ E_{T_2} \end{pmatrix} \stackrel{\text{def}}{=} \begin{pmatrix} \mathbf{E}\cdot\hat{\mathbf{T}}_1 \\ \dfrac{1}{\epsilon_0}\mathbf{D}\cdot\hat{\mathbf{N}} \\ \mathbf{E}\cdot\hat{\mathbf{T}}_2 \end{pmatrix} \tag{29}$$

is continuous across the object surface S, where the permittivity is discontinuous. Let us underline the fact that F_ϵ is not a vector: each of its elements represents a scalar. The elements can be expressed through the components of $\mathbf{E}$ using a square matrix A_ϵ,

$$F_\epsilon = A_\epsilon \mathbf{E}, \tag{30}$$

which can be determined by taking into account that

$$\frac{1}{\epsilon_0}D_N = \frac{1}{\epsilon_0}\mathbf{D}\cdot\hat{\mathbf{N}} = \hat{\mathbf{N}}\cdot(\tilde{\tilde{\epsilon}}\mathbf{E})$$
$$= N_r(\epsilon_{rr}E_r + \epsilon_{r\theta}E_\theta + \epsilon_{r\varphi}E_\varphi) + N_\theta(\epsilon_{\theta r}E_r + \epsilon_{\theta\theta}E_\theta + \epsilon_{\theta\varphi}E_\varphi)$$
$$+ N_\varphi(\epsilon_{\varphi r}E_r + \epsilon_{\varphi\theta}E_\theta + \epsilon_{\varphi\varphi}E_\varphi). \tag{31}$$

As a result, one obtains

$$A_\epsilon = \begin{bmatrix} T_{1,r} & T_{1,\theta} & 0 \\ (N_r\epsilon_{rr} + N_\theta\epsilon_{\theta r} + N_\varphi\epsilon_{\varphi r}) & (N_r\epsilon_{r\theta} + N_\theta\epsilon_{\theta\theta} + N_\varphi\epsilon_{\varphi\theta}) & (N_r\epsilon_{r\varphi} + N_\theta\epsilon_{\theta\varphi} + N_\varphi\epsilon_{\varphi\varphi}) \\ T_{2,r} & T_{2,\theta} & T_{2,\varphi} \end{bmatrix}, \tag{32}$$

which can be written in a more compact form by introducing a dot product ($\mathbf{N}\cdot\tilde{\tilde{\epsilon}}$) denoting a contraction over the first tensorial subscript of $\tilde{\tilde{\epsilon}}$:

$$A_\epsilon = \begin{bmatrix} T_{1,r} & T_{1,\theta} & 0 \\ (\hat{\mathbf{N}}\cdot\tilde{\tilde{\epsilon}})_r & (\hat{\mathbf{N}}\cdot\tilde{\tilde{\epsilon}})_\theta & (\hat{\mathbf{N}}\cdot\tilde{\tilde{\epsilon}})_\varphi \\ T_{2,r} & T_{2,\theta} & T_{2,\varphi} \end{bmatrix}. \tag{33}$$

After tedious but elementary calculations, it can be shown that its inverse matrix has the form

$$C \overset{\text{def}}{=} A_\epsilon^{-1} = \frac{1}{\xi_0} \begin{bmatrix} [(\hat{\mathbf{N}}\cdot\tilde{\tilde{\epsilon}})\times\hat{\mathbf{T}}_2]_r & N_r & [\hat{\mathbf{T}}_1\times(\hat{\mathbf{N}}\cdot\tilde{\tilde{\epsilon}})]_r \\ [(\hat{\mathbf{N}}\cdot\tilde{\tilde{\epsilon}})\times\hat{\mathbf{T}}_2]_\theta & N_\theta & [\hat{\mathbf{T}}_1\times(\hat{\mathbf{N}}\cdot\tilde{\tilde{\epsilon}})]_\theta \\ [(\hat{\mathbf{N}}\cdot\tilde{\tilde{\epsilon}})\times\hat{\mathbf{T}}_2]_\varphi & N_\varphi & [\hat{\mathbf{T}}_1\times(\hat{\mathbf{N}}\cdot\tilde{\tilde{\epsilon}})]_\varphi \end{bmatrix}, \tag{34}$$

where $\xi_0 = \hat{\mathbf{N}}\cdot\tilde{\tilde{\epsilon}}\cdot\hat{\mathbf{N}}$ is the determinant of A_ϵ. Using the mutual orthogonality of $\hat{\mathbf{N}}$, $\hat{\mathbf{T}}_1$, and $\hat{\mathbf{T}}_2$, and the fact that the mixed product of three vectors is null when two of the vectors are identical, one can easily verify that $A_\epsilon A_\epsilon^{-1} = \mathbb{I}$. In addition, due to the symmetry of $\tilde{\tilde{\epsilon}}$, the determinant ξ_0 of A_ϵ is a positive quadratic form and thus is never null. By using Eqs. (25) and (26), we can write matrix C in another form:

$$C = \begin{pmatrix} T_{1,r} - \dfrac{\xi_1}{\xi_0}N_r & \dfrac{1}{\xi_0}N_r & T_{2,r} - \dfrac{\xi_2}{\xi_0}N_r \\[2mm] T_{1,\theta} - \dfrac{\xi_1}{\xi_0}N_\theta & \dfrac{1}{\xi_0}N_\theta & T_{2,\theta} - \dfrac{\xi_2}{\xi_0}N_\theta \\[2mm] T_{1,\varphi} - \dfrac{\xi_1}{\xi_0}N_\varphi & \dfrac{1}{\xi_0}N_\varphi & T_{2,\varphi} - \dfrac{\xi_2}{\xi_0}N_\varphi \end{pmatrix} = (\mathbf{C}_1, \mathbf{C}_2, \mathbf{C}_3), \tag{35}$$

where $\xi_1 = \hat{\mathbf{N}}\cdot\tilde{\tilde{\epsilon}}\cdot\hat{\mathbf{T}}_1$ and $\xi_2 = \hat{\mathbf{N}}\cdot\tilde{\tilde{\epsilon}}\cdot\hat{\mathbf{T}}_2$ are scalars. As can be observed, the three vectors $(\mathbf{C}_1, \mathbf{C}_2, \mathbf{C}_3)$ representing the three columns of C consist of a linear combination of the normal ($\hat{\mathbf{N}}$) and tangential ($\hat{\mathbf{T}}_1, \hat{\mathbf{T}}_2$) vectors, whatever the coordinated system used. In the anisotropic case, $\mathbf{C}_1, \mathbf{C}_2, \mathbf{C}_3$ are not mutually orthogonal, while they are orthogonal in isotropic media, with $\xi_1 = \xi_2 = 0$.

Inversing Eq. (30) gives

$$\mathbf{E} = CF_\epsilon, \tag{36}$$

and thus

$$\mathbf{D} = \epsilon_0\tilde{\tilde{\epsilon}}\mathbf{E} = \epsilon_0\tilde{\tilde{\epsilon}}CF_\epsilon. \tag{37}$$

Let us recall that the aim is to express the components of the column [$\mathbf{D}$], made of three block columns [D_Y], [D_X], and [D_Z] in terms of the column [$\mathbf{E}$], made of [E_Y], [E_X], and [E_Z]. To achieve this goal we have to pass through the column F_ϵ, which is composed of those components of the

electric and induction field that are continuous across the diffractive object surface S.

A. Direct Factorization Rule

All the components of the column F_ϵ are continuous across S, while some of the components of $\mathbf{D}$ are discontinuous and some are continuous. We can then apply the direct factorization rule to Eq. (37) by projecting $\mathbf{D}$ onto the basis of vector spherical harmonics [see Eq. (10)] and projecting the scalar elements of F_ϵ onto the basis of scalar spherical harmonics. Then Eq. (37) takes the form

$$\sum_{p,\eta} D_{\eta,p}(r)\mathbf{W}_p^{(\eta)}(\theta,\varphi) = \epsilon_0\tilde{\tilde{\epsilon}}(r,\theta,\varphi)C(r,\theta,\varphi)$$
$$\times \sum_p \begin{pmatrix} F_{\epsilon,1,p}(r) \\ F_{\epsilon,2,p}(r) \\ F_{\epsilon,3,p}(r) \end{pmatrix} Y_p(\theta,\varphi), \tag{38}$$

where $\tilde{\tilde{\epsilon}}$ is a square matrix of size 3×3 with elements $\tilde{\tilde{\epsilon}}_{ij}$. Matrix C is also a square matrix of size 3×3 with elements $C_{i,J}$ representing the components of the three vectors $\mathbf{C}_J$, $J=1,2,3$, Eq. (35), expressed in the same coordinate system as $\tilde{\tilde{\epsilon}}$. Their product ($\tilde{\tilde{\epsilon}}C$) has the same form with elements

$$(\tilde{\tilde{\epsilon}}C)_{iJ} = \sum_{j=r,\theta,\varphi} \tilde{\tilde{\epsilon}}_{ij}C_{jJ}. \tag{39}$$

If the basis used to represent the tensor elements differs from the set of unit vectors of the spherical coordinate system, then i and j stay for the basic vectors, for example, in the Cartesian coordinate system $i,j=x,y,z$. In contrast, the last subscript $J=1,2,3$ corresponds to the tangential or normal field components, which form the column F_ϵ, Eq. (29). Since they are scalars, they do not depend on the coordinate system. Using this convention, we can write Eq. (38) in a more compact form:

$$\sum_{p,\eta} D_{\eta,p}\mathbf{W}_p^{(\eta)} = \epsilon_0\sum_{J,p} (\tilde{\tilde{\epsilon}}\mathbf{C}_J)F_{\epsilon,J,p}Y_p. \tag{40}$$

The next step is to use the orthogonality of the vector spherical harmonics with respect to their argument:

$$\int_0^{4\pi} d\Omega \mathbf{W}_p^{(\eta)}(\theta,\varphi)\cdot\mathbf{W}_q^{*(\tau)}(\theta,\varphi) = \delta_{pq}\delta_{\eta\tau}. \tag{41}$$

Multiplying Eq. (40) by $\mathbf{W}_q^{*(\tau)}$ and integrating over the entire solid angle, one obtains

$$D_{\tau,q}(r) = \epsilon_0\sum_{J,p} \langle\mathbf{W}_q^{(\tau)}|(\tilde{\tilde{\epsilon}}\mathbf{C}_J)Y_p\rangle F_{\epsilon,J,p}(r)$$
$$= \epsilon_0\sum_{J,p} \{\tilde{\tilde{\epsilon}}C\}_{\tau,J,qp}F_{\epsilon,J,p}(r), \tag{42}$$

where

$$\{\tilde{\bar{\epsilon}}C\}_{\tau J,qp} = \langle \mathbf{W}_q^{(\tau)}|(\tilde{\bar{\epsilon}}\mathbf{C}_J)Y_p\rangle = \int_0^{4\pi} d\Omega \mathbf{W}_q^{*(\tau)}(\theta,\varphi) \cdot (\tilde{\bar{\epsilon}}\mathbf{C}_J)Y_p(\theta,\varphi),$$

$$(43)$$

and the dot product here is reduced to the ordinary scalar product. This equation is written in a form independent of the coordinate system used, owing to the scalar product, which has to be explicitly calculated in each specific coordinate system.

Owing to Eq. (A22) of Part I,[9] the φ dependence of the integrand in Eq. (43) is exponential, $\exp\{i[m(p)-m(q)]\varphi\}$, so that the integration with respect to φ represents a Fourier transform of $(\tilde{\bar{\epsilon}}C)_{iJ}$. In addition, the facts that $\mathbf{Y}_p$ are parallel to $\hat{\mathbf{r}}$ and that $\mathbf{X}_p$ and $\mathbf{Z}_p$ are perpendicular to $\hat{\mathbf{r}}$ simplify the form of $\{\tilde{\bar{\epsilon}}C\}$ when it is represented in spherical coordinates:

$$\{\tilde{\bar{\epsilon}}C\}_{YJ,pq} = \langle Y_p|(\tilde{\bar{\epsilon}}C)_{rJ}Y_q\rangle,$$

$$\{\tilde{\bar{\epsilon}}C\}_{XJ,pq} = \sum_{i=\theta,\varphi} \langle X_{p,i}|(\tilde{\bar{\epsilon}}C)_{iJ}Y_q\rangle,$$

$$\{\tilde{\bar{\epsilon}}C\}_{ZJ,pq} = \sum_{i=\theta,\varphi} \langle Z_{p,i}|(\tilde{\bar{\epsilon}}C)_{iJ}Y_q\rangle. \qquad (44)$$

The integration with respect to θ is significantly simplified when $(\tilde{\bar{\epsilon}}C)_{iJ}$ can be represented in the form of series of scalar spherical harmonics. This is the case of isotropic media, as discussed in detail in Ref. 1. Another situation is discussed in Section 5 and concerns the case of absence of discontinuity of the permittivity tensor inside the modulated region, for example, gradient-index anisotropy. Two more cases are described in detail in Appendix A.

Equations (42) and (43) establish the direct factorization rule.

B. Inverse Rule

As already discussed, all the components of the column F_ϵ are continuous across S. However, some of the components of $\mathbf{E}$ may be discontinuous there. Thus, it is necessary to apply the inverse rule to Eq. (30). This is simply done by applying the direct factorization rule as stated in Eqs. (42) and (43) to Eq. (36), taking into account that C is discontinuous, while F_ϵ is continuous. Thus, Eq. (36) can be written in components

$$E_{\tau,q}(r) = \sum_{J,p} C_{\tau J,qp} F_{\epsilon,J,p}(r), \qquad (45)$$

where the elements

$$C_{\tau J,qp} = \langle \mathbf{W}_q^{(\tau)}|(\mathbf{C}_J)Y_p\rangle = \int_0^{4\pi} d\Omega \mathbf{W}_q^{*(\tau)}(\theta,\varphi) \cdot (\mathbf{C}_J)Y_p(\theta,\varphi)$$

$$(46)$$

form a square matrix $\{C\}$ with nine blocks $C_{\tau J}$. Its numerical inversion makes it possible to express the components of F_ϵ as function of $[E_Y]$, $[E_X]$, and $[E_Z]$:

$$[F_\epsilon] = \{C\}^{-1}[\mathbf{E}]. \qquad (47)$$

The remarks following Eq. (43) and concerning $\{\tilde{\bar{\epsilon}}C\}$ also hold for the matrix $\{C\}$ derived in Eq. (46). Equation (44) again apply by replacement of $\tilde{\bar{\epsilon}}C$ with C.

Equations (46) and (47) state the inverse factorization rule extended to anisotropic materials.

C. Fast Numerical Factorization Equation

It is now straightforward to determine the relation between $[D_Y]$, $[D_X]$, and $[D_Z]$ on one side and $[E_Y]$, $[E_X]$, and $[E_Z]$ on the other side. Combining Eqs. (42) and (47), we obtain

$$[\mathbf{D}] = \epsilon_0\{\tilde{\bar{\epsilon}}C\}\{C\}^{-1}[\mathbf{E}]. \qquad (48)$$

Thus the matrix Q_ϵ takes the form

$$Q_\epsilon = \{\tilde{\bar{\epsilon}}C\}\{C\}^{-1}. \qquad (49)$$

It is worth noticing that Eq. (49), together with Eqs. (43) and (46), generalize Eq. (114) of Ref. 1 to anisotropic media. When applied to isotropic medium, they lead to Eqs. (76), (82), (83), (88), and (89) of Ref. 1 with ϵ being a scalar. This can be easily observed by taking into account that for isotropic media the triad $(\mathbf{C}_1,\mathbf{C}_2,\mathbf{C}_3)$ simplifies into $(\hat{\mathbf{T}}_1,1/\epsilon\hat{\mathbf{N}},\hat{\mathbf{T}}_2)$. When projected onto the basis $(\mathbf{Y}_p,\mathbf{X}_p,\mathbf{Z}_p)$ as stated by Eq. (46), matrix $\{C\}$ becomes

$$\{C\} = \left(\{\hat{\mathbf{T}}_1\}, \left\{\frac{1}{\epsilon}\right\}\{\hat{\mathbf{N}}\}, \{\hat{\mathbf{T}}_2\} \right) \qquad (50)$$

and can be inverted analytically:

$$\{C\}^{-1} = \begin{pmatrix} \{\hat{\mathbf{T}}_1\}^{\mathrm{T}} \\ \left\{\dfrac{1}{\epsilon}\right\}^{-1}\{\hat{\mathbf{N}}\}^{\mathrm{T}} \\ \{\hat{\mathbf{T}}_2\}^{\mathrm{T}} \end{pmatrix}. \qquad (51)$$

On the other hand, Eq. (43) simplifies to the form

$$\{\tilde{\bar{\epsilon}}C\} = (\{\epsilon\}\{\hat{\mathbf{T}}_1\}, \{\hat{\mathbf{N}}\}, \{\epsilon\}\{\hat{\mathbf{T}}_2\}) \qquad (52)$$

so that matrix Q_ϵ takes the form written in Eq. (116) of Ref. 1 when we take into account the relation $\hat{\mathbf{T}}_1\hat{\mathbf{T}}_1 + \hat{\mathbf{T}}_2\hat{\mathbf{T}}_2 + \hat{\mathbf{N}}\hat{\mathbf{N}} = \mathbb{I}$.

In contrast to the isotropic case, in the anisotropic case the elements of matrix Q_ϵ are determined numerically and cannot be explicitly written, as they were in Ref. 1. We also note that the matrix product in Eq. (49) cannot cancel matrix C and its inverse, because the matrix elements of $\{\tilde{\bar{\epsilon}}C\}$ are not represented as elements of the product of two matrices, $\{\tilde{\bar{\epsilon}}C\} \neq \{\tilde{\bar{\epsilon}}\}\{C\}$, owing to the integration in Eq. (43). $\{\tilde{\bar{\epsilon}}C\}$ would be the product of two matrices only if one worked in a nontruncated basis, which is impossible numerically.

5. INHOMOGENEOUS SPHERICAL BODY

If the permittivity tensor does not present any discontinuity inside the modulated region but presents only smooth inhomogeneity, it is not necessary to use the fast numerical factorization (FNF) rules. Such an example contains a spherical optically inhomogeneous anisotropic body with the elements of $\bar{\epsilon}$ being continuously varying

functions of (x,y,z), for example, a graded-permittivity anisotropic sphere. In that case both **D** and **E** are continuous and the first relation in Eq. (37) can be directly used: $\mathbf{D} = \epsilon_0 \tilde{\tilde{\epsilon}} \mathbf{E}$. Both **D** and **E** are expressed in terms of vector spherical harmonics, Eq. (10), and the left-hand side of Eq. (38), so that

$$\mathbf{D} = \epsilon_0 \tilde{\tilde{\epsilon}} \mathbf{E} \Rightarrow \sum_{\eta,p} D_{\eta p}(r) \mathbf{W}_p^{(\eta)}(\theta,\varphi)$$

$$= \epsilon_0 \tilde{\tilde{\epsilon}}(r,\theta,\varphi) \sum_{\tau,q} E_{\tau q}(r) \mathbf{W}_q^{(\tau)}(\theta,\varphi). \tag{53}$$

Multiplying by $\mathbf{W}_p^{*(\tau)}$ and integrating over the entire solid angle leads to a simplified form of matrix Q_ϵ in Eq. (18):

$$Q_\epsilon = \{\tilde{\tilde{\epsilon}}\}, \tag{54}$$

where the elements of the matrix $\{\tilde{\tilde{\epsilon}}\}$ are given by

$$\{\tilde{\tilde{\epsilon}}\}_{\tau\eta,pq}(r) = \langle \mathbf{W}_p^{(\tau)} | (\tilde{\tilde{\epsilon}}) \mathbf{W}_q^{(\eta)} \rangle$$

$$= \int_0^{4\pi} d\Omega \mathbf{W}_p^{*(\tau)}(\theta,\varphi) \cdot \tilde{\tilde{\epsilon}}(r,\theta,\varphi) \mathbf{W}_q^{(\eta)}(\theta,\varphi). \tag{55}$$

Each element $\{\tilde{\tilde{\epsilon}}\}_{\tau\eta,pq}$ is a scalar independent of the coordinate system and contains a product of the tensor $\tilde{\tilde{\epsilon}}$ with the vector $\mathbf{W}_p^{*(\tau)}$ on the left and $\mathbf{W}_q^{(\eta)}$ on the right. In a specific coordinate system it is represented as a summation over the tensorial indices i and j of $\tilde{\tilde{\epsilon}}$:

$$\mathbf{W}_p^{*(\tau)} \cdot \tilde{\tilde{\epsilon}} \mathbf{W}_q^{(\eta)} = \sum_{i,j} W_{p,i}^{*(\tau)} \tilde{\tilde{\epsilon}}_{ij} W_{q,j}^{(\eta)}, \tag{56}$$

where $W_{q,j}^{(\eta)} = \mathbf{W}_q^{(\eta)} \cdot \hat{\mathbf{j}}$ is the projection of $\mathbf{W}_q^{(\eta)}$ onto the coordinate unit vector $\hat{\mathbf{j}}$.

Unfortunately, Eq. (55) requires a numerical integration of the products of spherical harmonics. However, in some cases, it is possible to avoid this by using Eq. (5). If the inhomogeneity of $\tilde{\tilde{\epsilon}}$ is such that its elements can be represented with only a few terms in the expansion on scalar spherical harmonics, Eq. (5), these terms can be used to rapidly calculate the integrals that appear in Eq. (55). In Cartesian or cylindrical coordinates, the projection $\mathbf{W}_p^{(\eta)}(\theta,\varphi) \cdot \hat{\mathbf{j}}$ of $\mathbf{W}_p^{(\eta)}(\theta,\varphi)$ on the axis $\hat{\mathbf{j}}$ takes a simple form (see Appendix B) proportional to the scalar spherical harmonics $Y_{nm}(\theta,\varphi)$:

$$\mathbf{W}_{nm}^{(\eta)}(\theta,\varphi) \cdot \hat{\mathbf{j}} = \sum_{\nu=-1}^{+1} b_{nm,\mu\nu,j}^{(\eta)} Y_{n+\nu,m+\mu}(\theta,\varphi). \tag{57}$$

with coefficients $b_{nm,\mu\nu,j}^{(\eta)}$ proportional to the projections of the vector spherical harmonics on the basis $(\hat{\mathbf{j}})$, as given in Appendix B. With the use of Eq. (57), the integrand in Eq. (55) becomes a triple product of scalar spherical harmonics. As discussed in Appendix D of Ref. 1, the integrals of triple products represent the normalized Gaunt coefficients $\bar{a}$[12]:

$$\bar{a}(\{\nu',\mu'\},\{\nu,\mu\},\{n,m\}) = \int_0^{2\pi} d\varphi \int_0^\pi \sin\theta d\theta Y_{\nu',\mu'}(\theta,\varphi)$$

$$\times Y_{\nu,\mu}(\theta,\varphi) Y_{nm}(\theta,\varphi), \tag{58}$$

which can be calculated rapidly through recursion

relations.[13] Then each element $\{\tilde{\tilde{\epsilon}}\}_{\tau\eta,qp}$ is given as a linear combination of the products of Gaunt coefficients $\bar{a}$ and the coefficients $b_{nm,\mu\nu,j}^{(\eta)}$ seen in Eq. (57), which depend on the coordinate system used to represent the permittivity tensor.

6. RESOLUTION OF THE BOUNDARY-VALUE PROBLEM

The integration of Eq. (20) can be done numerically between R_1 and R_2. However, this requires starting values of the components of the unknown column $[F(r)]$. In addition, as long as this column contains electromagnetic field components that are continuous across S_1 and S_2, it is necessary to match the results of the integration with the corresponding field components outside S_2 and inside S_1.

Using the expansion of a plane wave on the vector spherical harmonic basis in an anisotropic material, Eqs. (50) and (55) of Part I,[9] the column $[F]$ at the innermost sphere S_1 takes the form

$$[F(R_j)] = \Psi_{\text{aniso}}(R_1)[\tilde{A}] \tag{59}$$

with a column $[\tilde{A}]$ containing the unknown amplitudes inside S_1,

$$[\tilde{A}] = \begin{pmatrix} [\tilde{A}_1] \\ [\tilde{A}_2] \end{pmatrix} = \begin{pmatrix} \vdots \\ \tilde{A}_{1,\nu} \\ \vdots \\ \tilde{A}_{2,\nu} \\ \vdots \end{pmatrix}, \tag{60}$$

and the matrix Ψ_{aniso} having a block form,

$$\Psi_{\text{aniso}} = (\Psi_{1,\text{aniso}} \quad \Psi_{2,\text{aniso}}), \tag{61}$$

in which each block consists of four subblocks with rank $p_{\text{Max}} - 1$:

$$\Psi_{j,\text{aniso}}(r) = \begin{pmatrix} \left[\dfrac{1}{k_{j,r}r} a_{h,p,j,\nu} \psi_n(k_{j,r}r) \right] \\ \left[\dfrac{1}{k_{j,r}r} [a_{e,p,j,\nu} \psi_n'(k_{j,r}r) + a_p a_{o,p,j,\nu} j_n(k_{j,r}r)] \right] \\ \left[\dfrac{1}{ik_0 r} a_{e,p,j,\nu} \psi_n(k_{j,r}r) \right] \\ \left[\dfrac{1}{ik_0 r} a_{h,p,j,\nu} \psi_n'(k_{j,r}r) \right] \end{pmatrix}. \tag{62}$$

As usual, j_n and h_n^+ are the spherical Bessel functions and ψ_n and ξ_n are the Ricatti–Bessel functions:

$$\psi_n(z) = z j_n(z), \qquad \xi_n(z) = z h_n^+(z). \tag{63}$$

The matrix Ψ_{aniso} can be used as a starting matrix at $r = R_1$ in the process of numerical integration of Eq. (20). At the end of the integration, the integrated matrix $[F_{\text{integ}}]$ represents the transmission matrix of the system:

$$T(R_2, R_1) = [F_{\text{integ}}], \tag{64}$$

which links the field on S_2 to the unknown amplitudes $[\tilde{A}]$ inside S_1:

$$[F(R_2)] = T(R_2, R_1)[\tilde{A}]. \qquad (65)$$

On the other hand, the field components $[F(R_2)]$ are continuous across S_2 and can be expressed through the incident and diffracted field amplitudes in the outermost homogeneous and isotropic medium, discussed in detail in Part I[9]:

$$E_{X,p}(r = R_2) = [A_{h,p}^{(i)} j_n(n_{\text{out}} k_0 R_2) + B_{h,p} h_n^+(n_{\text{out}} k_0 R_2)],$$

$$E_{Z,p}(r = R_2) = \frac{1}{n_{\text{out}} k_0 R_2}[A_{e,p}^{(i)} \psi_n'(n_{\text{out}} k_0 R_2)$$

$$+ B_{e,p} \xi_n'(n_{\text{out}} k_0 R_2)], \qquad (66)$$

$$\tilde{H}_{X,p}(r = R_2) = \frac{1}{ik_0 R_2}[A_{e,p}^{(i)} \psi_n(n_{\text{out}} k_0 R_2)$$

$$+ B_{e,p} \xi_n(n_{\text{out}} k_0 R_2)],$$

$$\tilde{H}_{Z,p}(r = R_2) = \frac{1}{ik_0 R_2}[A_{h,p}^{(i)} \psi_n'(n_{\text{out}} k_0 R_2)$$

$$+ B_{h,p} \xi_n'(n_{\text{out}} k_0 R_2)], \qquad (67)$$

where $A_{h,p}^{(i)}$ and $A_{e,p}^{(i)}$ are the incident (known) field amplitudes and $B_{h,p}$ and $B_{e,p}$ are the diffracted (unknown) field amplitudes in the outermost region. With these expressions, the column $[F]$ in the outermost region takes the form

$$[F(R_2)] = \Psi_{\text{iso}}(n_{\text{out}} k_0 R_2) \begin{pmatrix} \vdots \\ A_{e,p}^{(i)} \psi_n'(n_{\text{out}} k_0 R_2)/n_{\text{out}} k_0 R_2 \\ \vdots \\ A_{h,p}^{(i)} \psi_n(n_{\text{out}} k_0 R_2)/n_{\text{out}} k_0 R_2 \\ \vdots \\ B_{e,p} \xi_n'(n_{\text{out}} k_0 R_2)/n_{\text{out}} k_0 R_2 \\ \vdots \\ B_{h,p} \xi_n(n_{\text{out}} k_0 R_2)/n_{\text{out}} k_0 R_2 \\ \vdots \end{pmatrix}, \qquad (68)$$

where

$$\Psi_{\text{iso}} = \begin{pmatrix} 0 & \mathbb{I} & 0 & \mathbb{I} \\ \mathbb{I} & 0 & \mathbb{I} & 0 \\ \dfrac{-in_{\text{out}}}{p(n_{\text{out}} k_0 R_2)} & 0 & \dfrac{-in_{\text{out}}}{q(n_{\text{out}} k_0 R_2)} & 0 \\ 0 & -in_{\text{out}} p(n_{\text{out}} k_0 R_2) & 0 & -in_{\text{out}} q(n_{\text{out}} k_0 R_2) \end{pmatrix} \qquad (69)$$

and

$$p_{p,q}(z) = \delta_{p,q} \frac{\psi_n'(z)}{\psi_n(z)}, \quad q_{p,q}(z) = \delta_{p,q} \frac{\xi_n'(z)}{\xi_n(z)}. \qquad (70)$$

Equations (65) and (68) represent the same column $[F(R_2)]$, and thus they form a set of $4(N_\nu - 1) = 4(p_{\text{Max}} - 1)$ linear algebraic equations for the unknown field amplitudes $[\tilde{A}_1]$, $[\tilde{A}_2]$, $[B_e]$, and $[B_h]$. The set can be solved numerically when the incident field amplitudes $A_{h,p}^{(i)}$ and $A_{e,p}^{(i)}$ are known.

During the integration process, one can expect the appearance of numerical problems, and it is necessary to divide the integration region into subregions so that inside each subregion the integration remains possible. Instead of obtaining the transmission matrix T, it is possible to directly determine the scattering matrix S, which links the diffracted to the incident amplitudes. This procedure is well known in the diffraction theories in Cartesian and cylindrical coordinates and is explained in detail in Ref. 1. The equations in the case of anisotropic media do not differ from the formulas developed in the isotropic case; the interested reader can find them in Ref. 1. The first difference is the start of the integration, which uses as a shoot-

ing matrix the matrix Ψ_{aniso}, defined by Eqs. (61) and (62), which requires $2(p_{\text{Max}} - 1)$ independent starting vectors. The second difference is the form of the Q_ϵ matrix, discussed in detail in Section 4.

7. CONCLUSION

This work extends the differential theory of diffraction to an arbitrary-shaped 3D body made of arbitrary anisotropic lossless or lossy material. The theory extends the fast numerical factorization (FNF) of products of continuous and discontinuous vector functions to anisotropic media described in vector spherical harmonic basis. It is able to analyze uniaxial, biaxial or chiral materials. Moreover, the theory can be applied to ferromagnetic materials, described by a tensorial magnetic permeability.

Some particular cases permit significant simplifications that avoid numerical integration of the products of spherical harmonics. Certain examples are the optically uniaxial finite-length cylinder and arbitrary-anisotropic parallelepiped, described in detail in Appendix A. In addition, the theory can be directly applied to graded-permittivity materials by using only the direct rule of factorization.

APPENDIX A: TWO PARTICULAR GEOMETRIES

Let us consider two particular cases, which permit significant simplifications in calculating the matrix elements of $\{C\}$ and $\{\tilde{\epsilon}C\}$.

1. Finite-Length Circular Cylinder with Uniaxial Anisotropy

Let us consider a finite-length circular cylinder with height H and radius R with axis coinciding with the z axis and the origin of the coordinate system located in the center of the body, Fig. 2. The numerical integration of Eq. (20) has to be performed from $r=R_1=\min(R,H/2)$ to $R_2 =[R^2+(H/2)^2]^{1/2}$, and it is necessary to extend the definition of the normal vectors defined at the surface to the entire region of integration. This can be done, for example, as represented in Fig. 2. If the cylinder material has uniaxial anisotropy with the optic axis coinciding with the axis of symmetry, the permittivity tensor has the same form in a Cartesian and in a cylindrical coordinate system:

$$\tilde{\tilde{\epsilon}} = \begin{pmatrix} \epsilon_x & 0 & 0 \\ 0 & \epsilon_x & 0 \\ 0 & 0 & \epsilon_z \end{pmatrix}. \tag{A1}$$

Since the normal and the tangential vectors can be simply expressed in cylindrical coordinates, we represent the matrices C and $(\tilde{\epsilon}C)$ in cylindrical basis $(\hat{\boldsymbol{\rho}},\hat{\boldsymbol{\varphi}},\hat{\mathbf{z}})$. We distinguish two cases:

(1) $\theta \in (\theta_c, \pi-\theta_c)$. In this interval, we can write

$$\hat{\mathbf{N}} = \hat{\boldsymbol{\rho}}, \qquad \hat{\mathbf{T}}_1 = \hat{\mathbf{z}}, \qquad \hat{\mathbf{T}}_2 = \hat{\boldsymbol{\varphi}}, \tag{A2}$$

so that $\xi_0 = \epsilon_x$ in Eq. (35) and matrices C and $(\tilde{\epsilon}C)$ become

$$C = \begin{pmatrix} 0 & 1/\epsilon_x & 0 \\ 0 & 0 & 1 \\ 1 & 0 & 0 \end{pmatrix}, \qquad (\tilde{\epsilon}C) = \begin{pmatrix} 0 & 1 & 0 \\ 0 & 0 & \epsilon_x \\ \epsilon_z & 0 & 0 \end{pmatrix}. \tag{A3}$$

(2) $\theta \notin (\theta_c, \pi-\theta_c)$. Equations (A2) and (A3) become, respectively,

$$\hat{\mathbf{N}} = \hat{\mathbf{z}}, \qquad \hat{\mathbf{T}}_1 = -\hat{\boldsymbol{\rho}}, \qquad \hat{\mathbf{T}}_2 = \hat{\boldsymbol{\varphi}}, \tag{A4}$$
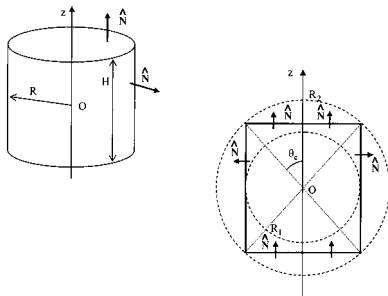

Fig. 2. Finite-length cylinder and notation.

$$C = \begin{pmatrix} -1 & 0 & 0 \\ 0 & 0 & 1 \\ 0 & 1/\epsilon_z & 0 \end{pmatrix}, \qquad (\tilde{\epsilon}C) = \begin{pmatrix} -\epsilon_x & 0 & 0 \\ 0 & 0 & \epsilon_x \\ 0 & 1 & 0 \end{pmatrix}. \tag{A5}$$

As can be observed, both C and $(\tilde{\epsilon}C)$ are piecewise-constant functions of θ and do not depend on φ. Moreover, the components of $\hat{\mathbf{T}}_2$ are constant in θ as well. It is straightforward to represent the elements of (C) and $(\tilde{\epsilon}C)$ in the basis of scalar spherical functions, Eq. (5):

$$(C)_{ij}(\theta) = \sum_{n=0}^{\infty} (C)_{ij,n} Y_{n0}(\theta,\varphi) \equiv \sum_{n=0}^{\infty} (C)_{ij,n} \bar{P}_n^0(\cos\theta),$$

$$(\tilde{\epsilon}C)_{ij}(\theta) = \sum_{n=0}^{\infty} (\tilde{\epsilon}C)_{ij,n} Y_{n0}(\theta,\varphi) \equiv \sum_{n=0}^{\infty} (\tilde{\epsilon}C)_{ij,n} \bar{P}_n^0(\cos\theta). \tag{A6}$$

Their components $(C)_{ij,n}$ and $(\tilde{\epsilon}C)_{ij,n}$ do not depend on r and can be evaluated analytically, taking into account the relations (see Appendix A of Ref. 1):

$$\bar{P}_n^0 = \sqrt{\frac{2n+1}{4\pi}} P_n^0,$$

$$\int_{\theta_1}^{\theta_2} P_n^0(\cos\theta)\sin\theta\,d\theta = \frac{1}{n}[\cos\theta P_n^0(\cos\theta) \\ - P_{n+1}^0(\cos\theta)]\Bigg|_{\theta_1}^{\theta_2}. \tag{A7}$$

To obtain the components of $\{C\}$ and $(\tilde{\epsilon}C)$, Eqs. (46) and (43), it is necessary to project the vector spherical harmonics onto the same basis of coordinate vectors $(\hat{\boldsymbol{\rho}},\hat{\boldsymbol{\varphi}},\hat{\mathbf{z}})$. This can be done using the form of $\mathbf{W}_p^{(\eta)}$ in the basis of Cartesian spherical vectors $\hat{\boldsymbol{\chi}}_\mu$, presented in Appendix B. The transformation matrix $\mathfrak{R}$ is obtained by calculating the scalar products of the basic vectors:

$$\mathfrak{R} = \begin{pmatrix} \hat{\boldsymbol{\chi}}_{-1}\cdot\hat{\boldsymbol{\rho}} & \hat{\boldsymbol{\chi}}_{-1}\cdot\hat{\boldsymbol{\varphi}} & \hat{\boldsymbol{\chi}}_{-1}\cdot\hat{\mathbf{z}} \\ \hat{\boldsymbol{\chi}}_0\cdot\hat{\boldsymbol{\rho}} & \hat{\boldsymbol{\chi}}_0\cdot\hat{\boldsymbol{\varphi}} & \hat{\boldsymbol{\chi}}_0\cdot\hat{\mathbf{z}} \\ \hat{\boldsymbol{\chi}}_{+1}\cdot\hat{\boldsymbol{\rho}} & \hat{\boldsymbol{\chi}}_{+1}\cdot\hat{\boldsymbol{\varphi}} & \hat{\boldsymbol{\chi}}_{+1}\cdot\hat{\mathbf{z}} \end{pmatrix}$$

$$= \begin{pmatrix} \dfrac{1}{\sqrt{2}}\exp(-i\varphi) & \dfrac{-i}{\sqrt{2}}\exp(-i\varphi) & 0 \\ 0 & 0 & 1 \\ \dfrac{-1}{\sqrt{2}}\exp(i\varphi) & \dfrac{-i}{\sqrt{2}}\exp(i\varphi) & 0 \end{pmatrix}. \tag{A8}$$

Let us first consider Eq. (46). The projections of $\mathbf{W}_{n'm'}^{*(\tau)}$ onto $(\hat{\boldsymbol{\rho}}, \hat{\boldsymbol{\varphi}}, \hat{\mathbf{z}})$ are represented as a product of $\mathbf{W}_p^{*(\tau)} \cdot \hat{\boldsymbol{\chi}}_\mu$ and the transformation matrix in Eq. (A8) and are expressed through the coefficients $b_{nm,\mu\nu j}^{(\eta)}$, $j = \rho, \varphi, z$, obtained using Eqs. (B6)–(B9). They are used together with expansion (A6) to give for the integrand in Eq. (46) the form

$$
\mathbf{W}_{n'm'}^{*(\tau)}(\theta,\varphi) \cdot (\mathbf{C}_J) Y_{nm}(\theta,\varphi) = \sum_{\mu,\nu=-1}^{+1} \sum_{j=\rho,\varphi,z} \sum_{n''=0}^{\infty} b_{n'm',\mu\nu j}^{*(\tau)}
$$
$$
\times Y_{n'+\nu,m'+\mu}^{*}(C)_{jJ,n''} Y_{n''0} Y_{nm}.
$$
$$
\text{(A9)}
$$

Thus the integrand is represented as a triple product of scalar spherical harmonics. The only other dependence is the φ dependence of some of the elements of $\mathfrak{R}$ stated in Eq. (A8). Given the simple form of this dependence, the integration in φ can easily be performed, while the θ integration can be avoided by using Gaunt coefficients, Eq. (58). Thus, the elements of $\{C\}$ can be obtained without numerical integration.

The same reasoning applies for $(\tilde{\boldsymbol{\epsilon}}C)$.

2. Optically Anisotropic Brick

Let us consider a parallelepiped consisting of anisotropic material (see Fig. 3). The parallelepiped is divided into six pyramids each of which contains a wall of the parallelepiped and has an apex at the origin of coordinates. The prolongation of the vectors normal and tangential to each wall is made inside the pyramidal regions. Let us denote each region as $V_j^\pm$, $j = x, y, z$, so that, for example, V_x^+ is the
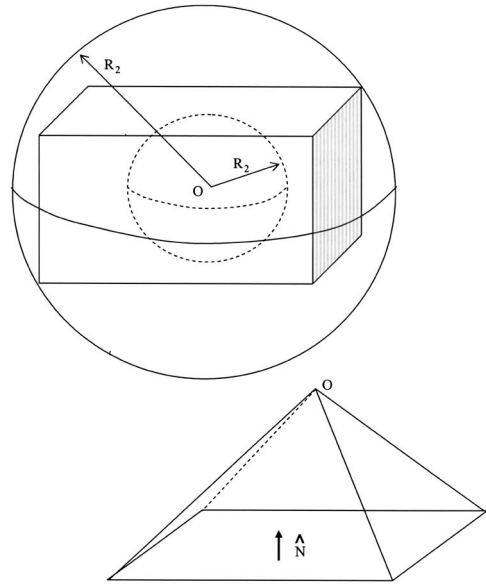
Fig. 3.   Anisotropic brick and notation.

pyramid containing the wall perpendicular to the x axis and crossing it at $x > 0$, V_x^- is the opposite wall, etc. The three vectors have the following form in V_x^+:

$$
\hat{\mathbf{T}}_1 = \hat{\mathbf{z}}, \qquad \hat{\mathbf{N}} = \hat{\mathbf{x}}, \qquad \hat{\mathbf{T}}_2 = \hat{\mathbf{y}}, \qquad \text{(A10)}
$$

and thus

$$
\xi_0 = \epsilon_{xx}, \qquad \xi_1 = \epsilon_{xz}, \qquad \xi_2 = \epsilon_{xy}. \qquad \text{(A11)}
$$

Matrix C is written in $V_x^\pm$ as

$$
C \equiv (\mathbf{C}_1, \mathbf{C}_2, \mathbf{C}_3) = \begin{cases} \left(\hat{\mathbf{z}} - \dfrac{\epsilon_{xz}}{\epsilon_{xx}} \hat{\mathbf{x}}, \dfrac{1}{\epsilon_{xx}} \hat{\mathbf{x}}, \hat{\mathbf{y}} - \dfrac{\epsilon_{xy}}{\epsilon_{xx}} \hat{\mathbf{x}} \right), & \text{inside the parallelepiped} \\[2ex] \left(\hat{\mathbf{z}}, \dfrac{1}{\epsilon_{\text{out}}} \hat{\mathbf{x}}, \hat{\mathbf{y}} \right), & \text{outside the parallelepiped} \end{cases} \qquad \text{(A12)}
$$

Similar expressions are obtained in $V_y^\pm$ and $V_z^\pm$. As can be observed, matrix C is a piecewise-constant function of θ and φ. The same is valid for $(\tilde{\boldsymbol{\epsilon}}C)$, as the permittivity tensor is independent of (x, y, z) inside each medium. Thus, the two matrices can be represented in the form of Eq. (5). The main difference from the matrices for the finite-length cylinder is that now they depend on φ and thus will contain spherical harmonics Y_{nm} with $m \neq 0$, in addition to Y_{n0}. These supplementary components cannot be evaluated analytically, unlike in the case of Eq. (A7), so that it is necessary to numerically integrate the integrals in θ.

The second difference from the cylindrical structure comes from the transformation matrix $\mathfrak{R}$, which here has a simpler form and has constant components:

$$
\mathfrak{R} = \begin{pmatrix} \hat{\boldsymbol{\chi}}_{-1} \cdot \hat{\mathbf{x}} & \hat{\boldsymbol{\chi}}_{-1} \cdot \hat{\mathbf{y}} & \hat{\boldsymbol{\chi}}_{-1} \cdot \hat{\mathbf{z}} \\ \hat{\boldsymbol{\chi}}_0 \cdot \hat{\mathbf{x}} & \hat{\boldsymbol{\chi}}_0 \cdot \hat{\mathbf{y}} & \hat{\boldsymbol{\chi}}_0 \cdot \hat{\mathbf{z}} \\ \hat{\boldsymbol{\chi}}_{+1} \cdot \hat{\mathbf{x}} & \hat{\boldsymbol{\chi}}_{+1} \cdot \hat{\mathbf{y}} & \hat{\boldsymbol{\chi}}_{+1} \cdot \hat{\mathbf{z}} \end{pmatrix} = \begin{pmatrix} \dfrac{1}{\sqrt{2}} & \dfrac{-i}{\sqrt{2}} & 0 \\ 0 & 0 & 1 \\ \dfrac{-1}{\sqrt{2}} & \dfrac{-i}{\sqrt{2}} & 0 \end{pmatrix}.
$$
$$
\text{(A13)}
$$

The coefficients $b_{nm,\mu,\nu j}^{(\eta)}$, $j = x, y, z$ are obtained from Eq. (B12), they are independent of θ and φ because $\mathfrak{R} = \text{const}$. The integrand in Eq. (46) has the same form as that in Eq. (A9), adding a summation over the second index m'' of $Y_{n''m''}$:

$$\mathbf{W}_{n'm'}^{*(\tau)} \cdot (\mathbf{C}_J) Y_{nm} = \sum_{\mu,\nu=-1}^{+1} \sum_{j=xy,z} \sum_{n''=0}^{\infty} \sum_{m''=-n''}^{n''} b_{n'm',\mu\nu j}^{*(\tau)}$$

$$\times Y_{n'+\nu,m'+\mu}^{*} (\tilde{\epsilon}C)_{jJ,n''m''} Y_{n''m''} Y_{nm}.$$

$$(A14)$$

APPENDIX B: PROJECTION OF VECTOR SPHERICAL HARMONICS ONTO DIFFERENT BASIS

Let us recall the definition of Cartesian spherical unit vectors:

$$\hat{\boldsymbol{\chi}}_{-1} = \frac{1}{\sqrt{2}} (\hat{\mathbf{x}} - i\hat{\mathbf{y}}),$$

$$\hat{\boldsymbol{\chi}}_0 = \hat{\mathbf{z}},$$

$$\hat{\boldsymbol{\chi}}_{+1} = -\frac{1}{\sqrt{2}} (\hat{\mathbf{x}} + i\hat{\mathbf{y}}). \qquad (B1)$$

The vector spherical harmonics can be defined as a linear combination of these vectors, as discussed in Appendix A of Part I.[9] This fact makes them extremely suitable for projecting $\mathbf{W}_p^{(\eta)}$ onto a basis, independent of the observation point. Using the formulas in Appendix A of Part I, one obtains

$$\mathbf{Y}_{nm} \cdot \hat{\boldsymbol{\chi}}_\mu = \left(\sqrt{\frac{n}{2n+1}} \mathbf{Y}_{n,n-1}^m - \sqrt{\frac{n+1}{2n+1}} \mathbf{Y}_{n,n+1}^m \right) \cdot \boldsymbol{\chi}_\mu$$

$$= \sqrt{\frac{n}{2n+1}} \sum_{\mu'=-1}^{1} (n-1,m-\mu';1,\mu'|n,m)$$

$$\times Y_{n-1,m-\mu'} \hat{\boldsymbol{\chi}}_{\mu'} \cdot \hat{\boldsymbol{\chi}}_\mu$$

$$-\sqrt{\frac{n+1}{2n+1}} \sum_{\mu'=-1}^{1} (n+1,m-\mu';1,\mu'|n,m)$$

$$\times Y_{n+1,m-\mu'} \hat{\boldsymbol{\chi}}_{\mu'} \cdot \hat{\boldsymbol{\chi}}_\mu, \qquad (B2)$$

$$\mathbf{X}_{nm} \cdot \hat{\boldsymbol{\chi}}_\mu = \frac{1}{i} \mathbf{Y}_{n,n}^m \cdot \hat{\boldsymbol{\chi}}_\mu$$

$$= -i \sum_{\mu'=-1}^{1} (n,m-\mu';1,\mu'|n,m) Y_{n,m-\mu'} \hat{\boldsymbol{\chi}}_{\mu'} \cdot \hat{\boldsymbol{\chi}}_\mu. \qquad (B3)$$

$$\mathbf{Z}_{nm} \cdot \hat{\boldsymbol{\chi}}_\mu = \left(\sqrt{\frac{n+1}{2n+1}} \mathbf{Y}_{n,n-1}^m + \sqrt{\frac{n}{2n+1}} \mathbf{Y}_{n,n+1}^m \right) \cdot \hat{\boldsymbol{\chi}}_\mu$$

$$= \sqrt{\frac{n+1}{2n+1}} \sum_{\mu'=-1}^{1} (n-1,m-\mu';1,\mu'|n,m)$$

$$\times Y_{n-1,m-\mu'} \hat{\boldsymbol{\chi}}_{\mu'} \cdot \hat{\boldsymbol{\chi}}_\mu$$

$$+ \sqrt{\frac{n}{2n+1}} \sum_{\mu'=-1}^{1} (n+1,m-\mu';1,\mu'|n,m)$$

$$\times Y_{n+1,m-\mu'} \hat{\boldsymbol{\chi}}_{\mu'} \cdot \hat{\boldsymbol{\chi}}_\mu. \qquad (B4)$$

On the other hand, the scalar products of the Cartesian spherical vectors give, by use of Eq. (B1),

$$\hat{\boldsymbol{\chi}}_\mu \cdot \hat{\boldsymbol{\chi}}_\nu^{*} = \delta_{\mu\nu},$$

$$\hat{\boldsymbol{\chi}}_{-1} \cdot \hat{\boldsymbol{\chi}}_{-1} = 0, \qquad \hat{\boldsymbol{\chi}}_{-1} \cdot \hat{\boldsymbol{\chi}}_0 = 0,$$

$$\hat{\boldsymbol{\chi}}_{-1} \cdot \hat{\boldsymbol{\chi}}_{+1} = -1,$$

$$\hat{\boldsymbol{\chi}}_0 \cdot \hat{\boldsymbol{\chi}}_0 = 1, \qquad \hat{\boldsymbol{\chi}}_1 \cdot \hat{\boldsymbol{\chi}}_0 = 0,$$

$$\hat{\boldsymbol{\chi}}_{+1} \cdot \hat{\boldsymbol{\chi}}_{+1} = 0. \qquad (B5)$$

These relations finally produce

$$\mathbf{Y}_{nm} \cdot \hat{\boldsymbol{\chi}}_{-1} = -\sqrt{\frac{n}{2n+1}} (n-1,m-1;1,1|n,m) Y_{n-1,m-1} + \sqrt{\frac{n+1}{2n+1}} (n+1,m-1;1,1|n,m) Y_{n+1,m-1},$$

$$\mathbf{Y}_{nm} \cdot \hat{\boldsymbol{\chi}}_0 = \sqrt{\frac{n}{2n+1}} (n-1,m;1,0|n,m) Y_{n-1,m} - \sqrt{\frac{n+1}{2n+1}} (n+1,m;1,0|n,m) Y_{n+1,m},$$

$$\mathbf{Y}_{nm} \cdot \hat{\boldsymbol{\chi}}_1 = -\sqrt{\frac{n}{2n+1}} (n-1,m+1;1,-1|n,m) Y_{n-1,m+1} + \sqrt{\frac{n+1}{2n+1}} (n+1,m+1;1,-1|n,m) Y_{n+1,m+1}. \qquad (B6)$$

$$\mathbf{X}_{nm} \cdot \hat{\boldsymbol{\chi}}_{-1} = i(n,m-1;1,1|n,m) Y_{n,m-1},$$

$$\mathbf{X}_{nm} \cdot \hat{\boldsymbol{\chi}}_0 = -i(n,m;1,0|n,m) Y_{n,m},$$

$$\mathbf{X}_{nm} \cdot \hat{\boldsymbol{\chi}}_1 = i(n,m+1;1,-1|n,m) Y_{n,m+1}. \qquad (B7)$$

$$\mathbf{Z}_{nm} \cdot \hat{\boldsymbol{\chi}}_{-1} = -\sqrt{\frac{n+1}{2n+1}}(n-1,m-1;1,1|n,m)Y_{n-1,m-1} - \sqrt{\frac{n}{2n+1}}(n+1,m-1;1,1|n,m)Y_{n+1,m-1},$$

$$\mathbf{Z}_{nm} \cdot \hat{\boldsymbol{\chi}}_{0} = \sqrt{\frac{n+1}{2n+1}}(n-1,m;1,0|n,m)Y_{n-1,m} + \sqrt{\frac{n}{2n+1}}(n+1,m;1,0|n,m)Y_{n+1,m},$$

$$\mathbf{Z}_{nm} \cdot \hat{\boldsymbol{\chi}}_{1} = -\sqrt{\frac{n+1}{2n+1}}(n-1,m+1;1,-1|n,m)Y_{n-1,m+1} - \sqrt{\frac{n}{2n+1}}(n+1,m+1;1,-1|n,m)Y_{n+1,m+1}. \qquad \text{(B8)}$$

The coefficients in front of $Y_{n,m}$ in Eqs. (B6)–(B8) represent the coefficients $b^{(\eta)}_{nm,\mu\nu,\chi}$, which express the projections of the vector spherical harmonics $\mathbf{W}^{(\eta)}_{nm}$ on $\hat{\boldsymbol{\chi}}_\mu$ in terms of scalar spherical harmonics $Y_{n,m}$:

$$\mathbf{W}^{(\eta)}_{nm} \cdot \hat{\boldsymbol{\chi}}_\mu = \sum_{\nu=-1}^{1} b^{(\eta)}_{nm,\mu,\nu,\chi} Y_{n+\nu,m+\mu}. \qquad \text{(B9)}$$

A similar expression applies in an arbitrary basis $(\hat{\mathbf{j}}_\mu)$:

$$\mathbf{W}^{(\eta)}_{nm} \cdot \hat{\mathbf{j}}_\mu = \sum_{\nu=-1}^{1} b^{(\eta)}_{nm,\mu,\nu,j} Y_{n+\nu,m+\mu}. \qquad \text{(B10)}$$

The transfer from the basis $(\hat{\boldsymbol{\chi}}_\mu)$ to the basis $(\hat{\mathbf{j}}_\mu)$ is made through the corresponding transformation matrix $\mathfrak{R} = (\hat{\mathbf{j}} \cdot \hat{\boldsymbol{\chi}}^*)$, so that $(\hat{\mathbf{j}}_\mu) = \mathfrak{R}(\hat{\boldsymbol{\chi}}_\nu)$. The components of vector spherical harmonics in different basis sets are related through the same transformation matrix:

$$\mathbf{W}^{(\eta)}_{nm} \cdot \hat{\mathbf{j}}_\mu \equiv \hat{\mathbf{j}}_\mu \cdot \mathbf{W}^{(\eta)}_{nm} = \sum_{\mu'} \mathfrak{R}_{\mu\mu'} \hat{\boldsymbol{\chi}}_{\mu'} \cdot \mathbf{W}^{(\eta)}_{nm}. \qquad \text{(B11)}$$

This relation ensures the transfer between the two sets of b coefficients:

$$b^{(\eta)}_{nm,\mu,\nu,j} = \sum_{\mu'} \mathfrak{R}_{\mu\mu'} b^{(\eta)}_{nm,\mu',\nu,\chi}. \qquad \text{(B12)}$$

The corresponding author's e-mail address is brian.stout@fresnel.fr.

REFERENCES

1. B. Stout, M. Nevière, and E. Popov, "Light diffraction by a three-dimensional object: differential theory," J. Opt. Soc. Am. A **22**, 2385–2404 (2005).
2. B. T. Draine, "Interstellar dust," in *Origin and Evolution of the Elements*, A. McWilliams and M. Rauch, eds. (Cambridge U. Press, 2004), p. 230.
3. M. Gottlied, C. L. M. Ireland, and J. M. Ley, *Electro-Optic and Acousto-Optic Scanning and Defection*, Optical Engineering Series (Marcel Dekker, New York, 1983).
4. S. N. Papadakis, N. K. Uzunoglu, and C. N. Capsalis, "Scattering of a plane wave by a general anisotropic dielectric ellipsoid," J. Opt. Soc. Am. A **7**, 991–997 (1990).
5. J. C. Monzon, "Three-dimensional field expansion in the most general rotationally symmetric anisotropic material: application to the scattering by a sphere," IEEE Trans. Antennas Propag. **37**, 728–735 (1989).
6. W. Ren and X. B. Wu, "Application of an eigenfunction representation to the scattering of a plane wave by an anisotropically coated circular cylinder," J. Phys. D **28**, 1031–1039 (1995).
7. A. D. Kiselev, V. Yu. Reshetnyaba, and T. J. Sluckain, "Light scattering by optically anisotropic scatterers: T-matrix theory for radial and uniform anisotropies," Phys. Rev. E **65**, 056609 (2002).
8. M. Nevière and E. Popov, *Light Propagation in Periodic Media: Differential Theory and Design* (Marcel Dekker, New York, 2003).
9. B. Stout, M. Nevière, and E. Popov, "Mie scattering by an anisotropic object. Part I. Homogeneous sphere," J. Opt. Soc. Am. A **23**, 1111–1123 (2006).
10. L. Li, "Use of Fourier series in the analysis of discontinuous periodic structures," J. Opt. Soc. Am. A **13**, 1870–1876 (1996).
11. E. Popov, M. Nevière, and N. Bonod, "Factorization of products of discontinuous functions applied to Fourier–Bessel basis," J. Opt. Soc. Am. A **21**, 46–51 (2004).
12. A. R. Edmonds, *Angular Momentum in Quantum Mechanics* (Princeton U. Press, 1960).
13. Y. L. Xu, "Fast evaluation of the Gaunt coefficients," Math. Comput. **65**, 1601–1612 (1996).

Auger *et al.*

Scattering efficiency of aggregated clusters of spheres: dependence on configuration and composition

Jean-Claude Auger

Centro de Investigación en Polímeros, Grupo COMEX, Boulevar M.A. Camacho No 138, Lomas de Chapultepec, 11560 Mexico D.F., México

Brian Stout

Institut Fresnel, Centre de St. Jérôme UMR 6133, 13397 Marseille Cedex 20, France

Vincent Martinez

Centro de Investigación en Polímeros, Grupo COMEX, Boulevar M.A. Camacho No 138, Lomas de Chapultepec, 11560 Mexico D.F., México

We study the orientation average scattering cross section of various isolated aggregates of identical spherical particles as functions of their size, optical properties, and spatial configurations. Two kinds of aggregates are studied: latex particles in water and rutile titanium dioxide pigments in a polymeric resin, with size parameters varying from 0.6 to 2.3. Calculations are performed by using a recursive centered T-matrix algorithm solution of the multiple scattering equation that we previously developed [J. Quant. Spectrosc. Radiat. Transfer **79–80**, 533 (2003)]. We show that for a specific size of the constituent spheres, their respective couplings apparently vanish, regardless of the aggregate configuration, and that the scattering cross section of the entire cluster behaves as if its constituents were isolated. We found that the particular radius for which this phenomenon occurs is a function of the relative refractive index of the system. We also study the correlations between the strength of the coupling among the constituent spheres, and the pseudofractal dimension of the aggregate as it varies from 1 to 30. © 2005 Optical Society of America

OCIS codes: 290.4020, 290.4210, 290.5850.

1. INTRODUCTION

The study of the optical properties of granular materials is a subject of broad interest on account of the various applications that can be encountered in academic research and industry. Numerous studies have already been performed concerning, for example, remote atmospheric sensing[1] or the characterization of interstellar dust and its effect on the propagation of stellar radiation in astrophysics.[2] Also, various theoretical approaches have been proposed to calculate light scattering properties by clusters composed of spheres having sizes comparable with the wavelength of the incident field.[3,4] Numerous studies have been conducted in the quasi-static approximation, for example to reproduce experimental Raman scattering data obtained for silica aerogels[5] or to study resonant extinction in colloidal systems containing either nonabsorbing or strongly absorbing spherical particles.[6] From the industrial point of view, such as in the coating industry, manufacturers study the influence of aggregation and flocculation phenomena of rutile titanium dioxide pigment on opacity and gloss of dried paint films.[7]

Optical properties of inhomogeneous media can be studied at two levels. On the microscopic scale, one is typically concerned with the scattering and/or absorption processes that occur between the incident radiation and the heterogeneities of the dispersed phase. In such studies, the nature, size, shape, orientation, volume fraction, and spatial dispersion of the scatterers are the primary parameters affecting the physical response. The principal theoretical challenge is then to relate such variables to the amplitude scattering matrix elements and total cross sections of the volume element of the medium under study.

Rayleigh[8] and Mie[9] introduced the first formalisms to describe the interaction of a monochromatic plane wave with isolated dielectric or metallic spherical particles embedded in a nonabsorbing media. Subsequently, numerous other formalisms were developed in order to calculate the light scattering and absorption properties of nonspherical or aggregated particles. Among the most prevalent are the discrete dipole approximation,[10] the T-matrix formalism,[11,12] the finite-element method,[13,14] and the finite-difference time-domain method.[15–17]

On the macroscopic scale, optical properties such as the total reflection and transmission coefficients, in addition to having a dependence on the local parameters cited above, also have a strong dependence on the thickness of the medium, the roughness of the interfaces, and the type

of illumination. They are generally evaluated from the radiative transfer equation formalism[18] or the analytical theory of the multiple scattering equation.[19]

If limited computing capabilities at first prevented or limited exhaustive multiple scattering studies, nowadays, they can be performed much more rapidly. Typical studies consist in analyzing the correctness and consistency of theoretical predictions through comparisons with experimental measurements[20] or in the characterization of the dispersion medium.[21] One can also perform systematic studies relating the change in optical properties of a well-defined system as a function of the variation of one or several key parameters, allowing a better understanding of the fundamental processes under study.[22] In this work, we focus on the latter approach and study the relation between the orientation average scattering cross section of clusters composed of aggregated spherical particles and their configurations. Such studies are usually applied within the quasi-static approximation by using the discrete dipole approximation[23,24] or within an approximation of the analytical theory of multiple scattering.[25] Here, we propose a numerical study in the Mie scattering regime by using a recursive centered T-matrix algorithm (RCTMA)[26] that is an exact solution of the vector multiple scattering equation.[27]

As our primary concern is the optical properties of architectural white paint films, our study is applied to systems composed of rutile titanium dioxide pigments in a polymer resin and latex particles in water. Nevertheless, the methodology and principal results that we encountered could be useful in the different fields of research mentioned earlier. The reason for studying such systems is that water-based architectural paints are composed of a combination of Latex emulsions and rutile titanium dioxide suspensions. Both colloidal systems are thermodynamically unstable, and eventually, dispersion forces will lead to flocculation and sedimentation. Stability can be promoted with surface-active agents, also called surfactants, that adsorb on the particle surface and prevent aggregation by means of electrostatic and/or steric repulsions. Nevertheless, cluster formation cannot be totally avoided, and its presence affects the performance of the paint. Rutile titanium dioxide aggregates decrease the opacity of white paint, whereas flocculation of latex particles can lead to a premature coalescence of the polymer chains. Also, emulsion stability is often monitored by measuring particle size distribution with dynamic light scattering. It is therefore important and of interest to study the optical properties of such systems as functions of cluster characteristics such as size, shape, and configuration.

The paper is constructed as follows: In Section 2, we briefly introduce the multiple scattering theory that has been used throughout the numerical study. Section 3 is devoted to the description of the cluster generation process, the presentation of the statistical analysis that we performed, and the associated data treatment that we applied. Section 4 is dedicated to the presentation of the main results and to the discussion of the principal effects encountered. To clarify the discussion, the concept of transition radius and the possible extrapolation of our results to much larger clusters are studied in two different paragraphs. Finally, in Section 5, we conclude with our final observations and comments.

2. THEORY

To calculate the orientation average scattering cross section of an ensemble of aggregated dielectric or metallic spheres immersed in an infinite nonabsorbing medium, we adopted a multiple T-matrix formalism[26] of the multiple scattering equation.[27,28] In this approach, the incident, internal, and scattered electromagnetic fields are expanded in terms of vector spherical wave functions and one associates with each particle in the system both single T matrices $\bar{T}^{i(1)}$ and multiple scattering T matrices $\bar{T}^{i(N)}$ (i being the particle label).

The $\bar{T}^{i(1)}$ characterize the intrinsic optical properties of the isolated scatterers and can be calculated from the extended boundary condition technique introduced by Waterman.[10] The multiple scattering T matrices $\bar{T}^{i(N)}$ are obtained from a complete solution of the multiple scattering equations and describe the optical response of a scatterer while taking into account the presence of all the other particles. In our formalism, the $\bar{T}^{i(N)}$ satisfy the equation

$$\bar{T}^{i(N)} = \bar{T}^{i(1)}\left[\bar{I} + \sum_{\substack{j=1 \\ j\neq i}}^{N} \bar{H}^{(i,j)}\bar{T}^{j(N)}\bar{J}^{(j,i)}\right], \qquad i = 1, \ldots, N, \quad (1)$$

where $\bar{J}^{(i,j)}$ and $\bar{H}^{(i,j)}$ are the matrices that translate the incident and the scattered fields, respectively, from the ith to the jth reference frames.[29] We solved Eq. (1) with a RCTMA that we have introduced in previous works.[26,27] In this formalism, the $\bar{T}^{i(N)}$ matrices can be expressed in terms of centered T matrices, denoted $\bar{\tau}_N^{(i,j)}$ such that

$$\bar{T}^{i(N)} = \sum_{j=1}^{j=N} \bar{\tau}_N^{(i,j)}\bar{J}^{(j,i)}. \qquad (2)$$

The fundamental relations of the RCTMA are given in Appendix A. A great advantage of multiple T-matrix formalism is that one can easily perform an analytical evaluation of the orientation average cross section of the system under study.[30] In the present work, we study nonabsorbing particles for which the scattering cross section is equal to the more simply formulated extinction cross section that can be expressed[31] as

$$\langle C_{ext} \rangle = \frac{2\pi}{k_0^2}\mathrm{Tr}\sum_{i=1}^{N}\sum_{j=1}^{N} \bar{\tau}_N^{(i,j)}\bar{J}^{(j,i)}, \qquad (3)$$

where k_0 is the wave vector of the incident radiation and Tr stands for trace. Once the position, size, and complex index of refraction of each sphere is given, one can use Eqs. (A1)–(A4) in Appendix A to calculate the centered T matrix associated with each scatterer. Finally, with Eq. (3) the orientation average extinction cross section of the system can be evaluated.

3. CLUSTER CONFIGURATION AND DATA TREATMENT

A. Cluster Configuration

In a previous work,[32] we calculated the orientation average scattering cross section (OASCS) of linear and compact arrangements of aggregated spheres of rutile titanium dioxide with radii ranging from 0.04 to 0.132 μm. The compact configurations in these studies were constructed from simple crystalline lattice models. Conclusions of this work were that the OASCS showed three distinctive behaviors as functions of the particle radii: Near $r_s \cong 0.08$ μm, the OASCS of the aggregate was very close to the sum of the scattering cross sections of the isolated spheres, and for larger and smaller radii, the OASCS was smaller and larger than the independent scattering sum, respectively.

In this work, we study the influence of the cluster arrangements on the OASCS for more realistic configurations than those studied previously. For this purpose, in addition to linear arrangements of spheres, we have studied clusters formed from two different aggregation processes.[33] The first model is the diffusion-limited cluster–cluster aggregation (DLCCA). It assumes that the colloids stick permanently as soon as they touch, and thus the mechanism is limited by the time taken for the particles to diffuse through the suspension and meet. Such a mechanism leads to clusters with fractal dimension of $f_d \cong 1.8$. The second model, known as the reaction-limited particle–cluster aggregation (RLPCA), assumes that the particles do not necessarily stick at first contact and that they can rearrange themselves. Thus, the aggregation process is limited by the time taken for a sticking encounter to occur. Such an assumption leads to more compact clusters than those in the previous model, with fractal dimension close to $f_d \cong 3.0$.

B. Numerical Calculations and Data Treatment

The different aggregates were generated thanks to a FORTRAN source code provided by R. Botet. Based on the variations of the OASCS as a function of particle size observed in our previous study, the sizes of the constituent spheres studied were chosen as $r_s = 0.04$, 0.08, and 0.132 μm for each fractal dimension (linear, DLCCA, and RLPCA). The wavelength of the incident radiation was taken as 0.546 μm corresponding to the center of the visible range. The complex indices of refraction were taken to be 1.5 for the latex particles and polymer resin and 1.33 for water. Rutile titanium dioxide is birefringent and thus possesses two distinctive indices of refraction. For the purpose of this study, we choose a commonly used approximation[34] that consists of a weighted average of both indices, which yields 2.8 for the chosen wavelength. The indices of the particles and of the surrounding medium are denoted n_s and n_m, respectively.

Once the aggregates were generated (Figs. 1 and 2), the following methodology was applied: We calculated the OASCS associated with 1000 different configurations of the DLCCA and RLPCA families of clusters composed of 6, 9, 12, 15, 18, and 21 spheres with particle radii of 0.04, 0.08, and 0.132 μm for both systems. Figure 3 represents the OASCS, also denoted $\langle C_{ext} \rangle$, determined in the differ-
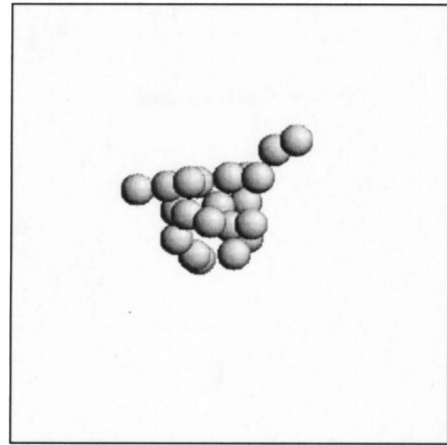

Fig. 1.   Aggregate composed of 21 spheres generated from the RLPCA process.
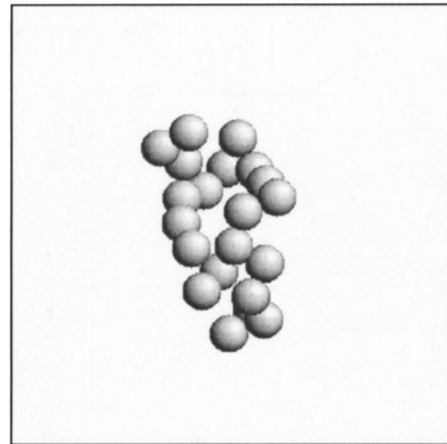

Fig. 2.   Aggregate composed of 21 spheres generated from the DLCCA process.
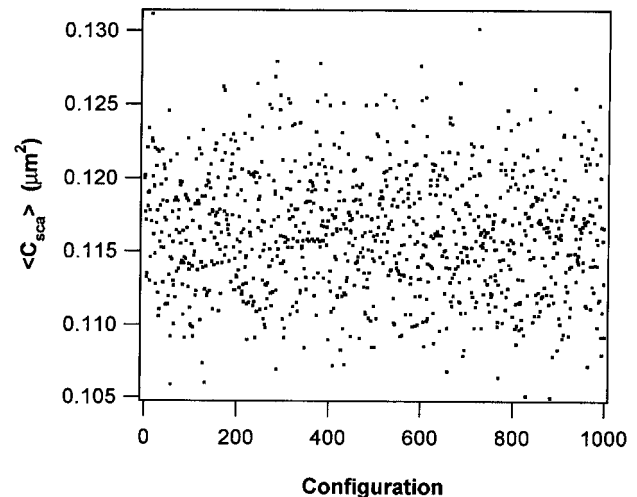

Fig. 3.   OASCS $\langle C_{sca} \rangle$ as a function of 1000 different configurations. The aggregates are composed of 12 spheres of radius $r_s = 0.132$ μm generated from the RLPCA process with index of refraction $n_s = 1.5$ embedded in water with index of refraction $n_m = 1.33$. The wavelength of the incident radiation is 0.546 μm.

ent configuration trials for a 12-sphere cluster of latex particles in water, generated from the RLPCA process. Histograms (Fig. 4) of the occupation number were then constructed and fitted with a Gaussian probability function by adjusting the average cross section $\langle C_{ext} \rangle_c$ and the standard deviation σ_c. The $\langle C_{ext} \rangle_c$ represents the configuration average of the OASCS, while σ_c describes the deviation from this average value of the statistical ensemble. To check the reliability of the sample number, we performed the same adjustments on an ensemble of 3000 configurations. Relative errors inferior to 1% were found on $\langle C_{ext} \rangle_c$ and σ_c, allowing us to conclude that 1000 configurations represent a sufficiently accurate sampling of the possible configurations for each family.

4. RESULTS AND DISCUSSION

Figures 5(a), 5(b), and 5(c) represent the Gaussian adjustments related to the occupation probabilities of the 6-, 9-, 12-, 15-, 18-, and 21-sphere clusters of rutile titanium dioxide immersed in the polymer resin, as functions of the OASCS. The radii of the constituent spheres are respectively $r_s = 0.04$, 0.08, and 0.132 μm, whereas the solid and dashed curves are associated with clusters generated from the DLCCA and RLPCA aggregation processes, respectively. Also, because all adjustments are calculated from the same number of different configurations, the corresponding areas under each Gaussian fit are identical.

The case of linear clusters is particular and much simpler to treat, since only one configuration is possible. The latter leads to $\langle C_{ext} \rangle_c = \langle C_{ext} \rangle$ and $\sigma_c = 0$, and consequently no Gaussian adjustment is necessary. Also, in order to study the electromagnetic coupling between the constituent spheres, we have represented in Figs. 6(a), 6(b), and 6(c) the variation of $\langle C_{ext} \rangle_c$ as a function of the number of particles for the independent-spheres assumption, the RLPCA, DLCCA, and linear aggregates with a radius of 0.04, 0.08, and 0.132 μm, respectively. Let us recall that in the independent scattering assumption, the scattering cross section of the aggregate is calculated supposing that each constituent sphere scatters light as if it were iso-

lated. In this case, one has $\langle C_{ext} \rangle = N_s C_{ext}^I$ and $\sigma_c = 0$, where C_{ext}^I represents the scattering cross section of an isolated particle.

(a)

(b)
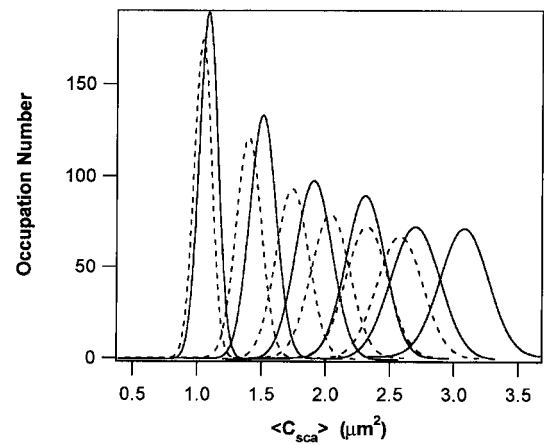
(c)

Fig. 5.   Gaussian adjustments for the 6-, 9-, 12-, 15-, 18-, and 21-sphere clusters of rutile titanium dioxide ($n_s = 2.8$) in a polymer resin ($n_m = 1.5$) for 1000 different configurations. The solid and dashed curves indicate aggregates generated from the DL-CCA and RLPCA, respectively. The radii of the spheres are equal to (a) 0.040 μm, (b) 0.080 μm, and (c) 0.132 μm.
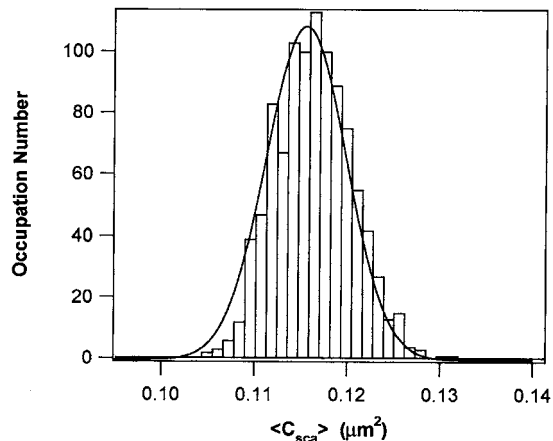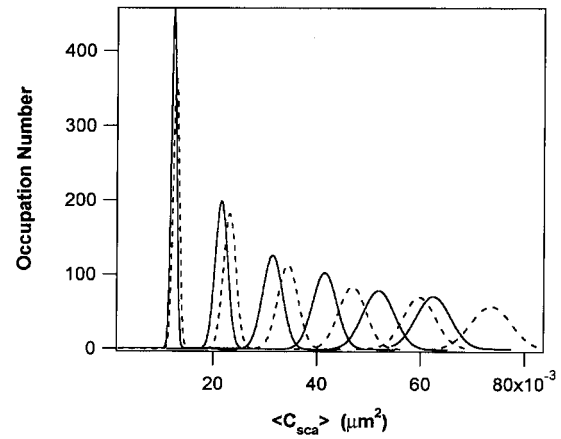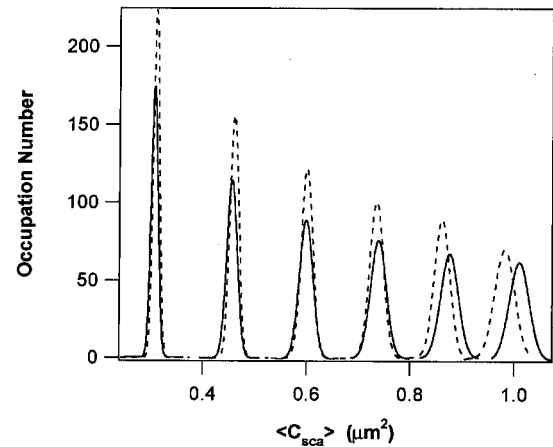
Fig. 4.   Histogram constructed from the values of Fig. 3, where the occupation frequency is plotted as a function of $\langle C_{sca} \rangle$ and fitted with a Gaussian probability function.
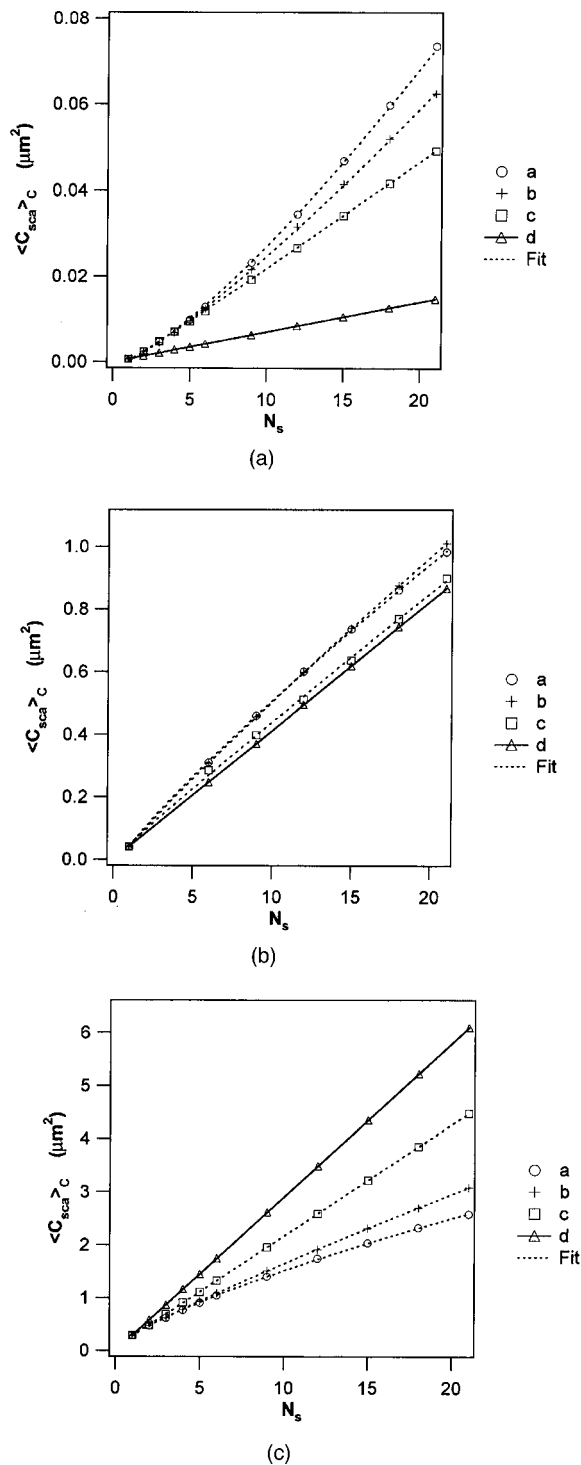
increase as a function of the number of spheres N_s in the cluster. Indeed, since the incident radiation is a monochromatic plane wave of infinite spatial extent, the average amplitude of the scattering interaction process $\langle C_{ext} \rangle_c$ is directly related to the size of the scattering object. Also, for a small number of constituent spheres, the quantity of possible configurations is limited and both the DLCCA and RLPCA give rise to very similar aggregates.

Taking into account the discussion in previous paragraphs together with the fact that the incident radiation cannot discern the details of the cluster structure, at least insofar as their dimensions are smaller than the wavelength, the OASCS does not undergo large variations from one configuration to another, and σ_c remains small for small clusters. However, as the number of constituent spheres increases, the number of different configurations, as well as the overall dimension of the aggregates, also increases. For this reason, the optical response given by the OASCS is spread over a larger range of different values, inducing larger values of σ_c. As a consequence, there is an increase of the overlap zone between the Gaussian adjustments. This overlap is essentially negligible between the six- and nine-sphere clusters, whereas it is quite noticeable between the 18- and 21-sphere systems. In short, essentially none of the six-sphere configurations scatters with the same strength as that of the nine-sphere clusters, but numerous 18-sphere configurations have the same OASCS as that of aggregates composed of 21 particles.

B. Effects of the Cluster Pseudofractal Dimension on the Orientation Average Scattering Cross Section

We now focus on the comparison between the optical responses of clusters having the same number of constituent spheres but generated from different aggregation process. Inspection of Figs. 5(a) and 5(c) shows that values of σ_c are always larger for the RLPCA than for the DLCCA aggregates. Also, because of the condition of constant area under the Gaussian adjustments mentioned above, this implies that the occupation probabilities associated with the values of $\langle C_{ext} \rangle_c$ are always smaller for the former than for the latter. In other words, the denser the aggregate's configuration (higher pseudofractal dimension), the wider the optical response in term of OASCS. This phenomenon can be explained by assuming that the probability of the electromagnetic coupling is directly proportional to the average number of particles directly touching in the aggregates. Then, constituent spheres in clusters generated from the RLPCA process ($f_d = 3$) undergo more coupling phenomena, and the resulting OASCS is spread over a larger range of possible values. Consequently, the pseudofractal dimension gives important information on the possible electromagnetic coupling between the constituent particles of the aggregates.

The aforementioned tendency clearly appears in an inspection of Figs. 6(a) and 6(c), where the differences between the values of $\langle C_{ext} \rangle_c$ for the linear, DLCCA, and RLPCA become more significant as the number of constituent spheres increases. For large numbers of particles, each type of aggregate has a different optical response, which indicates distinctions in the degree of electromagnetic couplings between constituent spheres.

Fig. 6. (a) Variation of $\langle C_{ext} \rangle_c$ as a function of the number of particles for the (a) RLPCA, (b) DLCCA, and (c) linear chain with respective fractal dimensions of 3.0, 1.8, and 1.0, together with the value of $\langle C_{ext} \rangle_c$ in the case of isolated scatterers (d) for a cluster of rutile titanium dioxide particles in a polymer resin. The radius of the constituent spheres is $r_s = 0.04$ μm. (b) Same as (a) but for $r_s = 0.08$ μm. (c) Same as (a) but for $r_s = 0.132$ μm.

A. Effects of the Number of Particles in the Cluster on the Orientation Average Scattering Cross Section

Inspection of Fig. 5 shows that the width σ_c and the averaged value $\langle C_{ext} \rangle_c$ of the probability distribution always

The lower the pseudofractal dimension, the closer the response to the isolated case, whereas, the higher the fractal dimension, the larger the difference. In other words, superior and inferior limits of the variation of $\langle C_{ext}\rangle_c$ are given by the linear ($f_d = 1.0$) and compact ($f_d = 3.0$) cases. Between these limits, the optical response of different fractal dimensions follows the same tendency. Fractals having a variation of $\langle C_{ext}\rangle_c$ closest to the isolated scatterer response should have the lowest fractal dimension, whereas those with the larger discrepancies should have the higher fractal dimension.

C. Effects of the Size of the Constituent Spheres on the Orientation Average Scattering Cross Section

After having studied the influence of the clusters' pseudofractal dimension, we focus in this subsection on the effects of the size of the constituent spheres on the OASCS. From Figs. 5(a) and 5(c), it can be seen that at $r_s = 0.04$ μm, RLPCA aggregates scatter on the average more than DLCCA clusters (higher values of $\langle C_{ext}\rangle_c$), whereas the opposite is true at $r_s = 0.132$ μm. This behavior can also be illustrated by a careful analysis of the size of the normalized overlapping areas between the different Gaussian adjustments (Table 1), where the normalization is realized on the sum of both areas. It is seen that normalized overlapping areas between the $N_s = N$ and $N_s = N + 3$ clusters, where $N = 12$, 15, 18, and 21, is always larger for DLPCA than for RLPCA clusters at $r_s = 0.040$ μm, whereas the opposite holds at $r_s = 0.132$ μm. The strength and type of coupling between the constituent particles depends then not only on the configuration of the aggregate (and consequently on its fractal dimension), as shown previously, but also on the size of the constituent spheres.

One important feature also appearing from inspection of Figs. 6(a) and 6(c) is that for $r_s = 0.132$ μm, all cluster families have $\langle C_{ext}\rangle_c$ values inferior to those of the isolated case whereas for $r_s = 0.04$ μm they are all superior. Such behavior can be understood from Mie and Rayleigh scattering characteristics. In the $r_s = 0.132$ μm case, the scattering intensity is associated with the total surface area of the cluster, which decreases when one particle is added to the system. For this reason, the effect is amplified as the pseudofractal dimension increases. In the $r_s = 0.04$ μm case, particle dimensions are much smaller than the wavelength of the incident field, and the scattering intensity is proportional to scatterer size raised to the fourth power. Adding particles to the system will increase the scattering intensity compared with that in the isolated hypothesis. Finally, since the $r_s = 0.04$ and $r_s = 0.132$ μm cases respectively yield values of $\langle C_{ext}\rangle_c$ inferior and superior to those of the isolated system, one could assume that there exists one radius of the constituent spheres at which the OASCS of the coupled system is equal to the latter. This specific concept is discussed in detail in Subsection 4.D.

D. Concept of Transition Radius

An analysis of Fig. 5(b) that represents the variation of the occupation probabilities as a function of the OASCS for both families at $r_s = 0.08$ μm shows that there is no overlapping zone between the N_s and $N_s + 3$ clusters, indicating that the σ_c remain small. Also, both DLCCA and RLPCA clusters lead to the same Gaussian fits, at least until $N_s = 15$. Such behavior is also revealed upon inspection of Fig. 6(b) by remarking that the fractal dimension of the clusters seems to have a very small influence on the variation of $\langle C_{ext}\rangle_c$ as a function of N_s. Moreover, linear, RLPCA, and DLCCA clusters have an average OASCS that is very close to that under the isolated assumption. This confirms then the fact that this radius represents a transition where, for smaller and larger sizes, the $\langle C_{ext}\rangle_c$ is larger and smaller, respectively, than in the isolated case and that at this radius, each particle seems to scatter as if it were isolated from the others regardless of the fractal dimension. In other words, the electromagnetic coupling that comes from the interaction of the scattered fields is little affected by the cluster's configuration at this radius whereas it is strongly influenced for a larger or smaller one. We shall define the size of the constituent spheres at which such phenomena appear by the name transition radius.

Now, in Figs. 7(a) and 7(b), we present analogous results to those represented in Figs. 6(a) and 6(c) except that now the system under study is composed of latex particles in water. One can clearly observe that the influence of the fractal dimension discussed earlier on the variation of $\langle C_{ext}\rangle_c$ is still valid. However, for $r_s = 0.132$ μm, all the aggregates still scatter more than the isolated particles even if the difference is smaller than that for $r_s = 0.04$ μm. These results clearly indicate that the transition radius that we introduced earlier depends on the relative refractive index of the system (n_m/n_s), which is equal to 0.54 in the case of TiO_2 in a polymer resin and 0.89 for latex particles in water, and that for this latter system, the transition radius is superior to 0.132 μm.

To confirm this hypothesis, we performed a preliminary study, which consists in comparing the associated OASCS of two particles placed in contact with their isolated scattering cross section, varying r_s and the relative index of refraction, denoted N_{re}. The results of this study are shown in Fig. 8, where we plotted the transition radius, denoted R_t, as a function of N_{re}. The zone under the curve represents systems for which the OASCS is higher than that of isolated scatterers, whereas the zone above represents system parameters for which the OASCS is smaller than that of isolated scatterers. A curve passing through the points represents the transition between scattering

Table 1. Normalized Size of the Overlapping Areas for RLPCA and DLPCA Clusters

Particle Radius r_s (μm)	System	RLPCA	DLPCA
0.040	A[a]	0.003	0.008
	B[b]	0.012	0.026
	C[c]	0.025	0.050
0.132	A[a]	0.16	0.094
	B[b]	0.22	0.145
	C[c]	0.29	0.185

[a]Between the 12- and 15-sphere clusters.
[b]Between the 15- and 18-sphere clusters.
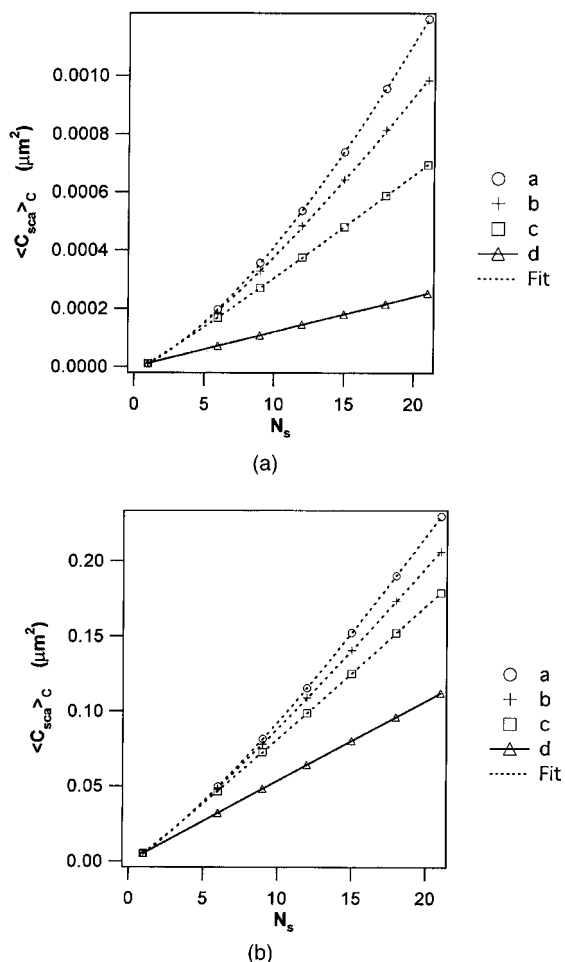[c]Between the 18- and 21-sphere clusters.

(a)

(b)

Fig. 7.   (a) Variation of $\langle C_{ext} \rangle_c$ as a function of the number of particles for the (a) RLPCA, (b) DLCCA, and (c) linear chain with respective fractal dimensions of 3.0, 1.8, and 1.0, together with the value of $\langle C_{ext} \rangle_c$ in the case of isolated scatterers (d) for a cluster of latex particles in water. The radius of the constituent spheres is $r_s = 0.04$ μm. (b) Same as (a) but for $r_s = 0.132$ μm.
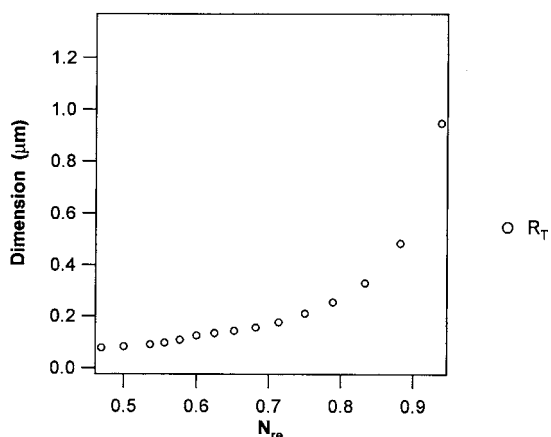

Fig. 8.   Transition radius R_T as a function of relative refraction index N_{re} for a polymer resin host medium ($n_m = 1.5$) and a wavelength of 0.546 μm.

regimes and thereby corresponds to the size regime for which where there is no apparent coupling between the spheres. The general tendency of this variation is that a

more pronounced contrast of the index of refraction between the particles and the surrounding medium corresponds to a smaller transition radius. Thus one can see that the transition radius for latex particles in water occurs around 0.4 μm and that this is the reason that we could not observe it in the study illustrated in Fig. 7.

E. Extrapolation of the Orientation Average Scattering Cross Section for Larger Numbers of Constituent Spheres

Due to the large number of cluster configurations necessary to accurately evaluate the average optical parameters, the numerical calculations are quite time-consuming and studies on larger clusters cannot be considered. For this reason, the discussion in this subsection is devoted to the study of the extrapolated values of the OASCS for aggregates having much larger numbers of constituent spheres than in those that we studied previously. Results are shown for rutile titanium dioxide clusters in water with constituent spheres of $r_s = 0.132$ μm.

Figure 9 represents the parameter $\langle C_{sca} \rangle_c$ normalized by the total volume of the aggregate, also denoted C_{sca}^N, as a function of the number of particles N_s for the linear, DL-CCA, and RLPCA clusters. The use of this parameter is convenient because its variation as a function of the number of spheres in the cluster is a constant line parallel to the Ox axis for the isolated assumption. Two interesting tendencies can be observed. The first is that the variation of C_{sca}^N seems to converge to an asymptotic value, denoted $C_{sca,A}^N$, as N_s increases. The smaller the fractal dimension of the aggregate, the smaller the discrepancy compared with that in the isolated case and therefore the higher the value of $C_{sca,A}^N$. The second remark is that the number of particles N_s, denoted N_A, at which the variation of C_{sca}^V reaches its asymptotic value $C_{sca,A}^V$ increases with the fractal dimension of the aggregates. As we explained earlier, these observations reflect the strong correlation between the coupling effects and the average number of neighboring particles, and consequently with the fractal
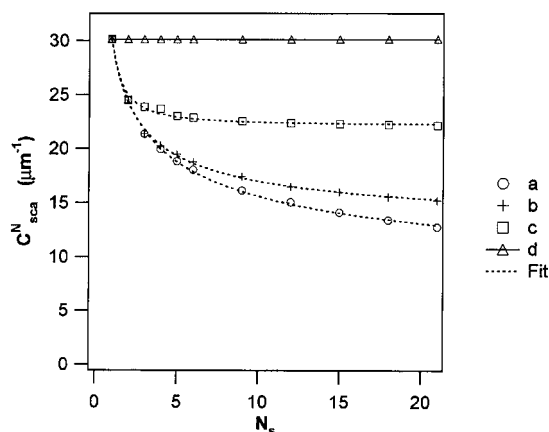

Fig. 9.   Variation of C_{sca}^N as a function of the number of particles for the (a) RLPCA, (b) DLCCA, and (c) linear chain with respective fractal dimensions of 3.0, 1.8, and 1.0, together with the value of C_{sca}^N of isolated scatterers (d) for clusters of rutile titanium dioxide particles in water. The radius of the constituent spheres is $r_s = 0.132$ μm.

Table 2. Adjustment Coefficients Given by the Power Law Functions

Coefficients	Linear	DLCCA	RLPCA
A_0	22.27	11.24	2.24
A_1	7.84	18.89	27.84
A_2	-1.75	-0.51	-0.31
χ	0.12	0.0035	0.043

dimension of the aggregate. The perturbation yielded by N_s+1 particles is weaker in a linear chain than in more compact configurations. For this reason, once that $\langle C_{sca}\rangle_c$ is normalized by the total volume of the cluster, the convergence is reached faster for a linear chain than for a compact configuration.

Taking into account those tendencies and variations, we have adjusted the data of Fig. 9 using a power law function such that $C_{sca}^N(N_s)=A_0+A_1 N_s^{A_2}$. The values of coefficients A_0, A_1, and A_2 are shown in Table 2 for each adjustment. The asymptotic value and the convergence rate introduced earlier are given by the A_0 and A_2 coefficients, respectively. One can note that the quality of the adjustments is better for higher pseudofractal dimension; however, even for small dimensions, the root mean square error on the fit is still relatively small. For this reason, the extrapolation of the values C_{sca}^N could be performed with good precision for clusters composed of a number of primary particles N_s superior to 21 even if the asymptotic trend given by the power law is not exact and the variation of C_{sca}^N slowly increases with N.

5. CONCLUSION

The recursive centered T-matrix algorithm (RCTMA) was used to calculate the optical properties of nonspherical objects composed of aggregated spherical particles. We studied the orientation average scattering cross section (OASCS) of different types of clusters as functions of their size, refractive index contrast, pseudofractal dimension, and size of their constituent spheres. The variations of the optical properties were clearly linked to the different types and strengths of the electromagnetic couplings between the scattering objects. We have introduced the concept of transition radius, which defines the size of the constituent particles for which the overall cluster scattering of light behaves as the sum of the independent constituents. For larger and smaller sizes, the OASCS has stronger and lower values, respectively. Also, the transition radius depends very strongly on the relative refractive index of the scattering particles.

The OASCS that we have studied characterizes the strength of the scattering interaction with the cluster but does not give any information on the spatial distribution of the scattered energy. Such effects could be taken into account by evaluating the orientation scattering efficiency of the aggregates. This quantity is defined as the product of the scattering cross section by unit volume with the term 1-g, where g represents the asymmetry parameters of the system.

Finally, further analysis should be carried out in order to retrieve C_{sca}^N as a function of the number of particles,

using a simple function of the size of the constituent spheres, the relative index of refraction of the system, and the fractal dimension, without the obligation to perform a full statistical study based on RCTMA calculations.

APPENDIX A

The recursive algorithm of the RCTMA is given by

$$\bar{\tau}_N^{(N,N)}=\left[\bar{\mathbf{I}}-\bar{\mathbf{T}}^{N(1)}\sum_{i=1}^{i=N-1}\bar{\mathbf{H}}^{(N,i)}\sum_{j=1}^{j=N-1}\bar{\tau}_{N-1}^{(i,j)}\bar{\mathbf{H}}^{(j,N)}\right]^{-1}\bar{\mathbf{T}}^{N(1)},\tag{A1}$$

$$\bar{\tau}_N^{(N,j)}=\bar{\tau}_N^{(N,N)}\sum_{i=1}^{i=N-1}\bar{\mathbf{H}}^{(N,i)}\bar{\tau}_{N-1}^{(i,j)},\quad j\neq N,\tag{A2}$$

$$\bar{\tau}_N^{(k,i)}=\bar{\tau}_{N-1}^{(k,i)}+\sum_{j=1}^{j=N-1}\bar{\tau}_{N-1}^{(k,j)}\bar{\mathbf{H}}^{(j,N)}\bar{\tau}_N^{(N,i)},\quad i\neq N,\tag{A3}$$

$$\bar{\tau}_N^{(k,N)}=\sum_{j=1}^{j=N-1}\bar{\tau}_{N-1}^{(k,j)}\bar{\mathbf{H}}^{(j,N)}\bar{\tau}_N^{(N,N)},\quad i=N.\tag{A4}$$

REFERENCES

1. L. Tsang, J. Kong, and R. Shin, *Theory of Microwave Remote Sensing* (Wiley, 1985).
2. R. H. Zerull, B. A. S. Gustafson, K. Schultz, and E. Thiele-Corbach, "Scattering by aggregates with and without an absorbing mantle: microwave analog experiments," Appl. Opt. **32**, 4088–4100 (1993).
3. F. Borghese and P. Denti, "Electromagnetic scattering by a cluster of spheres," Appl. Opt. **18**, 116–120 (1979).
4. A.-K. Hamid, I. R. Ciric, and M. Hamid, "Iterative solution of the scattering by a system of multilayered dielectric spheres," IEEE Trans. Antennas Propag. **41**, 172–175 (1992).
5. A. Rahmani, C. Benoit, R. Jullien, G. Poussigue, and A. Sakout, "Light scattering in fractals with scalar and bond-bending models," J. Phys.: Condens. Matter **9**, 2149–2164 (1997).
6. M. Quinten and J. Stier, "Absorption of scattered light in colloidal systems of aggregated particles," Colloid Polym. Sci. **273**, 233–241 (1995).
7. S. Fitzwater and J. W. Hook III, "Dependent scattering theory: a new approach to predicting scattering in paints," J. Coat. Technol. **57**, 39–47 (1985).
8. Lord Rayleigh, "On the electromagnetic theory of light," Philos. Mag., 1881, pp. 12–81.
9. C. F. Bohren and D. R. Huffman, *Absorption and Scattering of Light by Small Particles* (Wiley-Interscience, 1983).
10. E. M. Purcell and C. R. Pennypacker, "Scattering and absorption of light by non-spherical dielectric grains," Astrophys. J. **186**, 705–714 (1973).

11. P. C. Waterman, "Matrix formulation of electromagnetic scattering," Proc. IEEE **53**, 805–812 (1965).
12. P. C. Waterman, "Symmetry, unitarity, and geometry in electromagnetic scattering," Phys. Rev. D **3**, 825–839 (1971).
13. M. A. Morgan and K. K. Mei, "Finite-element computation of scattering by inhomogeneous penetrable bodies of revolution," IEEE Trans. Antennas Propag. **AP-27**, 202–214 (1979).
14. P. P. Silvester and R. L. Ferrari, *Finite Elements for Electrical Engineers* (Cambridge U. Press, 1996).
15. K. S. Yee, "Numerical solution of initial boundary value problems involving Maxwell's equations in isotropic media," IEEE Trans. Antennas Propag. **AP-14**, 302–307 (1966).
16. A. Taflove, *Computational Electrodynamics: The Finite-Difference Time-Domain Method* (Artech House, 1995).
17. P. Yang and K.-N. Liou, "Finite-difference time domain method for light scattering by non spherical and inhomogeneous particles," in *Light Scattering by Nonspherical Particles: Theory, Measurements, and Applications*, M. I. Mishchenko, J. W. Hovenier, and L. D. Travis, eds. (Academic, 2000), pp. 173–221.
18. S. Chandrasekhar, *Radiative Transfer* (Dover, 1960).
19. U. Frisch, "Wave propagation in random media," in *Probabilistic Methods in Applied Mathematics*, A. T. Barucha-Reid, ed. (Academic, 1968), Vol. 1, pp. 75–191.
20. F. Curiel, W. Vargas, and R. G. Barrera, "Visible spectral dependence of the scattering and absorption coefficients of pigmented coatings from inversion of diffuse reflectance spectra," Appl. Opt. **41**, 5968–5978 (2002).
21. D. Bhanti, S. Manickavasagam, and M. P. Mengüç, "Identification of non-homogeneous spherical particles from their scattering matrix elements," J. Quant. Spectrosc. Radiat. Transf. **56**, 591–607 (1996).
22. M. I. Mishchenko, "Light scattering by size–shape distributions of randomly oriented axially symmetric particles of a size comparable to a wavelength," Appl. Opt. **32**, 4652–4666 (1993).
23. P. Rannou, C. P. McKay, R. Botet, and M. Cabane, "Semi-empirical model of absorption and scattering by isotropic fractal aggregates of sphere," Planet. Space Sci. **47**, 385–396 (1999).
24. R. Botet and P. Rannou, "Optical anisotropy of an ensemble of aligned fractal aggregates," J. Quant. Spectrosc. Radiat. Transf. **79-80**, 569–576 (2003).
25. R. Botet, P. Rannou, and M. Cabane, "Mean-field approximation of Mie scattering by fractal aggregates of identical spheres," Appl. Opt. **36**, 8791–8796 (1997).
26. J. C. Auger and B. Stout, "A recursive *T*-matrix algorithm to solve the multiple scattering equation: numerical validation," J. Quant. Spectrosc. Radiat. Transf. **79–80**, 533–547 (2003).
27. B. Stout, J. C. Auger, and J. Lafait, "A transfer matrix approach to local field calculations in multiple scattering problems," J. Mod. Opt. **49**, 2129–2152 (2002).
28. A. Ishimaru, *Wave Propagation and Scattering in Random Media* (Academic, 1978).
29. S. Stein, "Addition theorems for spherical wave functions," Q. Appl. Math. **19**, 15–24 (1961).
30. D. Mackowski, "Calculation of total cross sections of multiple-sphere clusters," J. Opt. Soc. Am. A **11**, 2851–2861 (1994).
31. B. Stout, J. C. Auger, and J. Lafait, "Individual and aggregate scattering matrices and cross-sections: conservation laws and reciprocity," J. Mod. Opt. **48**, 2105–2128 (2001).
32. J. C. Auger, R. G. Barrera, and B. Stout, "Scattering efficiencies of aggregates of spherical particles," J. Quant. Spectrosc. Radiat. Transf. **79–80**, 521–531 (2003).
33. R. Julien and R. Botet, *Aggregation and Fractal Aggregates* (World Scientific, 1987).
34. E. S. Thiele and R. H. French, "Light-scattering properties of representative, morphological rutile titania particles studied using a finite-element method," J. Am. Ceram. Soc. **81**, 469–479 (1998).

Light diffraction by a three-dimensional object: differential theory

Brian Stout, Michel Nevière, and Evgeny Popov

Institut Fresnel, Unité Mixte de Recherche 6133, Case 161 Faculté des Sciences et Techniques, Centre de Saint Jérôme, 13397 Marseille Cedex 20, France

The differential theory of diffraction of light by an arbitrary object described in spherical coordinates is developed. Expanding the fields on the basis of vector spherical harmonics, we reduce the Maxwell equations to an infinite first-order differential set. In view of the truncation required for numerical integration, correct factorization rules are derived to express the components of **D** in terms of the components of **E**, a process that extends the fast Fourier factorization to the basis of vector spherical harmonics. Numerical overflows and instabilities are avoided through the use of the *S*-matrix propagation algorithm for carrying out the numerical integration. The method can analyze any shape and/or material, dielectric or conducting. It is particularly simple when applied to rotationally symmetric objects. © 2005 Optical Society of America

OCIS codes: 290.5850, 050.1940, 000.3860, 000.4430.

1. INTRODUCTION

Light scattering from arbitrarily shaped 3D objects comparable in size to the wavelength of the scattering radiation is an important problem with applications covering a vast range of fields of science and technology, including astrophysics, atmospheric physics, radiative transfer in optically thick media such as paints and papers, and remote detection. By "comparable in size with the wavelength," we are most often speaking of particles having a characteristic size D within an order of magnitude of the wavelength, $\lambda/10 \lesssim D \lesssim 10\lambda$. In this size regime, and for scatterers of sufficiently high dielectric contrast, popular approximations such as the Rayleigh–Gans[1,2] or geometric optics approximations[1,2] are invalid; one must resort to an essentially full solution of the Maxwell equations.

The first full solution to the electromagnetic scattering by a fully 3D object is that of Lorenz and Mie for the scattering by a single homogeneous isotropic spherical object embedded in a homogeneous isotropic external medium.[3–5] This renowned solution takes the form of an infinite (but rapidly converging) series of coefficients involving spherical Bessel functions. Being the only analytically manageable exact solution to the full electromagnetic scattering problem, the Mie solution has played a preponderate role in light-scattering calculations for nearly a century.

In view of the size range in which the Mie theory is most useful, it comes as no surprise that Mie theory is most frequently applied to media containing a large number of scattering inclusions. Since the Mie theory is a solution only to an isolated particle, it has frequently been coupled with the independent scattering approximation and applied to tenuous media systems containing only a week volume density of scatterers.[6]

The increasing interest in recent decades of light scattering by aggregates and light propagation in dense media such as composites, containing a high volume density of inclusions, has fueled considerable progress in the multiple-scattering problem of such dense media.[7–9] In view of the already considerable difficulty of the multiple-scattering equations, a majority of these studies have continued to use spheres as the fundamental scattering element. In reality, of course, it is extremely rare for scattering inclusions to be so obliging as to separate themselves into distinct compact spheres, even though an impressive number of mechanical and chemical processes in a number of industries have been developed with exactly this goal in mind (grinding, surfactants,…). Furthermore, it has long been clear that nonspherical inclusions can yield quantitatively different results on the macroscopic scale than spherical inclusions.

Many multiple-scattering codes and theories have employed with considerable success the notion of a transfer matrix (frequently called the *T* matrix in the multiple-scattering community; see the note[10]) that consists of a linear transformation between the excitation field incident on a scatterer and the scattered field emanating from it.[2,7–9,11] The transfer matrix is more than a single solution to the scattering problem corresponding to a given incident field; rather it can be viewed as a complete solution to the scattering problem for any possible incident field. In the multiple-scattering theories employing transfer matrices, the Mie solution to the sphere takes the form of a diagonal transfer matrix in a basis of the vector spherical wave functions. It has long been recognized by those working in this field that nonspherical scatterers can rather readily be integrated into existing multiple-scattering theories by simply replacing the diagonal Mie transfer matrices of spheres by the full transfer matrices of nonspherical objects.

There exist a number of techniques for treating scattering by nonspherical objects, but not all of these can readily provide the complete solution required to derive a transfer matrix, and the reliability and applicability of these various techniques is a recurring stumbling bock. One of the most popular techniques in the literature is

the Waterman (or extended boundary condition) method, whose popularity is in large part due to the fact that one can readily obtain from it a full transfer matrix for a large variety of nonspherical shapes.[12] It has been shown, however, that the Waterman technique yields the same algorithm as one obtains from a Rayleigh hypothesis.[11] Both the Rayleigh hypothesis and the Waterman technique have been demonstrated to have considerable limitations in the theories of diffraction gratings,[13] and it is well established that both the Waterman technique and the Rayleigh hypothesis can break down for scatterers with high aspect ratios.[11]

The above remarks have in part provided our motivation to propose a new differential theory for deriving the transfer matrix of nonspherical scatterers. Although differential theories have been studied previously for 3D scatterers, we have developed our theory from first principles and made full use of recent breakthroughs in the differential theory of 1D, 2D, and 3D diffraction gratings that have greatly improved the reliability and convergence of differential theories. The new methods in question have been presented and elaborated in a number of articles[14–19] and a recent book,[20] but these works are not a prerequisite for understanding the present work, which has been conceived to be self-contained. The differential technique in diffraction gratings makes extensive use of Fourier series, and their extension to the 3D problem leads us to make considerable use of vector spherical harmonics (VSHs) in the derivation of our formulas. The VSHs, however, do not appear in the final computational method, and the finer details of the VSH manipulations are provided in Appendix C.

The work is organized as follows. We present the problem in Section 2. We introduce the VSHs in Section 3 and introduce their applications to field expansions in Section 4. The propagation equations are derived in Section 5, and the fast numerical factorization (FNF) required for convergence of the series is thoroughly discussed in Section 6. We study field developments outside the modulated region in Section 7 and present the prescription for resolving the boundary-value problem in Section 8. We conclude this work by briefly illustrating the necessary formula for extracting physically relevant quantities such as cross sections and scattering matrices.

2. PRESENTATION OF THE PROBLEM

Figure 1 shows a finite object, made of an isotropic material, with arbitrary shape limited by a surface (S). This surface is described in spherical coordinates (r, θ, ϕ), with $\theta \in [0, \pi]$ defined in the figure by the equation

$$f(r, \theta, \phi) = 0 \qquad (1)$$

or

$$r = g(\theta, \phi). \qquad (2)$$

At a given point M on the surface, the external normal unit vector is $\hat{\mathbf{N}}$, and the unit vectors of spherical coordinates are denoted $\hat{r}$, $\hat{\theta}$, $\hat{\phi}$. The surface (S) divides the space into two regions. The first region, contained within (S), is filled with a linear, homogeneous, and isotropic me-

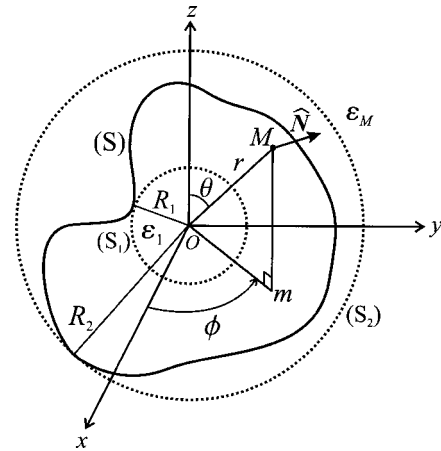Fig. 1.   Description of the diffracting object and notations.

dium, dielectric or conducting, described by complex permittivity ϵ_1. The second region lies outside (S) and has real permittivity ϵ_m. In view of developing the differential theory, we divide space into three regions by introducing the inscribed sphere (S_1) with radius R_1 and the circumscribed sphere (S_2) with radius R_2; the region between (S_1) and (S_2) is called the "modulated region," a denotation that recalls that for any constant value r_0 of r between R_1 and R_2, the permittivity, ϵ, is a function of θ and ϕ and, furthermore, is obviously periodic with respect to ϕ with a period of 2π and piecewise constant with respect to θ and ϕ.

The object is subject to an incident harmonic electromagnetic field described by its electric field, $\mathbf{E}_i$, with an $\exp(-i\omega t)$ time dependence. As is well known in quantum mechanics and electromagnetism,[21–23] any function of angular variables θ and ϕ can be developed on the basis of scalar spherical harmonics $Y_{nm}(\theta, \phi)$. The dimensionless relative dielectric constant, $\varepsilon(r, \theta, \phi)$, defined such that $\epsilon_0 \varepsilon(r, \theta, \phi) \equiv \epsilon(r, \theta, \phi)$ can therefore be expressed as

$$\varepsilon(r, \theta, \phi) = \sum_{n=0}^{\infty} \sum_{m=-n}^{n} \varepsilon_{nm}(r) Y_{nm}(\theta, \phi), \qquad (3)$$

which implies that $\varepsilon_{nm}(r)$ can be obtained from the Hermitian product:

$$\varepsilon_{nm}(r) = \langle Y_{nm} | \varepsilon \rangle \equiv \int_0^{4\pi} Y_{nm}^*(\theta, \phi) \varepsilon(r, \theta, \phi) d\Omega. \qquad (4)$$

The reader should note that in Eq. (4) and throughout this work we have adopted the convention for scalar Hermitian products such that

$$\langle g | f \rangle \equiv \int g^*(x) f(x) dx. \qquad (5)$$

In Eq. (4), the asterisk denotes the complex conjugate, and Ω is the solid angle. Equation (4) can thus be rewritten as

$$\varepsilon_{nm}(r) = \int_0^{2\pi} \int_0^{\pi} \varepsilon(r, \theta, \phi) Y_{nm}^*(\theta, \phi) \sin \theta \, d\theta \, d\phi. \qquad (6)$$

A development of the vector electromagnetic field is a more complicated affair. One might first be tempted to ex-

pand each spherical coordinate component of the total field ($\mathbf{E}, \mathbf{H}$) on the basis of the scalar spherical harmonics, similar to Eq. (3). But when such expansions are put into the Maxwell equations, derivatives of the Y_{nm} functions arise that are difficult to calculate and manipulate. Consequently, we choose another way to expand vector fields; i.e., we represent them on the basis of VSHs.

3. VECTOR SPHERICAL HARMONICS

VSHs are described in several reference books,[6,21–23] although their definitions and notations vary with the authors. They arise in vector solutions of the wave equation (Helmholtz equation) and when appropriately defined can form an orthogonal complete basis to represent the electromagnetic field. We choose to define and denote them by the following equations:

$$\mathbf{Y}_{nm}(\theta, \phi) \equiv \hat{\mathbf{r}} Y_{nm}(\theta, \phi), \tag{7}$$

$$\mathbf{X}_{nm}(\theta, \phi) \equiv \mathbf{Z}_{nm}(\theta, \phi) \times \hat{\mathbf{r}}, \tag{8}$$

where

$$\mathbf{Z}_{nm}(\theta, \phi) \equiv \frac{r \, \boldsymbol{\nabla} \, Y_{nm}(\theta, \phi)}{\sqrt{n(n+1)}}$$

$$\text{if } n \neq 0, \ \mathbf{Z}_{00}(\theta, \phi) \equiv 0. \tag{9}$$

Equation (8) implies that

$$\mathbf{Z}_{nm}(\theta, \phi) = \hat{\mathbf{r}} \times \mathbf{X}_{nm}(\theta, \phi). \tag{10}$$

All the VSHs are mutually orthonormal in the sense that if $\mathbf{W}_{nm}^{(i)}$ ($i = 1, 2, 3$) denotes the vector harmonics $\mathbf{Y}_{nm}$, $\mathbf{X}_{nm}$, or $\mathbf{Z}_{nm}$, we have

$$\langle \mathbf{W}_{nm}^{(i)} | \mathbf{W}_{\nu\mu}^{(j)} \rangle \equiv \int_0^{4\pi} \mathbf{W}_{nm}^{(i)*} \cdot \mathbf{W}_{\nu\mu}^{(j)} d\Omega = \delta_{ij} \delta_{n\nu} \delta_{m\mu}, \tag{11}$$

where δ_{ij} is the Kronecker symbol and the Hermitian product of Eq. (4) has been extended to vector fields. We also remark from Eqs. (7)–(9) that if the $\mathbf{W}_{nm}^{(i)}(\theta, \phi)$ were real the trihedral ($\mathbf{Y}_{nm}, \mathbf{X}_{nm}, \mathbf{Z}_{nm}$) would be direct.

Let us recall that the scalar spherical harmonics $Y_{nm}(\theta, \phi)$ are expressed in terms of associated Legendre functions $P_n^m(\cos \theta)$ as[23]

$$Y_{nm}(\theta, \phi) = \left[\frac{2n+1}{4\pi} \frac{(n-m)!}{(n+m)!} \right]^{1/2} P_n^m(\cos \theta) \exp(im\phi) \tag{12}$$

or by including the square root in the definitions of normalized associated Legendre functions $\bar{P}_n^m$:

$$Y_{nm}(\theta, \phi) = \bar{P}_n^m(\cos \theta) \exp(im\phi). \tag{13}$$

Introducing functions $\bar{u}_n^m$ and $\bar{s}_n^m$ defined by

$$\bar{u}_n^m(\cos \theta) = \frac{1}{\sqrt{n(n+1)}} \frac{m}{\sin \theta} \bar{P}_n^m(\cos \theta), \tag{14}$$

$$\bar{s}_n^m(\cos \theta) = \frac{1}{\sqrt{n(n+1)}} \frac{d}{d\theta} \bar{P}_n^m(\cos \theta), \tag{15}$$

we can express the vector harmonics $\mathbf{X}_{nm}$ and $\mathbf{Z}_{nm}$ as

$$\mathbf{X}_{nm}(\theta, \phi) = i\bar{u}_n^m(\cos \theta) \exp(im\phi) \hat{\boldsymbol{\theta}} - \bar{s}_n^m(\cos \theta) \exp(im\phi) \hat{\boldsymbol{\phi}}, \tag{16}$$

$$\mathbf{Z}_{nm}(\theta, \phi) = \bar{s}_n^m(\cos \theta) \exp(im\phi) \hat{\boldsymbol{\theta}} + i\bar{u}_n^m(\cos \theta) \exp(im\phi) \hat{\boldsymbol{\phi}}. \tag{17}$$

Equations (16) and (17), combined with Eq. (7), clearly show that for a given n, m the ($\mathbf{Y}_{nm}, \mathbf{X}_{nm}, \mathbf{Z}_{nm}$) are mutually perpendicular in the sense that $\mathbf{W}_{nm}^{(i)} \cdot \mathbf{W}_{nm}^{(j)} = 0$ for $i \neq j$.

Other interesting relations are the curl of products of a radially dependent function $h(r)$ by a $\mathbf{W}_{nm}^{(i)}$. These relations will prove to be useful in the derivation of the propagation equations and are given by

$$\mathbf{curl}[h(r)\mathbf{Y}_{nm}] = [n(n+1)]^{1/2} \frac{h(r)}{r} \mathbf{X}_{nm}, \tag{18}$$

$$\mathbf{curl}[h(r)\mathbf{X}_{nm}] = \frac{h(r)}{r}[n(n+1)]^{1/2}\mathbf{Y}_{nm} + \left[\frac{h(r)}{r} + h'(r) \right] \mathbf{Z}_{nm}, \tag{19}$$

$$\mathbf{curl}[h(r)\mathbf{Z}_{nm}] = - \left[\frac{h(r)}{r} + h'(r) \right] \mathbf{X}_{nm}. \tag{20}$$

4. FIELD EXPANSIONS

An arbitrary vector field $\mathbf{U}(r, \theta, \phi)$ can be expressed in a development of the VSHs as stated by

$$\mathbf{U}(r, \theta, \phi) = \sum_{n=0}^{\infty} \sum_{m=-n}^{n} [A_{Ynm}(r)\mathbf{Y}_{nm}(\theta, \phi) + A_{Xnm}(r)\mathbf{X}_{nm}(\theta, \phi) + A_{Znm}(r)\mathbf{Z}_{nm}(\theta, \phi)]. \tag{21}$$

Such a development will be subsequently applied to the total electric field $\mathbf{E}$, the total magnetic field $\mathbf{H}$, the displacement $\mathbf{D}$, the incident electric field $\mathbf{E}_i$, and the unit normal vector $\hat{\mathbf{N}}$. However, in view of a numerical treatment, the summation in Eq. (21) will have to be limited to a value of n equal to $n_{\max}$. Also, the double subscript (n, m) will be replaced by a single subscript p, varying from 1 to N. It is then easy to establish that Eq. (21) takes the form

$$\mathbf{U}(r, \theta, \phi) = \sum_{p=1}^{N} [A_{Yp}(r)\mathbf{Y}_p(\theta, \phi) + A_{Xp}(r)\mathbf{X}_p(\theta, \phi) + A_{Zp}(r)\mathbf{Z}_p(\theta, \phi)], \tag{22}$$

where $N \equiv (n_{\max} + 1)^2$ and

$$p = n(n + 1) + m + 1. \tag{23}$$

On the other hand, if p is given, n and m can be derived from it through the equations

$$n = \text{Int}\sqrt{p - 1}, \quad m = p - 1 - n(n + 1), \tag{24}$$

where the function $\text{Int}(x)$ calculates the integer part of x.

Throughout the rest of the work, the coefficients of the various field vectors will frequently be put in columns. As a result of Eq. (22), the total field **E**, for example, will be represented by a column $[E]$ composed of three blocks containing the functions E_{Yp}, E_{Xp}, and E_{Zp}. Since $p \in [1, (n_{\max} + 1)^2]$, the vector **E** will have $3 \times (n_{\max} + 1)^2$ components $E_l : \mathbf{E} \leftrightarrow [E]$, i.e.,

$$
\begin{bmatrix} \vdots \\ E_l \\ \vdots \end{bmatrix} \equiv
\left.\begin{bmatrix} - \\ \vdots \\ E_{Y,p} \\ \vdots \\ - \\ \vdots \\ E_{X,p} \\ \vdots \\ - \\ \vdots \\ E_{Z,p} \\ \vdots \\ - \end{bmatrix}\right\} 3 \times (n_{\max} + 1)^2. \tag{25}
$$

The unit vector $\hat{\mathbf{N}}$ can be represented in such a column once the surface S is specified; i.e., the function $f(r, \theta, \phi)$ is known. Since $\hat{\mathbf{N}}$ is given by

$$\hat{\mathbf{N}}(\theta, \phi) = \left.\frac{\mathbf{grad}\, f}{\|\mathbf{grad}\, f\|}\right|_{f=0}, \tag{26}$$

we obtain in spherical coordinates

$$N_r = \left.\frac{\dfrac{\partial f}{\partial r}}{\|\mathbf{grad}\, f\|}\right|_{f=0}, \quad N_\theta = \left.\frac{\dfrac{1}{r}\dfrac{\partial f}{\partial \theta}}{\|\mathbf{grad}\, f\|}\right|_{f=0},$$

$$N_\phi = \left.\frac{\dfrac{1}{r\sin\theta}\dfrac{\partial f}{\partial \phi}}{\|\mathbf{grad}\, f\|}\right|_{f=0}. \tag{27}$$

With $\hat{\mathbf{N}}$ known, its components on the VSHs are derived from the scalar products

$$N_{Ynm} = \langle \mathbf{Y}_{nm} | \hat{\mathbf{N}} \rangle = \langle Y_{nm}\hat{\mathbf{r}} | \hat{\mathbf{r}} N_r \rangle = \int_0^{4\pi} Y_{nm}^*(\theta, \phi) N_r(\theta, \phi) \mathrm{d}\Omega$$

$$= \int_0^{2\pi}\int_0^{\pi} N_r \bar{P}_n^m(\cos\theta)\exp(-im\phi)\sin\theta\,\mathrm{d}\theta\,\mathrm{d}\phi, \tag{28}$$

$$N_{Xnm} = \int_0^{2\pi}\int_0^{\pi} [iN_\theta \bar{u}_n^m(\cos\theta) - N_\phi \bar{s}_n^m(\cos\theta)]$$

$$\times \exp(-im\phi)\sin\theta\,\mathrm{d}\theta\,\mathrm{d}\phi, \tag{29}$$

$$N_{Znm} = \int_0^{2\pi}\int_0^{\pi} [N_\theta \bar{s}_n^m(\cos\theta) + iN_\phi \bar{u}_n^m(\cos\theta)]$$

$$\times \exp(-im\phi)\sin\theta\,\mathrm{d}\theta\,\mathrm{d}\phi. \tag{30}$$

From Eqs. (28)–(30), the column associated with vector $\hat{\mathbf{N}}$, containing the three blocks N_{Yp}, N_{Xp}, and N_{Zp}, $p \in [1, (n_{\max} + 1)^2]$, is fully determined. The case of a diffracted object with a revolution symmetry is especially simple. Then not only is N_ϕ null [which eliminates a term in Eqs. (29) and (30)] but more interesting is the fact that N_r and N_θ, are then ϕ independent. Then all terms with subscript m different from zero are null, and Eqs. (28)–(30) reduce to

$$N_{Yn0} = 2\pi\int_0^{\pi} N_r(\theta)\bar{P}_n^0(\cos\theta)\sin\theta\,\mathrm{d}\theta, \tag{31}$$

$$N_{Xn0} = 0, \tag{32}$$

$$N_{Zn0} = 2\pi\int_0^{\pi} N_\theta(\theta)\bar{s}_n^0(\cos\theta)\sin\theta\,\mathrm{d}\theta, \tag{33}$$

where we have used the fact that $\bar{u}_n^0(\cos\theta) = 0$.

Of course, replacing double integrals by single ones, combined with the reduction of their number from $3 \times (n_{\max} + 1)^2$ to $2 \times (n_{\max} + 1)$ leads to great savings in computation time. The same remark also applies to $\varepsilon(r, \theta, \phi)$, whose components on the $Y_n^m(\theta, \phi)$ basis reduce to $\varepsilon_{n,0}$, given by

$$\varepsilon_{n,0} = 2\pi\int_0^{\pi} \varepsilon(r, \theta)\bar{P}_n^0(\cos\theta)\sin\theta\,\mathrm{d}\theta. \tag{34}$$

Details concerning an analytical calculation of $\varepsilon_{n,0}$ are given in Appendix A.

5. PROPAGATION EQUATIONS

The main advantage of the field representation over the basis of VSHs lies in the simplicity of the propagation equations resulting from Maxwell equations. Writing $\mathbf{curl}\, \mathbf{E} = i\omega\mu\mu_0 \mathbf{H}$, with μ as the dimensionless relative magnetic permeability, and representing **E** and **H** by expansions of the form given by Eq. (22), we find

$$\sum_{p=1}^{N} \{\mathbf{curl}[E_{Yp}(r)\mathbf{Y}_p] + \mathbf{curl}[E_{Xp}(r)\mathbf{X}_p] + \mathbf{curl}[E_{Zp}(r)\mathbf{Z}_p]\}$$

$$= i\omega\mu\mu_0\sum_{p=1}^{N} (H_{Yp}\mathbf{Y}_p + H_{Xp}\mathbf{X}_p + H_{Zp}\mathbf{Z}_p). \tag{35}$$

Using Eqs. (18)–(20) and equating the p components on both sides in Eq. (35), we also have

$$\sqrt{n(n+1)}\frac{E_{Yp}(r)}{r}\mathbf{X}_p + \sqrt{n(n+1)}\frac{E_{Xp}(r)}{r}\mathbf{Y}_p + \left[\frac{E_{Xp}(r)}{r}\right.$$

$$\left. + \frac{dE_{Xp}(r)}{dr}\right]\mathbf{Z}_p - \left[\frac{E_{Zp}(r)}{r} + \frac{dE_{Zp}(r)}{dr}\right]\mathbf{X}_p$$

$$= i\omega\mu\mu_0(H_{Yp}\mathbf{Y}_p + H_{Xp}\mathbf{X}_p + H_{Zp}\mathbf{Z}_p). \tag{36}$$

Introducing $a_p = \sqrt{n(n+1)}$, where $n = \mathrm{Int}\sqrt{p-1}$, and projecting both members of Eq. (36) on vectors $\mathbf{Y}_p$, $\mathbf{X}_p$, and $\mathbf{Z}_p$, we obtain

$$a_p\frac{E_{Xp}}{r} = i\omega\mu\mu_0 H_{Yp}, \tag{37}$$

$$a_p\frac{E_{Yp}}{r} - \frac{E_{Zp}}{r} - \frac{dE_{Zp}}{dr} = i\omega\mu\mu_0 H_{Xp}, \tag{38}$$

$$\frac{E_{Xp}}{r} + \frac{dE_{Xp}}{dr} = i\omega\mu\mu_0 H_{Zp}. \tag{39}$$

Similarly, the Maxwell equation, **curl H** $= -i\omega\mathbf{D}$ leads to

$$a_p\frac{H_{Xp}}{r} = -i\omega D_{Yp}, \tag{40}$$

$$a_p\frac{H_{Yp}}{r} - \frac{H_{Zp}}{r} - \frac{dH_{Zp}}{dr} = -i\omega D_{Xp}, \tag{41}$$

$$\frac{H_{Xp}}{r} + \frac{dH_{Xp}}{dr} = -i\omega D_{Zp}. \tag{42}$$

Since we work in linear optics ($\mathbf{D} = \epsilon_0\varepsilon\mathbf{E}$), and since $\mathbf{E}$ and $\mathbf{D}$ are represented on the same basis, there exists a square matrix Q_ε that links the column $[E]$ to the column $[D]$ such that

$$[D] = \epsilon_0 Q_\varepsilon[E]. \tag{43}$$

This Q_ε matrix is made of nine square blocks, each block having dimension $(n_{\max}+1)^2$, which depend on the components of ε defined in Eq. (6), and will be calculated in Subsection 6.C. We represent Q_ε by the following block structure:

$$Q_\varepsilon = \begin{pmatrix} Q_{\varepsilon YY} & Q_{\varepsilon YX} & Q_{\varepsilon YZ} \\ Q_{\varepsilon XY} & Q_{\varepsilon XX} & Q_{\varepsilon XZ} \\ Q_{\varepsilon ZY} & Q_{\varepsilon ZX} & Q_{\varepsilon ZZ} \end{pmatrix}. \tag{44}$$

From Eqs. (43) and (44), we thus obtain

$$\frac{1}{\epsilon_0}[D_Y] = Q_{\varepsilon YY}[E_Y] + Q_{\varepsilon YX}[E_X] + Q_{\varepsilon YZ}[E_Z], \tag{45}$$

which gives

$$[E_Y] = (Q_{\varepsilon YY})^{-1}\left(\frac{1}{\epsilon_0}[D_Y] - Q_{\varepsilon YX}[E_X] - Q_{\varepsilon YZ}[E_Z]\right). \tag{46}$$

Moreover,

$$\frac{1}{\epsilon_0}[D_X] = Q_{\varepsilon XY}[E_Y] + Q_{\varepsilon XX}[E_X] + Q_{\varepsilon XZ}[E_Z], \tag{47}$$

$$\frac{1}{\epsilon_0}[D_Z] = Q_{\varepsilon ZY}[E_Y] + Q_{\varepsilon ZX}[E_X] + Q_{\varepsilon ZZ}[E_Z]. \tag{48}$$

We first insert Eq. (40) into Eq. (46). We then insert Eq. (46) into Eqs. (47) and (48) in order to express $[D_X]$ and $[D_Z]$ in terms of $[E_X]$, $[E_Z]$, and $[H_X]$, expressions that are then inserted into Eqs. (41) and (42). In Eq. (41) $[H_{Yp}]$ is eliminated thanks to Eq. (37). In Eq. (38) $[E_Y]$ is eliminated thanks to Eqs. (40) and (46). Introducing a diagonal matrix a with elements $a_p\delta_{p,q}$, we finally reduce the set of six equations, Eqs. (37)–(42), to four equations with unknowns E_{Xp}, E_{Zp}, H_{Xp}, and H_{Zp} only:

$$\frac{E_{Xp}}{r} + \frac{dE_{Xp}}{dr} = i\omega\mu\mu_0 H_{Zp} \tag{49}$$

$$\frac{a_p}{r}\left((Q_{\varepsilon YY})^{-1}\left[\frac{ia}{\omega\epsilon_0 r}[H_X] - Q_{\varepsilon YX}[E_X] - Q_{\varepsilon YZ}[E_Z]\right]\right)_p$$

$$- \frac{E_{Zp}}{r} - \frac{dE_{Zp}}{dr} = i\omega\mu\mu_0 H_{Xp}, \tag{50}$$

$$\frac{H_{Xp}}{r} + \frac{dH_{Xp}}{dr} = -i\omega\epsilon_0(Q_{\varepsilon ZX}[E_X])_p - i\omega\epsilon_0(Q_{\varepsilon ZZ}[E_Z])_p$$

$$- i\omega\epsilon_0\left(Q_{\varepsilon ZY}Q_{\varepsilon YY}^{-1}\left(\frac{ia}{\omega\epsilon_0 r}[H_X] - Q_{\varepsilon YX}[E_X]\right.\right.$$

$$\left.\left. - Q_{\varepsilon YZ}[E_Z]\right)\right)_p, \tag{51}$$

$$i\frac{a_p^2}{\omega\mu\mu_0}\frac{E_{Xp}}{r^2} + \frac{H_{Zp}}{r} + \frac{dH_{Zp}}{dr} = i\omega\epsilon_0(Q_{\varepsilon XX}[E_X])_p$$

$$+ i\omega\epsilon_0(Q_{\varepsilon XZ}[E_Z])_p$$

$$+ i\omega\epsilon_0\left(Q_{\varepsilon XY}Q_{\varepsilon YY}^{-1}\left(\frac{ia}{\omega\epsilon_0 r}[H_X]\right.\right.$$

$$\left.\left. - Q_{\varepsilon YX}[E_X] - Q_{\varepsilon YZ}[E_Z]\right)\right)_p. \tag{52}$$

It is now useful to construct a column $[F]$ containing the unknowns of the problem, made with four blocks, each block having $(n_{\max}+1)^2$ components:

$$[F] = \begin{bmatrix} [E_X] \\ [E_Z] \\ [\tilde{H}_X] \\ [\tilde{H}_Z] \end{bmatrix}, \tag{53}$$

where the tilde means that the magnetic field is multiplied by the vacuum impedance Z_0 so that it has the same dimension as an electric field:

$$\tilde{\mathbf{H}} \equiv Z_0 \mathbf{H} = \sqrt{\frac{\mu_0}{\epsilon_0}}\mathbf{H} = \frac{1}{c\,\epsilon_0}\mathbf{H}. \qquad (54)$$

The propagation equations, Eqs. (49)–(52), can then be written in matrix form:

$$\frac{\mathrm{d}[F]}{\mathrm{d}r} = M(r)[F], \qquad (55)$$

where $M(r)$ is a square matrix made with 16 square blocks, each of them having dimension $(n_{\max}+1)^2$, which can be explicitly written as

$$M_{11} = -\frac{1}{r}, \quad M_{12} = M_{13} = 0, \quad M_{14} = i\mu\frac{\omega}{c}1,$$

$$M_{21} = -\frac{a}{r}Q_{\varepsilon YY}^{-1}Q_{\varepsilon YX}, \quad M_{22} = -\frac{1}{r} - \frac{a}{r}Q_{\varepsilon YY}^{-1}Q_{\varepsilon YZ},$$

$$M_{23} = i\frac{\omega}{c}\left(\left(\frac{c}{r\omega}\right)^2 aQ_{\varepsilon YY}^{-1}a - \mu 1\right), \quad M_{24} = 0,$$

$$M_{31} = i\frac{\omega}{c}(Q_{\varepsilon ZY}Q_{\varepsilon YY}^{-1}Q_{\varepsilon YX} - Q_{\varepsilon ZX}),$$

$$M_{32} = i\frac{\omega}{c}(Q_{\varepsilon ZY}Q_{\varepsilon YY}^{-1}Q_{\varepsilon YZ} - Q_{\varepsilon ZZ}),$$

$$M_{33} = \frac{1}{r}(Q_{\varepsilon ZY}Q_{\varepsilon YY}^{-1}a - 1), \quad M_{34} = 0,$$

$$M_{41} = i\frac{\omega}{c}\left(Q_{\varepsilon XX} - Q_{\varepsilon XY}Q_{\varepsilon YY}^{-1}Q_{\varepsilon YX} - \frac{1}{\mu}\left(\frac{ac}{\omega r}\right)^2\right),$$

$$M_{42} = i\frac{\omega}{c}(Q_{\varepsilon XZ} - Q_{\varepsilon XY}Q_{\varepsilon YY}^{-1}Q_{\varepsilon YZ}),$$

$$M_{43} = -Q_{\varepsilon XY}Q_{\varepsilon YY}^{-1}\frac{a}{r}, \quad M_{44} = -\frac{1}{r}, \qquad (56)$$

where 1 is the unit matrix.

Equations (55) and (56) are the propagation equations. They will have to be numerically integrated across the modulated region, and the numerical solution will have to be matched with analytical expressions of the field in each homogeneous region ($r < R_1$ and $r > R_2$). It is known that such a process will determine the field everywhere. However, two difficulties are common in the process.[20] The first difficulty is the exponential growth of the numerical solutions during the integration process. This will have to be avoided by using the S-matrix propagation algorithm.[14,20] The second difficulty comes with the slow convergence of the field expansions, which requires integrating overly large sets of equations, which aggravates the exponential growth. In the case of grating theory, the difficulty has been resolved[15,16,20] by developing a technique called fast Fourier factorization (FFF), which is

based on factorization rules developed by Li.[17] Such a technique has been recently extended to basis functions different from the Fourier basis[18] and is then called fast numerical factorization (FNF). It has been applied with success to the Bessel–Fourier basis used to analyze objects in cylindrical coordinates.[19] Its extension to spherical harmonics is not trivial and is described in Section 6.

6. FAST NUMERICAL FACTORIZATION APPLIED TO A SPHERICAL HARMONIC BASIS

The difficulty of slow convergence of field expansion is linked to the necessity of truncating the set of propagation equations. From a mathematical point of view, field expansions are infinite series, as stated by Eq. (21). Thus the set of Eqs. (37)–(42) should be infinite, as should be the set in Eq. (55). The truncation of Eq. (21) performed in Eq. (22) limits the range of p in Eqs. (37)–(42) to $(n_{\max+1})^2$, and the question that arises is how can D_{Yp}, D_{Xp}, and D_{Zp} in Eqs. (40)–(42) be correctly expressed in terms of E_{Yp}, E_{Xp}, and E_{Zp}.

It has been known for a long time that reconstructing a discontinuous function from its Fourier series leads to the Gibbs phenomenon, which means that, at the discontinuity points, the sum of the truncated series does not converge to the value of the function. Such a phenomenon does not exist for continuous functions, which results in the fact that continuous functions are better reconstructed by summing their truncated Fourier series than discontinuous ones. This remark was used by Li to propose factorization rules[17] that allowed a breakthrough in grating theory.[15,16,20] Extending the previous hypothesis to arbitrary basis functions, namely, that continuous functions are better reconstructed than discontinuous functions by summing their truncated expansion on an arbitrary continuous function basis, we were able to establish factorization rules valid for an arbitrary basis. We briefly recall the basic ideas here.

A. Factorization Rules
Let us consider three functions f, g, and h of a common variable x with $h = gf$ and assume that the truncation expansion of f over a continuous function basis φ_m is known: $f(x) = \sum_{m=1}^{N} f_m\varphi_m(x)$. The function $g(x)$ may be known explicitly or from an expansion over a different or identical function basis. The question is how to determine with the best accuracy the coefficients h_m of the development of $h = gf$ over the φ_m basis: $h(x) = \sum_{m=1}^{N} h_m\varphi_m(x)$. The answer depends on whether f and g are discontinuous at a same value of x or not.

1. Direct Rule
If f is a continuous function while g is discontinuous, which implies that h is discontinuous, we have

$$h_m = \langle\varphi_m|h\rangle = \langle\varphi_m|gf\rangle = \left\langle \varphi_m\Big|g\sum_p f_p\varphi_p\right\rangle. \qquad (57)$$

In Eq. (57), the summation is a rapidly converging series, since f is continuous. From the linearity of the scalar product we find

$$h_m = \sum_p \langle \varphi_m | g f_p \varphi_p \rangle = \sum_p \langle \varphi_m | g \varphi_p \rangle f_p. \qquad (58)$$

Defining

$$g_{mp} \equiv \langle \varphi_m | g \varphi_p \rangle, \qquad (59)$$

we obtain the direct rule

$$h_m = \sum_p g_{mp} f_p. \qquad (60)$$

Since the sum in Eq. (57) is rapidly converging, so is the sum in Eq. (60), which means that the h_m components are well calculated with p limited to small values. It is worth noticing that the components g_n of the function g are not involved in the direct rule. It is the g_{mp} coefficients given by Eq. (59) that are required.

2. Inverse rule
Let us now assume that f and g are functions that are discontinuous at the same point, with a continuous product h. In order to find the same situation as in Subsection 6.A.1, we then consider $f = (1/g)h$, where h is continuous and $1/g$ and f are discontinuous. We thus find

$$f_m = \langle \varphi_m | f \rangle = \left\langle \varphi_m \left| \frac{1}{g} h \right. \right\rangle = \left\langle \varphi_m \left| \frac{1}{g} \sum_p h_p \varphi_p \right. \right\rangle$$

$$= \sum_p \left\langle \varphi_m \left| \frac{1}{g} \varphi_p \right. \right\rangle h_p, \qquad (61)$$

which will be a rapidly converging summation. Defining

$$g_{\mathrm{inv},mp} \equiv \left\langle \varphi_m \left| \frac{1}{g} \varphi_p \right. \right\rangle, \qquad (62)$$

we obtain

$$f_m = \sum_p g_{\mathrm{inv},mp} h_p. \qquad (63)$$

Again, the fast convergence of the summation in Eq. (61) due to the continuity of h ensures that the coefficients f_m are well calculated. Inverting the relation in Eq. (63), we have

$$h_m = \sum_p [(g_{\mathrm{inv}})^{-1}]_{mp} f_p, \qquad (64)$$

which is the inverse rule.

B. Factorization Rules for Spherical Harmonic Expansions
In electromagnetism, the tangential component $\mathbf{D}_{\mathrm{T}}$ of the displacement is the product of a discontinuous function ε by a continuous vector $\mathbf{E}_{\mathrm{T}}$. The calculation of its component on any basis will thus require using the direct rule. On the other hand, the components of $\mathbf{D}_{\mathrm{N}} = \hat{\mathbf{N}}(\hat{\mathbf{N}} \cdot \mathbf{D})$ will have to be obtained using the inverse rule.

1. Direct Rule
Representing both $\mathbf{D}_{\mathrm{T}}$ and $\mathbf{E}_{\mathrm{T}}$ by truncated expansions (21), we have

$$\mathbf{E}_{\mathrm{T}} = \sum_{n,m} (E_{\mathrm{TY}nm} \mathbf{Y}_{nm} + E_{\mathrm{TX}nm} \mathbf{X}_{nm} + E_{\mathrm{TZ}nm} \mathbf{Z}_{nm}), \qquad (65)$$

$$\mathbf{D}_{\mathrm{T}} = \sum_{n,m} (D_{\mathrm{TY}nm} \mathbf{Y}_{nm} + D_{\mathrm{TX}nm} \mathbf{X}_{nm} + D_{\mathrm{TZ}nm} \mathbf{Z}_{nm}). \qquad (66)$$

The $\mathbf{D}_{\mathrm{T}}$ and $\mathbf{E}_{\mathrm{T}}$ vectors are linked through the relation

$$\mathbf{D}_{\mathrm{T}} = \epsilon_0 \varepsilon \mathbf{E}_{\mathrm{T}}, \qquad (67)$$

and we want to express this in terms of a matrix relation among their components on the spherical harmonic basis:

$$[\mathbf{D}_{\mathrm{T}}] = \epsilon_0 \{\varepsilon^{(\mathrm{T})}\}[\mathbf{E}_{\mathrm{T}}], \qquad (68)$$

where

$$\{\varepsilon^{(\mathrm{T})}\} = \begin{pmatrix} \{\varepsilon_{YY}\} & \{\varepsilon_{YX}\} & \{\varepsilon_{YZ}\} \\ \{\varepsilon_{XY}\} & \{\varepsilon_{XX}\} & \{\varepsilon_{XZ}\} \\ \{\varepsilon_{ZY}\} & \{\varepsilon_{ZX}\} & \{\varepsilon_{ZZ}\} \end{pmatrix} \qquad (69)$$

and each square block has dimension $(n_{\max}+1)^2$. Our aim in what follows is to explicitly determine these blocks.

As established in Appendix B, since a given $\mathbf{Y}_{nm}$ is perpendicular to all $\mathbf{X}_{\nu\mu}$ and $\mathbf{Z}_{\nu\mu}$ vectors, we have $\{\varepsilon_{YX}\} = \{\varepsilon_{XY}\} = \{\varepsilon_{YZ}\} = \{\varepsilon_{ZY}\} = 0$, and $\varepsilon^{(\mathrm{T})}$ takes the form

$$\{\varepsilon^{(\mathrm{T})}\} = \begin{pmatrix} \{\varepsilon_{YY}\} & 0 & 0 \\ 0 & \{\varepsilon_{XX}\} & \{\varepsilon_{XZ}\} \\ 0 & \{\varepsilon_{ZX}\} & \{\varepsilon_{ZZ}\} \end{pmatrix}. \qquad (70)$$

Putting Eqs. (65) and (66) in Eq. (67) above, we have

$$\sum_{n',m'} (D_{\mathrm{TY}n'm'} \mathbf{Y}_{n'm'} + D_{\mathrm{TX}n'm'} \mathbf{X}_{n'm'} + D_{\mathrm{TZ}n'm'} \mathbf{Z}_{n'm'})$$

$$= \epsilon_0 \varepsilon(r,\theta,\phi) \sum_{\nu,\mu} (E_{\mathrm{TY}\nu\mu} \mathbf{Y}_{\nu\mu} + E_{\mathrm{TX}\nu\mu} \mathbf{X}_{\nu\mu} + E_{\mathrm{TZ}\nu\mu} \mathbf{Z}_{\nu\mu}). \qquad (71)$$

If we perform an ordinary scalar product of both sides of Eq. (71) by $\mathbf{Y}_{nm}^*$, we obtain

$$\mathbf{Y}_{nm}^* \cdot \sum_{n',m'} (D_{\mathrm{TY}n'm'} \mathbf{Y}_{n'm'} + D_{\mathrm{TX}n'm'} \mathbf{X}_{n'm'} + D_{\mathrm{TZ}n'm'} \mathbf{Z}_{n'm'})$$

$$= \epsilon_0 \varepsilon(r,\theta,\phi) \mathbf{Y}_{nm}^* \cdot \sum_{\nu,\mu} (E_{\mathrm{TY}\nu\mu} \mathbf{Y}_{\nu\mu} + E_{\mathrm{TX}\nu\mu} \mathbf{X}_{\nu\mu} + E_{\mathrm{TZ}\nu\mu} \mathbf{Z}_{\nu\mu}), \qquad (72)$$

and, using the fact that

$$\mathbf{Y}_{nm}^* \cdot \mathbf{X}_{n'm'} = \mathbf{Y}_{nm}^* \cdot \mathbf{Z}_{n'm'} = \mathbf{Y}_{nm}^* \cdot \mathbf{X}_{\nu\mu} = \mathbf{Y}_{nm}^* \cdot \mathbf{Z}_{\nu\mu} = 0,$$

we find

$$\sum_{n',m'} D_{\mathrm{TY}n'm'} \mathbf{Y}_{nm}^* \cdot \mathbf{Y}_{n'm'} = \epsilon_0 \varepsilon(r,\theta,\phi) \sum_{\nu,\mu} E_{\mathrm{TY}\nu\mu} \mathbf{Y}_{nm}^* \cdot \mathbf{Y}_{\nu\mu}. \qquad (73)$$

Integrating both sides of this equation over the solid angles,

$$\sum_{n',m'} D_{\text{TY}n'm'} \int_0^{4\pi} d\Omega \mathbf{Y}_{nm}^* \cdot \mathbf{Y}_{n'm'}$$

$$= \epsilon_0 \sum_{\nu,\mu} E_{\text{TY}\nu\mu} \int_0^{4\pi} d\Omega \varepsilon(r,\theta,\phi) \mathbf{Y}_{nm}^* \cdot \mathbf{Y}_{\nu\mu}, \qquad (74)$$

and using the functional orthonormality of the VSHs, we then obtain

$$D_{\text{TY}nm} = \epsilon_0 \sum_{\nu,\mu} E_{\text{TY}\nu\mu} \int_0^{4\pi} d\Omega \varepsilon(r,\theta,\phi) \mathbf{Y}_{nm}^* \cdot \mathbf{Y}_{\nu\mu}. \qquad (75)$$

Defining

$$\varepsilon_{\text{YY}nm,\nu\mu} \equiv \int_0^{4\pi} d\Omega \varepsilon(r,\theta,\phi) \mathbf{Y}_{nm}^* \cdot \mathbf{Y}_{\nu\mu} \equiv \langle \mathbf{Y}_{nm} | \varepsilon \mathbf{Y}_{\nu\mu} \rangle, \qquad (76)$$

we find the linear relation between $D_{\text{TY}nm}$ and $E_{\text{TY}\nu\mu}$ reads as

$$D_{\text{TY}nm} = \epsilon_0 \sum_{\nu,\mu} \varepsilon_{\text{YY}nm,\nu\mu} E_{\text{TY}\nu\mu}. \qquad (77)$$

Of course, the double subscripts (n,m) and (ν,μ) can, respectively, be replaced by single subscripts, p and q, using Eq. (23). Then Eq. (77) takes a compact form:

$$D_{\text{TY}p} = \epsilon_0 \sum_q \varepsilon_{\text{YY}p,q} E_{\text{TY}q}, \qquad (78)$$

which defines the elements of the block $\{\varepsilon_{\text{YY}}\}$ and where we recall that $\{\varepsilon_{\text{YY}}\}$ is a square block with dimensions $(n_{\max}+1)^2$.

We derive the expressions of the other blocks in a similar way. Multiplying both sides of Eq. (71) now by $\mathbf{X}_{nm}^*$, we obtain

$$\mathbf{X}_{nm}^* \cdot \sum_{n',m'} (D_{\text{TY}n'm'} \mathbf{Y}_{n'm'} + D_{\text{TX}n'm'} \mathbf{X}_{n'm'} + D_{\text{TZ}n'm'} \mathbf{Z}_{n'm'})$$

$$= \epsilon_0 \varepsilon(r,\theta,\phi) \mathbf{X}_{nm}^* \cdot \sum_{\nu,\mu} (E_{\text{TY}\nu\mu} \mathbf{Y}_{\nu\mu} + E_{\text{TX}\nu\mu} \mathbf{X}_{\nu\mu} + E_{\text{TZ}\nu\mu} \mathbf{Z}_{\nu\mu}). \qquad (79)$$

Using the fact that $\mathbf{X}_{nm}^* \cdot \mathbf{Y}_{n'm'} = \mathbf{X}_{nm}^* \cdot \mathbf{Y}_{\nu\mu} = 0$, we obtain

$$\sum_{n',m'} (D_{\text{TX}n'm'} \mathbf{X}_{nm}^* \cdot \mathbf{X}_{n'm'} + D_{\text{TZ}n'm'} \mathbf{X}_{nm}^* \cdot \mathbf{Z}_{n'm'})$$

$$= \epsilon_0 \varepsilon(r,\theta,\phi) \mathbf{X}_{nm}^* \cdot \sum_{\nu,\mu} (E_{\text{TX}\nu\mu} \mathbf{X}_{\nu\mu} + E_{\text{TZ}\nu\mu} \mathbf{Z}_{\nu\mu}). \qquad (80)$$

Integrating over the solid angle Ω, we obtain

$$D_{\text{TX}nm} = \epsilon_0 \sum_{\nu,\mu} \int_0^{4\pi} d\Omega \varepsilon(r,\theta,\phi) \mathbf{X}_{nm}^* \cdot (E_{\text{TX}\nu\mu} \mathbf{X}_{\nu\mu} + E_{\text{TZ}\nu\mu} \mathbf{Z}_{\nu\mu}). \qquad (81)$$

We then define

$$\varepsilon_{\text{XX}nm,\nu\mu} \equiv \int_0^{4\pi} d\Omega \varepsilon(r,\theta,\phi) \mathbf{X}_{nm}^* \cdot \mathbf{X}_{\nu\mu} \equiv \langle \mathbf{X}_{nm} | \varepsilon \mathbf{X}_{\nu\mu} \rangle, \qquad (82)$$

$$\varepsilon_{\text{XZ}nm,\nu\mu} \equiv \int_0^{4\pi} d\Omega \varepsilon(r,\theta,\phi) \mathbf{X}_{nm}^* \cdot \mathbf{Z}_{\nu\mu} \equiv \langle \mathbf{X}_{nm} | \varepsilon \mathbf{Z}_{\nu\mu} \rangle, \qquad (83)$$

so that, after the single-subscript notation is introduced, Eq. (81) reduces to

$$\frac{1}{\epsilon_0} D_{\text{TX}p} = \sum_q \varepsilon_{\text{XX}p,q} E_{\text{TX}q} + \sum_q \varepsilon_{\text{XZ}p,q} E_{\text{TZ}q}, \qquad (84)$$

which gives the $\{\varepsilon_{\text{XX}}\}$ and $\{\varepsilon_{\text{XZ}}\}$ blocks.

In a third step, multiplying both sides of Eq. (71) by $\mathbf{Z}_{nm}^*$, we find

$$\mathbf{Z}_{nm}^* \cdot \sum_{n',m'} (D_{\text{TY}n'm'} \mathbf{Y}_{n'm'} + D_{\text{TX}n'm'} \mathbf{X}_{n'm'} + D_{\text{TZ}n'm'} \mathbf{Z}_{n'm'})$$

$$= \epsilon_0 \varepsilon(r,\theta,\phi) \mathbf{Z}_{nm}^* \cdot \sum_{\nu,\mu} (E_{\text{TY}\nu\mu} \mathbf{Y}_{\nu\mu} + E_{\text{TX}\nu\mu} \mathbf{X}_{\nu\mu} + E_{\text{TZ}\nu\mu} \mathbf{Z}_{\nu\mu}), \qquad (85)$$

and, using the fact that $\mathbf{Z}_{nm}^* \cdot \mathbf{Y}_{n'm'} = \mathbf{Z}_{nm}^* \cdot \mathbf{Y}_{\nu\mu} = 0$, we obtain

$$\sum_{n',m'} (D_{\text{TX}n'm'} \mathbf{Z}_{nm}^* \cdot \mathbf{X}_{n'm'} + D_{\text{TZ}n'm'} \mathbf{Z}_{nm}^* \cdot \mathbf{Z}_{n'm'})$$

$$= \epsilon_0 \varepsilon(r,\theta,\phi) \mathbf{Z}_{nm}^* \cdot \sum_{\nu,\mu} (E_{\text{TX}\nu\mu} \mathbf{X}_{\nu\mu} + E_{\text{TZ}\nu\mu} \mathbf{Z}_{\nu\mu}). \qquad (86)$$

Integrating over the solid angle Ω, we obtain

$$D_{\text{TZ}nm} = \epsilon_0 \sum_{\nu,\mu} \int_0^{4\pi} d\Omega \varepsilon(r,\theta,\phi) \mathbf{Z}_{nm}^* \cdot (E_{\text{TX}\nu\mu} \mathbf{X}_{\nu\mu} + E_{\text{TZ}\nu\mu} \mathbf{Z}_{\nu\mu}). \qquad (87)$$

We then define

$$\varepsilon_{\text{ZX}nm,\nu\mu} \equiv \int_0^{4\pi} d\Omega \varepsilon(r,\theta,\phi) \mathbf{Z}_{nm}^* \cdot \mathbf{X}_{\nu\mu} \equiv \langle \mathbf{Z}_{nm} | \varepsilon \mathbf{X}_{\nu\mu} \rangle, \qquad (88)$$

$$\varepsilon_{\text{ZZ}nm,\nu\mu} \equiv \int_0^{4\pi} d\Omega \varepsilon(r,\theta,\phi) \mathbf{Z}_{nm}^* \cdot \mathbf{Z}_{\nu\mu} \equiv \langle \mathbf{Z}_{nm} | \varepsilon \mathbf{Z}_{\nu\mu} \rangle. \qquad (89)$$

After introducing the simplified subscript notation, we find that Eq. (87) reduces to

$$\frac{1}{\epsilon_0} D_{\text{TZ}P} = \sum_q \varepsilon_{\text{ZX}p,q} E_{\text{TX}q} + \sum_q \varepsilon_{\text{ZZ}p,q} Z_{\text{TX}q}, \qquad (90)$$

which gives the elements of the $\{\varepsilon_{\text{ZX}}\}$ and $\{\varepsilon_{\text{ZZ}}\}$ blocks. It is worth noticing a simplification that comes from the expression of $\mathbf{X}_{nm}$ and $\mathbf{Z}_{nm}$ established in Eqs. (16) and (17). It is straightforward to verify that $\mathbf{X}_{nm}^* \cdot \mathbf{X}_{\nu\mu} = \mathbf{Z}_{nm}^* \cdot \mathbf{Z}_{\nu\mu}$ and that $\mathbf{X}_{nm}^* \cdot \mathbf{Z}_{\nu\mu} = -\mathbf{Z}_{nm}^* \cdot \mathbf{X}_{\nu\mu}$. From Eqs. (82), (83), (88), and (89), we then obtain

$$\{\varepsilon_{\text{XX}}\} = \{\varepsilon_{\text{ZZ}}\}, \quad \{\varepsilon_{\text{XZ}}\} = -\{\varepsilon_{\text{ZX}}\}. \qquad (91)$$

In summary, the matrix $\{\varepsilon^{(\text{T})}\}$ in Eq. (70) will include the following blocks:

$$\{\varepsilon^{(T)}\} = \begin{pmatrix} \{\varepsilon_{YY}\} & 0 & 0 \\ 0 & \{\varepsilon_{XX}\} & \{\varepsilon_{XZ}\} \\ 0 & -\{\varepsilon_{XZ}\} & \{\varepsilon_{XX}\} \end{pmatrix}. \tag{92}$$

Considering Eqs. (76), (82), (83), (88), and (89), we remark that the blocks of the matrix in Eqs. (68) and (69) can be expressed in the concise form $\varepsilon_{ij,nm,\nu\mu} = \langle \mathbf{W}_{nm}^{(i)} | \varepsilon \mathbf{W}_{\nu\mu}^{(j)} \rangle$, with $i, j = 1, 2, 3$ and $\varepsilon_{11} \equiv \varepsilon_{YY}$, $\varepsilon_{23} \equiv \varepsilon_{XZ}$, etc. Furthermore, Eqs. (91) and (92) can be seen as specifying certain interesting properties of these matrix elements.

2. Inverse Rule
Concerning the normal components $\mathbf{D}_N$ and $\mathbf{E}_N$ of $\mathbf{D}$ and $\mathbf{E}$, which are related by

$$\mathbf{D}_N = \epsilon_0 \varepsilon \mathbf{E}_N, \tag{93}$$

we want to find the matrix relation that links their components in the form

$$[\boldsymbol{D}_N] = \epsilon_0 \{\varepsilon^{(N)}\}[\boldsymbol{E}_N], \tag{94}$$

where, for the same reasons as pointed out for $\{\varepsilon^{(T)}\}$, $\{\varepsilon^{(N)}\}$ will have the following block structure:

$$\{\varepsilon^{(N)}\} = \begin{pmatrix} \{\varepsilon_{YY}^{(N)}\} & 0 & 0 \\ 0 & \{\varepsilon_{XX}^{(N)}\} & \{\varepsilon_{XZ}^{(N)}\} \\ 0 & -\{\varepsilon_{XZ}^{(N)}\} & \{\varepsilon_{XX}^{(N)}\} \end{pmatrix}. \tag{95}$$

From Eq. (93), we have $\mathbf{E}_N = (1/\epsilon_0 \varepsilon)\mathbf{D}_N$ where $1/\varepsilon$ is discontinuous while $\mathbf{D}_N$ is continuous. Thus the direct rule has to be used to calculate the components of $\mathbf{E}_N$ from those of $1/\varepsilon$ and $\mathbf{D}_N$. Following the line stated in Subsection 6.A.2 and similar to Eq. (71), we write

$$\sum_{n',m'} (E_{NYn'm'}\mathbf{Y}_{n'm'} + E_{NXn'm'}\mathbf{X}_{n'm'} + E_{NZn'm'}\mathbf{Z}_{n'm'})$$

$$= \frac{1}{\epsilon_0 \varepsilon(r,\theta,\phi)} \sum_{\nu,\mu} (D_{NY\nu\mu}\mathbf{Y}_{\nu\mu} + D_{NX\nu\mu}\mathbf{X}_{\nu\mu} + D_{NZ\nu\mu}\mathbf{Z}_{\nu\mu}). \tag{96}$$

We continue the process as we did for obtaining Eqs. (76) and (77); defining

$$\left(\frac{1}{\varepsilon}\right)_{YYnm;\nu\mu} \equiv \int_0^{4\pi} d\Omega \frac{1}{\varepsilon(r,\theta,\phi)} \mathbf{Y}_{nm}^* \cdot \mathbf{Y}_{\nu\mu} \equiv \left\langle \mathbf{Y}_{nm} \Big| \frac{1}{\varepsilon} \mathbf{Y}_{\nu\mu} \right\rangle, \tag{97}$$

we obtain

$$\epsilon_0 E_{NYnm} = \sum_{\nu\mu} \left(\frac{1}{\varepsilon}\right)_{YYnm,\nu\mu} D_{NY\nu\mu} \tag{98}$$

or, with the single subscript,

$$\epsilon_0 E_{NYp} = \sum_q \left(\frac{1}{\varepsilon}\right)_{YYp,q} D_{NYq}. \tag{99}$$

Inversing this relation, we obtain an equation identical to the inverse rule in Eq. (64) that we established for scalar functions:

$$D_{NYp} = \epsilon_0 \sum_q \left[\left(\frac{1}{\varepsilon}\right)_{YY}^{-1}\right]_{p,q} E_{NYq}, \tag{100}$$

which is to be expected, since D_{NYq} depend only on E_{NYq} and thus behave like scalars. Equation (100) provides the first block in $\{\varepsilon^{(N)}\}$:

$$\{\varepsilon_{YY}^{(N)}\} = \left(\left(\frac{1}{\varepsilon}\right)_{YY}\right)^{-1}. \tag{101}$$

Things are a bit more complicated for the other blocks, since both $[D_{NX}]$ and $[D_{NZ}]$ depend on $[E_{NX}]$ and $[E_{NZ}]$. But, following the same lines, we obtain

$$\epsilon_0 E_{NXnm} = \sum_{\nu,\mu} \left(\frac{1}{\varepsilon}\right)_{XXnm,\nu\mu} D_{NX\nu\mu} + \sum_{\nu,\mu} \left(\frac{1}{\varepsilon}\right)_{XZnm,\nu\mu} D_{NZ\nu\mu}, \tag{102}$$

where

$$\left(\frac{1}{\varepsilon}\right)_{XXnm,\nu\mu} \equiv \left\langle \mathbf{X}_{nm} \Big| \frac{1}{\varepsilon} \mathbf{X}_{\nu\mu} \right\rangle, \tag{103}$$

$$\left(\frac{1}{\varepsilon}\right)_{XZnm,\nu\mu} \equiv \left\langle \mathbf{X}_{nm} \Big| \frac{1}{\varepsilon} \mathbf{Z}_{\nu\mu} \right\rangle. \tag{104}$$

Put in matrix form, Eq. (102) reads as

$$\epsilon_0[E_{NX}] = \left(\frac{1}{\varepsilon}\right)_{XX} [D_{NX}] + \left(\frac{1}{\varepsilon}\right)_{XZ} [D_{NZ}], \tag{105}$$

which, with the help of Eq. (95), gives

$$\epsilon_0[E_{NZ}] = -\left(\frac{1}{\varepsilon}\right)_{XZ} [D_{NX}] + \left(\frac{1}{\varepsilon}\right)_{XX} [D_{NZ}]. \tag{106}$$

Inverting Eqs. (105) and (106) leads to

$$\begin{bmatrix} [D_{NX}] \\ [D_{NZ}] \end{bmatrix} = \epsilon_0 \begin{pmatrix} \left(\frac{1}{\varepsilon}\right)_{XX} & \left(\frac{1}{\varepsilon}\right)_{XZ} \\ -\left(\frac{1}{\varepsilon}\right)_{XZ} & \left(\frac{1}{\varepsilon}\right)_{XX} \end{pmatrix}^{-1} \begin{bmatrix} [E_{NX}] \\ [E_{NZ}] \end{bmatrix}, \tag{107}$$

and Eq. (95) reads as

$$\{\varepsilon^{(N)}\} = \begin{pmatrix} \{\varepsilon_{YY}^{(N)}\} & 0 & 0 \\ 0 & \{\varepsilon_{XX}^{(N)}\} & \{\varepsilon_{XZ}^{(N)}\} \\ 0 & -\{\varepsilon_{XZ}^{(N)}\} & \{\varepsilon_{XX}^{(N)}\} \end{pmatrix}$$

$$= \begin{pmatrix} \left(\left(\frac{1}{\varepsilon}\right)_{YY}\right)^{-1} & 0 & 0 \\ 0 & \begin{pmatrix} \left(\frac{1}{\varepsilon}\right)_{XX} & \left(\frac{1}{\varepsilon}\right)_{XZ} \\ -\left(\frac{1}{\varepsilon}\right)_{XZ} & \left(\frac{1}{\varepsilon}\right)_{XX} \end{pmatrix}^{-1} & \end{pmatrix}. \tag{108}$$

Equations (94) and (108), together with Eqs. (97), (103),

and (104), state the inverse rule that applies to the vectorial functions **D** and **E** represented on the basis of VSHs.

The determination of the various blocks of $\{\varepsilon^{(T)}\}$ and $\{\varepsilon^{(N)}\}$ requires computing integrals involving scalar products of two VSHs, as shown in Eqs. (82) and (83), for example. The introduction of the Gaunt coefficients[23] developed by theoreticians working in quantum mechanics gives analytic expressions for these integrals. This is explained in Appendix D.

C. Total Field Representation: Fast Numerical Factorization Applied to Spherical Harmonic Basis

The concept of normal and tangential components of **E** or **D** is defined only on a surface S, whereas the direct and inverse rules have to be applied into the entire modulated region in order to calculate the **D** components on the VSHs. The basic idea of what was first called the fast Fourier factorization (FFF) in grating theory[16,20] consisted of extending the definition of $\hat{\mathbf{N}}$ stated by Eq. (26) toward the entire modulated area by simply stating that

$$\forall r \in [R_1, R_2], \quad \hat{\mathbf{N}}(r, \theta, \phi) = \left.\frac{\mathbf{grad}\, f}{\|\mathbf{grad}\, f\|}\right|_{f=0}. \quad (109)$$

Equation (109) allows one to derive a normal component $\mathbf{E}_N$ of the field E via

$$\mathbf{E}_N = \hat{\mathbf{N}}(\hat{\mathbf{N}} \cdot \mathbf{E}), \quad (110)$$

and its tangential component, $\mathbf{E}_T$, is given by

$$\mathbf{E}_T = \mathbf{E} - \mathbf{E}_N = \mathbf{E} - \hat{\mathbf{N}}(\hat{\mathbf{N}} \cdot \mathbf{E}); \quad (111)$$

these definitions hold in the entire modulated area. Dealing with an isotropic medium then leads to

$$\mathbf{D} = \epsilon_0 \varepsilon \mathbf{E} = \epsilon_0 \varepsilon (\mathbf{E}_T + \mathbf{E}_N) = \epsilon_0 \varepsilon (\mathbf{E} - \hat{\mathbf{N}}(\hat{\mathbf{N}} \cdot \mathbf{E})) + \epsilon_0 \varepsilon \hat{\mathbf{N}}(\hat{\mathbf{N}} \cdot \mathbf{E}). \quad (112)$$

Expressing the components of $\mathbf{D}_T = \epsilon_0 \varepsilon (\mathbf{E} - \hat{\mathbf{N}}(\hat{\mathbf{N}} \cdot \mathbf{E}))$ implies the direct rule that requires $\{\varepsilon^{(T)}\}$, whereas the components of $\mathbf{D}_N = \epsilon_0 \varepsilon \hat{\mathbf{N}}(\hat{\mathbf{N}} \cdot \mathbf{E})$ requires the inverse rule and thus requires $\{\varepsilon^{(N)}\}$. Introducing the matrix $\{\hat{\mathbf{N}}\hat{\mathbf{N}}\}$, with nine blocks $\{N_i N_j\}$, with i and j equal to Y, X, and Z, which relates $[E]$ to $[E_N]$, we thus have

$$\frac{1}{\epsilon_0}[D] = \{\varepsilon^{(T)}\}[E_T] + \{\varepsilon^{(N)}\}[E_N]$$

$$= (\{\varepsilon^{(T)}\}(1 - \{\hat{\mathbf{N}}\hat{\mathbf{N}}\}) + \{\varepsilon^{(N)}\}\{\hat{\mathbf{N}}\hat{\mathbf{N}}\})[E]. \quad (113)$$

As a result, matrix Q_ε defined in Eq. (44) reads

$$Q_\varepsilon = \{\varepsilon^{(T)}\} + (\{\varepsilon^{(N)}\} - \{\varepsilon^{(T)}\})\{\hat{\mathbf{N}}\hat{\mathbf{N}}\},$$

an equation that has to be interpreted in block form as

$$Q_{\varepsilon ij} = \{\varepsilon_{ij}^{(T)}\} + \sum_k (\{\varepsilon_{ik}^{(N)}\} - \{\varepsilon_{ik}^{(T)}\})\{\hat{\mathbf{N}}_k \hat{\mathbf{N}}_j\}. \quad (114)$$

In order to state explicitly the various blocks, we first introduce the matrix $\Delta \equiv \{\varepsilon^{(N)}\} - \{\varepsilon^{(T)}\}$, with blocks $\Delta_{ij} = \{\varepsilon_{ij}^{(N)}\} - \{\varepsilon_{ij}^{(T)}\}$, which reads

$$\Delta = \begin{pmatrix} \Delta_{YY} & 0 & 0 \\ 0 & \Delta_{XX} & \Delta_{XZ} \\ 0 & -\Delta_{XZ} & \Delta_{XX} \end{pmatrix}. \quad (115)$$

Thus, finally, Q_ε has the following blocks:

$$Q_{\varepsilon YY} = \Delta_{YY}\{N_Y N_Y\} + \{\varepsilon_{YY}\}, \quad Q_{\varepsilon YX} = \Delta_{YY}\{N_Y N_X\},$$

$$Q_{\varepsilon YZ} = \Delta_{YY}\{N_Y N_Z\},$$

$$Q_{\varepsilon XY} = \Delta_{XX}\{N_X N_Y\} + \Delta_{XZ}\{N_Z N_Y\},$$

$$Q_{\varepsilon XX} = \Delta_{XX}\{N_X N_X\} + \Delta_{XZ}\{N_Z N_X\} + \{\varepsilon_{XX}\},$$

$$Q_{\varepsilon XZ} = \Delta_{XX}\{N_X N_Z\} + \Delta_{XZ}\{N_Z N_Z\} + \{\varepsilon_{XZ}\},$$

$$Q_{\varepsilon ZY} = \Delta_{XX}\{N_Z N_Y\} - \Delta_{XZ}\{N_X N_Y\},$$

$$Q_{\varepsilon ZX} = \Delta_{XX}\{N_Z N_X\} - \Delta_{XZ}\{N_X N_X\} - \{\varepsilon_{XZ}\},$$

$$Q_{\varepsilon ZZ} = \Delta_{XX}\{N_Z N_Z\} - \Delta_{XZ}\{N_X N_Z\} + \{\varepsilon_{XX}\}. \quad (116)$$

The differential set written in Eqs. (55) and (56) with matrix Q_ε given by Eqs. (116) is the fast converging formulation of the Maxwell equations projected onto a truncated spherical harmonic basis, and the way of deriving them is the fast numerical factorization (FNF) in spherical coordinates.

7. FIELD EXPANSIONS OUTSIDE THE MODULATED REGION

Inside a homogeneous isotropic medium characterized by the relative electric and magnetic permitivities, ε_j and μ_j, the two Maxwell curl equations result in a second-order propagation equation involving the electric field:

$$\mathbf{curl}(\mathbf{curl}\,\mathbf{E}) - (\omega/c)^2 \varepsilon_j \mu_j \mathbf{E} = \mathbf{0}. \quad (117)$$

In a source-free medium, div $\mathbf{E} = \mathbf{0}$, and Eq. (117) leads to the vector Helmholtz equation:

$$\Delta \mathbf{E} + k_j^2 \mathbf{E} = \mathbf{0}, \quad (118)$$

where

$$k_j^2 = (\omega/c)^2 \varepsilon_j \mu_j. \quad (119)$$

Classical textbooks[1] explain how to construct the general solution of Eq. (117). Searching for a general vectorial solution of the form $\mathbf{M} \propto \mathbf{curl}(r\psi)$ and expressing the Laplacian operator in spherical coordinates, we find that ψ is a solution of the scalar Helmholtz equation:

$$\frac{1}{r^2}\frac{\partial}{\partial r}\left(r^2 \frac{\partial \psi}{\partial r}\right) + \frac{1}{r^2 \sin \theta}\frac{\partial}{\partial \theta}\left(\sin \theta \frac{\partial \psi}{\partial \theta}\right) + \frac{1}{r^2 \sin^2 \theta}\frac{\partial^2 \psi}{\partial \phi^2} + k_j^2 \psi$$

$$= 0. \quad (120)$$

Expressing ψ on the basis of scalar spherical harmonics,

$$\psi(r, \theta, \phi) = \sum_{n,m} R(r) Y_{nm}(\theta, \phi), \quad (121)$$

we find that $R(r)$ verifies

$$\frac{\mathrm{d}}{\mathrm{d}r}\left(r^2\frac{\mathrm{d}R}{\mathrm{d}r}\right)+[k_j^2r^2-n(n+1)]R(r)=0. \qquad (122)$$

Introducing the dimensionless variable $\rho\equiv k_jr$ and the function $\check{R}\equiv R\sqrt{\rho}$ we find that Eq. (122) leads to

$$\frac{\mathrm{d}^2\check{R}}{\mathrm{d}^2\rho}+\frac{1}{\rho}\frac{\mathrm{d}\check{R}}{\mathrm{d}\rho}+\left[1-\frac{\left(n+\frac{1}{2}\right)^2}{\rho^2}\right]\check{R}(\rho)=0. \qquad (123)$$

Equation (123) is the Bessel equation with half-integer order $n+1/2$; its independent solutions are thus the half-integer Bessel functions $\check{R}=J_{n+1/2}(\rho)$ and $Y_{n+1/2}(\rho)$ or Hankel functions $\check{R}=H_{n+1/2}^+(\rho)$ and $H_{n+1/2}^-(\rho)$. Consequently, linearly independent solutions of Eq. (122) are called spherical Bessel functions and are defined by

$$R(r)=j_n(k_jr)\equiv\sqrt{\frac{\pi}{2k_jr}}J_{n+1/2}(k_jr),$$
$$\qquad (124)$$
$$R(r)=y_n(k_jr)\equiv\sqrt{\frac{\pi}{2k_jr}}Y_{n+1/2}(k_jr),$$

where the factor $\sqrt{\pi/2}$ is introduced for convenience.

Any combination of $j_n(\rho)$ and $y_n(\rho)$ is also a solution to Eq. (122). Two such combinations deserve special attention, which are called spherical Bessel functions of the third and fourth kind, or spherical Hankel functions:

$$h_n^+(\rho)=j_n(\rho)+iy_n(\rho),$$

$$h_n^-(\rho)=j_n(\rho)-iy_n(\rho). \qquad (125)$$

It will be useful to designate one of the four spherical Bessel functions by the generic notation $z_n(k_jr)$. Following Eqs. (121)–(125), ψ can be expressed as a series of elementary functions ψ_{nm}, with

$$\psi_{nm}(r,\theta,\varphi)=z_n(k_jr)Y_{nm}(\theta,\phi). \qquad (126)$$

Each ψ_{nm} can be used to generate a solution to Eq. (117) (frequently called a vector spherical wave function):

$$\mathbf{M}_{nm}\equiv\frac{\mathbf{curl}(\mathrm{r}\psi_{nm})}{\sqrt{n(n+1)}}. \qquad (127)$$

From $\mathbf{M}_{nm}$, a second solution to Eq. (117) can be constructed[1] by taking $\mathbf{N}_{nm}\equiv\mathbf{curl}\,\mathbf{M}_{nm}/k_j$. Classical textbooks[1] then establish that one can write

$$\mathbf{M}_{nm}(\rho,\theta,\phi)=z_n(\rho)\mathbf{X}_{nm}(\theta,\phi), \qquad (128)$$

$$\mathbf{N}_{nm}(\rho,\theta,\phi)=\frac{1}{\rho}\{\sqrt{n(n+1)}z_n(\rho)\mathbf{Y}_{nm}(\theta,\phi)$$
$$+[\rho z_n(\rho)]'\mathbf{Z}_{nm}(\theta,\phi)\}, \qquad (129)$$

where the prime here, and from here on, is a shorthand for expressing derivatives with respect to the argument of the Bessel function; i.e., explicitly we have

$$f'(x_0)\equiv\left.\frac{\mathrm{d}}{\mathrm{d}x}f(x)\right|_{x=x_0}. \qquad (130)$$

From Eq. (128) and (129), it is established that $\mathbf{N}_{nm}(\rho)$ are orthogonal to $\mathbf{M}_{nm}(\rho)$ and are thus linearly independent. As a result, the general solution of the propagation equation inside a homogeneous medium, Eq. (117), can be written as

$$\mathbf{E}(\mathbf{r})=\sum_{n,m}\left\{A_{h,nm}^{(j)}j_n(k_jr)\mathbf{X}_{nm}+\frac{A_{e,nm}^{(j)}}{k_jr}\right.$$
$$\times[\sqrt{n(n+1)}j_n(k_jr)\mathbf{Y}_{nm}+(k_jrj_n(k_jr))'\mathbf{Z}_{nm}]\Big\}$$
$$+\sum_{n,m}\left\{B_{h,nm}^{(j)}h_n^+(k_jr)\mathbf{X}_{nm}+\frac{B_{e,nm}^{(j)}}{k_jr}\right.$$
$$\times[\sqrt{n(n+1)}h_n^+(k_jr)\mathbf{Y}_{nm}+(k_jrh_n^+(k_jr))'\mathbf{Z}_{nm}]\Big\}.$$
$$\qquad (131)$$

The coefficients $A_{h,nm}^{(j)}$, $A_{e,nm}^{(j)}$, and $B_{h,nm}^{(j)}$, $B_{e,nm}^{(j)}$, play in the 3D scattering problem the same role as Rayleigh coefficients in grating theory.[20] The choice made among the $z_n(k_jr)$ functions allows one to distinguish the terms that remain bounded at the coordinate origin (corresponding to $A_{h,nm}^{(j)}$, $A_{e,nm}^{(j)}$,) from terms that correspond to outgoing waves or waves decaying at infinity (corresponding to $B_{h,nm}^{(j)}$, $B_{e,nm}^{(j)}$,).

The general expression for $\mathbf{E}$ in Eq. (131) is applicable to the inner region ($r\leq R_1$) and the outer region ($r>R_2$). For $r\leq R_1$, in order to obtain a solution that remains bounded, we impose

$$B_{e,nm}^{(1)}=0=B_{h,nm}^{(1)} \qquad \forall\,n,m. \qquad (132)$$

Let us introduce the Ricatti–Bessel functions, $\psi_n(z)$ and $\xi_n(z)$, defined in Appendix E, so that Eq. (131) for $r\leq R_1$ reduces to

$$\mathbf{E}=\sum_{n,m}\left\{A_{h,nm}^{(1)}j_n(k_1r)\mathbf{X}_{nm}+\frac{A_{e,nm}^{(1)}}{k_1r}\right.$$
$$\times[\sqrt{n(n+1)}j_n(k_1r)\mathbf{Y}_{nm}+\psi_n'(k_1r)\mathbf{Z}_{nm}]\Big\}. \qquad (133)$$

On the other hand, if $r>R_2$, the field must be the sum of the diffracted field, expressed by the second summation in Eq. (131), and the incident field. This means that the first summation in Eq. (131) must here reduce to the incident field, with coefficients denoted $A_{h,nm}^{\mathrm{i}}$, and $A_{e,nm}^{\mathrm{i}}$. Expressed in terms of the polarization vector, $\hat{e}_{\mathrm{i}}$, these coefficients for an incident plane wave $\mathbf{E}_{\mathrm{i}}=\exp(i\mathbf{k}_M\cdot\mathbf{r})\hat{e}_{\mathrm{i}}$ have analytic expressions[2,6,24]:

$$A_{h,nm}^{\mathrm{i}}=4\pi i^n\mathbf{X}_{nm}^*(\theta_{\mathrm{i}},\phi_{\mathrm{i}})\cdot\hat{e}_{\mathrm{i}}, \qquad (134)$$

$$A_{e,nm}^{\mathrm{i}}=4\pi i^{n-1}\mathbf{Z}_{nm}^*(\theta_{\mathrm{i}},\phi_{\mathrm{i}})\cdot\hat{e}_{\mathrm{i}}, \qquad (135)$$

where θ_{i} and ϕ_{i} specify the direction of the incident wave, $\theta_{\mathrm{i}}=|(\hat{z},\mathbf{k}_M)|$, with $\theta_{\mathrm{i}}\in[0,\pi]$, and $\phi_{\mathrm{i}}=(\hat{x},\mathbf{k}_{Mt})$, where $\mathbf{k}_{Mt}$ is the projection of $\mathbf{k}_M$ on the xOy plane while $\hat{z}$ and $\hat{x}$ are the unit vectors of the z and x axes. It could be useful to notice that in order to be able to analyze a circularly polarized incident plane wave, we allow $\hat{e}_{\mathrm{i}}$ to be a complex

unit vector. Defining $k_M = (\omega/c)\sqrt{\varepsilon_M \mu_M}$, we find that the field for $r \geqslant R_2$ reads as

$$
\mathbf{E} = \sum_{n,m} \left\{ A^{\mathrm{i}}_{h,nm} j_n(k_M r)\mathbf{X}_{nm} + \frac{A^{\mathrm{i}}_{e,nm}}{k_M r} \times [\sqrt{n(n+1)} j_n(k_M r)\mathbf{Y}_{nm} \right.
$$
$$
\left. + \psi'_n(k_M r)\mathbf{Z}_{nm}] \right\} + \sum_{n,m} \left\{ B^{(M)}_{h,nm} h^+_n(k_M r)\mathbf{X}_{nm} + \frac{B^{(M)}_{e,nm}}{k_M r} \right.
$$
$$
\left. \times [\sqrt{n(n+1)} h^+_n(k_M r)\mathbf{Y}_{nm} + \xi'_n(k_M r)\mathbf{Z}_{nm}] \right\}. \tag{136}
$$

8. RESOLUTION OF THE BOUNDARY-VALUE PROBLEM

The problem is now reduced to the numerical integration on the $[R_1, R_2]$ interval of the first-order differential set stated by Eqs. (55), (56), and (114)–(116) in such a way that the numerical solution matches the boundary conditions stated by Eqs. (133) and (136), concerning both the unknown functions and their derivatives. When dealing with objects far different from a sphere, the distance $R_2 - R_1$ can be large enough so that numerical overflows and instabilities may appear. It is then safer to make a partition of the modulated region and to use the S-matrix propagation algorithm.

A. Partition of the Modulated Area and S-Matrix Propagation Algorithm

We follow a process similar to that performed in grating theory.[20] As illustrated in Fig. 2 for an example with $M = 6$, the modulated region with thickness $R_2 - R_1$ is cut into $M - 1$ slices with equal thicknesses at radial distances $r_j = R_1 + [(R_2 - R_1)/(M-2)](j-1)$, so that $r_1 = R_1$ and $r_{M-1} = R_2$. With this partition, a region labeled by the subscript j lies between r_{j-1} and r_j, region 1 lying between 0 and R_1, while region M extends from $r_{M-1}(\equiv R_2)$ toward infinity. At each distance $r_j(j > 1)$, we introduce infinitely thin slices of a medium with electric and magnetic permittivity ε_M and μ_M. In each of these infinitely thin homogeneous regions, the general expansion in Eq. (131) fully defines the field, provided that k_j is taken equal to k_M, that

Fig. 2.   Example of the partition of the modulated region in which $M = 6$, and an illustration of the notation for the coefficients appearing in Eq. (131) used inside the various homogeneous regions.

$r = r_j$, and that we use primed coefficients (see Ref. 20 and the following paragraph for a discussion of the primed coefficients). We thus consider a column matrix $V^{(j)}$ constructed with the Z and X components of the impinging and outgoing waves, defined by

$$
[V^{(j)}] = \begin{bmatrix} \vdots \\ A'^{(j)}_{e,p} \psi'_n(k_M r_j)/(k_M r_j) \\ \vdots \\ A'^{(j)}_{h,p} j_n(k_M r_j) \\ \vdots \\ B'^{(j)}_{e,p} \xi'_n(k_M r_j)/(k_M r_j) \\ \vdots \\ B'^{(j)}_{h,p} h^+_n(k_M r_j) \\ \vdots \end{bmatrix}, \tag{137}
$$

where p is related to (n,m) through Eq. (23). One should note that the prime on the coefficients serves as a reminder that the field is developed inside one of the infinitesimal homogeneous slices within the modulated region (the prime on the coefficients does not stand for the derivative). Inside the circumscribed sphere, the field is developed in a truly homogeneous region and

$$
A'^{(1)}_{e,p} = A^{(1)}_{e,p}; \quad A'^{(1)}_{h,p} = A^{(1)}_{h,p}; \quad B'^{(1)}_{e,p} = B^{(1)}_{e,p}; \quad B'^{(1)}_{h,p} = B^{(1)}_{h,p}, \tag{138}
$$

while

$$
A'^{(M-1)}_{e,p} = A^{(M)}_{e,p}; \quad A'^{(M-1)}_{h,p} = A^{(M)}_{h,p}; \quad B'^{(M-1)}_{e,p} = B^{(M)}_{e,p}; \tag{139}
$$

$$
B'^{(M-1)}_{h,p} = B^{(M)}_{h,p}.
$$

Since we are working in linear optics, there exists a linear relation between the field at ordinate r_{j-1} and the field at ordinate r_j. We thus have

$$
[V^{(j)}] = T^{(j)}[V^{(j-1)}], \tag{140}
$$

a relation that defines the transmission matrix, $T^{(j)}$, of the region (j) (not to be confused with the transfer matrix of the object).

When the four-block S matrix of the stack including j regions (not to be confused with the S matrix of the jth region nor with the S matrix of scattering theory!) is defined by
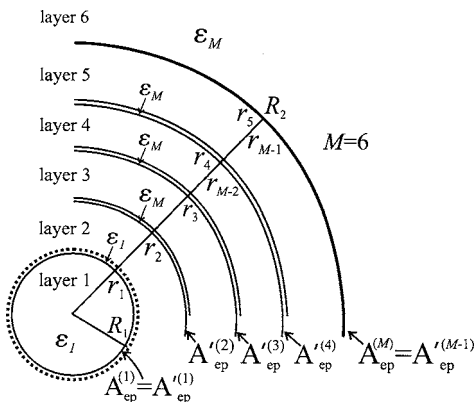
$$
\begin{bmatrix}
\vdots \\
B'^{(j)}_{e,p}\xi'_n(k_Mr_j)/(k_Mr_j) \\
\vdots \\
B'^{(j)}_{h,p}h^+_n(k_Mr_j) \\
\vdots \\
\text{---} \\
\vdots \\
A^{(1)}_{e,p}\psi'_n(k_1r_1)/(k_1r_1) \\
\vdots \\
A^{(1)}_{h,p}j_n(k_1r_1) \\
\vdots
\end{bmatrix}
=
\left(
\begin{array}{c|c}
S^{(j)}_{11} & S^{(j)}_{12} \\
\hline
S^{(j)}_{21} & S^{(j)}_{22}
\end{array}
\right)
$$

$$
\times
\begin{bmatrix}
\vdots \\
B^{(1)}_{e,q}\xi'_n(k_1r_1)/(k_1r_1) \\
\vdots \\
B^{(1)}_{h,q}h^+_n(k_1r_1) \\
\vdots \\
\text{---} \\
\vdots \\
A'^{(j)}_{e,q}\psi'_n(k_Mr_j)/(k_Mr_j) \\
\vdots \\
A'^{(j)}_{h,q}j_n(k_Mr_j) \\
\vdots
\end{bmatrix},
\tag{141}
$$

the S-matrix propagation algorithm[14,20] reads as

$$
S^{(j)}_{12} = (T^{(j)}_{21} + T^{(j)}_{22}S^{(j-1)}_{12})Z^{(j-1)},
\tag{142}
$$

$$
S^{(j)}_{22} = S^{(j-1)}_{22}Z^{(j-1)},
\tag{143}
$$

where

$$
Z^{(j-1)} = (T^{(j)}_{11} + T^{(j)}_{12}S^{(j-1)}_{12})^{-1}.
\tag{144}
$$

The recursive evaluation for the $S^{(j)}$ matrices is started[20] by taking $S^{(1)}_{12} = 0$ and $S^{(1)}_{22} = 1$, which means that when there is no boundary, no reflection occurs, and the transmission is unity. Each recursive step requires the corresponding $T^{(j)}$ matrix, which is determined through the following shooting method.

B. Shooting Method: Determination of the $T^{(j)}$ Matrices
Considering the jth region, we have to integrate numerically, from r_{j-1} to r_j, the differential set stated by Eqs. (55), (56), and (116) in order to construct the matrix $T^{(j)}$. However, Eq. (55) deals with the column $[F]$, while $T^{(j)}$ links columns $[V^{(j)}]$. The first step is to express the link between these two columns via a matrix $\Psi(r)$.

Indeed, at any value of $r_j(j \neq 1)$, from Eq. (131) we have

$$
[E_X]_p = A'^{(j)}_{h,p}j_n(k_Mr_j) + B'^{(j)}_{h,p}h^+_n(k_Mr_j),
\tag{145}
$$

$$
[E_Z]_p = \frac{1}{k_Mr_j}\{A'^{(j)}_{e,p}\psi'_n(k_Mr_j) + B'^{(j)}_{e,p}\xi'_n(k_Mr_j)\}.
\tag{146}
$$

Equations (38), (54), and (131) yield

$$
[\tilde{H}_X]_p = \frac{1}{i\omega\mu_M\sqrt{\epsilon_0\mu_0}}\left\{\frac{n(n+1)}{k_Mr_j^2}[A'^{(j)}_{e,p}j_n(k_Mr_j) + B'^{(j)}_{e,p}h^+_n(k_Mr_j)] \right.
$$
$$
- \frac{1}{k_Mr_j^2}[A'^{(j)}_{e,p}\psi'_n(k_Mr_j) + B'^{(j)}_{e,p}\xi'_n(k_Mr_j)]
$$
$$
\left. - \frac{d}{dr}\left[A'^{(j)}_{e,p}\frac{\psi'_n(k_Mr_j)}{k_Mr_j} + B'^{(j)}_{e,p}\frac{\xi'_n(k_Mr_j)}{k_Mr_j}\right]\right\}
$$
$$
= \frac{1}{i\omega\mu_M\sqrt{\epsilon_0\mu_0}}\frac{1}{k_Mr_j^2}\left\{n(n+1)[A'^{(j)}_{e,p}j_n(k_Mr_j)\right.
$$
$$
+ B'^{(j)}_{e,p}h^+_n(k_Mr_j)] - [A'^{(j)}_{e,p}(k_Mr_j)^2j'_n(k_Mr_j)
$$
$$
\left. + B'^{(j)}_{e,p}(k_Mr_j)^2(h^+_n)'(k_Mr_j)]'\right\},
\tag{147}
$$

where we have used the relation

$$
\rho^2\frac{d}{d\rho}\left(\frac{1}{\rho}(\rho z_n(\rho))'\right) + (\rho z_n(\rho))' = \frac{d}{d\rho}(\rho^2z'_n(\rho)).
\tag{148}
$$

Using now the fact that the spherical Bessel functions satisfy Eq. (122) shows us that

$$
n(n+1)z_n(\rho) - \frac{d}{d\rho}(\rho^2z'_n(\rho)) = \rho^2z_n(\rho).
$$

One obtains finally the compact result:

$$
[\tilde{H}_X]_p = -i\sqrt{\frac{\epsilon_M}{\mu_M}}[A'^{(j)}_{e,p}j_n(k_Mr_j) + B'^{(j)}_{e,p}h^+_n(k_Mr_j)].
\tag{149}
$$

Moreover, with Eqs. (39), (54), and (131) one finds

$$
[\tilde{H}_Z]_p = -i\sqrt{\frac{\epsilon_M}{\mu_M}}\frac{1}{k_Mr_j}\{A'^{(j)}_{h,p}\psi'_n(k_Mr_j) + B'^{(j)}_{h,p}\xi'_n(k_Mr_j)\}.
\tag{150}
$$

As a result, we obtain

$$
[F^{(j)}] \equiv
\begin{bmatrix}
[E_X^{(j)}] \\
[E_Z^{(j)}] \\
[\tilde{H}_X^{(j)}] \\
[\tilde{H}_Z^{(j)}]
\end{bmatrix}
\equiv \Psi^{(j)}
\begin{bmatrix}
\vdots \\
A'^{(j)}_{e,p}\psi'_n(k_Mr_j)/(k_Mr_j) \\
\vdots \\
A'^{(j)}_{h,p}j_n(k_Mr_j) \\
\vdots \\
B'^{(j)}_{e,p}\xi'_n(k_Mr_j)/(k_Mr_j) \\
\vdots \\
B'^{(j)}_{h,p}h^+_n(k_Mr_j) \\
\vdots
\end{bmatrix}
= \Psi^{(j)}[V^{(j)}],
\tag{151}
$$

which entails

$$\Psi^{(j)} = \begin{pmatrix} 0 & 1 & 0 & 1 \\ 1 & 0 & 1 & 0 \\ -i\sqrt{\dfrac{\varepsilon_M}{\mu_M}}/p^{(j)} & 0 & -i\sqrt{\dfrac{\varepsilon_M}{\mu_M}}/q^{(j)} & 0 \\ 0 & -i\sqrt{\dfrac{\varepsilon_M}{\mu_M}}p^{(j)} & 0 & -i\sqrt{\dfrac{\varepsilon_M}{\mu_M}}q^{(j)} \end{pmatrix}, \tag{152}$$

with

$$p_{p,q}^{(j)} \equiv \delta_{p,q} \left. \frac{\psi_n'(z)}{\psi_n(z)} \right|_{z=k_M r_j}, \quad q_{p,q}^{(j)} \equiv \delta_{p,q} \left. \frac{\xi_n'(z)}{\xi_n(z)} \right|_{z=k_M r_j}. \tag{153}$$

The calculation of the $p_{p,q}^{(j)}$ and $q_{p,q}^{(j)}$ matrix elements is simplified by invoking the recurrence relations of the Ricatti–Bessel functions as shown in Appendix E.

The matrix $\Psi^{(j-1)}$ (at r_{j-1}) links the column $[V^{(j-1)}]$ to the field $[F]$, noted $[F^{(j-1)}]$, and, since the columns $[V^{(j)}]$ have $4 \times (n_{max}+1)^2$ components, we perform successively $4 \times (n_{max}+1)^2$ numerical integrations with linearly independent columns $[V^{(j-1)}]_i$, $i \in [1, 4(n_{max}+1)^2]$, by taking their elements as $V_{p,i}^{(j-1)} = \delta_{pi}$. As a result, these vectors form a square matrix $[\hat{V}^{(j-1)}]$ with

$$[\hat{V}^{(j-1)}] = 1. \tag{154}$$

We thus take, for initiating the integration, columns $[F^{(j-1)}(r_{j-1})]_i = \Psi^{(j-1)}[V^{(j-1)}]_i$, which form a square matrix $[\hat{F}(r_{j-1})] = \Psi^{(j-1)}1 = \Psi^{(j-1)}$. Performing the numerical integration with a standard subroutine leads to numerical values at $r = r_j$, which form a matrix named $[\hat{F}_{int}(r_j)]$. Inverting the matrix relation of Eq. (151), $[F^{(j)}] = \Psi^{(j)}[V^{(j)}]$, we then deduce

$$[\hat{V}_{int}^{(j)}] = [\Psi^{(j)}(r_j)]^{-1}[\hat{F}_{int}(r_j)], \tag{155}$$

which, thanks to Eq. (154), results in

$$[\hat{V}_{int}^{(j)}] = [\Psi^{(j)}(r_j)]^{-1}[\hat{F}_{int}(r_j)][\hat{V}^{(j-1)}]. \tag{156}$$

Comparison with Eq. (140) shows that

$$T^{(j)} = [\Psi^{(j)}(r_j)]^{-1}[\hat{F}_{int}(r_j)]. \tag{157}$$

Thus the shooting method provides the transmission matrix at the end of the integration process.

C. Determination of the Diffracted Field

Once the $T^{(j)}$ matrices for each region have been calculated, the S-matrix propagation algorithm given by Eqs. (142)–(144) is performed in order to find the S matrix of the total modulated area $S^{(M-1)}$. Using a block notation that includes the various Bessel and Ricatti functions, we thus obtain

$$\begin{bmatrix} [B_e'^{(M-1)}] \\ [B_h'^{(M-1)}] \\ [A_e^{(1)}] \\ [A_h^{(1)}] \end{bmatrix} = S^{(M-1)} \begin{bmatrix} [B_e^{(1)}] \\ [B_h^{(1)}] \\ [A_e'^{(M-1)}] \\ [A_h'^{(M-1)}] \end{bmatrix}, \tag{158}$$

and, from Eq. (139), we obtain

$$\begin{bmatrix} [B_e^{(M)}] \\ [B_h^{(M)}] \\ [A_e^{(1)}] \\ [A_h^{(1)}] \end{bmatrix} = \left(\begin{array}{c|c} S_{11} & S_{12} \\ \hline S_{21} & S_{22} \end{array} \right)^{(M-1)} \begin{bmatrix} [B_e^{(1)}] \\ [B_h^{(1)}] \\ [A_e^{(M)}] \\ [A_h^{(M)}] \end{bmatrix}. \tag{159}$$

Recalling that inside the sphere S_1 the field must remain bounded, especially at $r=0$, we must state $B_{eq}^{(1)}=0=B_{hq}^{(1)} \forall q$. Thus Eq. (159) gives the diffracted field through

$$\begin{bmatrix} [B_e^{(M)}] \\ [B_h^{(M)}] \end{bmatrix} = S_{12}^{(M-1)} \begin{bmatrix} [A_e^{(M)}] \\ [A_h^{(M)}] \end{bmatrix}, \tag{160}$$

where $B_{eq}^{(M)}$, $B_{hq}^{(M)}$ will be called the scattering coefficients and the union of the two $(n_{max}+1)^2$ column matrices $[B_e^{(M)}]$, $[B_h^{(M)}]$ will henceforth simply be denoted $[B^{(M)}]$.

The $A_{e,p}^{(M)}$, $A_{e,p}^{(M)}$ are provided by the incident field:

$$A_{e,p}^{(M)} = A_{e,p}^i, \quad A_{h,p}^{(M)} = A_{h,p}^i, \tag{161}$$

which for an incident plane wave are given by Eqs. (134) and (135). It may be useful in some problems to determine the field inside sphere S_1. Equation (159) indeed leads to

$$\begin{bmatrix} [A_e^{(1)}] \\ [A_h^{(1)}] \end{bmatrix} = S_{22}^{(M-1)} \begin{bmatrix} [A_e^{(M)}] \\ [A_h^{(M)}] \end{bmatrix}. \tag{162}$$

From the coefficients $A_{e,p}^{(1)}$ and $A_{h,p}^{(1)}$, the field everywhere inside the modulated area could be computed if necessary.

9. EXTRACTION OF PHYSICAL QUANTITIES

One should remark that the $S_{22}^{(M-1)}$ and $S_{12}^{(M-1)}$ block matrices obtained by our method are rather complicated objects owing to the fact they contain a great deal of physical information in both near and far fields. This detailed information is essential if we wish to use these matrices as the basic building blocks for multiple-scattering codes.[2,25] For a given single-scattering situation, however, one is typically interested in studying more limited, but more physical accessible, quantities such as cross sections. This extraction of physical quantities has been ex-

tensively studied elsewhere,[24–27] and we content our-selves here with a few illustrative formulas.

Physical quantities of interest can usually be obtained directly from analytical formulas of the coefficients of the incident and scattered fields. We recall that for a given incident field, with expansion coefficients placed in a $[A^i]$ column vector and multiplied by suitable Bessel and Ricatti functions to obtain the vector $[A^{(M)}]$, Eq. (160) allows us to obtain the scattering vector $[B^{(M)}]$ via

$$[B^{(M)}] = S_{12}^{(M-1)}[A^{(M)}], \qquad (163)$$

from which a vector $[B_c^{(M)}]$ containing only the scattering coefficients can be derived. We shall define the Hermitian conjugate or adjoint vector $[B_c]^\dagger$, which takes the form of a row matrix of the complex conjugates of the $[B_c^{(M)}]$ elements:

$$[B_c^{(M)}]^\dagger \equiv [\ldots, B_{eq}^{(M),*}, \ldots | \ldots, B_{hq}^{(M),*}, \ldots]. \qquad (164)$$

The T-matrix, denoted here by t, familiar to the 3D scattering community is defined by the equation

$$[B_c^{(M)}] \equiv t[A^i], \qquad (165)$$

and a comparison with Eqs. (141), (160), and (163) shows that the elements of t can be obtained from the elements of $S_{12}^{(M-1)}$ through the multiplication by appropriate ratios of Ricatti–Bessel functions.

With $[B_c^{(M)}]$, one can readily express the total scattering, extinction, and absorption cross sections, respectively, given by[24,26]

$$\sigma_s = \frac{1}{k_M^2}[B_c]^\dagger[B_c],$$

$$\sigma_e = \mathrm{Re}\left\{\frac{1}{k_M^2}[B_c]^\dagger[A^i]\right\},$$

$$\sigma_a = \sigma_e - \sigma_s. \qquad (166)$$

For a number of applications, however, total cross sections provide too-crude information, and one is interested in the angular distribution of the scattered radiation in the far field. For such situations, it is frequently useful to define an amplitude scattering matrix,[2,6] F [not to be confused with the F column used in propagation equations (53) and (55) nor with the S matrix of Eqs. (141) and (159)]. The scattering matrix is defined in the context of an incident plane wave, which we express as $\mathbf{E}_i = E \exp(i\mathbf{k}_M \cdot \mathbf{r})(e_\theta \hat{\boldsymbol{\theta}}_i + e_\phi \hat{\boldsymbol{\phi}}_i)$, where $\hat{\boldsymbol{\theta}}_i$ and $\hat{\boldsymbol{\phi}}_i$ are the spherical unit vectors associated with the incident wave vector, $\mathbf{k}_M$. The scalar E has the dimensions of an electric field. We are in the habit of normalizing the polarization factors e_θ and e_ϕ such that $|e_\theta|^2 + |e_\phi|^2 = 1$, in which case E is simply the electric field amplitude $\|E_i\| = E$. In the far-field limit, the scattered field at $r \to \infty$ will have the form

$$\lim_{r \to \infty} \mathbf{E}_s(\mathbf{r}) = E \frac{\exp(ikr)}{ikr}(E_{s,\theta}\hat{\boldsymbol{\theta}} + E_{s,\phi}\hat{\boldsymbol{\phi}}), \qquad (167)$$

where $\hat{\boldsymbol{\theta}}$ and $\hat{\boldsymbol{\phi}}$ are the spherical unit vectors associated with the vector $\mathbf{r}$. The scattered field factors $E_{s,\theta}$ and $E_{s,\phi}$

can be calculated in terms of the 2×2 scattering matrix F:

$$\begin{pmatrix} E_{s,\theta} \\ E_{s,\phi} \end{pmatrix} = E\frac{\exp(ikr)}{ikr}\begin{pmatrix} F_{\theta\theta} & F_{\theta\phi} \\ F_{\phi\theta} & F_{\phi\phi} \end{pmatrix}\begin{pmatrix} e_\theta \\ e_\phi \end{pmatrix}, \qquad (168)$$

where each of the F elements is a function of the incident field direction θ_i, ϕ_i and the observation angle of the scattered field θ, ϕ. They can be calculated by defining the scattering dyadic $\bar{\bar{F}}$:

$$\bar{\bar{F}} \equiv 4\pi[\boldsymbol{\mathcal{X}}^*(\hat{\mathbf{r}}), \boldsymbol{\mathcal{Z}}^*(\hat{\mathbf{r}})]t\begin{bmatrix} \boldsymbol{\mathcal{X}}(\hat{\mathbf{k}}_i) \\ \boldsymbol{\mathcal{Z}}(\hat{\mathbf{k}}_i) \end{bmatrix}, \qquad (169)$$

where we call $\boldsymbol{\mathcal{X}}$ and $\boldsymbol{\mathcal{Z}}$ the phase-modified VSH[24]:

$$\boldsymbol{\mathcal{X}}_{nm}(\hat{\mathbf{r}}) \equiv i^n \mathbf{X}_{nm}^*(\hat{\mathbf{r}}), \quad \boldsymbol{\mathcal{Z}}_{nm}(\hat{\mathbf{r}}) \equiv i^{n-1}\mathbf{Z}_{nm}^*(\hat{\mathbf{r}}). \qquad (170)$$

The F elements of Eq. (168) can then be readily expressed as

$$F_{\theta\theta} \equiv \hat{\boldsymbol{\theta}} \cdot \bar{\bar{F}} \cdot \hat{\boldsymbol{\theta}}_i, \quad F_{\theta\phi} \equiv \hat{\boldsymbol{\theta}} \cdot \bar{\bar{F}} \cdot \hat{\boldsymbol{\phi}}_i, \quad F_{\phi\theta} \equiv \hat{\boldsymbol{\phi}} \cdot \bar{\bar{F}} \cdot \hat{\boldsymbol{\theta}}_i,$$

$$F_{\phi\phi} \equiv \hat{\boldsymbol{\phi}} \cdot \bar{\bar{F}} \cdot \hat{\boldsymbol{\phi}}_i. \qquad (171)$$

The scattering matrix can subsequently be invoked to derive other angularly dependent physical quantities such as the Stokes matrix.[6,24,27] Here we simply remark that a quantity of frequent interest is the differential cross section $d\sigma/d\Omega$, which in our notation can be computed from[6,24,27]

$$\frac{d\sigma}{d\Omega}(\theta, \phi; \theta_i, \phi_i) = \lim_{r \to \infty} r^2 \frac{\|\mathbf{E}_s(\mathbf{r})\|^2}{E^2} = \frac{|E_{s,\theta}|^2 + |E_{s,\phi}|^2}{k^2}$$

$$= \frac{|F_{\theta\theta}e_\theta + F_{\theta\phi}e_\phi|^2 + |F_{\phi\theta}e_\theta + F_{\phi\phi}e_\phi|^2}{k^2}.$$

$$(172)$$

10. CONCLUSION

This achieves the detailed presentation of the differential theory of light diffraction by a 3D object. Although the theory makes use of the basis of vector spherical harmonics, which is much more complicated to manipulate than the Fourier basis used in Cartesian coordinates, the final result looks quite simple in the sense that it is not more complicated than analyzing crossed gratings,[20] for which the propagation equations are quite similar.

The current theory can also be extended to treat the diffraction from anisotropic materials. A forthcoming paper will present numerical results concerning prolate and oblate spheroids and will include comparisons with results given by approximate methods in view of studying their domain of validity.

The authors thank Sophie Stout for helpful contributions.

Corresponding author B. Stout can be reached by e-mail at brian.stout@fresnel.fr

APPENDIX A: CALCULATION OF $\varepsilon_{N,0}$

In the case of an axisymmetric object, in the modulated region the permittivity $\varepsilon(r,\theta)$ is a piecewise constant function with step discontinuities. With $c = \cos\theta$, $\varepsilon(r,\theta)$ is transformed into $\tilde{\varepsilon}(r,c)$, and Eq. (34) reads as $\varepsilon_{n,0} = 2\pi\int_{-1}^{1}\tilde{\varepsilon}(r,c)\bar{P}_n^0(c)dc$, where $\bar{P}_n^0$ are the normalized Legendre polynomials:

$$\bar{P}_n^0(\cos\theta) = \left(\frac{2n+1}{4\pi}\right)^{1/2}P_n^0(\cos\theta). \tag{A1}$$

We can evaluate this integral by invoking the recurrence relation

$$(n+1)P_n^0(c) = \frac{d}{dc}P_{n+1}^0(c) - c\frac{d}{dc}P_n^0(c). \tag{A2}$$

Using the relation

$$\frac{d}{dc}(cP_n^0(c)) = c\frac{d}{dc}P_n^0(c) + P_n^0(c), \tag{A3}$$

we find

$$c\frac{d}{dc}P_n^0(c) = \frac{d}{dc}(cP_n^0(c)) - P_n^0(c), \tag{A4}$$

and the recurrence relation becomes

$$P_n^0(c) = \frac{1}{n}\frac{d}{dc}P_{n+1}^0(c) - \frac{1}{n}\frac{d}{dc}(cP_n^0(c)). \tag{A5}$$

We have then

$$\int_{c_2}^{c_1}P_n^0(c)dc = \frac{1}{n}\int_{c_2}^{c_1}\frac{d}{dc}P_{n+1}^0(c)dc - \frac{1}{n}\int_{c_2}^{c_1}\frac{d}{dc}(cP_n^0(c))dc, \tag{A6}$$

and the piecewise integral is then

$$\int_{c_2}^{c_1}P_n^0(c)dc = \frac{1}{n}[P_{n+1}^0(c_1) - P_{n+1}^0(c_2)] + \frac{1}{n}[c_2P_n^0(c_2) - c_1P_n^0(c_1)]. \tag{A7}$$

An example of the determination of the $\varepsilon_{n,0}$ coefficients is illustrated on a spheroid with half large and small axes a and b, respectively; Oz is the symmetry axis, and, in the yOz plane, its Cartesian equation is

$$\frac{z^2}{a^2} + \frac{y^2}{b^2} = 1. \tag{A8}$$

Since $z = r\cos\theta$ and $y = r\sin\theta$, this equation in spherical coordinates reads as

$$r(\theta) = \frac{ab}{\sqrt{a^2 + (b^2 - a^2)\cos^2\theta}}. \tag{A9}$$

Inversing this relation leads to

$$\theta(r) = \arccos\left(\frac{a}{r}\sqrt{\frac{r^2 - b^2}{a^2 - b^2}}\right) \tag{A10}$$

$\forall r \in [b,a]$; Eq. (A10) defines a value $\theta_1(r)$, with $\theta_1(r) \in [0,\pi/2]$. Defining $\theta_2(r) = \pi - \theta_1(r)$, we have

$$\varepsilon(r,\theta) = \varepsilon_1 \quad \text{if } \theta \in [0,\theta_1(r)] \cup [\theta_2(r),\pi],$$

$$\varepsilon(r,\theta) = \varepsilon_M \quad \text{if } \theta \in [\theta_1(r),\theta_2(r)]. \tag{A11}$$

The limits c_1 and c_2 that appear in Eq. (A7) are $\cos\theta_1(r)$ and $\cos\theta_2(r)$.

APPENDIX B: VANISHING OF SOME ELEMENTS OF THE Q_ε MATRIX

Expanding $\mathbf{D}$ and $\mathbf{E}$ on the basis of VSH, the equation $\mathbf{D} = \epsilon_0\varepsilon\mathbf{E}$ gives

$$\sum_{n',m'}(D_{Yn'm'}\mathbf{Y}_{n'm'} + D_{Xn'm'}\mathbf{X}_{n'm'} + D_{Zn'm'}\mathbf{Z}_{n'm'})$$

$$= \epsilon_0\varepsilon(r,\theta,\phi)\sum_{\nu,\mu}(E_{Y\nu\mu}\mathbf{Y}_{\nu\mu} + E_{X\nu\mu}\mathbf{X}_{\nu\mu} + E_{Z\nu\mu}\mathbf{Z}_{\nu\mu}). \tag{B1}$$

Performing an ordinary scalar product of both sides of Eq. (B1) with $\mathbf{Y}_{nm}^*$, we obtain

$$\mathbf{Y}_{nm}^* \cdot \sum_{n',m'}(D_{Yn'm'}\mathbf{Y}_{n'm'} + D_{Xn'm'}\mathbf{X}_{n'm'} + D_{Zn'm'}\mathbf{Z}_{n'm'})$$

$$= \epsilon_0\varepsilon(r,\theta,\phi)\mathbf{Y}_{nm}^* \cdot \sum_{\nu,\mu}(E_{Y\nu\mu}\mathbf{Y}_{\nu\mu} + E_{X\nu\mu}\mathbf{X}_{\nu\mu} + E_{Z\nu\mu}\mathbf{Z}_{\nu\mu}). \tag{B2}$$

Using the fact as one can see from Eqs. (7), (16), and (17) that $\mathbf{Y}_{nm}^* \cdot \mathbf{X}_{n'm'} = \mathbf{Y}_{nm}^* \cdot \mathbf{Z}_{n'm'} = \mathbf{Y}_{nm}^* \cdot \mathbf{X}_{\nu\mu} = \mathbf{Y}_{nm}^* \cdot \mathbf{Z}_{\nu\mu} = 0$, we find

$$\sum_{n',m'}D_{Ynm}\mathbf{Y}_{nm}^* \cdot \mathbf{Y}_{n'm'} = \epsilon_0\varepsilon(r,\theta,\phi)\sum_{\nu,\mu}E_{Y\nu\mu}\mathbf{Y}_{nm}^* \cdot \mathbf{Y}_{\nu\mu}. \tag{B3}$$

This equation establishes a linear relation between D_{Ynm} and $E_{Y\nu\mu}$ only; thus $Q_{\varepsilon YX}$ and $Q_{\varepsilon YZ}$ must be null.

Now, performing a scalar product on both sides of Eq. (B1) with $\mathbf{X}_{nm}^*$, we find that

$$\mathbf{X}_{nm}^* \cdot \sum_{n',m'}(D_{Yn'm'}\mathbf{Y}_{n'm'} + D_{Xn'm'}\mathbf{X}_{n'm'} + D_{Zn'm'}\mathbf{Z}_{n'm'})$$

$$= \epsilon_0\varepsilon(r,\theta,\phi)\mathbf{X}_{nm}^* \cdot \sum_{\nu,\mu}(E_{Y\nu\mu}\mathbf{Y}_{\nu\mu} + E_{X\nu\mu}\mathbf{X}_{\nu\mu} + E_{Z\nu\mu}\mathbf{Z}_{\nu\mu}). \tag{B4}$$

Using the fact that $\mathbf{X}_{nm}^* \cdot \mathbf{Y}_{n'm'} = \mathbf{X}_{nm}^* \cdot \mathbf{Y}_{\nu\mu} = 0$, we obtain

$$\frac{1}{\epsilon_0} \sum_{n',m'} (D_{Xn'm'} \mathbf{X}^*_{nm} \cdot \mathbf{X}_{n'm'} + D_{Zn'm'} \mathbf{X}^*_{nm} \cdot \mathbf{Z}_{n'm'})$$

$$= \varepsilon(r,\theta,\phi) \mathbf{X}^*_{nm} \cdot \sum_{\nu,\mu} (E_{X\nu\mu} \mathbf{X}_{\nu\mu} + E_{Z\nu\mu} \mathbf{Z}_{\nu\mu}). \tag{B5}$$

Integrating over the solid angles Ω, we obtain, taking into account Eq. (11),

$$D_{Xnm} = \epsilon_0 \sum_{\nu,\mu} \int_0^{4\pi} d\Omega \varepsilon(r,\theta,\phi) \mathbf{X}^*_{nm} \cdot (E_{X\nu\mu} \mathbf{X}_{\nu\mu} + E_{Z\nu\mu} \mathbf{Z}_{\nu\mu}). \tag{B6}$$

Since D_{Xnm} does not depend on $E_{Y\nu\mu}$, we deduce that $Q_{\varepsilon XY}=0$.

A similar calculation starting from multiplying both sides of Eq. (B1) by $\mathbf{Z}^*_{nm}$ leads to $Q_{\varepsilon ZY}=0$.

APPENDIX C: TWO RELATIONS BETWEEN VECTOR SPHERICAL HARMONICS

In order to derive two relations between VSHs that are necessary to construct the theory, it is useful to invoke another set of VSHs, denoted $\mathbf{Y}^m_{n,n+1}$, $\mathbf{Y}^m_{n,n}$, and $\mathbf{Y}^m_{n,n-1}$, as introduced by quantum-mechanic theoreticians who worked on the angular-momentum coupling formalism.[23] We first recall the definition of the Cartesian spherical unit vectors[23]:

$$\boldsymbol{\mathcal{X}}_1 = -\frac{1}{\sqrt{2}}(\hat{\mathbf{x}}+i\hat{\mathbf{y}}), \quad \boldsymbol{\mathcal{X}}_0 = \hat{\mathbf{z}}, \quad \boldsymbol{\mathcal{X}}_{-1} = \frac{1}{\sqrt{2}}(\hat{\mathbf{x}}-i\hat{\mathbf{y}}), \tag{C1}$$

where $\hat{\mathbf{x}}$, $\hat{\mathbf{y}}$, $\hat{\mathbf{z}}$ are the unit vectors of the Cartesian coordinate system. Making use of the Clebsch–Gordan coefficients,[23] we then define the new set of VSHs as

$$\mathbf{Y}^m_{n,l} = \sum_{\mu=-1}^1 (l,m-\mu;1,\mu|n,m) Y_{l,m-\mu} \boldsymbol{\mathcal{X}}_\mu, \tag{C2}$$

with $l=n-1, n, n+1$.

Using the conversion from spherical to Cartesian coordinates and the expressions of our $\mathbf{Y}_{nm}$, $\mathbf{X}_{nm}$, $\mathbf{Z}_{nm}$ VSHs in a spherical coordinate system of Eqs. (7), (16), and (17), we can painstakingly verify that our $\mathbf{Y}_{nm}$, $\mathbf{X}_{nm}$, and $\mathbf{Z}_{nm}$ VSHs can be expressed in terms of the $\mathbf{Y}^m_{n,n+1}$, $\mathbf{Y}^m_{n,n+1}$, $\mathbf{Y}^m_{n,n+1}$ spherical harmonics via the relations

$$\mathbf{X}_{nm} = \frac{\mathbf{Y}^m_{n,n}}{i}, \tag{C3}$$

$$\mathbf{Z}_{nm} = \left(\frac{n+1}{2n+1}\right)^{1/2} \mathbf{Y}^m_{n,n-1} + \left(\frac{n}{2n+1}\right)^{1/2} \mathbf{Y}^m_{n,n+1}, \tag{C4}$$

$$\mathbf{Y}_{nm} = \left(\frac{n}{2n+1}\right)^{1/2} \mathbf{Y}^m_{n,n-1} - \left(\frac{n+1}{2n+1}\right)^{1/2} \mathbf{Y}^m_{n,n+1}. \tag{C5}$$

With the above equations in place, we first calculate the following two products.

1. $\mathbf{X}_{\nu\mu} \cdot \mathbf{X}^*_{nm}$

Using Eq. (C3), we find

$$\mathbf{X}_{\nu\mu} \cdot \mathbf{X}^*_{nm} = \mathbf{Y}^\mu_{\nu,\nu} \cdot (\mathbf{Y}^m_{n,n})^*. \tag{C6}$$

Putting Eq. (C2) in Eq. (C6) and calculating the Clebsch–Gordan coefficients lead us to

$$\mathbf{X}_{\nu\mu} \cdot \mathbf{X}^*_{nm} = \left[\frac{1}{n(n+1)\nu(\nu+1)}\right]^{1/2}$$

$$\times \left\{ \frac{1}{2}[(n+m+1)(n-m)(\nu+\mu+1)(\nu-\mu)]^{1/2} \right.$$

$$\times Y_{\nu,\mu+1} Y^*_{n,m+1} + m\mu Y_{\nu\mu} Y^*_{nm}$$

$$+ \frac{1}{2}[(n+m)(n-m+1)$$

$$\left. \times (\nu+\mu)(\nu-\mu+1)]^{1/2} Y_{\nu,\mu-1} Y^*_{n,m-1} \right\}. \tag{C7}$$

2. $\mathbf{X}_{\nu\mu} \cdot \mathbf{Z}^*_{nm}$

In order to calculate this scalar product, we use the fact that $\mathbf{X}_{\nu\mu} \cdot \mathbf{Y}^*_{nm}=0$. Thus Eq. (C5) gives

$$\left(\frac{n+1}{2n+1}\right)^{1/2} \mathbf{X}_{\nu\mu} \cdot \mathbf{Y}^{m,*}_{n,n+1} = \left(\frac{n}{2n+1}\right)^{1/2} \mathbf{X}_{\nu\mu} \cdot \mathbf{Y}^{m,*}_{n,n-1}, \tag{C8}$$

i.e.,

$$\mathbf{X}_{\nu\mu} \cdot \mathbf{Y}^{m,*}_{n,n+1} = \left(\frac{n}{n+1}\right)^{1/2} \mathbf{X}_{\nu\mu} \cdot \mathbf{Y}^{m,*}_{n,n-1}. \tag{C9}$$

Using Eq. (C4), we then obtain

$$\mathbf{X}_{\nu\mu} \cdot \mathbf{Z}^*_{nm} = \left(\frac{n+1}{2n+1}\right)^{1/2} \mathbf{X}_{\nu\mu} \cdot \mathbf{Y}^{m,*}_{n,n-1}$$

$$+ \left(\frac{n}{2n+1}\right)^{1/2} \mathbf{X}_{\nu\mu} \cdot \mathbf{Y}^{m,*}_{n,n+1}$$

$$= \left(\frac{2n+1}{n+1}\right)^{1/2} \mathbf{X}_{\nu\mu} \cdot \mathbf{Y}^{m,*}_{n,n-1}$$

$$= -i\left(\frac{2n+1}{n+1}\right)^{1/2} \mathbf{Y}^\mu_{\nu,\nu} \cdot \mathbf{Y}^{m,*}_{n,n-1}. \tag{C10}$$

Inserting Eq. (C2) and the expression of the Clebsch–Gordan coefficients into Eq. (C10) leads to

$$\mathbf{X}_{\nu\mu} \cdot \mathbf{Z}^*_{nm} = i\left(\frac{1}{n(n+1)\nu(\nu+1)} \frac{2n+1}{2n-1}\right)^{1/2}$$

$$\times \left\{ -\frac{Y_{\nu,\mu-1} Y^*_{n-1,m-1}}{2} \right.$$

$$\times [(n+m)(n+m-1)(\nu+\mu)(\nu-\mu+1)]^{1/2}$$

$$+ \mu[(n^2 - m^2)]^{1/2} Y_{\nu,\mu} Y^*_{n-1,m} + \frac{Y_{\nu,\mu+1} Y^*_{n-1,m+1}}{2}$$

$$\times [(n-m)(n-m-1)(\nu-\mu)(\nu+\mu+1)]^{1/2} \Big\}.$$

$$\text{(C11)}$$

APPENDIX D: USE OF THE GAUNT COEFFICIENTS

Theoreticians working on the coupling of angular momentum in quantum mechanics have introduced the concepts of Gaunt coefficients and Wigner 3J coefficients.[23,28] With our definitions, the normalized Gaunt coefficients, $\bar{a}$, arise from solid-angle integration of the product of three scalar spherical harmonics[23]:

$$\bar{a}(\{\nu',\mu'\},\{\nu,\mu\},\{n,m\}) \equiv \int_0^{2\pi} \int_0^{\pi} Y_{\nu'\mu'}(\theta,\phi) Y_{\nu\mu}(\theta,\phi)$$

$$\times Y_{nm}(\theta,\phi) \sin\theta \, d\theta \, d\phi. \qquad \text{(D1)}$$

These coefficients can be rapidly calculated through recursion relations.[29] They naturally appear if, starting from Eq. (71), we expand in it the $\varepsilon(r,\theta,\phi)$ function as stated in Eq. (3):

$$\sum_{n'm'} (D_{\text{TY}n'm'} \mathbf{Y}_{n'm'} + D_{\text{TX}n'm'} \mathbf{X}_{n'm'} + D_{\text{TZ}n'm'} \mathbf{Z}_{n'm'})$$

$$= \epsilon_0 \sum_{\nu',\mu'} \sum_{\nu,\mu} \varepsilon_{\nu'\mu'} Y_{\nu'\mu'} (E_{\text{TY}\nu\mu} \mathbf{Y}_{\nu\mu} + E_{\text{TX}\nu\mu} \mathbf{X}_{\nu\mu} + E_{\text{TZ}\nu\mu} \mathbf{Z}_{\nu\mu}).$$

$$\text{(D2)}$$

Multiplying both sides by $\mathbf{Y}^*_{nm}(\theta,\phi)$ and integrating over the angular variables θ, ϕ, we obtain

$$\frac{1}{\epsilon_0} D_{\text{TY}nm} = \sum_{\nu',\mu'} \sum_{\nu,\mu} \varepsilon_{\nu'\mu'} E_{\text{TY}\nu\mu} \iint Y_{\nu'\mu'}(\theta,\phi) Y_{\nu\mu}(\theta,\phi) \cdot Y^*_{nm}(\theta,\phi) \sin\theta \, d\theta \, d\phi$$

$$= \sum_{\nu',\mu'} \sum_{\nu,\mu} \varepsilon_{\nu'\mu'} E_{\text{TY}\nu\mu} (-1)^m \iint Y_{\nu'\mu'}(\theta,\phi) Y_{\nu\mu}(\theta,\phi) \cdot Y_{n,-m}(\theta,\phi) \sin\theta \, d\theta \, d\phi$$

$$= \sum_{\nu',\mu'} \sum_{\nu,\mu} \varepsilon_{\nu'\mu'} E_{\text{TY}\nu\mu} (-1)^m \iint Y_{\nu'\mu'}(\theta,\phi) Y_{\nu\mu}(\theta,\phi) Y_{n,-m}(\theta,\phi) \sin\theta \, d\theta \, d\phi$$

$$= \sum_{\nu',\mu'} \sum_{\nu,\mu} \varepsilon_{\nu'\mu'} E_{\text{TY}\nu\mu} (-1)^m \bar{a}(\{\nu',\mu'\},\{\nu,\mu\},\{n,-m\}). \qquad \text{(D3)}$$

A useful property of Gaunt coefficients defined in Eq. (D1) is that they are null except if $\mu' = m - \mu$ and $\nu' \in [|n - \nu|, n + \nu]$. Thus the summation over μ' is eliminated, and Eq. (D3) reduces to

$$D_{\text{TY}nm} = \epsilon_0 \sum_{\nu'=|n-\nu|}^{n+\nu} \sum_{\nu=0}^{N} \sum_{\mu=-\nu}^{\nu} (-1)^m \bar{a}(\{\nu',m-\mu\},$$

$$\{\nu,\mu\},\{n,-m\}) \varepsilon_{\nu',m-\mu} E_{\text{TY}\nu\mu}. \qquad \text{(D4)}$$

A comparison with Eq. (77) shows that

$$\varepsilon_{\text{YY}nm,\nu\mu} = (-1)^m \sum_{\nu'=|n-\nu|}^{n+\nu} \bar{a}(\{\nu',m-\mu\},\{\nu,\mu\},\{n,$$

$$- m\}) \varepsilon_{\nu',m-\mu}(r), \qquad \text{(D5)}$$

in which the calculation of $\varepsilon_{\nu',m-\mu}(r)$ involves computing the integrals stated in Eq. (6), which implies integrating single spherical harmonics multiplied by piecewise constant functions, a task that can readily be performed analytically as described in Appendix A.

We now can derive similar expressions for the other blocks. Multiplying both sides of Eq. (71) by $\mathbf{X}^*_{nm}(\theta,\phi)$, integrating over the angular variables θ, ϕ, and expanding ε as stated by Eq. (3), we obtain

$$D_{\text{TX}nm} = \epsilon_0 \sum_{\nu',\mu'} \sum_{\nu,\mu} \varepsilon_{\nu'\mu'} E_{\text{TX}\nu\mu} \int Y_{\nu'\mu'}(\theta,\phi) \mathbf{X}_{\nu\mu}(\theta,\phi) \cdot \mathbf{X}^*_{nm}(\theta,\phi) \sin\theta \, d\theta \, d\phi$$

$$+ \sum_{\nu',\mu'} \sum_{\nu,\mu} \varepsilon_{\nu'\mu'} E_{\text{TZ}\nu\mu} \int Y_{\nu'\mu'}(\theta,\phi) \mathbf{Z}_{\nu\mu}(\theta,\phi) \cdot \mathbf{X}^*_{nm}(\theta,\phi) \sin\theta \, d\theta \, d\phi. \qquad \text{(D6)}$$

From Eq. (C7) in Appendix C we thus obtain

$$\varepsilon_{XXnm,\nu\mu} = \left[\frac{1}{n(n+1)\nu(\nu+1)}\right]^{1/2}(-1)^{-m}\sum_{\nu'=|n-\nu|}^{n+\nu}\varepsilon_{\nu',m-\mu}\times\left\{-\frac{1}{2}[(n+m+1)(n-m)(\nu+\mu+1)(\nu-\mu)]^{1/2}\bar{a}(\{\nu',m-\mu\},\{\nu,\mu+1\},\{n,\right.$$

$$\left. -m-1\}) + \bar{a}(\{\nu',m-\mu\},\{\nu,\mu\},\{n,-m\}) - \frac{1}{2}[(n+m)(n-m+1)(\nu+\mu)(\nu-\mu+1)]^{1/2}\bar{a}(\{\nu',m-\mu\},\{\nu,\mu-1\},\{n,-m\right.$$

$$\left. +1\})\right\}. \tag{D7}$$

From Eq. (C11) in Appendix C, we obtain

$$\varepsilon_{XZnm,\nu\mu} = \frac{i}{2}\left(\frac{1}{n(n+1)\nu(\nu+1)}\frac{2n+1}{2n-1}\right)^{1/2}(-1)^{m}\sum_{\nu'=|n-1-\nu|}^{n+\nu-1}\varepsilon_{\nu',m-\mu}\times\left\{-[(n+m)(n+m-1)(\nu+\mu)(\nu-\mu+1)]^{1/2}\bar{a}(\{\nu',m\right.$$

$$\left. -\mu\},\{\nu,\mu\},\{n-1,-m+1\}) + 2\mu[(n^2-m^2)]^{1/2}\bar{a}(\{\nu',m-\mu\},\{\nu,\mu\},\{n-1,-m\}) + [(n-m)(n-m-1)(\nu-\mu)(\nu+\mu\right.$$

$$\left. +1)]^{1/2}\bar{a}(\{\nu',m-\mu\},\{\nu,\mu+1\},\{n-1,-m-1\})\right\}. \tag{D8}$$

An alternative exists to determine the Gaunt coefficients. Introducing the Wigner 3*J* coefficients

$$\begin{pmatrix} n_1 & n_2 & n_3 \\ m_1 & m_2 & m_3 \end{pmatrix},$$

which are given by standard subroutines, we can calculate the normalized Gaunt coefficients from

$$\bar{a}(\{\nu',\mu'\},\{\nu,\mu\},\{n,m\}) = \left[\frac{(2\nu'+1)(2\nu+1)(2n+1)}{4\pi}\right]^{1/2}$$
$$\times\begin{pmatrix} \nu' & \nu & n \\ 0 & 0 & 0 \end{pmatrix}\begin{pmatrix} \nu' & \nu & n \\ \mu' & \mu & m \end{pmatrix}.$$

APPENDIX E: RICATTI–BESSEL FUNCTIONS

We recall the definition of the Ricatti–Bessel functions $\psi_n(z)$ and $\xi_n(z)$:

$$\psi_n(z) \equiv zj_n(z), \quad \xi_n(z) \equiv zh_n^+(z). \tag{E1}$$

Their derivatives $\psi'_n(z)$ and $\xi'_n(z)$ can be readily calculated using the Bessel function recursion relations:

$$\psi'_n(z) = \frac{(n+1)}{z}\psi_n(z) - \psi_{n+1}(z),$$

$$\xi'_n(z) = \frac{(n+1)}{z}\xi_n(z) - \xi_{n+1}(z). \tag{E2}$$

We note, for example, the elements of the $p^{(j)}$ and $q^{(j)}$ matrices of Eq. (152) are simply the logarithmic derivatives of the Ricatti–Bessel functions:

$$p_{p,q}^{(j)} \equiv \delta_{pq}\Phi_n(k_M r_j) \equiv \left.\delta_{pq}\frac{\psi'_n(z)}{\psi_n(z)}\right|_{z=k_M r_j},$$

$$q_{p,q}^{(j)} \equiv \delta_{pq}\Psi_n(k_M r_j) \equiv \left.\delta_{pq}\frac{\xi'_n(z)}{\xi_n(z)}\right|_{z=k_M r_j}, \tag{E3}$$

which can be rapidly and reliably calculated[1] from recurrence relations derived from Eqs. (E2),

$$\Phi_{n-1}(z) = \frac{n}{z} - \frac{1}{\Phi_n(z)+n/z},$$

or

$$\Psi_n(z) = \frac{1}{n/z-\Psi_{n-1}(z)} - \frac{n}{z}, \tag{E4}$$

so that Ricatti–Bessel functions simplify the initialization of the shooting method. Of course, the partition of the modulated area should be done in such a way that no value of r_j coincides with a zero of a Ricatti $\psi_n(z)$ function.

REFERENCES AND NOTES

1. C. F. Bohren and D. R. Huffman, *Absorption and Scattering of Light by Small Particles* (Wiley-Interscience, 1983).
2. M. I. Mischenko L. D. Travis, and A. A. Lacis, *Scattering, Absorption, and Emission of Light by Small Particles* (Cambridge U. Press, 2002).
3. L. Lorenz, "Lysbevaegelsen i og uden for en af plane Lysbølger belyst Kulge," Vidensk. Selk. Skr. **6**, 1–62 (1890).
4. L. Lorenz, "Sur la lumière réfléchie et réfractée par une sphère transparente," Librairie Lehmann et Stage, Oeuvres scientifique de L. Lorenz, revues et annotées par H. Valentiner, 1898 (transl. of Ref. 3).
5. G. Mie, "Beiträge zur Optik Trüber Medien speziell kolloidaler Metallosungen," Ann. Phys. **25**, 377–452 (1908).
6. L. Tsang, J. A. Kong, and R. T. Shin, *Theory of Microwave Remote Sensing* (Wiley, 1985).
7. L. Tsang, J. A. Kong, and K.-H. Ding, *Scattering of Electromagnetic Waves, Theories and Applications* (Wiley, 2000).
8. L. Tsang, J. A. Kong, K.-H. Ding, and C. O. Ao, *Scattering of Electromagnetic Waves, Numerical Simulations* (Wiley, 2001).
9. L. Tsang and J. A. Kong, *Scattering of Electromagnetic Waves, Advanced Topics* (Wiley, 2001).
10. In the community of grating theoreticians, as well as in the one of waveguides, this matrix is called the *S* matrix or

scattering matrix. It is essentially the S_{12} block of the $S^{(M-1)}$ matrix appearing later on in Eq. (158); see also Eqs. (163) and (165).

11. W. C. Chew, *Waves and Fields in Inhomogeneous Media*, IEEE Press Series on Electromagnetic Waves (IEEE, 1994).
12. P. C. Waterman, "Matrix methods in potential theory and electromagnetic scattering," J. Appl. Phys. **50**, 4550–4566 (1979).
13. M. Bagieu and D. Maystre, "Waterman and Rayleigh methods for diffraction grating problems: extension of the convergence domain," J. Opt. Soc. Am. A **15**, 1566–1576 (1998).
14. L. Li, "Formulation and comparison of two recursive matrix algorithms for modeling layered diffraction gratings," J. Opt. Soc. Am. A **13**, 1024–1035 (1996).
15. E. Popov and M. Nevière, "Grating theory: new equations in Fourier space leading to fast converging results for TM polarization," J. Opt. Soc. Am. A **17**, 1773–1784 (2000).
16. E. Popov and M. Nevière, "Maxwell equations in Fourier space: fast converging formulation for diffraction by arbitrary shaped, periodic, anisotropic media," J. Opt. Soc. Am. A **18**, 2886–2894 (2001).
17. L. Li, "Use of Fourier series in the analysis of discontinuous periodic structures," J. Opt. Soc. Am. A **13**, 1870–1876 (1996).
18. E. Popov, M. Nevière, and N. Bonod, "Factorization of products of discontinuous functions applied to Fourier–Bessel basis," J. Opt. Soc. Am. A **21**, 46–51 (2004).

19. N. Bonod, E. Popov, and M. Neviere, "Differential theory of diffraction by finite cylindrical objects," J. Opt. Soc. Am. A **22**, 481–490 (2005).
20. M. Nevière and E. Popov, *Light Propagation in Periodic Media: Diffraction Theory and Design* (Marcel Dekker, 2003).
21. C. Cohen-Tannoudji, *Photons & Atomes—Introduction à l'électrodynamique quantique* (InterEdition/ Editions du CNRS, 1987).
22. J. D. Jackson, *Classical Electrodynamics* (Wiley, 1965).
23. A. R. Edmonds, *Angular Momentum in Quantum Mechanics* (Princeton U. Press, 1960).
24. B. Stout, J.-C. Auger, and J. Lafait, "Individual and aggregate scattering matrices and cross-sections: conservation laws and reciprocity," J. Mod. Opt. **48**, 2105–2128 (2001).
25. B. Stout, J. C. Auger, and J. Lafait, "A transfer matrix approach to local field calculations in multiple scattering problems," J. Mod. Opt. **49**, 2129–2152 (2002).
26. D. W. Mackowski, "Calculation of total cross sections of multiple-sphere clusters," J. Opt. Soc. Am. A **11**, 2851–2861 (1994).
27. D. W. Mackowski, and M. I. Mishchenko, "Calculation of the T matrix and the scattering matrix for ensembles of spheres," J. Opt. Soc. Am. A **13**, 2266–2278 (1996).
28. J. A. Gaunt, "On the triplets of Helium," Philos. Trans. R. Soc. London, Ser. A **228**, 151–196 (1929).
29. Y. L. Xu, "Fast evaluation of the Gaunt coefficients," Math. Comput. **65**, 1601–1612 (1996).

Optical force calculations in arbitrary beams by use of the vector addition theorem

Olivier Moine and Brian Stout

Institut Fresnel, Unité Mixte de Recherche 6133, Université Aix-Marseille I, Case 161 Faculté des Sciences et Techniques, Centre de Saint Jérome, 13397 Marseille Cedex 20, France.

We derive and apply formulas that employ the vector-wave addition theorem and rotation matrices for quantitative calculations of both radial and axial optical forces exerted on particles trapped in arbitrarily shaped tweezer beams. For the tightly focused beams encountered in optical tweezers, we shall highlight the importance of formulating the optical forces and beam symmetries in terms of the irradiance and total beam power. A major interest of the addition theorem treatment of optical forces is that it opens up the possibility of modeling a wide variety of beam shapes while automatically ensuring that the beams satisfy the Maxwell equations. In some of the first numerical applications of our method, we shall illustrate that resonance effects play an important role in the axial trapping position of particles comparable in size with the wavelength of the trapping beam. © 2005 Optical Society of America

OCIS codes: 140.7010, 140.3300, 120.5820, 290.4020.

1. INTRODUCTION

Optical tweezers and traps have opened up a new domain of laser applications in that they allow the mechanical manipulation of particles via light-induced forces.[1] The essential aspect of optical tweezers is to create large gradients in the field intensity that induce optical forces that attract dielectric particles toward regions of high intensity. Outside their demonstrated usefulness to trap, displace, and rotate particles, a major interest of optical tweezers is the measurement of molecular scale forces that, like typical optical forces, are frequently in the 1–100 (pN) range.[2–6] A reliable theory of optical forces is therefore useful in this regard.

Particles commonly trapped in optical tweezers experiments of characteristic size D are frequently too large to be reliably treated in a simple dipole model,[7] $D \ll \lambda$, and not large enough to be reliably treated via a geometrical optics approach,[8] $D \gg \lambda$. The weak dielectric contrast of many optically trapped particles has motivated the use of Born-type approximations[9] for particles in the intermediate or resonant size regime, $D \sim \lambda$, but this method is reliable only to the extent in which the particle only weakly modifies the incident beam, and the precise domain of validity of this approximation is not known. Consequently, optical force experiments are frequently carried out by one's experimentally measuring the forces on spherical particles and then attaching these calibrated optical handles to the molecules, membranes, or cells under study.[10]

Optical force calculations based on transition matrices[11,12] (or a Lorentz–Mie-type theory for spheres[13]) are an obvious choice for rigorous numerical calculations of the optical force. We demonstrate in this paper that quantitative calculations of the force along an arbitrary direction can be performed by invoking the translation-addition matrices familiar from analytic multiple-scattering calculations.[11] Another important aspect of quantitative calculations is the necessity to accurately model realistic optical tweezer beams. Space does not permit a detailed discussion of the various possible beam shapes in this paper, but we shall discuss the partial-wave decomposition of focused laser beams and the importance of irradiance when evaluating beam symmetries and optical forces.

Although our transition-matrix formulas can be applied to arbitrary scatterers, in the interest of simplicity, we shall restrict our attention to the optical forces on dielectric spheres suspended in liquid dielectrics. For the purpose of theoretical comparisons, we simply study here some simple models based on Davis-type corrections to Gaussian-type focused beams.[14,15] Although these models are rather poor approximations to realistic tweezer beams, they have the advantage of having rather simple partial-wave expansions. These models suffice, nevertheless, to illustrate the necessity of proper beam normalization and the importance of an irradiance formulation of the beam symmetries.

The principal goal of this paper is to present our technique of calculation and to illustrate its ability to perform quantitative calculation of optical forces on resonant dielectric particles $D \gtrsim \lambda$. Our techniques can be adopted to the study of non-Gaussian beams (doughnut beams, top-hat beams, Bessel beams, etc.) and can be used to systematically test the domain of application of the various approximate theories. These topics, however, shall be treated in subsequent publications.

We use SI units throughout this paper. In view of the scale-invariant nature of the electromagnetic equations,

we shall formulate our results in terms of dimensionless parameters wherever possible. Nevertheless, numerical applications will be formulated for the commonly employed infrared optical tweezer beams with a vacuum wavelength of $\lambda_0 = 1.064$ (μm). Water is assumed for the background liquid dielectric media, $n_b \simeq 1.32$, and the trapped particles will be either silica $n_s \simeq 1.46$ or latex $n_s \simeq 1.59$.

We have broken this paper up into three largely independent sections. Section 2 is dedicated to introducing the partial-wave developments of the electromagnetic fields and a discussion of beam symmetries and normalization. Section 3 presents our expressions for the optical forces derived from the Maxwell constraint tensor. The translation-addition theorem of scattering theory permits the calculation of the forces at different positions, whereas the angular-momentum rotation formulas permit the calculation of the forces in different directions. Indicative calculations are presented in this section for both radial and axial forces. We also present some preliminary results demonstrating the importance of resonance effects on the trapping position of large particles.

2. ELECTROMAGNETIC PARTIAL WAVES

We adopt a time-harmonic incident field with an $\exp(-i\omega t)$ time dependence and assume that trapped particles are suspended in a homogeneous absorption-free liquid dielectric medium. The time-harmonic Maxwell equations then require that the electric field in a homogenous medium satisfies the following second-order differential equation:

$$\nabla \times \nabla \times \mathbf{E}(\mathbf{r}) - k^2 \mathbf{E}(\mathbf{r}) = 0, \qquad (1)$$

with $k = \sqrt{\varepsilon_b \mu_0}\sqrt{\epsilon_0 \mu_0}\,\omega = n_b \omega/c$, where ($\epsilon_0, \mu_0$) are the permittivity and the permeability of the vacuum and (ε_b, μ_b) are the relative permittivity and the permeability of the background dielectric medium. The electromagnetic partial waves or vector spherical wave functions (VSWFs) are a set of spherical waves centered on a given origin and form a complete basis set of solutions to Eq. (1).

The set of outgoing (or irregular[11]) VSWFs is traditionally denoted by $\mathbf{M}_{n,m}$, $\mathbf{N}_{n,m}$ and satisfies Eq. (1) with outgoing boundary conditions:

$$\mathbf{M}_{nm}(k\mathbf{r}) \equiv h_n(kr)\mathbf{X}_{nm}(\theta, \phi),$$

$$\mathbf{N}_{nm}(k\mathbf{r}) \equiv \frac{1}{kr}\{\sqrt{n(n+1)}h_n(kr)\mathbf{Y}_{nm}(\theta, \phi)$$

$$+ [krh_n(kr)]'\mathbf{Z}_{nm}(\theta, \phi)\}, \qquad (2)$$

where h_n are the spherical Hankel functions of the first kind and $[krh_n(kr)]'$ is the derivative of $krh_n(kr)$ with respect to kr. We use a normalized version of the $\mathbf{M}$ and $\mathbf{N}$ functions,[11] which can be conveniently expressed in terms of the normalized vector spherical harmonics (VSHs) $\mathbf{X}$, $\mathbf{Y}$, and $\mathbf{Z}$[16]:

$$\mathbf{X}_{nm}(\theta, \phi) \equiv \mathbf{Z}_{nm}(\theta, \phi) \times \hat{\mathbf{r}} = \gamma_{nm}\mathbf{C}_{nm}(\theta, \phi),$$

$$\mathbf{Y}_{nm}(\theta, \phi) \equiv \hat{\mathbf{r}}Y_{nm}(\theta, \phi) \equiv \gamma_{nm}\sqrt{n(n+1)}\mathbf{P}_{nm}(\theta, \phi),$$

$$\mathbf{Z}_{nm}(\theta, \phi) \equiv \frac{r\nabla Y_{nm}(\theta, \phi)}{\sqrt{n(n+1)}} = \hat{\mathbf{r}} \times \mathbf{X}_{nm}(\theta, \phi)$$

$$= \gamma_{nm}\mathbf{B}_{nm}(\theta, \phi), \qquad (3)$$

where $Y_{nm}(\theta, \phi)$ are the normalized scalar spherical harmonics and $\mathbf{C}$, $\mathbf{P}$, $\mathbf{B}$ are the VSHs used by Tsang et al.[11] (see also Appendix A). Nondivergent (i.e., incident) fields should be developed on the basis of regular partial waves, $\mathcal{R}g\{[\mathbf{M}_{n,m}]\}$, $\mathcal{R}g\{[\mathbf{N}_{n,m}]\}$,[11] which are obtained by one's replacing the spherical Hankel functions, h_n, in Eqs. (2) with spherical Bessel functions j_n.

A. Partial-Wave Developments of the Incident Field
The above results permit the development of an arbitrary incident electric field, $\mathbf{E}_i(\mathbf{r})$, on the basis of the regular VSWFs:

$$\mathbf{E}_i(\mathbf{r}) = A\sum_{n,m} \mathcal{R}g\{[\mathbf{M}_{n,m}(k\mathbf{r})]\}a_{n,m}^M + \mathcal{R}g\{[\mathbf{N}_{n,m}(k\mathbf{r})]\}a_{n,m}^N$$

$$\equiv A\mathcal{R}g\{[\mathbf{M}(k\mathbf{r}), \mathbf{N}(k\mathbf{r})]\}a$$

$$\equiv A\mathcal{R}g\{\mathbf{\Psi}^t(k\mathbf{r})\}a, \qquad (4)$$

where A is an overall field amplitude coefficient with the dimensions of an electric field and $a_{n,m}^M$, $a_{n,m}^N$ are dimensionless partial-wave expansion coefficients. The second and third lines of Eq. (4) introduce a compact vector notation that allows the suppression of the bothersome summation over index labels, n, m.[11,12] In the compact notation, a is a shorthand symbol representing an infinite column vector composed of the $a_{n,m}^M$, $a_{n,m}^N$ coefficients, and $\mathbf{\Psi}^t$ (the t indicating the transpose) represents an infinite row vector composed of the VSWFs:

$$\mathbf{\Psi}(k\mathbf{r}) = [\mathbf{M}_{1,1}(k\mathbf{r}), \mathbf{M}_{1,0}(k\mathbf{r}), \mathbf{M}_{1,-1}(k\mathbf{r}), \ldots, \mathbf{N}_{1,1}(k\mathbf{r}), \mathbf{N}_{1,0}(k\mathbf{r}), \mathbf{N}_{1,-1}(k\mathbf{r}), \ldots]. \qquad (5)$$

O. Moine and B. Stout

One can find the incident magnetic field corresponding to a given incident electric field by invoking Faraday's law,

$$\mathbf{H}_i(\mathbf{r}) = \frac{1}{i\omega\mu_b\mu_0} \nabla \times \mathbf{E}_i(\mathbf{r}) = \frac{A}{i\omega\mu_b\mu_0} \mathcal{R}g\{\nabla \times \mathbf{\Psi}^t(k\mathbf{r})\}a$$

$$= A\left(\frac{\varepsilon_b\epsilon_0}{\mu_b\mu_0}\right)^{1/2} \mathcal{R}g\{[\mathbf{N}(k\mathbf{r}),\mathbf{M}(k\mathbf{r})]\}a, \qquad (6)$$

and the convenient rotational properties of the VSWFs, $\nabla \times \mathbf{M} = k\mathbf{N}$ and $\nabla \times \mathbf{N} = k\mathbf{M}$.

The most common theoretical choice for incident fields in electromagnetic theory is that of polarized homogenous incident plane waves of the form $\mathbf{E}_i^{p.w.} = A \exp(i\mathbf{k}_i \cdot \mathbf{r})\hat{\mathbf{e}}_i$, where $\hat{\mathbf{e}}_i$ is a (possibly complex) polarization vector with unit norm $|\hat{\mathbf{e}}_i| = 1$. For this choice, the incident-field coefficients can be determined analytically and can be conveniently expressed in terms of the VSHs[16]:

$$[p]_{nm}^M \equiv 4\pi\mathcal{X}_{nm}(\hat{\mathbf{k}}_i) \cdot \hat{\mathbf{e}}_i \equiv 4\pi i^n \mathbf{X}_{nm}^*(\hat{\mathbf{k}}_i) \cdot \hat{\mathbf{e}}_i,$$

$$[p]_{nm}^N = 4\pi\mathcal{Z}_{nm}(\hat{\mathbf{k}}_i) \cdot \hat{\mathbf{e}}_i \equiv 4\pi i^{n-1} \mathbf{Z}_{nm}^*(\hat{\mathbf{k}}_i) \cdot \hat{\mathbf{e}}_i, \qquad (7)$$

where we replace the arbitrary incident-field coefficient vector a with the symbol p as a reminder that the $[p]_{nm}^{M,N}$ are the coefficients of an incident plane wave. It proves convenient to define the phase-modified VSH, $\mathcal{X}_{nm}$ and $\mathcal{Z}_{nm}$, in Eqs. (7) because these quantities appear repeatedly in far-field calculations.

For inhomogeneous beams such as those used in optical tweezers, the normalization of the field amplitude coefficient A in Eq. (4) can easily become a point of confusion and erroneous results. For the common optical tweezer beams formed from a lowest-order T_{00}-type laser mode, we choose to normalize the field amplitude at the maximal symmetry point of the beam (i.e., the center of the Rayleigh region—typically being the point of maximal field amplitude). When this maximal symmetry point is taken to be the system origin, O, the connection with experimental irradiance is facilitated if we define A such that

$$A^2 \equiv 2|\mathbf{S}_i(\mathbf{0})|\left(\frac{\mu_b\mu_0}{\varepsilon_b\epsilon_0}\right)^{1/2}, \qquad (8)$$

where $\mathbf{S}_i(\mathbf{0})$ is the time-averaged incident Poynting vector, $\mathbf{S}_i(\mathbf{r}) \equiv \frac{1}{2}\text{Re}\{\mathbf{E}_i^* \times \mathbf{H}_i\}$, evaluated at the origin.

For an incident homogeneous plane-polarized wave, the normalization of Eq. (8) is consistent with A being the amplitude of a complex electric field, $|\mathbf{E}_i^{p.w.}| = A$. The adoption of Eq. (8) imposes a normalization condition on the dimensionless a coefficients. A computation of $|\mathbf{S}_i(\mathbf{0})|$ using the field developments of Eqs. (4) and (6) and the value Eq. (8) of A shows that the dimensionless incident-field coefficient vector a must consequently be normalized such that the dipole beam coefficients satisfy (see Appendix D)

$$\text{Re}\{[a]_{1,-1}^{N,*}[a]_{1,-1}^M - [a]_{1,1}^{N,*}[a]_{1,1}^M\} = 6\pi. \qquad (9)$$

One can verify that the plane-wave coefficients of Eqs. (7) [see also Eqs. (15) below] always satisfy this normalization condition.

The direction of incidence, $\hat{\mathbf{u}}_i$, of the incident field is defined as

$$\hat{\mathbf{u}}_i \equiv \mathbf{S}_i(\mathbf{0})/|\mathbf{S}_i(\mathbf{0})|, \qquad (10)$$

with $\hat{\mathbf{u}}_i$ characterized by two angles, θ_i and ϕ_i. For axisymmetric beams, $\hat{\mathbf{u}}_i$ will lie along the symmetry axis. We henceforth define the incident irradiance, $I(\mathbf{r})$, of the incident field as the beam power flux along the direction of incidence:

$$I(\mathbf{r}) \equiv \mathbf{S}_i(\mathbf{r}) \cdot \hat{\mathbf{u}}_i, \qquad (11)$$

where it is important to note that $I(\mathbf{r})$ for inhomogeneous beams is not equal to the norm of the Poynting vector, $|\mathbf{S}_i(\mathbf{r})|$ (except at the origin).

The total beam power, P_i, is a more readily obtainable experimental quantity than $I(\mathbf{0})$. Furthermore, for more exotic beams (doughnut beams, asymmetric beams, etc.), the maximal symmetry point may not always be readily identifiable or may be located in a region of near-zero irradiance. We will see in Section 3 below how one can reformulate the force in terms of a beam power normalization that is independent of a chosen point of system origin. For the moment, we remark that P_i can be obtained by integrating the irradiance over any plane perpendicular to $\hat{\mathbf{u}}_i$; i.e., when $\hat{\mathbf{z}} \equiv \hat{\mathbf{u}}_i$, P_i is given by

$$P_i = \int I(x,y,z)\mathrm{d}x\mathrm{d}y\big|_{z=\text{const.}} = \int_0^\infty \rho\mathrm{d}\rho \int_0^{2\pi} \mathrm{d}\phi I(\rho,\phi,z)\big|_{z=\text{const.}}, \qquad (12)$$

independent of z.

B. Axisymmetric Beams

In this paper, we will consider only beams whose irradiance is axisymmetric. We shall see below, however, that this does not, in general, imply an axial symmetric intensity, $|\mathbf{E}|^2$. It suffices for this demonstration to perform calculations for models based on low-order Davis corrections[14,15] to moderately divergent beams.

If one develops the partial-wave expansion of a beam with an axisymmetric irradiance in a system whose origin is placed at the center of the maximum beam constriction, the partial-wave expansion coefficients can be conveniently expressed[15] as

$$[a]_{n,m}^A = [g]_n[p]_{n,m}^A, \quad A = M,N, \qquad (13)$$

where the $[p]_{n,m}^A$ are the plane-wave expansion coefficients of a plane wave with $\hat{\mathbf{k}} = \hat{\mathbf{u}}_i$ and the $[g]_n$ coefficients depend only on the n number. Following the terminology of Gouesebet et al., we refer to these $[g]_n$ coefficients as the beam shape coefficients.

Strictly speaking, the models that we shall consider lie somewhat outside the paraxial approximation invoked in the derivation of a Gaussian beam. Nevertheless, the low-order Davis corrections that we have chosen to work with allow us to roughly apply Gaussian beam terminology such as diffraction length, waist, etc. For near-Gaussian beams, the tightness of the beam focusing can be parameterized via the dimensionless beam shape parameter s:

$$s \equiv \frac{1}{kw_0} \equiv \frac{w_0}{2z_R} \simeq \frac{\tan\theta_d}{2}, \tag{14}$$

where w_0 in the paraxial approximation is the minimal beam radius or waist, z_R is the Rayleigh diffraction length, and θ_d is the beam angle of divergence. The first equality in expression (14) gives us a physically transparent expression of the s parameter as the wavelength divided by beam circumference at the minimal focus (i.e., the circumference of the beam spot).

Using the values of the plane-wave coefficients given in Eqs. (7) and defining the $\hat{\mathbf{z}}$ axis to lie along the incident-beam direction, we find that the analytic expressions of the $|m|=1$ plane-wave coefficients are

$$[p]^{\mathrm{M}}_{n,1} \equiv 4\pi\mathcal{X}_{n1}(0,0)\cdot\hat{\mathbf{e}}_{\mathrm{i}} = i^n\sqrt{\pi(2n+1)}(i\hat{\theta}+\hat{\phi})\cdot\hat{\mathbf{e}}_{\mathrm{i}},$$

$$[p]^{\mathrm{N}}_{n,1} \equiv 4\pi\mathcal{Z}_{n1}(0,0)\cdot\hat{\mathbf{e}}_{\mathrm{i}} = i^n\sqrt{\pi(2n+1)}(i\hat{\theta}+\hat{\phi})\cdot\hat{\mathbf{e}}_{\mathrm{i}},$$

$$[p]^{\mathrm{M}}_{n,-1} = i^n\sqrt{\pi(2n+1)}(i\hat{\theta}-\hat{\phi})\cdot\hat{\mathbf{e}}_{\mathrm{i}},$$

$$[p]^{\mathrm{N}}_{n,-1} = i^n\sqrt{\pi(2n+1)}(-i\hat{\theta}+\hat{\phi})\cdot\hat{\mathbf{e}}_{\mathrm{i}}, \tag{15}$$

with $[p]^{\mathrm{M,N}}_{n,m}=0$, when $|m|\neq 1$. Under our chosen conditions that the origin is the maximum symmetry point of the beam, the beam shape coefficients can be chosen to be real.[15] One further ensures that the beam expansion coefficients, $[a]^{\mathrm{A}}_{n,m}$ [Eq. (13)], satisfy the normalization condition of Eq. (9) by simply imposing $[g]_1=1$ [in that the plane-wave coefficients, $[p]^{\mathrm{A}}_{1,m}$, already satisfy Eq. (9)].

C. Beam Power Normalization

We saw in Eq. (8) that the beam amplitude constant, A, was determined by the irradiance at the origin $I(\mathbf{0})$. This beam center irradiance is rarely a precisely known quantity, and the relationship between $I(\mathbf{0})$ and the total beam power depends strongly on the beam shape. It is therefore preferable to formulate the force in terms of the total beam power P_{i}. Dimensional arguments lead us to a convenient definition of a dimensionless shape normalization parameter, φ, defined such that

$$I(\mathbf{0}) \equiv \varphi\frac{k^2 P_{\mathrm{i}}}{\pi}, \tag{16}$$

where $k=2\pi/\lambda_b$, the factor π is for later convenience, and φ is a geometric factor calculated from the irradiance profile of the beam. For an axisymmetric beam, the total power is

$$P_{\mathrm{i}} = \frac{2\pi}{k^2}\int_0^\infty I(\mathbf{r})k\rho(k\,\mathrm{d}\rho)\bigg|_{z=\mathrm{const.}}. \tag{17}$$

A comparison with Eq. (16) shows that φ is expressed as

$$\varphi = \left[2\int_0^\infty \frac{I(\mathbf{r})}{I(\mathbf{0})}k\rho(k\,\mathrm{d}\rho)\bigg|_{z=\mathrm{const.}}\right]^{-1}. \tag{18}$$

The extent to which an optical tweezer beam differs from a paraxial Gaussian beam approximation is an important question in optical tweezers, and it may therefore prove instructive for comparison to calculate φ for a Gaussian beam. We recall that Gaussian beams are an approximate solution of the Maxwell equations in free space for which the irradiance is expressed as

$$I_g(\mathbf{r}) = I_g(\mathbf{0})\left[\frac{w_0}{w(z)}\right]^2\exp\left[-\frac{2\rho^2}{w^2(z)}\right];$$

$$w(z) = w_0\left[1+\left(\frac{z}{z_R}\right)^2\right]^{1/2}, \tag{19}$$

where $z_R=kw_0^2/2=w_0/2s$ is the Rayleigh length and s is the beam parameter of expression (14). The power integral of Eq. (17) for a Gaussian irradiance yields

$$P_{\mathrm{i}}^g = \frac{\pi}{2}w_0^2 I_g(\mathbf{0}) = \frac{\pi}{2}\frac{1}{k^2 s^2}I_g(\mathbf{0}),$$

which corresponds to a normalization factor from Eq. (18) of $\varphi_g=2s^2$.

For non-Gaussian beams, one can readily evaluate φ numerically by carrying out the integral of Eq. (18) in an arbitrary $z=$constant plane. With a bit of effort, one can alternatively obtain an analytic expression for φ in terms of the shape coefficients. One possible derivation of this analytic expression is outlined in Appendix C by our carrying out an analytic integration of the irradiance in the $z=0$ plane. The result in terms of the shape coefficients, $[g]_n$, of Eq. (13) is

$$\varphi = \left\{ \sum_{p,q=0}^{(N_{\max}-1)/2} [g]_{2p+1}[g]_{2q+1}(4p+3)(4q+3) \right.$$
$$\times\frac{(2p-1)!!}{(2p+2)!!}\frac{(2q-1)!!}{(2q+2)!!}(-1)^{p-q}$$
$$+2\sum_{p=1}^{N_{\max}/2}\sum_{q=0}^{(N_{\max}-1)/2}[g]_{2p}[g]_{2q+1}\frac{(2q+1)!!}{(2q)!!}$$
$$\left.\times\frac{(2p-1)!!}{(2p)!!}\frac{(4p+1)(4q+3)}{2p(2p+1)-(2q+1)(2q+2)}(-1)^{p-q+1}\right\}^{-1}. \tag{20}$$

We note that a statement has erroneously appeared in the literature that the power of inhomogeneous beams is simply $P_{\mathrm{i}}\propto\Sigma_{n,m}\{|a^{\mathrm{M}}_{n,m}|^2+|a^{\mathrm{N}}_{n,m}|^2\}$. This result is apparently derived through far-field considerations of the intensity and an overly hasty appeal to the orthonormality of the VSHs. It is worth remarking that the erroneous result predicts that the total power flux of an inhomogeneous beam is simply the sum of the power flux of the individual partial waves (without interference effects). If any further evidence were necessary, we remark that it is a relatively simple matter to numerically compute the beam irradiance over any infinite plane intercepting the beam and that this calculation supports Eq. (20).

D. Davis-Type Beams

We have chosen to work with Davis-type models here because they allow us to use familiar Gaussian beam terminology and because, in the localization approximation of

O. Moine and B. Stout

Gouesebet *et al.*,[15] one obtains simple analytic expressions for their beam coefficients. Nonparaxial corrections in the Davis prescription take the form of an s^2 power series of approximations to the vector potential, and the first-, third-, and fifth-order Davis beams are given, respectively, by[15]

$$[g_1]_n = \exp[-s^2(n-1)(n+2)],$$

$$[g_3]_n = [g_1]_n + \exp[-s^2(n-1)(n+2)](n-1)(n+2)s^4[3-(n-1)(2+n)s^2],$$

$$[g_5]_n = [g_3]_n + \exp[-s^2(n-1)(n+2)]\{(n-1)^2(n+2)^2s^8[10 - 5(n-1)(2+n)s^2 + 0.5(n-1)^2(n+2)^2s^4]\}, \quad (21)$$

where g_1 corresponds to the commonly used paraxial, i.e., Gaussian approximation to focused beams with axial, i.e., E_z, field corrections.[14]

The diffraction limit of focusing is generally accepted to be $w_0 \simeq \lambda_b/2$, which corresponds to an s parameter of $s \equiv \lambda_b/2\pi w_0 \simeq 1/\pi \simeq 0.32$, which we shall adopt from here on. This does not mean that $s \simeq 1/\pi$ is the largest possible beam shape parameter but rather that higher s parameters would require corrections beyond that of the low-order Davis corrections in order to reconcile high beam divergence with diffraction considerations. Taking $s = 1/\pi$ (corresponding to a beam divergence of $\theta_d \simeq 33°$), we illustrate the focal-plane irradiance and intensity profiles for a g_5 beam in Fig. 1. The shape normalization factor for

Fig. 1.   Focal-plane irradiance and intensity of a $\hat{\mathbf{y}}$-polarized fifth-order Davis beam with $s = 1/\pi$.

this beam is $\varphi_{g_5} \simeq 0.130$ (as opposed to a Gaussian value of $\varphi = 2s^2 \simeq 0.2$; we note that the considerable difference between these two values of φ is due in part to the non-Gaussian nature of the g_5 beam and in part to ambiguities involving the determination of w_0 in terms of irradiance or intensity).

3. CROSS SECTIONS AND OPTICAL FORCES IN INHOMOGENEOUS BEAMS

For inhomogeneous beams, it proves essential to define position-dependent cross sections and efficiencies. We introduce our notation and justify our terminology by first studying the position-dependent scattering cross section in inhomogeneous beams. We then tackle the somewhat more difficult problem of optical force cross sections and efficiencies.

A. Position-Dependent Cross Sections

Before generalizing to inhomogeneous beams, let us first recall the traditional definition of the scattering cross section. For incident plane waves, the total electromagnetic power scattered by a particle is given by $P_s = I\sigma_s$, where the scattering cross section, σ_s, has the dimension of a surface. The irradiance is defined by $I \equiv \mathbf{S}_i \cdot \hat{\mathbf{k}}_i = |\mathbf{S}_i|$, where $\mathbf{S}_i$ is the complex Poynting vector of the chosen incident plane wave. The σ_s depends on the physical properties of the particle, as well as the wavelength, direction, and polarization of the incident field, but not on the particle position or incident-field strength. By definition, σ_s is the solid-angle integral of the differential cross section, $d\sigma_s/d\Omega$:

$$\sigma_s(\theta_i, \phi_i) = \int_0^\pi \sin\theta d\theta \int_0^{2\pi} d\phi \frac{d\sigma_s(\theta, \phi, \theta_i, \phi_i)}{d\Omega}, \quad (22)$$

where θ_i, ϕ_i specify the direction of $\hat{\mathbf{k}}_i$. The differential cross section, $d\sigma_s/d\Omega$, is defined via the ratio of scattered to incident flux:

$$\frac{d\sigma_s(\theta, \phi, \theta_i, \phi_i)}{d\Omega} \equiv \lim_{r \to \infty} r^2 \frac{\hat{\mathbf{r}} \cdot \mathbf{S}_s(\mathbf{r})}{I}, \quad (23)$$

where $\mathbf{S}_s(r\hat{\mathbf{r}})$ is the Poynting vector of the scattered field and the angles θ, ϕ specify the direction of $\hat{\mathbf{r}}$.

For inhomogeneous beams, the irradiance [see Eqs. (10) and (11)] is no longer a constant, and the scattered flux will depend on the particles' position. For a particle centered on $\mathbf{x}$, we can generalize the cross-section formula of Eq. (23) by dividing by the irradiance at the system origin, $I(\mathbf{0}) \equiv \mathbf{S}_i(\mathbf{0}) \cdot \hat{\mathbf{u}}_i = |\mathbf{S}_i(\mathbf{0})|$:

$$\frac{d\sigma_s(\mathbf{x})}{d\Omega} \equiv \lim_{r \to \infty} r^2 \frac{\hat{\mathbf{r}} \cdot \mathbf{S}_s(\mathbf{r})}{I(\mathbf{0})} = \lim_{r \to \infty} \frac{r^2}{2} \left(\frac{\varepsilon_b \epsilon_0}{\mu_b \mu_0} \right)^{1/2} \frac{\mathbf{E}_s^*(\mathbf{r}) \cdot \mathbf{E}_s(\mathbf{r})}{I(\mathbf{0})}. \quad (24)$$

The power of the radiation scattered by a particle at position $\mathbf{x}$ is then $P_s(\mathbf{x}) = I(\mathbf{0})\sigma_s(\mathbf{x})$.

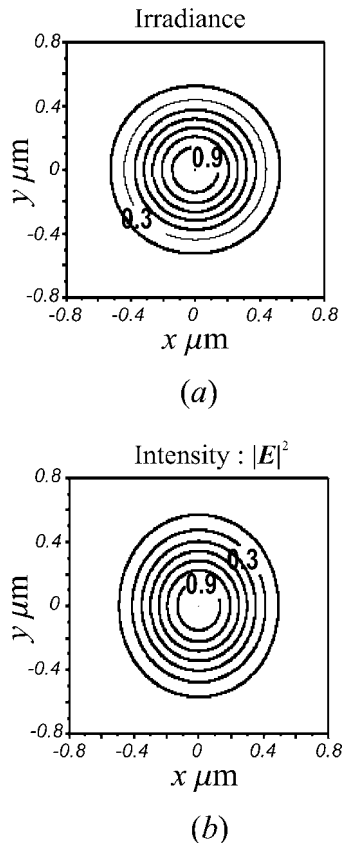The position dependence in Eq. (24) enters into the calculations via the VSWF development of the scattered field:

$$\mathbf{E}_s(\mathbf{r}') = A\mathcal{R}g\{\mathbf{\Psi}^t[k(\mathbf{r}-\mathbf{x})]\}f(\mathbf{x}), \qquad (25)$$

where $\mathbf{r}' \equiv \mathbf{r}-\mathbf{x}$ and $f(\mathbf{x})$ is the column vector composed of the scattering coefficients for a particle centered on $\mathbf{x}$. One obtains an analytic expression for $\sigma_s(\mathbf{x})$ in terms of $f(\mathbf{x})$ by inserting the partial-wave development of Eq. (25) into Eq. (24), invoking Eq. (8) for the value of A, and carrying out an analytic integration over the solid angles in Eq. (22) to obtain[11,16]

$$\sigma_s(\mathbf{x}) = \frac{1}{k^2}f^{\dagger}(\mathbf{x})f(\mathbf{x}). \qquad (26)$$

For incident-field coefficients, $a(\mathbf{x})$, developed around an origin located at $\mathbf{x}$ in the system reference frame, the scattering coefficients can be conveniently obtained from transition-matrix theory as

$$f(\mathbf{x}) = Ta(\mathbf{x}), \qquad (27)$$

where T is the transition matrix of the scattering particle.[11,16] The translation-addition theorem (see Appendix B) allows us to express $a(\mathbf{x})$ in terms of the incident-field coefficients, a, established in the system reference frame:

$$a(\mathbf{x}) = J(k\mathbf{x})a, \qquad (28)$$

where $J(k\mathbf{x})$ is the regular translation-addition matrix. This leaves us with a final expression for the position-dependent cross section:

$$\sigma_s(\mathbf{x}) = \frac{1}{k^2}a^{\dagger}J^{\dagger}(k\mathbf{x})T^{\dagger}TJ(k\mathbf{x})a. \qquad (29)$$

This expression for $\sigma_s(\mathbf{x})$ has two inconvenient aspects: The value of $\sigma_s(\mathbf{x})$ will depend on the choice of the system origin, and the formula in Eq. (29) is valid only if the system incident-field coefficients, a, satisfy the normalization of Eq. (9). Both problems can be removed by one's formulating the scattering power in terms of the total incident-beam power. Invoking the shape normalization parameter, φ, of Eq. (16), we can write the expression for the scattered power, $P_s(\mathbf{x})=I(\mathbf{0})\sigma_s(\mathbf{x})$, in terms of the total power, P_i, of the incident beam:

$$P_s(\mathbf{x}) = P_i\frac{k^2}{\pi}\varphi\sigma_s(\mathbf{x}) \equiv P_iQ_s(\mathbf{x}),$$

$$Q_s(\mathbf{x}) \equiv k^2\frac{\varphi}{\pi}\sigma_s(\mathbf{x}) = \frac{\varphi}{\pi}a^{\dagger}J^{\dagger}(k\mathbf{x})T^{\dagger}TJ(k\mathbf{x})a,$$

$$(30)$$

where the dimensionless beam efficiency factor, $Q_s(\mathbf{x})$, is independent of the normalization of the incident-field coefficients, a. Furthermore, $Q_s(\mathbf{x})$ is independent of the choice of system origin.

Having familiarized ourselves with position-dependent cross sections, we will apply analogous considerations and formulations to the force cross sections and efficiencies in Subsection 3.B.

B. Force Cross Formulation from the Maxwell Stress Tensor

Starting from the Lorentz force equations, one can calculate the time-averaged electromagnetic force, $\mathbf{F}$, on the induced charges in a material object by integrating the time-harmonic Maxwell stress tensor, $\overset{\leftrightarrow}{\mathbf{T}}$, over a closed surface, Γ, surrounding the object:

$$\mathbf{F} = \oint_{\Gamma} \overset{\leftrightarrow}{\mathbf{T}}\cdot\hat{\mathbf{n}}ds, \qquad (31)$$

where $\hat{\mathbf{n}}$ is the local unit normal of the closed surface. The time-averaged optical force is then obtained by our evaluating the following time-averaged constraint tensor $\overset{\leftrightarrow}{\mathbf{T}}$ expressed in terms of the total complex electromagnetic fields, $\mathbf{E}$ and $\mathbf{B}$:

$$\overset{\leftrightarrow}{\mathbf{T}}_{i,j}(\mathbf{r}) = \frac{1}{2}\text{Re}\left\{\varepsilon_b\epsilon_0 E_i^*(\mathbf{r})E_j(\mathbf{r}) + \frac{1}{\mu_b\mu_0}B_i^*(\mathbf{r})B_j(\mathbf{r})\right.$$
$$\left. - \frac{1}{2}\left[\varepsilon_b\epsilon_0|\mathbf{E}(\mathbf{r})|^2 + \frac{|\mathbf{B}(\mathbf{r})|^2}{\mu_b\mu_0}\right]\delta_{i,j}\right\}. \qquad (32)$$

One can readily verify that $\overset{\leftrightarrow}{\mathbf{T}}$ has the dimension of pressure.

To remove the dependence on the field strength, it is convenient to define a vector radiation force cross section $\boldsymbol{\sigma}_f$ and efficiency vector $\mathbf{Q}_f$ such that

$$\mathbf{F} \equiv \frac{I(\mathbf{0})}{v_b}\boldsymbol{\sigma}_f(\mathbf{r}) = \frac{P_i k^2\varphi}{v_b \pi}\boldsymbol{\sigma}_f(\mathbf{r}) \equiv \frac{P_i}{v_b}\mathbf{Q}_f(\mathbf{r}), \qquad (33)$$

where $v_b=c/n_b=\sqrt{\varepsilon_b\mu_b\epsilon_0\mu_0}^{-1}$ is the (real) phase velocity in the background medium. With these definitions, the vector $\boldsymbol{\sigma}_f(\mathbf{r})$ has the dimensions of a surface, and $\mathbf{Q}_f(\mathbf{r}) \equiv (k^2\varphi/\pi)\boldsymbol{\sigma}_f(\mathbf{r})$ is an efficiency vector that is independent of the normalization of the incident coefficient vector a.

Taking the closed surface in Eq. (31) to be a sphere at infinity, invoking the far-field limits, and comparing the result with the definitions in Eq. (33) show that $\boldsymbol{\sigma}_f$ can be expressed as

$$\boldsymbol{\sigma}_f = \boldsymbol{\sigma}_r - \boldsymbol{\sigma}_a, \qquad (34)$$

where $\boldsymbol{\sigma}_a$ characterizes the contribution to the force due to asymmetric scattering of the particle:

$$\boldsymbol{\sigma}_a = \frac{v_b}{4I(\mathbf{0})}\int_{\Omega}\hat{\mathbf{r}}\left\{\varepsilon_b\epsilon_0\mathbf{E}_s^*\cdot\mathbf{E}_s + \frac{1}{\mu_b\mu_0}\mathbf{B}_s^*\cdot\mathbf{B}_s\right\}d\Omega$$
$$\underset{r\to\infty}{=} \frac{1}{2I(\mathbf{0})}r^2\left(\frac{\varepsilon_b\epsilon_0}{\mu_b\mu_0}\right)^{1/2}\int_{\Omega}\hat{\mathbf{r}}\mathbf{E}_s^*\cdot\mathbf{E}_sd\Omega. \qquad (35)$$

We have eliminated the magnetic field from the expressions by using the vector identity $(\mathbf{a}\times\mathbf{b})\cdot(\mathbf{c}\times\mathbf{d})=(\mathbf{a}\cdot\mathbf{c})\times(\mathbf{b}\cdot\mathbf{d})-(\mathbf{a}\cdot\mathbf{d})(\mathbf{b}\cdot\mathbf{c})$, the far-field results $\lim_{r\to\infty}\hat{\mathbf{r}}\cdot\mathbf{E}_s=0$, and[13]

$$\mathbf{B}_s(\mathbf{r}) \underset{r\to\infty}{=} (\varepsilon_b\epsilon_0\mu_b\mu_0)^{1/2}\hat{\mathbf{r}}\times\mathbf{E}_s. \qquad (36)$$

O. Moine and B. Stout

The other contribution to the optical force, σ_r, corresponds to the momentum flux removed from the incident beam:

$$\sigma_r \underset{r\to\infty}{=} -\frac{v_b}{4I(0)}r^2\left\{\varepsilon_b\epsilon_0\int_\Omega \hat{\mathbf{r}}\,\mathrm{Re}\{\mathbf{E}_s^*\cdot\mathbf{E}_i + \mathbf{E}_i^*\cdot\mathbf{E}_s\}d\Omega\right.$$

$$\left.+\frac{1}{\mu_b\mu_0}\int_\Omega\hat{\mathbf{r}}\,\mathrm{Re}\{\mathbf{B}_s^*\cdot\mathbf{B}_i + \mathbf{B}_i^*\cdot\mathbf{B}_s\}d\Omega\right\}$$

$$= -\frac{1}{2I(0)}\lim_{r\to\infty}r^2\left(\frac{\varepsilon_b\epsilon_0}{\mu_b\mu_0}\right)^{1/2}\int_\Omega\hat{\mathbf{r}}\,\mathrm{Re}\{\mathbf{E}_s^*\cdot\mathbf{E}_i + \mathbf{E}_i^*\cdot\mathbf{E}_s\}d\Omega,$$

$$(37)$$

where we have again eliminated the magnetic field by employing the same techniques outlined after Eq. (35) and using $\lim_{r\to\infty}\mathbf{B}_i(\mathbf{r}) = (\varepsilon_b\epsilon_0\mu_b\mu_0)^{1/2}\hat{\mathbf{r}}\times\mathbf{E}_i$.

C. Axial Force Efficiency
In single-beam optical tweezers, trapping is consistently stronger along the radial direction than in the axial direction. To determine the existence of trapping, one must foremost look at the forces along the beam direction (henceforth referred to as the axial direction), which typically go under the name of optical pressure even though trapping can exist only when this quantity has a region of negative values.

Without loss of generality, we can define the $\hat{\mathbf{z}}$ axis to lie along the $\hat{\mathbf{z}} = \hat{\mathbf{u}}_i$ direction. The optical pressure force is thus $F_p = F_z = (P_i/v_b)(k^2\varphi/\pi)\sigma_p$ with

$$\sigma_p \equiv \hat{\mathbf{z}}\cdot\boldsymbol{\sigma}_r - \hat{\mathbf{z}}\cdot\boldsymbol{\sigma}_a \equiv \sigma_r - g\sigma_s, \qquad (38)$$

where σ_s is the scattering cross section of Eq. (29) and the asymmetry parameter, g, has a standard definition as the projection of the scattered radiation along the direction of incidence.[13] We obtain an analytic expression for g in terms of the scattering coefficient vector $f(\mathbf{x})$ by inserting the development of $\mathbf{E}_s$ on the VSWF basis, Eq. (25), and carrying out the angular integrations in the $\hat{\mathbf{z}}$ component of Eq. (35). The result is

$$g \equiv \frac{1}{\sigma_s}\hat{\mathbf{z}}\cdot\boldsymbol{\sigma}_a = \frac{1}{2I(0)\sigma_s}\left(\frac{\varepsilon_b\epsilon_0}{\mu_b\mu_0}\right)^{1/2}\lim_{r\to\infty}r^2\int_\Omega\hat{\mathbf{z}}\cdot\hat{\mathbf{r}}\mathbf{E}_s^*\cdot\mathbf{E}_s d\Omega$$

$$= \frac{1}{k^2\sigma_s}f^\dagger(\mathbf{x})$$

$$\times\left\{\int d\Omega\cos\theta\begin{bmatrix}\mathcal{X}(\theta,\phi)\\\mathcal{Z}(\theta,\phi)\end{bmatrix}\cdot[\mathcal{X}^*(\theta,\phi),\mathcal{Z}^*(\theta,\phi)]\right\}f(\mathbf{x})$$

$$= \frac{1}{\sigma_s k^2}f^\dagger(\mathbf{x})\Upsilon f(\mathbf{x}), \qquad (39)$$

where the Υ matrix is obtained by one's carrying out the solid-angle integration of the term in brackets and takes the form

$$\Upsilon = \begin{bmatrix}\Xi & \Theta\\\Theta & \Xi\end{bmatrix}, \qquad (40)$$

$$\Theta_{nm,\nu\mu} = \frac{m}{n(n+1)}\delta_{m,\mu}\delta_{n,\nu},$$

$$\Xi_{nm,\nu\mu} = \delta_{m,\mu}\frac{i}{\sqrt{(2n+1)(2\nu+1)}}\left[\frac{\delta_{\nu,n-1}}{n}\sqrt{(n^2-1)(n^2-m^2)}\right.$$

$$\left. -\frac{\delta_{\nu,n+1}}{\nu}\sqrt{(\nu^2-1)(\nu^2-m^2)}\right]. \qquad (41)$$

Carrying out similar manipulations for σ_r, we find

$$\sigma_r(\mathbf{x}) \equiv \hat{\mathbf{z}}\cdot\boldsymbol{\sigma}_r = -\frac{1}{2I(0)}\left(\frac{\varepsilon_b\epsilon_0}{\mu_b\mu_0}\right)^{1/2}\lim_{r\to\infty}r^2\int_\Omega\hat{\mathbf{z}}\cdot\hat{\mathbf{r}}\,\mathrm{Re}\{\mathbf{E}_s^*\cdot\mathbf{E}_i$$

$$+\mathbf{E}_i^*\cdot\mathbf{E}_s\}d\Omega = -\frac{1}{k^2}\mathrm{Re}\{a^\dagger(\mathbf{x})\Upsilon f(\mathbf{x})\}. \qquad (42)$$

Recalling the defining property of the transition matrix, Eq. (27), and invoking the regular translation-addition matrix, $J(k\mathbf{x})$ [see Eqs. (28) and (B2)], we find that $\sigma_p = \sigma_r - g\sigma_s$, and the corresponding efficiency vector, $Q_p(\mathbf{x})$, may be conveniently expressed as

$$\sigma_p(\mathbf{x}) = -\frac{1}{k^2}\mathrm{Re}\{a^\dagger J^\dagger(k\mathbf{x})\Upsilon T J(k\mathbf{x})a\}$$

$$-\frac{1}{k^2}a^\dagger J^\dagger(k\mathbf{x})T^\dagger\Upsilon T J(k\mathbf{x})a,$$

$$Q_p(\mathbf{x}) = -\frac{\varphi}{\pi}\mathrm{Re}\{a^\dagger J^\dagger(k\mathbf{x})\Upsilon T J(k\mathbf{x})a\}$$

$$-\frac{\varphi}{\pi}a^\dagger J^\dagger(k\mathbf{x})T^\dagger\Upsilon T J(k\mathbf{x})a, \qquad (43)$$

where we recall that in terms of $Q_p(\mathbf{x})$ the optical pressure force is simply

$$F_p = \frac{P_i}{v_b}Q_p(\mathbf{x}). \qquad (44)$$

The absolute value of the efficiency vector $Q_p(\mathbf{x})$ thus determines the fraction of the total beam momentum that is converted into a force along the direction of incidence. For numerical determinations of the force, the factor $1/v_b$ in Eq. (44) can be approximately expressed as

$$\frac{1}{v_b} \simeq \frac{n_b}{3}10^{-8}\frac{N}{W} = n_b\frac{10}{3}\frac{\mathrm{pN}}{\mathrm{mW}} \simeq 4.4\frac{\mathrm{pN}}{\mathrm{mW}}, \qquad (45)$$

where, in the last equality, we took our value for the refraction index of water, $n_b \simeq 1.32$. One can therefore obtain the force in piconewtons per milliwatt of beam power by multiplying $Q_p(\mathbf{x})$ by 4.4.

We remark that, although our force formulas are valid for inhomogeneous beams, one retrieves for incident plane waves the classic Debye–Mie results, $\sigma_p = \sigma_e - g\sigma_s$.[13,17,18] This can be verified by showing that the asymmetry factor contribution, $g\sigma_s$ [Eq. (39)], is identical to the plane-wave results[13] by simply inserting the
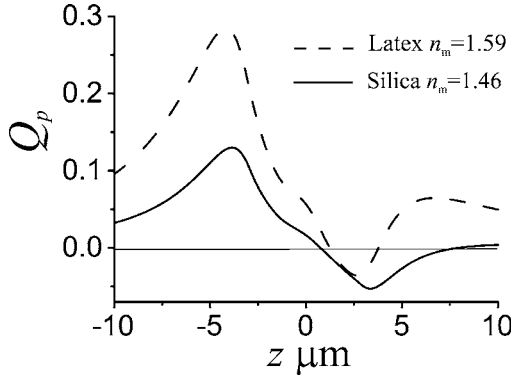
Fig. 2.   Axial trapping efficiency, $Q_p(z)$, for spheres of radii $R = 2.1$ (μm) composed of silica ($n_s = 1.46$) and latex ($n_s = 1.59$) immersed in water ($n_b = 1.32$) and exposed to a $\hat{\mathbf{y}}$-polarized fifth-order Davis beam.

coefficients for incident plane waves. One can also show that $\sigma_r(\mathbf{x})$ is identical to the extinction cross section σ_e in the plane-wave limit[19]:

$$\sigma_r \to \sigma_e = -\frac{1}{k^2}\mathrm{Re}\{p^\dagger T p\}. \qquad (46)$$

D. Applications to Trapping
In this paper we restrict ourselves to evaluating the forces on spherical objects in order to avoid the complications associated with torques and particle orientation. The transition matrix, T, is then diagonal with matrix elements corresponding to the Mie coefficients.[11,16] The axial force formula of expressions (43)–(45) permits us to quantitatively calculate the optical forces along the direction of the beam propagation and thereby determine the trapping position and stiffness.

We show in Fig. 2 the axial trapping efficiency of silica and latex spheres of radius $R = 2.1$ (μm) suspended in water and a $\hat{\mathbf{y}}$-polarized, $s = 1/\pi$ fifth-order Davis beam. The position $z = 0$ corresponds to the beam focus (i.e., center of the Rayleigh region). We note that the calculation predicts trapping for both the silica and the latex spheres because both curves contain regions for which the radiation pressure is negative. The stable trapping position, z_{tr}, is given by the point for which $Q_p(z_{tr}) = 0$ and $dQ_p(z)/dz|_{z=z_{tr}} < 0$. We remark that the trapping positions for the two types of sphere, though not the the same, are ~ 0.8–1 (μm) after the beam focus, which indicates that scattering forces (sometimes called radiation damping forces) along the direction of beam propagation are not entirely negligible compared with the gradient forces that draw the particle toward the beam focus.

Our rigorous calculations permit us to demonstrate the importance of resonance effects on optical forces. Such effects cannot be explored by any of the commonly used approximations such as dipole, geometrical optics, or Born-type approximations. We illustrate in Fig. 3 that resonance effects can have a sizable effect on the axial trapping position of a particle. In Fig. 3, the trapping position is calculated as a function of the sphere radius for silica and latex spheres trapped in water by a fifth-order Davis beam. For radii in which the points on the trapping

position curve lie above the $z = R$ dotted line, $R \lesssim 0.62$ (μm) for silica, the center of the beam focus lies outside the particle. For larger particles, $R \gtrsim 0.62$ (μm) for silica, the trapping position lies below the $z = R$ line, indicating that the center of the beam focus lies within the particle as arguments from geometrical optics indicate.

We interpret the oscillations in trapping positions as a function of the radii, observed in Fig. 3, as evidence for geometric resonance effects on the trapping force. This is a subject worthy of more detailed investigations. Notably, one should also investigate the behavior of resonance on the radial trapping force. It may also prove instructive to study the correlation of this phenomenon with the strengths of the scattering cross sections and with field energy densities.

E. Radial Force Efficiency
Let us label $\hat{\rho}$ a radial unit vector (in cylindrical coordinates) between the beam axis and the particle center (characterized by the azimuth angle ϕ). The force along this axis is given by

$$F_\rho \equiv \hat{\rho} \cdot \mathbf{F} = \frac{P_i}{v_b}\hat{\rho} \cdot \mathbf{Q}_f = \frac{P_i}{v_b}\hat{\rho} \cdot (\mathbf{Q}_r - \mathbf{Q}_a). \qquad (47)$$

The $\hat{\rho} \cdot \mathbf{Q}_a$ contribution to F_ρ can be expressed as

$$\hat{\rho} \cdot \mathbf{Q}_a = \frac{k^2 \varphi}{2\pi I(0)}\left(\frac{\varepsilon_b \epsilon_0}{\mu_b \mu_0}\right)^{1/2} \lim_{r\to\infty} r^2 \int_\Omega (\hat{\rho} \cdot \hat{\mathbf{r}}) \mathbf{E}_s^* \cdot \mathbf{E}_s d\Omega$$

$$= \frac{\varphi}{\pi} f^*(\mathbf{x}) \mathrm{D}\left(\phi, \frac{\pi}{2}, 0\right) \left\{ \int d\Omega' \cos\theta' \begin{bmatrix} \mathcal{X}(\theta', \phi') \\ \mathcal{Z}(\theta', \phi') \end{bmatrix} \right.$$

$$\left. \cdot [\mathcal{X}^*(\theta', \phi'), \mathcal{Z}^*(\theta', \phi')] \right\} \mathrm{D}^\dagger\left(\phi, \frac{\pi}{2}, 0\right) f(\mathbf{x}), \quad (48)$$

where the primed angles are measured with respect to the $\hat{\rho}$ axis as the polar direction and the rotation matrix of the VSHs, $\mathrm{D}(\alpha, \beta, \gamma)$, has the form

$$\mathrm{D}(\alpha, \beta, \gamma) \equiv \begin{bmatrix} \mathcal{D}(\alpha, \beta, \gamma) & 0 \\ 0 & \mathcal{D}(\alpha, \beta, \gamma) \end{bmatrix}, \qquad (49)$$

where α, β, γ are the Euler angles. The $\mathcal{D}(\alpha, \beta, \gamma)$ matrix elements are described in detail in Ref. 20 and are block diagonal in the orbital (multipole) quantum number, n:
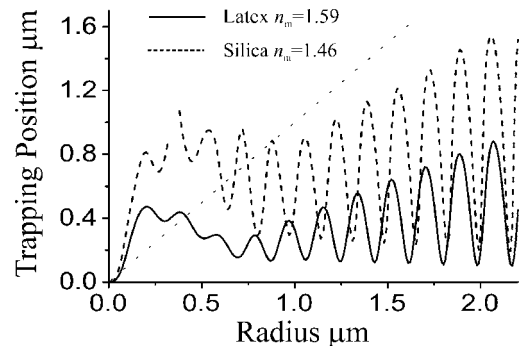

Fig. 3.   Trapping positions for silica and latex spheres in water in a $\hat{\mathbf{y}}$-polarized, $s = 1/\pi$, fifth-order Davis beam, as a function of the sphere radius.

$$[\mathcal{D}(\alpha,\beta,\gamma)]_{\nu\mu,nm} = \delta_{n,\nu}\exp(i\mu\alpha)d^{(n)}_{\mu m}(\beta)\exp(im\gamma). \quad (50)$$

The elements $d^{(n)}_{\mu m}$ are standard,[20] and expressions for them are given in Appendix B. The integral in brackets in Eq. (48) is the same as that encountered in the axial force, Eq. (39), and, again, yields Υ [see Eq. (40)].

Defining then the matrix

$$\Lambda(\theta,\phi) \equiv D(\phi,\theta,0)\Upsilon D^{\dagger}(\phi,\theta,0), \quad (51)$$

and carrying out analogous manipulations on $\hat{\rho}\cdot\mathbf{Q}_r$, we find the final result for Q_ρ is

$$Q_\rho \equiv \hat{\rho}\cdot\mathbf{Q}_f = -\frac{\varphi}{\pi}\mathrm{Re}\left[a^{\dagger}J^{\dagger}(k\mathbf{x})T^{\dagger}\Lambda\left(\frac{\pi}{2},\phi\right)J(k\mathbf{x})a\right.$$

$$\left. + a^{\dagger}J^{\dagger}(k\mathbf{x})\Lambda\left(\frac{\pi}{2},\phi\right)TJ(k\mathbf{x})a\right]$$

$$- \frac{\varphi}{\pi}a^{\dagger}J^{\dagger}(k\mathbf{x})T^{\dagger}\Lambda\left(\frac{\pi}{2},\phi\right)TJ(k\mathbf{x})a, \quad (52)$$

where ϕ is the azimuth angle of the particle position $\mathbf{x}$.

In Fig. 4(a), we present the results of calculations of the radial efficiency on a silica sphere with the same particle and beam parameters as in Fig. 2 with a $\hat{\mathbf{y}}$-polarized Davis beam. The particle displacements are restricted to a plane perpendicular to the beam direction $\hat{\mathbf{z}}$ at the axial trapping position determined from Fig. 2, $z_{\mathrm{tr}} \simeq 0.75$ (μm). The radial efficiencies for displacements along the direction of polarization $\hat{\mathbf{y}}$ and perpendicular to it, the $\hat{\mathbf{x}}$ direction, are both displayed.
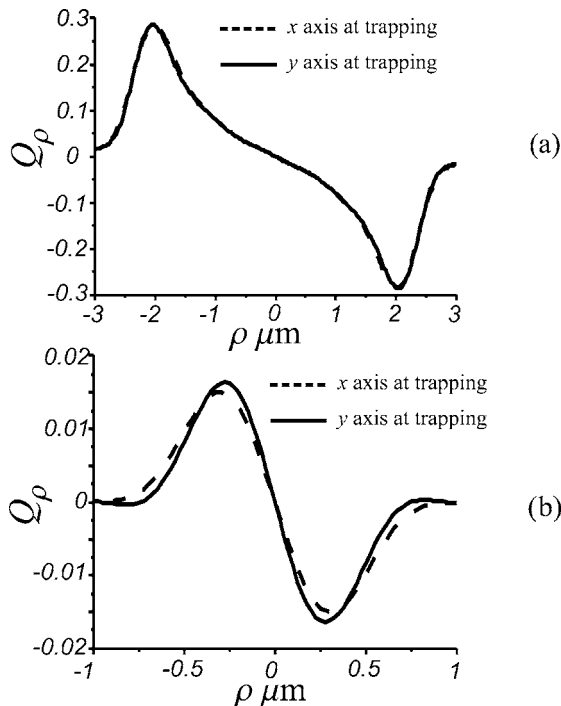

Fig. 4. (a) Radial trapping efficiency, Q_ρ, for a $R=2.1$ (μm) silica as a function of the radial displacements along the $\hat{\mathbf{x}}$ and $\hat{\mathbf{y}}$ axes at the trapping position, $z_{\mathrm{tr}} \simeq 0.75$ (μm). (b) Radial trapping efficiency, Q_ρ, for $\hat{\mathbf{x}}$ and $\hat{\mathbf{y}}$ axis displacements of a $R=0.2$ (μm) silica sphere evaluated at its trapping position $z_{\mathrm{tr}} \simeq 0.43$ (μm).

At least for the beams and particle sizes studied here, the axial asymmetry of the forces is essentially negligible, as can be seen in the example of Fig. 4(a). For smaller particles, the dipole approximation becomes increasingly valid, and it predicts forces more sensitive to the gradient of the axially asymmetric intensity, $|\mathbf{E}_i|^2$, than the (axisymmetric) irradiance, I.[7] We confirm this expectation by calculating in Fig. 4(b) the radial efficiency for a $R=0.2$ (μm) silica sphere at its trapping position, $z_{\mathrm{tr}} \simeq 0.43$ (μm). The axial asymmetry of the optical forces in this situation is considerably more pronounced.

4. CONCLUSIONS

We have hoped to illustrate in this paper that optical forces can be calculated by using rigorous electromagnetic theory in arbitrary directions and for arbitrary particle positions. The formulas that we have developed make use of a unique partial-wave development of the incident beam in an arbitrarily chosen coordinate system, which allows us to choose the system origin such that it facilitates the partial-wave development. Calculations for varying force directions employ the rotation matrices of angular momenta, and the calculation of the force at different particle positions employs the translation-addition theorem. Once one has developed the necessary computer codes, the calculation of the optical forces is generally quite rapid on modern computers and can be used to calculate optical forces in regions that fall outside the domain of validity of commonly invoked approximations. We feel that we have demonstrated the necessity of making such efforts by illustrating the important variations in trapping position that arise owing to geometric resonances within the scattered particles.

APPENDIX A: SPHERICAL WAVES AND VECTOR SPHERICAL HARMONICS

The three normalized VSHs, can be explicitly written in terms of the associated Legendre functions:

$$\mathbf{Y}_{nm}(\theta,\phi) = \gamma_{nm}\sqrt{n(n+1)}P^m_n(\cos\theta)\exp(im\phi)\hat{\mathbf{r}} \equiv Y_{nm}(\theta,\phi)\hat{\mathbf{r}},$$

$$\mathbf{X}_{nm}(\theta,\phi) = \gamma_{nm}\left[\frac{im}{\sin\theta}P^m_n(\cos\theta)\hat{\theta}\right.$$

$$\left. - \frac{\mathrm{d}}{\mathrm{d}\theta}P^m_n(\cos\theta)\hat{\phi}\right]\exp(im\phi) \equiv [i\bar{u}^m_n(\cos\theta)\hat{\theta}$$

$$- \bar{s}^m_n(\cos\theta)\hat{\phi}]\exp(im\phi),$$

$$\mathbf{Z}_{nm}(\theta,\phi) = \gamma_{nm}\left[\frac{\mathrm{d}}{\mathrm{d}\theta}P^m_n(\cos\theta)\hat{\theta}\right.$$

$$\left. + \frac{im}{\sin\theta}P^m_n(\cos\theta)\hat{\phi}\right]\exp(im\phi) \equiv [\bar{s}^m_n(\cos\theta)\hat{\theta}$$

$$+ i\bar{u}^m_n(\cos\theta)\hat{\phi}]\exp(im\phi), \quad (A1)$$

where the normalization coefficients γ_{nm} are defined

$$\gamma_{nm} \equiv \left[\frac{(2n+1)(n-m)!}{4\pi n(n+1)(n+m)!} \right]^{1/2}. \tag{A2}$$

APPENDIX B: ADDITION THEOREM AND ROTATION MATRICES

In optical tweezers containing a single particle, we need only the translation-addition theorem as it applies to regular partial waves. In the context of a given fixed coordinate system and origin, the translation-addition theorem[21,22] takes the form of a translation-addition matrix, $J(k\mathbf{x})$, which permits the development of a partial-wave basis centered on a point $\mathbf{x}$ [i.e., $\mathcal{R}g\{\Psi^t(k\mathbf{r}')\}$, $\mathbf{r}' \equiv \mathbf{r} - \mathbf{x}$] into the regular spherical wave basis centered on the system origin [$\mathcal{R}g\{\Psi(k\mathbf{r})\}$; see Eq. (5)]:

$$\mathcal{R}g\{\Psi(k\mathbf{r})\} = \mathcal{R}g\{\Psi^t(k\mathbf{r}')\}J(k\mathbf{x}), \quad \forall\, |\mathbf{r}_j|, \tag{B1}$$

where J is a matrix of the form

$$J(k\mathbf{x}) \equiv \begin{bmatrix} \bar{A}(k\mathbf{x}) & \bar{B}(k\mathbf{x}) \\ \bar{B}(k\mathbf{x}) & \bar{A}(k\mathbf{x}) \end{bmatrix}. \tag{B2}$$

The matrix elements $\bar{A}_{\nu\mu,nm}$ and $\bar{B}_{\nu\mu,nm}$ are normalized versions of the matrix elements derived by Stein and Cruzan.[11,21,22,23]

The $d_{\mu,m}^{(n)}$ of Eq. (50) can be expressed in terms of the Jacobi polynomials[20]:

$$d_{\mu m}^{(n)}(\beta) = \left[\frac{(n+\mu)!\,(n-\mu)!}{(n+m)!\,(n-m)} \right]^{1/2}$$

$$\times \left(\cos\frac{\beta}{2} \right)^{m+\mu} \left(\sin\frac{\beta}{2} \right)^{m-\mu} P_{n-\mu}^{(\mu-m,m+\mu)}(\cos\beta). \tag{B3}$$

APPENDIX C: BEAM IRRADIANCE

The power of an incident beam is calculated by one's integrating the normal component of the complex incident Poynting vector, $\mathbf{S}_i$, over any infinite surface intercepting the beam. As in the text, we find it convenient to adopt for this surface an infinite plane whose unit normal is parallel to the beam direction, $\hat{\mathbf{u}}_i$. The calculation of beam power then corresponds to an integration of the beam irradiance, $I(\mathbf{r}) \equiv \mathbf{S}_i \cdot \hat{\mathbf{u}}_i$, over this plane.

The fact that we use spherical coordinates for the wave functions makes it difficult to perform an analytical integration of $I(\mathbf{r})$ in an arbitrary $z=$constant plane (with $\hat{\mathbf{u}}_i = \hat{\mathbf{z}}$). It is possible, however, to perform analytic integrations in the $z=0$ plane. With the field VSWF field developments of Eqs. (4) and (6), the irradiance for time-harmonic fields is explicitly

$$I(\mathbf{r}) = \frac{1}{2}\mathrm{Re}\{\mathbf{E}_i^* \times \mathbf{H}_i\} \cdot \hat{\mathbf{z}}$$

$$= -\frac{1}{2}\left(\frac{\varepsilon_b \epsilon_0}{\mu_b \mu_0} \right)^{1/2} A^2 \sum_{n,m;\nu\mu} \mathrm{Re}\{-i[a_{nm}^{\mathrm{M},*}\mathcal{R}g\{\mathbf{M}_{nm}^*(k\mathbf{r})\}$$

$$+ a_{nm}^{\mathrm{N},*}\mathcal{R}g\{\mathbf{N}_{nm}^*(k\mathbf{r})\}] \times [a_{\nu\mu}^{\mathrm{M}}\mathcal{R}g\{\mathbf{N}_{\nu\mu}(k\mathbf{r})\}$$

$$+ a_{\nu\mu}^{\mathrm{N}}\mathcal{R}g\{\mathbf{M}_{\nu\mu}(k\mathbf{r})\}] \cdot \hat{\mathbf{z}}\}. \tag{C1}$$

The $z=0$ irradiance integral then corresponds to taking $\theta = \pi/2$ and integrating over $\phi = 0 \to 2\pi$ and $r = 0 \to \infty$.

An inspection of Eq. (C1) shows that an analytic calculation of the beam power, Eq. (17), will involve four integrals involving vector products of the VSWFs. The contribution to the total beam power involving the coefficient product $a_{nm}^{\mathrm{M},*}a_{\nu\mu}^{\mathrm{N}}$ (denoted δP^{MN}) is zero because $\mathcal{R}g\{\mathbf{M}_{nm}^*\} \times \mathcal{R}g\{\mathbf{M}_{\nu\mu}\} \cdot \hat{\mathbf{z}} = 0$ in the $z=0$ plane. The vector product involving $a_{nm}^{\mathrm{N},*}a_{\nu\mu}^{\mathrm{M}}$ (denoted δP^{NM}) does, however, have a nonzero contribution to the power integral of Eq. (17), namely,

$$\delta P^{\mathrm{NM}} = \int_0^\infty r\mathrm{d}r \int_0^{2\pi} \mathrm{d}\phi\, \mathrm{Re}\{-i[a_{nm}^{\mathrm{N},*}a_{\nu\mu}^{\mathrm{M}}\mathcal{R}g\{\mathbf{N}_{nm}^*(k\mathbf{r})\}$$

$$\times \mathcal{R}g\{\mathbf{N}_{\nu\mu}(k\mathbf{r})\}]\} \cdot \hat{\mathbf{z}}_{\theta=\pi/2}$$

$$= -A^2 \frac{\pi}{k^2}\left(\frac{\varepsilon_b \epsilon_0}{\mu_b \mu_0} \right)^{1/2} \sum_{n,\nu,m=\pm 1} \mathrm{Re}\{[a]_{nm}^{\mathrm{N*}}[a]_{\nu m}^{\mathrm{M}}\}$$

$$\times \frac{\bar{u}_n^m(0)\bar{u}_\nu^m(0)}{m} \times \left\{ n(n+1)\int_0^\infty \frac{j_n(x)}{x}[xj_\nu(x)]'\mathrm{d}x + \nu(\nu \right.$$

$$\left. + 1)\int_0^\infty [xj_n(x)]'\frac{j_\nu(x)}{x}\mathrm{d}x \right\}, \tag{C2}$$

where the $\bar{u}_n^m(\cos\theta)$ are defined in Eq. (A1). One finds that $\bar{u}_n^m(0)\bar{u}_\nu^m(0)$ with $|m|=1$ is nonzero only if both n and ν are odd. The analytic expression for $\bar{u}_n^m(0)\bar{u}_\nu^m(0)$ with both n and ν odd is

$$\bar{u}_n^m(0)\bar{u}_\nu^m(0)$$

$$= \frac{(-1)^{(n-\nu)/2}}{4\pi}\sqrt{(2n+1)(2\nu+1)}\frac{(n-2)!!\,(\nu-2)!!}{(n+1)!!\,(\nu+1)!!}. \tag{C3}$$

The Bessel function integral gives a particularly simple result,

$$n(n+1)\int_0^\infty \frac{j_n(x)}{x}[xj_\nu(x)]'\mathrm{d}x + \nu(\nu+1)\int_0^\infty [xj_n(x)]'\frac{j_\nu(x)}{x}\mathrm{d}x$$

$$= (-1)^{(n-\nu)/2}, \tag{C4}$$

to yield finally

O. Moine and B. Stout

$$\delta P^{\mathrm{NM}} = -\frac{|I(\mathbf{0})|}{2k^2} \sum_{p,q=0}^{(N_{\max}-1)/2} \sum_{m=\pm 1} \frac{\mathrm{Re}[\,[a]^{\mathrm{N},*}_{2p+1,m}[a]^{\mathrm{M}}_{2q+1,m}\}]}{m}$$

$$\times \sqrt{(4p+3)(4q+3)}\frac{(2p-1)!!}{(2p+2)!!}\frac{(2q-1)!!}{(2q+2)!!}, \quad (\mathrm{C5})$$

where $N_{\max}$ is an appropriate cutoff for the VSWF development of the incident beam and $2p+1$ and $2q+1$ are odd integers.

Finally, using the defining property of the beam shape coefficients, g_n, of Eq. (16) and the expressions for the $[p]^{\mathrm{M,N}}_{n,m}$ of Eqs. (15), we can write this sum directly in terms of g_n:

$$\delta P^{\mathrm{NM}} = I(\mathbf{0})\frac{\pi}{k^2} \sum_{p,q=0}^{(N_{\max}-1)/2} g_{2p+1}g_{2q+1}(4p+3)$$

$$\times (4q+3)\frac{(2p-1)!!}{(2p+2)!!}\frac{(2q-1)!!}{(2q+2)!!}(-1)^{p-q}. \quad (\mathrm{C6})$$

Evaluating the remaining δP^{MM} and δP^{NN} contributions to the total beam power in a similar manner and appealing to the defining relation, Eq. (13), for the beam shape normalization factor, φ, yield the analytic expression for φ found in Eq. (20).

APPENDIX D: NORMALIZATION CONDITION OF THE INCIDENT-FIELD COEFFICIENTS

From the partial-wave expression for the irradiance, Eq. (C1), one can determine the normalization condition for the incident-field coefficients, Eq. (9), by noting that, as $\mathbf{r}\to\mathbf{0}$, only the $\mathcal{R}g\{\mathbf{N}_{1,m}(k\mathbf{r})\}$ VSWFs are nonzero, and that

$$\mathcal{R}g\{\mathbf{N}^*_{1m}(k\mathbf{r})\} \times \mathcal{R}g\{\mathbf{N}_{1\mu}(k\mathbf{r})\} \cdot \hat{\mathbf{z}}$$

$$= \frac{\sqrt{2}j_1(kr)[krj_1(kr)]' Y^*_{1m}(\hat{\mathbf{r}})\mathbf{X}_{1\mu}(\hat{\mathbf{r}})}{k^2r^2}$$

$$- \frac{\sqrt{2}[krj_1(kr)]'j_1(kr)Y_{1\mu}(\hat{\mathbf{r}})\mathbf{X}^*_{1m}(\hat{\mathbf{r}})}{k^2r^2}$$

$$- \frac{[(krj_\nu(kr)]')^2\mathbf{Z}^*_{nm}(\theta,\phi)\cdot\mathbf{X}_{\nu\mu}(\theta,\phi)\hat{\mathbf{r}}}{k^2r^2}. \quad (\mathrm{D1})$$

Using the limits

$$\lim_{x\to 0}j_1(x)\approx \frac{x}{3}, \quad \lim_{x\to 0}[xj_\nu(x)]'\approx \frac{2x}{3}, \quad (\mathrm{D2})$$

we obtain

$$\frac{1}{2\pi}\int_0^{2\pi}\mathrm{d}\phi\sum_{m,\mu=-1}^{1}a^{\mathrm{N},*}_{1m}a^{\mathrm{M}}_{1\mu}\mathcal{R}g\{\mathbf{N}^*_{1m}(\mathbf{0})\}\times\mathcal{R}g\{\mathbf{N}_{1\mu}(\mathbf{0})\}\cdot\hat{\mathbf{z}}\bigg|_{\theta=\pi/2}$$

$$= -i\frac{8}{9}\sum_{m=\pm 1}ma^{\mathrm{N},*}_{1,m}a^{\mathrm{M}}_{1,m}\bar{u}^m_1(0)\bar{u}^m_1(0)$$

$$= \frac{i}{6\pi}\{a^{\mathrm{N},*}_{1,-1}a^{\mathrm{M}}_{1,-1} - a^{\mathrm{N},*}_{1,1}a^{\mathrm{M}}_{1,1}\}, \quad (\mathrm{D3})$$

where we used $\bar{u}^m_1(0)=-\frac{1}{4}\sqrt{3/\pi}$. Putting this result into Eq. (C1), we find that the irradiance at the system origin takes the form

$$I(\mathbf{0}) = \frac{1}{2}\left(\frac{\varepsilon_b\epsilon_0}{\mu_b\mu_0}\right)^{1/2}A^2\frac{1}{6\pi}\mathrm{Re}\{a^{\mathrm{N},*}_{1,-1}a^{\mathrm{M}}_{1,-1} - a^{\mathrm{N},*}_{1,1}a^{\mathrm{M}}_{1,1}\}$$

$$= \frac{|\mathbf{S}(\mathbf{0})|}{6\pi}\mathrm{Re}\{a^{\mathrm{N},*}_{1,-1}a^{\mathrm{M}}_{1,-1} - a^{\mathrm{N},*}_{1,1}a^{\mathrm{M}}_{1,1}\}, \quad (\mathrm{D4})$$

where we have invoked Eq. (8) for A^2. Because $I(\mathbf{0}) = |\mathbf{S}(\mathbf{0})|$, this leads to the normalization condition of Eq. (9) for $a^{\mathrm{M}}_{n,m}$.

As we have seen in the text, the resulting normalization condition, Eq. (9), is trivial to implement, but it is principally only of use when studying and comparing beam profiles. One should keep in mind that the final formulas for the optical forces, Eqs. (43) and (52), are independent of the normalization of the incident-beam coefficients.

REFERENCES

1. A. Ashkin, J. M. Dziedzic, J. E. Bjorkholm, and S. Chu, "Observation of a single-beam gradient force optical trap for dielectric particles," Opt. Lett. **11**, 288–290 (1986).
2. J. C. Crocker, J. A. Matteo, A. D. Dinsmore, and A. G. Yodh, "Entropic attraction and repulsion in binary colloids probed with a line optical tweezer," Phys. Rev. Lett. **82**, 4352–4355 (1999).
3. L. Paterson, M. P MacDonald, J. Arit, W. Dultz, H. Schmitzer, W. Sibett, and K. Dholakia, "Controlled simultaneous rotation of multiple optically trapped particles," J. Mod. Opt. **50**, 1591–1601 (2003).
4. H. Melville, G. F. Milne, G. C. Spalding, W. Sibbett, K. Dholakia, and D. McGloin, "Optical trapping of three-dimensional structures using dynamic holograms," Opt. Express **1**, 3562–3567 (2003).
5. G. Sinclair, J. Leach, P. Jordan, G. Gibson, E. Yao, Z. J. Laczik, M. J. Padgett, and J. Courtial, "Interactive application in holographic optical tweezers of a multiplane Gerchberg–Saxton algorithm for three-dimensional light shaping," Opt. Express **12**, 1665–1670 (2004).
6. J. Leach, G. Sinclair, P. Jordan, J. Courtil, and M. J. Padgett, "3D manipulation of particles into crystal structures using holographic optical tweezers," Opt. Express **12**, 220–226 (2004).
7. A. Ashkin and J. M. Dziedzic, "Optical trapping and manipulation of viruses and bacteria," Science **2335**, 1517–1520 (1987).
8. A. Ashkin, "Forces of a single-beam gradient laser trap on a dielectric sphere in the ray optics regime," Biophys. J. **61**, 569–582 (1992).
9. T. Tlusty, A. Meller, and R. Bar-Ziv, "Optical gradient forces of strongly localized fields," Phys. Rev. Lett. **81**, 1738–1741 (1998).
10. G. Lenormand, S. Hénon, A. Richert, J. Siméon, and F. Gallet, "Direct measurement of the area expansion and shear moduli of the human red blood cell membrane skeleton," Biophys. J. **81**, 43–56 (2001).
11. L. Tsang, J. A. Kong, and R. T. Shin, *Theory of Microwave Remote Sensing* (Wiley, 1985).

12. W. Chew, *Waves and Fields in Inhomogeneous Media*, Series on Electromagnetic Waves (IEEE, 1990).
13. C. F. Bohren and D. R. Huffman, *Absorption and Scattering of Light by Small Particles* (Wiley-Interscience, 1983).
14. L. W. Davis, "Theory of electromagnetic beams," Phys. Rev. A **19**, 1177–1179 (1979).
15. G. Gouesebet, J. A. Lock, and G. Gréhan, "Partial-wave representations of laser beams for use in light-scattering calculations," Appl. Opt. **34**, 2133–2143 (1995).
16. B. Stout, J.-C. Auger, and J. Lafait, "Individual and aggregate scattering matrices and cross-sections: conservation laws and reciprocity," J. Mod. Opt. **48**, 2105–2128 (2001).
17. H. C. Van de Hulst, *Light Scattering by Small Particles* (Dover, 1957).

18. P. Debye, "Der Lichtdruck auf Kugeln von beliebigem Material," Ann. Phys. (Leipzig) **30**, 57–136 (1909).
19. M. I. Mishchenko, "Radiation force caused by scattering, absorption, and emission of light by nonspherical particles," J. Quant. Spectrosc. Radiat. Transf. **70**, 811–816 (2001).
20. A. R. Edmonds, *Angular Momentum in Quantum Mechanics* (Princeton U. Press, 1960).
21. S. Stein, "Addition theorems for spherical wave function," Q. Appl. Math. **19**, 15–24 (1961).
22. O. R. Cruzan, "Translation addition theorems for spherical vector wave functions," Q. Appl. Math. **20**, 33–40 (1962).
23. B. Stout, J. C. Auger, and J. Lafait, "A transfer matrix approach to local field calculations in multiple-scattering problems," J. Mod. Opt. **49**, 2129–2152 (2002).